



VALIDATION AND CASE STUDIES

Section Coordinator: Anssi Laukkanen

VTT, Finland

13 Fracture module

13	Fracture module	13-1
13.1	Introduction.....	13-2
13.2	Case Studies for Fracture.....	13-3
13.2.1	Laser Beam (LB) and Friction Stir Welded (FSW) Wide Plate Tests of Al-Alloys	13-3
13.2.2	A533B Steel Wide Plate Tests	13-8
13.2.3	Wide Plate Tests on Aluminium Alloys	13-19
13.2.4	Canadian Pipe Bend Trials	13-21
13.2.5	A533B-1 Steel Residual Stress Experiments.....	13-25
13.2.6	Stainless Steel Large Plate Test SSTP10.....	13-36
13.2.7	Stainless Steel Large Plate Test SSTP12.....	13-46
13.2.8	Spinning Cylinder Test 1	13-54
13.2.9	Master Curve Analysis of the Point Pleasant Bridge Failure.....	13-58
13.2.10	Crack Arrest Evaluation.....	13-64
13.2.11	Weld Strength Mismatched Steel Specimens	13-70
13.2.12	Thin-Walled Specimens Tests.....	13-75
13.3	Case Studies for FATIGUE	13-80
13.3.1	Fatigue Routes 1 and 2 for Welded Structures, Nominal and Notch Stress Approaches	13-80
13.3.2	Fatigue Route 2, for Non Welded Components on Compressor Flange Made of Grey Iron ..	13-85
13.3.3	Fatigue Route 3, for Non-Welded Components: Local Stress-Strain Approach	13-89
13.3.4	Specific Applications: Structural Stress Approach on Welded Structures	13-94
13.3.5	Application of Fatigue Improvement Techniques to Welded Structures	13-98
13.4	Case Studies for CREEP.....	13-105
13.4.1	Flat Plate under Constant Tensile Load.....	13-105
13.4.2	Cylindrical Pipe With an External Crack under Constant Load.....	13-114
13.4.3	Cylindrical Pipe With an Internal Crack under Cyclic Loading	13-125
13.4.4	Flat Plate With a Part-Penetrating Defect under Cyclic Loading.....	13-139
13.5	Case Studies for CORROSION.....	13-165
13.5.1	Pipeline Local Thinned Area Assessment.....	13-165
13.5.2	Checklist for FFS Assessment.....	13-168

13.1 Introduction

FITNET Fitness-for-Service (FFS) Procedure consists of three volumes;

Volume I: FITNET FFS Procedure (Sections 1 to 12)

Volume II: Case Studies and Tutorials (Sections 13 and 14)

Volume III: FITNET FFS Annexes

This Volume II: Case studies and Tutorials, contains two Sections. **Section 13: Case studies and validation, Section 14: Tutorials.** First section aims to provide examples from validation works during the FITNET FFS Procedure development. Section 14 provides examples of the FFS applications in a more detailed manner.

This Volume presents the 7th version (MK7) of the FITNET FFS Procedure development work during the period of 2002 to 2006. It is called a “Final Draft”, implying for further revisions.

The FITNET FFS procedure has been validated in parallel with the development of the procedure. Numbers of case studies have been developed by the members and hence this section presents these case studies. The case studies themselves have been collected from a wide range of sources, such as international case benchmarks, integrity assessment trials, recent publications and works within the FITNET consortium etc., with the emphasis of covering the various aspects of the FITNET FFS procedure to produce verification of the different assessment modules.

Some well-documented examples presented in this Volume II have earlier been used in R6, BS7910 and SINTAP procedures. Therefore, this final draft has still tentative subsection and/or figure, equation numbers. They will be harmonised during the next revision.

Numbers of the case studies covered in this Section 13 are also presented in Section 14 (Tutorials) and covered in a much more detailed fashion to provide a clear and “step-by-step” use of the FITNET FFS Procedure. This is particularly important for the new users of the procedure in industry and academia.

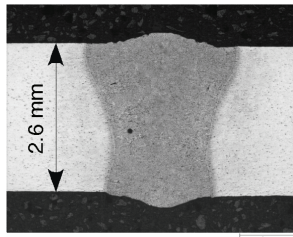
13.2 Case Studies for Fracture

13.2.1 Laser Beam (LB) and Friction Stir Welded (FSW) Wide Plate Tests of Al-Alloys

This case study covers the application of Fracture Module to welded (**with strong strength undermatching**) thin-walled Al-alloys of aerospace grades.

Specimen :	Middle cracked wide plate with transverse laser beam and FSW butt-joints. $2W=750$ mm, $a_0/W=0.33$, $B=2.2$ and 2.6 mm. Ligament ($W - a_0$) / Thickness (B) ratio = 193 to 228
Loading :	Tension
Material :	The material investigated within this work is an age-hardening Al-alloy 6013 in T6 temper condition. The thickness of the sheets was varied between 2.2 mm and 2.6 mm. The laser beam welding was carried out using a single CO ₂ laser source with an AISi12 filler wire. Both LBW and FSW produced strength under-matched welds, tested in the as-welded condition (Figure 13.1).
Defect :	Central through thickness notch with fatigue crack located at the centre of the weld metals, the HAZ of the LBW and the TMAZ (thermomechanically affected zone) of the FSW.
Temperature :	RT

LBW butt-joint



a)

FSW butt-joint



b)

Figure 13.1 – Macro-sections of a) LBW and b) FSW butt-joints

The current case study is presented in more detail in the FITNET Tutorials, chapter 14.3.

Generation of Material Data:

It is known that standard flat tensile specimens produce tensile properties characteristic of the whole joint, covering the interaction between base and weld areas. However, micro-flat tensile specimens enable the determination of local tensile properties. These 0.5 mm thick and 1.5 mm wide specimens were extracted using electrical discharge machining (EDM) from different locations of the LBW and FSW joints. Figure 13.2 shows the extraction technique. This technique yields full stress-strain curves obtained from the bulk material of the region of interest. The elongation was measured at a gauge length of $L_0 = 7$ mm. It should be noted that micro-flat tensile specimens are made of all-weld material and thus provide the intrinsic (local) material tensile properties. Table 13.1 gives the tensile strength and elongation values for all materials. For the LBW material, the standard specimens yielded much higher yield and ultimate tensile strengths than the micro-flat tensile specimens.

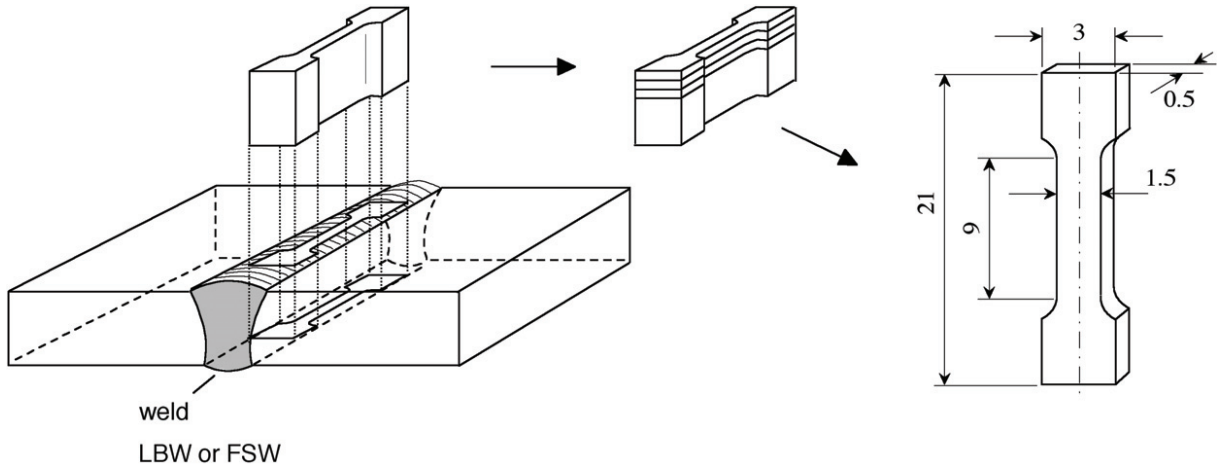


Figure 13.2 – Extraction of micro- flat tensile specimens

Table 13.1 – Material properties of the weld and base materials obtained from micro-flat and standard transverse flat tensile specimens (gauge length 50 mm).

Material	Yield strength $\sigma_Y = R_{p0.2}$ MPa	Tensile strength σ_{UTS} MPa	Elongation at fracture, A %	Mismatch factor, $M = \sigma_{YW} / \sigma_{YB}$
Micro-flat tensile specimens				
Base (LT)	330	365	11.5	
LBW (FZ)	145	165	2.0	0.44
FSW (nugget)	185	295	28.5	0.56
FSW (TMAZ)	200	285	13.0	0.61
Standard flat tensile specimens				
Base (LT)	360	395	12.6	
LBW	240	290	0.9	
FSW	210	285	2.6	

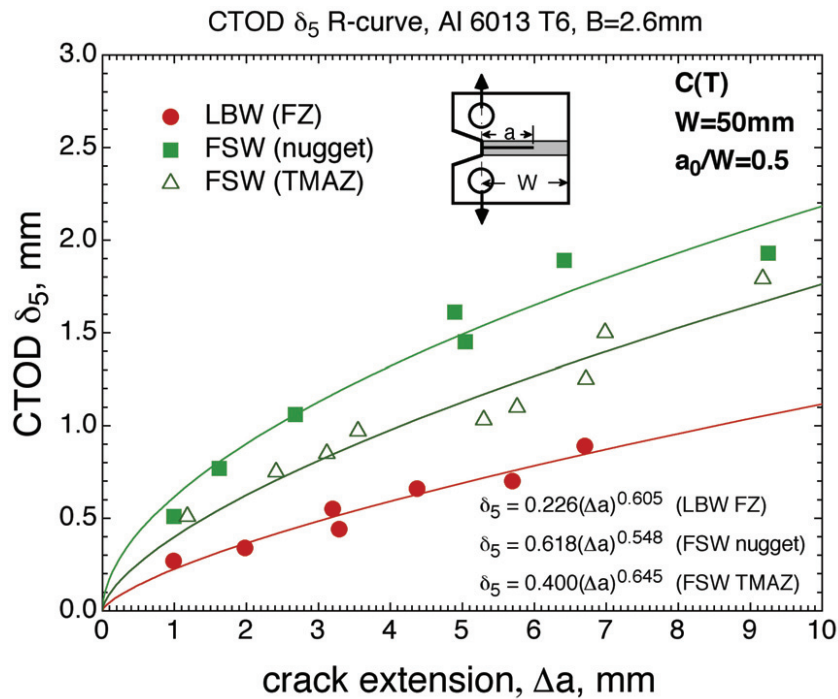


Figure 13.3 – R-curves of the materials as determined using C(T)50 type specimens.

Summary of Analysis and Results: FITNET analysis results in comparison with the experimental results are given in Figures 13.4 to 13.7 for various inputs and analysis options. Figure 13.4 shows the effect of the selection of the weld metal yield strength on the FITNET Option 2 predictions of Load vs. CTOD curves of the LBW panels with weld metal crack.

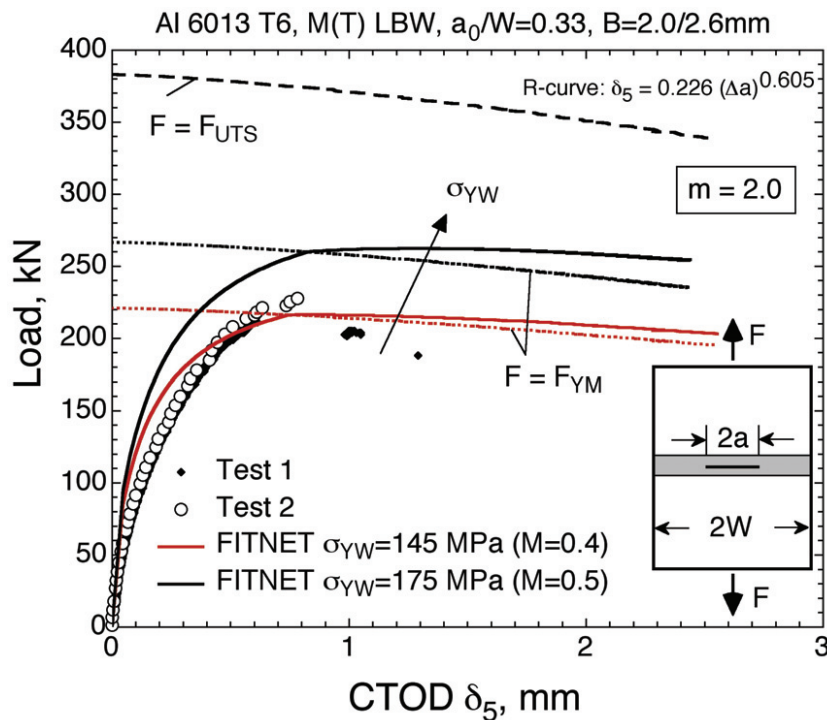


Figure 13.4 – Sensitivity of the residual strength prediction to the yield strength of the LBW material

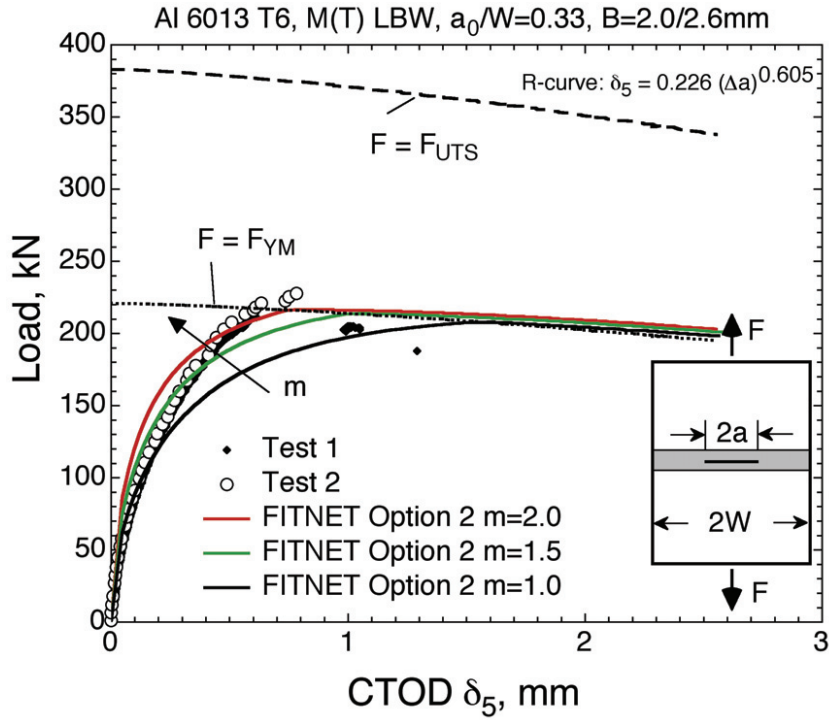


Figure 13.5 – Comparison between the predicted and experimental results of LBW panels including the variation of the constraint parameter m .

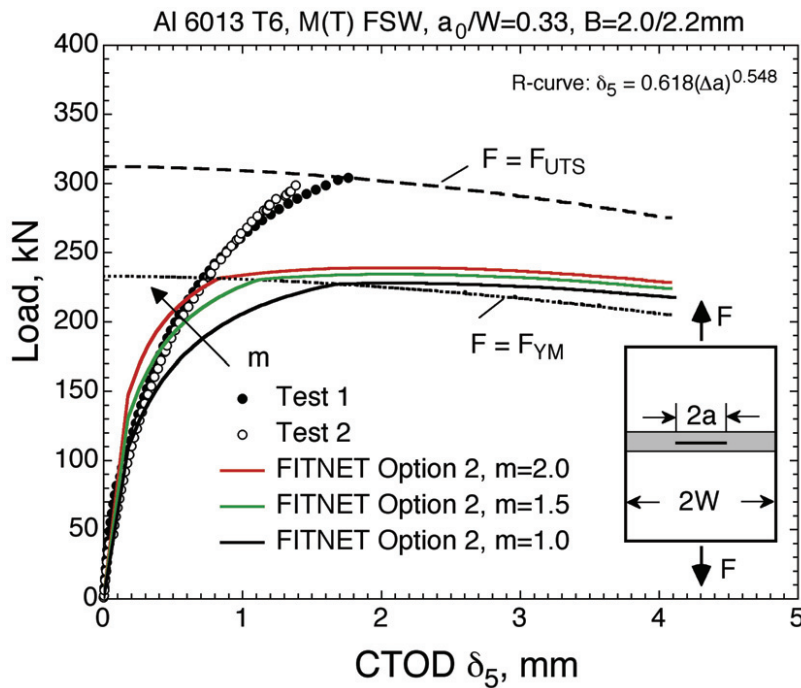


Figure 13.6 – Comparison between the predicted and experimental results of FSW panels including the variation of the constraint parameter m .

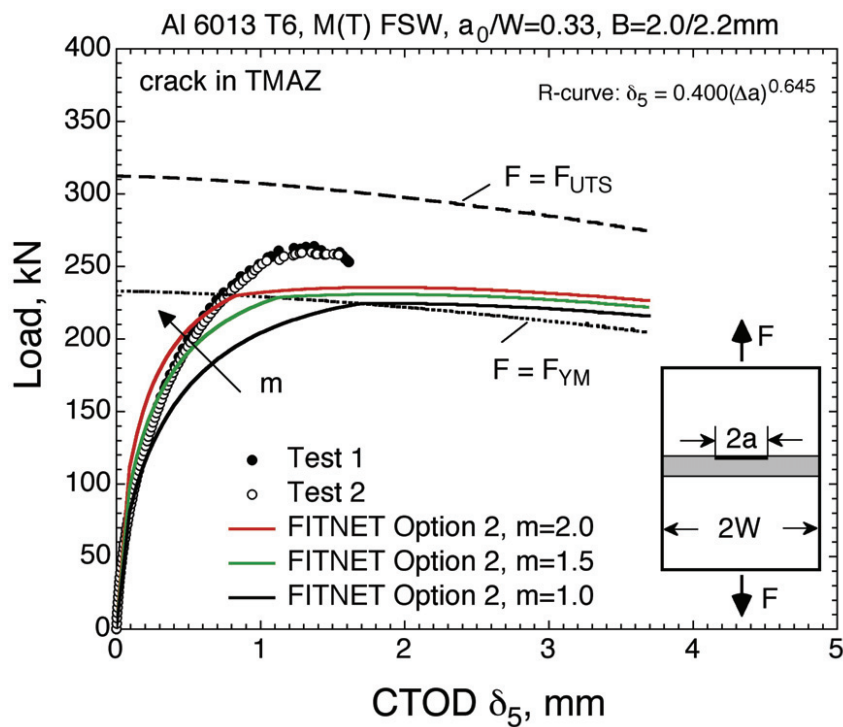


Figure 13.7 – Comparison between the predicted and experimental results of the TMAZ notched panels the variation of the constraint parameter m .

Assessment of Significance of Results: These case studies have shown the applicability of the FITNET FFS Fracture Module to the thin-walled welded panels. The cases are reported here covered advanced welds on high strength Al-alloys with significant strength undermatching. Comparison of the FITNET Option 2 predictions of the maximum load carrying capacities of the panels has shown conservative natures of the predictions for both LBW and FSW welds. An increase of constraint factor “ m ” towards plane strain condition has yielded, in general, prediction with less conservatism. Better prediction of the LBW joints compared to the FSW joints was observed.

An application of weld strength mis-match option (Option 2) of the FITNET FFS Fracture Module is further demonstrated by the cases covered in manuscript of the authors presented in FITNET 2006 Conference.

Bibliography

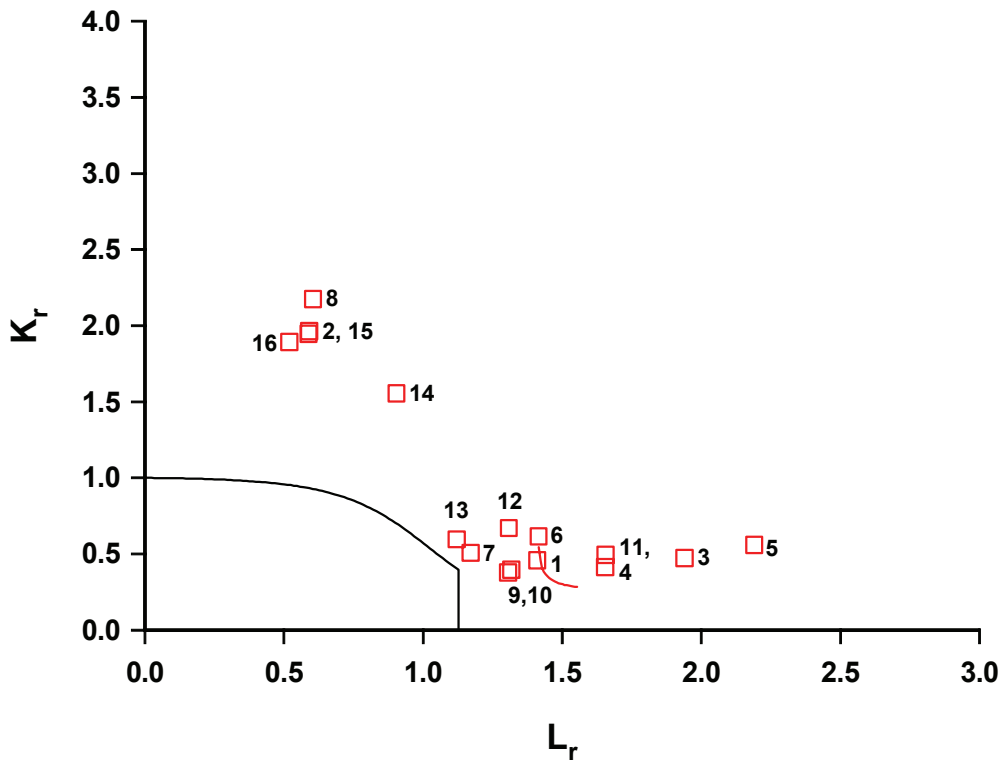
- [13.1] Seib E. and Koçak M., Fracture of Strength Under-matched Welds of Thin-walled Aluminium Structures using FITNET Procedure, IIW Doc.X-1577-2005, Welding in the World, Nov. Dec. 2005, Vol. 49, No. 11/12-2005, pp. 58-69.
- [13.2] FITNET FFS Procedure, Chapter 14.3

13.2.2 A533B Steel Wide Plate Tests

This case study presents an application of the Fracture Module to the A533B Steel wide plate

Specimen : Wide plates
 Loading : Monotonic uniaxial and biaxial tension, bending, WPS
 Material : A533B-1 steel
 Defect : Semi-elliptical and through-wall cracks
 Temperature : Temperatures ranging from -163°C to 70°C

Further details are contained in I Hadley and P Moore, Fracture case studies for validation of fitness-for-service procedures, TWI members' report 850/2006



Test Programme on 50mm Thick A533B Plate

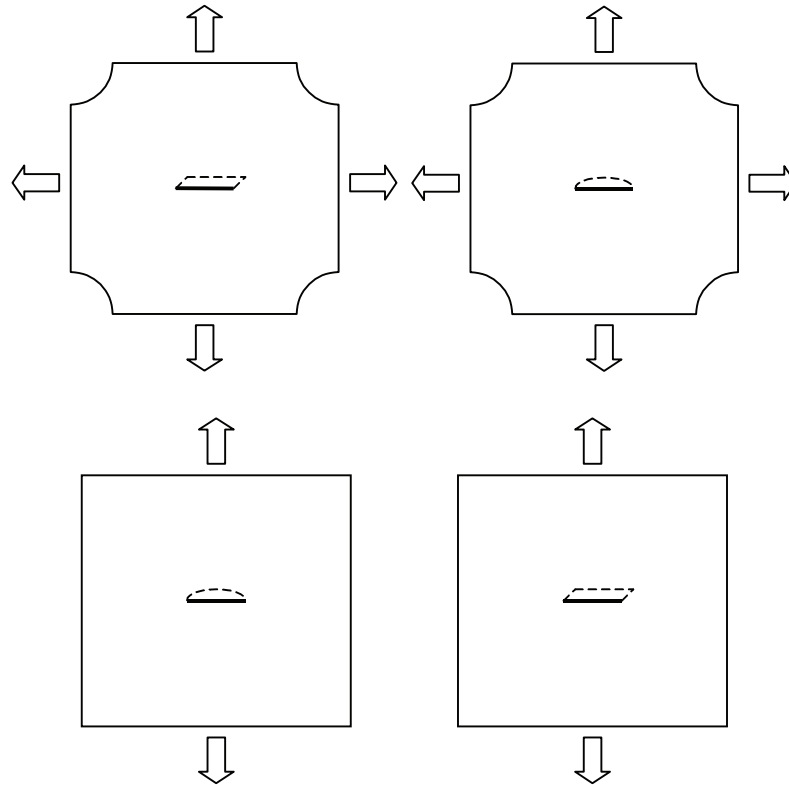


Figure 13.8 – Wide plate test specimens for tests on 50 mm plate.

A large programme of testing and analysis was carried out on 50mm thick A533B steel, Figure 13.8, (for selected tests, the material thickness was reduced to 25mm to allow testing within the capacity of the available equipment).

Material characterisation:

- Standard fracture mechanics testing (SENB specimens), to generate single-point values of toughness in terms of K_{Ic} , critical J and critical CTOD.
- Tearing resistance curves (R-curves) in terms of J and CTOD, at temperatures of -100, -70 and +70°C.
- Full stress-strain curves at +70, -70 and -96 °C.

Loading, temperatures and defects: Wide plate tests were carried out at a range of temperatures between +70°C and -163°C, covering the full ductile to brittle transition temperature curve. Biaxial ratios of $k=0$ (ie uniaxial loading), $k=0.5$, and $k=1$ (ie equibiaxial loading) are included in the data, where k represents the ratio of the load parallel to the flaw to that perpendicular to the flaw. Both semi-elliptical surface breaking and through-thickness flaws were introduced, ie SCT (surface-cracked tension) and CCT (centre-cracked tension) specimens as shown in Table 13.2.

Table 13.2 – Specimen identification and specifications

ID, this work	ID, original work	Crack type	Nominal thickness, [mm]	Test temperature, [°C]	Biaxiality ratio, k
1	M01-01	SCT	50	70	0
2	M01-10	SCT	25	-129	1
3	M01-11	SCT	50	70	1
4	M01-12	SCT	25	70	0
5	M01-13	SCT	25	70	0.5
6	M01-15	CCT	25	70	1
7	M01-16	CCT	25	70	0
8	M01-20(1)	SCT	50	-129	1
9	M01-20(2)	SCT	25	-77	0
10	M01-21	SCT	25	-70	1
11	M01-22	SCT	25	-70	0.5
12	M01-23	SCT	25	-94	0.5
13	M01-24	SCT	25	-97	1
14	M01-25	SCT	50	-103	1
15	M01-20	SCT	50	-157	0
16	M01-40	SCT	50	-163	1

Note:

k=0 denotes uniaxial loading, k=1 denotes equibiaxial loading, k=0.5 denotes twice as much loading perpendicular to the flaw as parallel to it (for example, the biaxiality conditions experienced by a seam weld in a closed pressurised pipe)

Analysis: The sixteen wide plate tests carried out in the first phase of the work, referred to as ID 1-16, have been analysed as follows:

- The membrane stress applied perpendicular to the flaw at the point of failure is treated as the primary stress, P_m .
- The fracture toughness K_J used in the analysis was taken as the lowest of three SENB test results or equivalent (ie Minimum of Three Equivalent or MOTE) at the appropriate temperature.
- A single case (ID 1) was re-analysed using a Option 1 tearing analysis, based on the J R-curve generated over the range $0.2\text{mm}\Delta a < 5\text{mm}$ for this material at 70°C.
- All analyses used an Option 1 or Option 3 FAD, with the appropriate tensile properties for the test temperature.

The results of the analysis are given in Figure 13.9. Numbers adjacent to each data point indicate the test ID as shown in the table. It can be seen that all the specimens failed in the 'unacceptable' region of the failure assessment diagram (FAD), as expected. Results fall in the fracture-dominated, (IDs 2, 8, 15, 16), 'knee' (ID

14) and collapse-dominated (all other data points) regions of the FAD, depending on the test temperature. The results of the Option 1 analysis of specimen ID 1 can be seen as a locus of points (only one Option 1 tearing analysis was carried out, to illustrate the difference between initiation and tearing analyses, although data are available for further tearing analyses if required). At low levels of tear length, Δa , the different option analyses are virtually coincident.

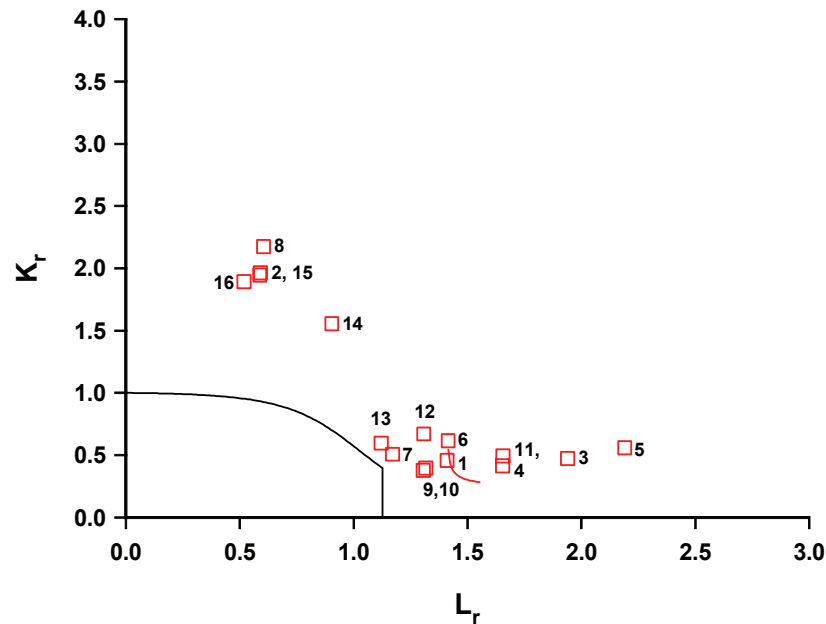


Figure 13.9 – Assessment results for wide plate IDs 1-16.

Further tests were later carried out on material from the same batch as that described above, along with numerical analyses of tests. The numerical analyses predicted a strong effect of biaxiality on the effective toughness of through-cracked plates tested in the lower transition, with uniaxial specimens showing an apparent toughness (defined in this case as J/J_{SSY}) some four times higher than that of SENB specimens, while equibiaxially loaded specimens would have a toughness approximately the same as that of an SENB specimen. For a surface-cracked specimen, the effect of biaxiality was predicted to be much less marked. The predicted effect of biaxiality on fracture of through-cracked plates was later confirmed by experiment at -100°C , as shown in Table 13.3.

Table 13.3 – Biaxially tested specimen identification and specifications

ID, this work	ID, original work	Crack type	Nominal thickness, [mm]	Test temperature, [$^{\circ}\text{C}$]	Biaxiality ratio, k
40	M01-26	CCT	50	-100	1
41	M01-28	CCT	50	-100	0

Results of the analysis in terms of a Option 3 analysis are shown in Figure 13.10. The result corresponding to the uniaxially loaded specimen (ID 40) lies further away from the failure assessment line than the result for the biaxially loaded specimen (ID 41); hence the safety factor associated with the analysis of the biaxially loaded specimen is lower, as would be expected from the numerical analysis results.

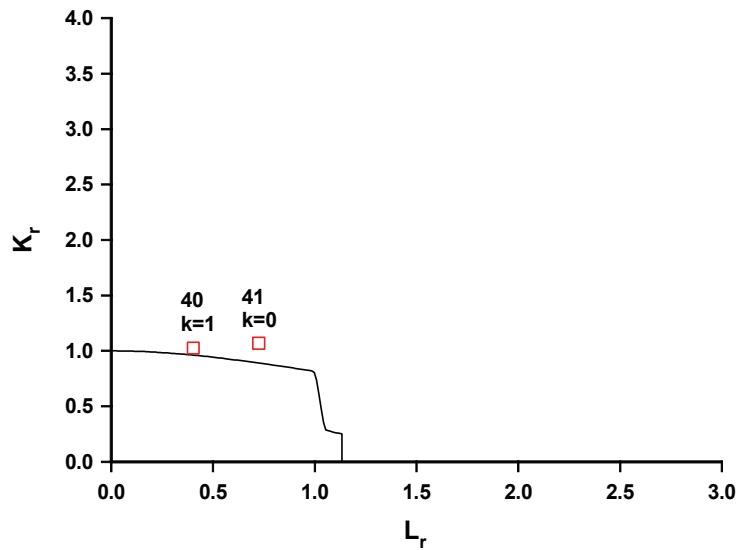


Figure 13.10 – Results of biaxial (ID 40) and uniaxial (ID 41) wide plate tests at –100°C.

A series of low-constraint fracture mechanics tests (using shallow-notched SENB specimens) was subsequently carried out as part of the SINTAP programme. The purpose of the work was to validate Appendix 3 of the SINTAP procedure, which addresses the treatment of crack tip constraint. The uniaxial wide plate test (ID 41) was re-analysed using the ‘constraint matching’ option. Figure 13.11 shows the results both for a standard analysis and a more advanced analysis using the constraint matching approach. The data point associated with ‘constraint-corrected’ data lies much closer to the failure analysis line, indicating the benefits to be gained from using constraint correction.

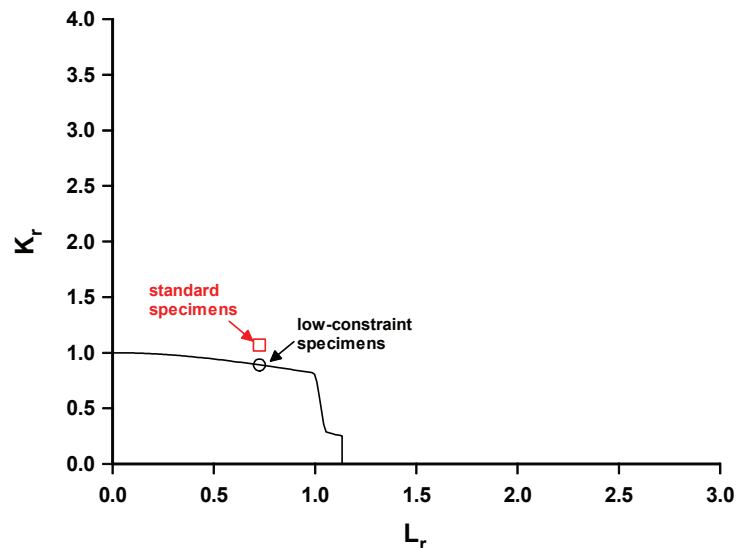


Figure 13.11 – Results of uniaxial wide plate test (ID 41) using a Level 3b BS 7910 analysis based on both standard and low-constraint specimens.

Test Programme on 85mm Thick A533B Specimens for Warm Pre-stress

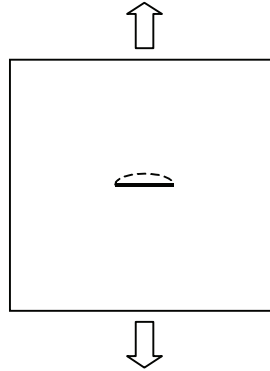


Figure 13.12 – Wide plate test specimens for WPS tests on 85 mm plate.

Uniaxial wide plate tests were carried out on four 85mm thick specimens, containing semi-elliptical notches sharpened by fatigue (Figure 13.12 and Table 13.4). Three (ID 17-19) comprised A533B material that had been quenched and tempered, whilst one (ID 20) was in the as-rolled condition, intended to be representative of an irradiation-embrittled material. Specimens ID 17 and 18 were pre-stressed at 70°C and then cooled to -44°C and loaded to failure. Around 20mm of ductile tearing occurred during the warm pre-stress period. Specimen ID 20 was warm pre-stressed and held at load while cooled to -20°C, where fracture occurred. Specimen ID 19 was not pre-stressed. All tests were loaded using a dual hydraulic loading ram to apply both membrane and bending stress.

Table 13.4 – Specimen identification and specifications.

ID, this work	ID, original work	Crack type	Nominal thickness, [mm]	Material condition	Pre-stress temperature [°C]	Test temperature, [°C]
17	22771/M01-01	SCT	85	Q&T	70	-44
18	22771/M01-02	SCT	85	Q&T	70	-44
19	23200/M01-01	SCT	85	Q&T	-	-44
20	22771/M01-01	SCT	85	as-rolled	70	-20

Fracture toughness data are available for this material in the form of single point values of K_J and CTOD, along with CTOD and J R-curves. Single point K_J data were used in the BS 7910 Level 2 analysis shown in Figure 13.13. Note that for one of the plates (ID 19), yield level residual stress was assumed to account for the fact that a weld associated with the bending capsule loading flange was located only 60mm from the notch.

The analysis of ID 19 gives the result closest to the FAD line, and if a negligible residual stress is assumed the result is not conservative. On the FAD, the higher value of L_r cut-off relates to specimens ID 17-19 (Q&T steel), while the lower value is that for ID 20 (as-rolled material).

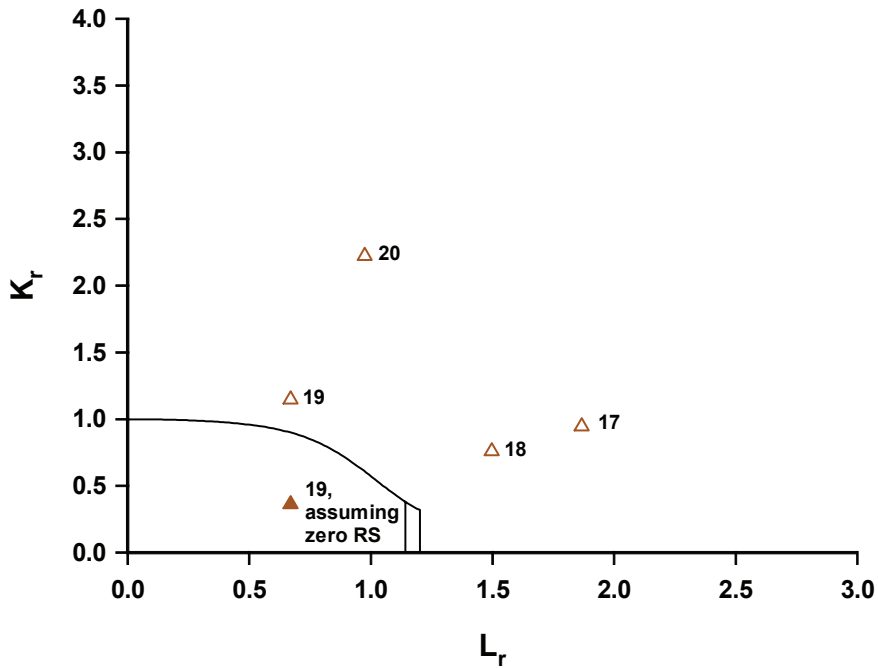


Figure 13.13 – BS 7910 failure assessment diagram for ID 17-20.

This case illustrates the importance of taking into account welding residual stress, even when the notch is placed in parent material, as was the case with specimen ID 19. For flaws close to a weld, welding residual stresses (Q_m) should be included in the analysis. If $Q_m=0$ is assumed for ID 19, the analysis point falls within the failure assessment line as shown (solid triangle).

Tests in the Upper Transition Region

The as-rolled A533B material considered in ID 20 above featured a high ductile-brittle transition temperature relative to the Q&T condition; the difference between the steels is qualitatively (although not microstructurally) similar to that between steel used in newly-built nuclear reactors and the same steel after long-term irradiation embrittlement. The as-rolled material was therefore used in a programme investigating the transferability of data from ‘surveillance’ specimens (12.5mm thick side-grooved CT specimens) to the fracture of large-scale specimens, and the temperature associated with onset of upper shelf temperature (OUST). Both are important issues for the nuclear power industry, especially in relation to ageing plant. Two wide plate tests (ID 42-43) were carried out at 40 and 50°C as part of this programme (40-50°C was associated with upper transitional behaviour in full-thickness SENB specimens); details are shown in Table 13.5. Both plates failed by ductile tearing followed by brittle fracture.

Table 13.5 – Specimen identification and specifications.

ID, this work	ID, original work	Crack type	Nominal thickness, [mm]	Material condition	Test temperature, [°C]
42	M03-01	SCT	85	as-rolled	50
43	M03-02	SCT	85	as-rolled	40

Fracture toughness data was available in the form of R-curves (determined at 70°C) and single-point fracture toughness data (determined over a range of temperatures in the upper transition region) from both side-grooved surveillance specimens and full-thickness SENB specimens. The value of J at initiation of stable ductile tearing ($J_{0.2B/L}$) and the form of the R-curve were not very sensitive to temperature in the range 40-70°C and the main effect of specimen geometry was to change OUST slightly.

The analysis shown in Figure 13.14 is therefore based on:

- $J_{0.2B/L}$ (square symbols, both tests).
- R-curves from surveillance specimens ($0.2 < \Delta a < 1.25\text{mm}$, ID 42 only).
- R-curves from full-thickness SENB specimens ($0.2 < \Delta a < 4\text{mm}$, ID 42 only).

The two Option 1 tearing analyses (one based on surveillance specimens, one on full-thickness SENB specimens) are superposed in the low Δa range and therefore indistinguishable in Figure 13.14.

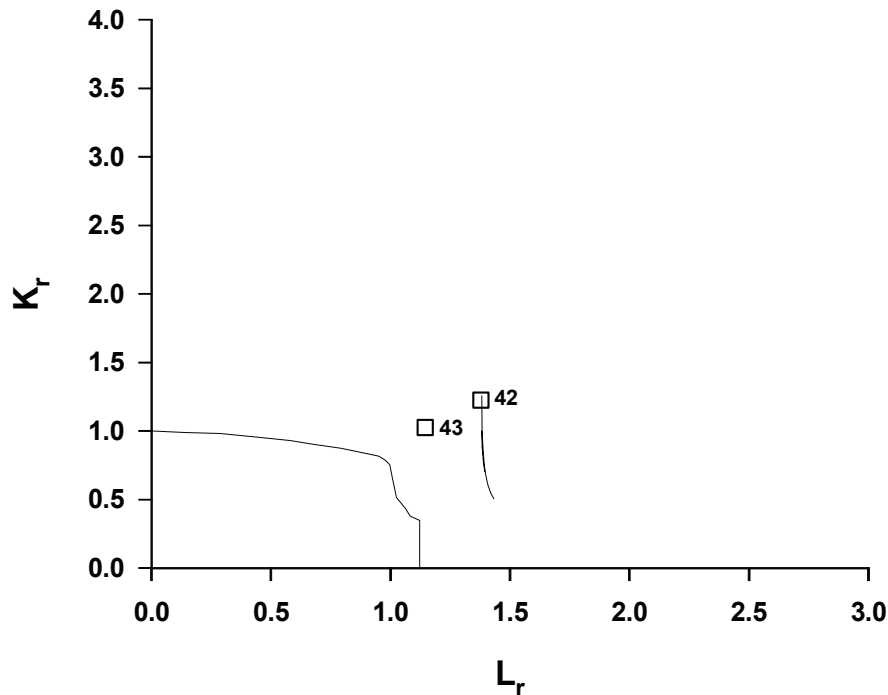


Figure 13.14 – Results of wide plate test on as-rolled A533B steel in the upper transition region (ID 42-43).

The analysis shows that both surveillance and full-thickness specimens can be safely used to predict fracture, in spite of the differences in OUST.

90-110mm Thick A533B Class 1 Wide Plate Tests

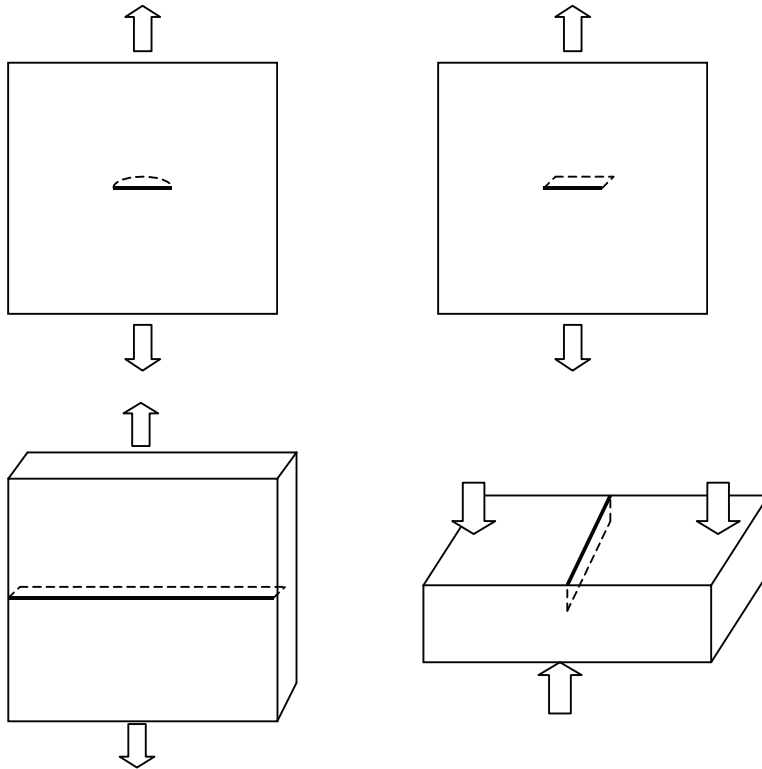


Figure 13.15 – Wide plate test specimens for 90-110 mm thick plate tests.

Further case studies on A533B pressure vessel steel are reported in this section. A series of nine wide plate tests was carried out on 500mm wide, 110mm thick A533B Class 1 steel with three specimens of three different notch geometries of CCT, SCT and extended surface crack tension tests (ESCT) (ID 21-29, Table 13.6).

Four further tests (ID 30-33) were carried out on 90mm thick plate of the same material to investigate ‘time-dependent crack growth’ due to ductile tearing from holding at increasing applied loads for periods of 100 hours; these had crack geometries of CCT and SCT.

A third programme tested six similar 90mm thick specimens to study the upper shelf behaviour of this steel. These specimens (ID 34-39) contained single edge notches and were tested under three point bending (SENB configuration). All 19 wide plate tests were tested at 70°C.

Table 13.6 – Specimen identification and specifications.

ID, this work	ID, original work	Crack type	Nominal thickness, [mm]
21	1008	CCT	110
22	1042	CCT	110
23	1043	CCT	110
24	1009	ESCT	110
25	1045	ESCT	110
26	1044	ESCT	110
27	1006	SCT	110
28	1007	SCT	110
29	1046	SCT	110
30	WP1	CCT	90
31	WP3	CCT	90
32	WP2	SCT	90
33	WP4	SCT	90
34	WP1	SENB	90
35	WP2	SENB	90
36	WP3	SENB	90
37	WP4	SENB	90
38	WP5	SENB	90
39	WP6	SENB	90

Analysis of these tests, as shown on the FAD below, was based on maximum load values of CTOD (δ_m), with the constraint factor set at $X=1.5$ to ensure compatibility with the FITNET procedure for treatment toughness data given in terms of CTOD only. All analysis points lie in the collapse-dominated part of the FAD; most are clustered close to each other, so have not been individually identified in Figure 13.16.

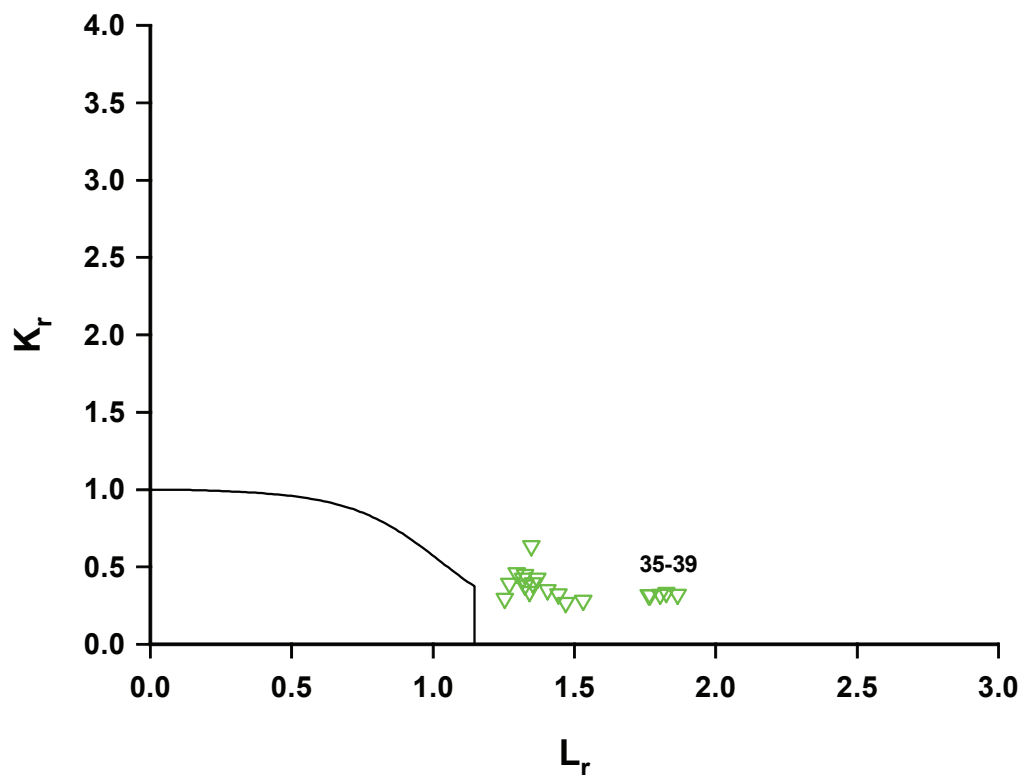


Figure 13.16 – BS 7910 failure assessment diagram for ID 21-39.

Bibliography

- [13.2] I Hadley and P Moore, Fracture case studies for validation of fitness-for-service procedures, TWI members' report 850/2006

13.2.3 Wide Plate Tests on Aluminium Alloys

Specimen : Wide plates
 Loading : Monotonic uniaxial tension
 Material : Various Al alloys including welds
 Defect : Semi-elliptical and through wall cracks
 Temperature : Ambient

Further details are contained in I Hadley and P Moore, Fracture case studies for validation of fitness-for-service procedures, TWI members' report 850/2006.

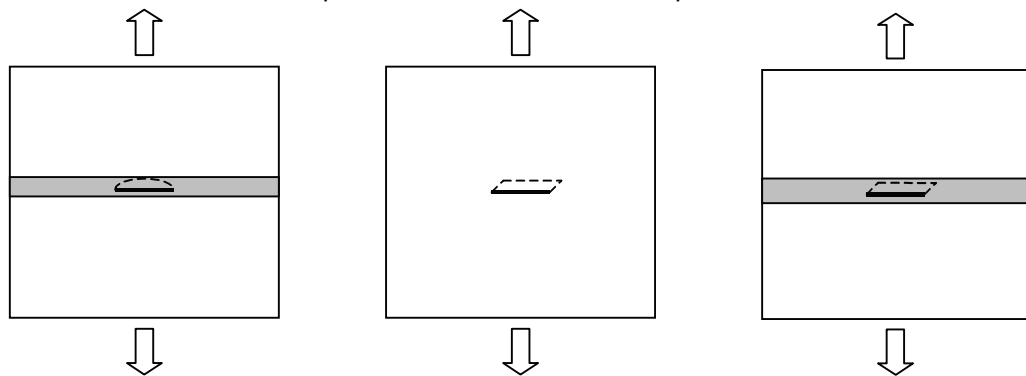


Figure 13.17 – Wide plate test specimens on aluminium alloys.

Wide plate tests on various aluminium alloys of different thicknesses conducted at TWI are designated ID 401-408, Table 13.7. Of the eight tests, one (ID 401) was notched in the parent metal and seven in the weld metal. The weld metal tests featured various degrees of strength mismatch, given by the ratio $M = \sigma_{yw}/\sigma_{yp}$, where σ_{yw} is the weld metal yield strength and σ_{yp} the parent metal yield strength ($0.39 < M < 1.17$ for this set of cases).

Table 13.7 – Specimen identification and specifications.

ID, this work	ID, original work	Parent material	Welding consumable	$M = \sigma_{yw}/\sigma_{yp}$	Nominal thickness, mm	Flaw geometry
401	M02	6061-T651	-	-	10	CCT
402	W12	5456-H116	5556	0.60	10	CCT
403	W14	6061-T651	5356	0.41	10	CCT
404	W16	6061-T651	4043	0.42	10	CCT
405	W17	5083-0	5183	1.17	50	CCT
406	W18	5083-0	5183	1.17	50	ESCT
407	W19	2219-T87	2319	0.39	50	CCT
408	W20	2219-T87	2319	0.39	50	ESCT

The plates have been analysed using the following assumptions:

- P_m represents the global failure stress.
- Residual stresses were taken from measurements, using a sectioning technique.
- The appropriate tensile properties are taken to be those of the parent for overmatched cases, but those of the weld metal for undermatched cases.
- The fracture toughness was measured in terms of maximum load CTOD, δ_m , from SENB specimens (CT specimen data and R-curve data are also available for selected cases).
- The CTOD analysis route was used, with $X=1.0$.

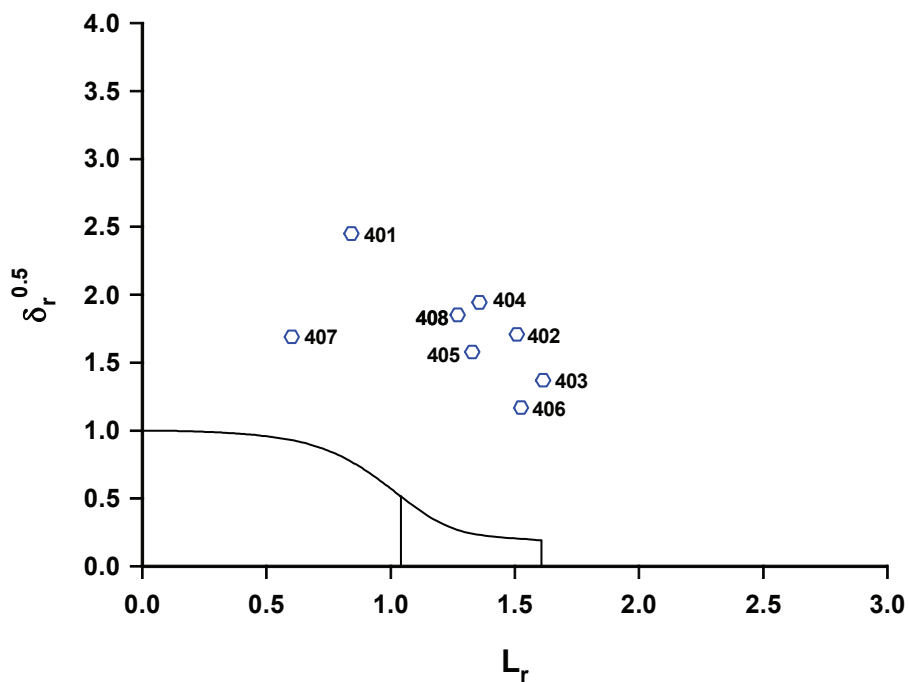


Figure 13.18 – Failure assessment diagram for ID 401-408 (the two values of $L_{r,max}$ represent the maximum and minimum of the range for this series of tests).

Bibliography

[13.3] I Hadley and P Moore, Fracture case studies for validation of fitness-for-service procedures, TWI members’ report 850/2006

13.2.4 Canadian Pipe Bend Trials

Specimen :	Full-scale pipes, range 600 to 1000 mm in diameter
Loading :	Three-point bending
Material :	X60, X65, X70, X75, X100 API grades and welds
Defect :	Circumferential surface and embedded cracks
Temperature :	Ambient

Further details are contained in I Hadley and P Moore, Fracture case studies for validation of fitness-for-service procedures, TWI members' report 850/2006.

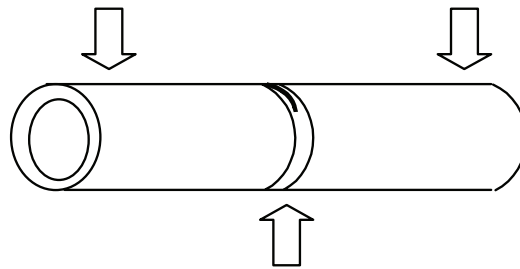


Figure 13.19 – Nominal description of the pipe bend configuration.

The results of 38 full-scale pipe bend tests carried out at various laboratories in support of Canadian standards (Table 13.8) have been analysed in accordance with BS7910 level 2a procedures (similar to FITNET Option 1). The pipes covered a range of dimensions from 600-1000mm in diameter and 7-25mm wall thickness. Most of the pipe specimens contained girth welds with circumferential surface cracks in them. Two specimens (ID 613, 614) contained circumferential embedded flaws in the girth weld. All the specimens were in the as-welded condition.

Table 13.8 – Specimen identification and specifications.

ID, this work	ID, original work	Pipe yield strength, N/mm ² (approx. equivalent API grade)	Flaw geometry
601	4	531 (X75)	Circumferential surface-breaking
602	5	531 (X75)	
603	6	531 (X75)	
604	7	531 (X75)	
605	8	531 (X75)	
606	9	531 (X75)	
607	10	531 (X75)	
608	11	531 (X75)	
609	12	531 (X75)	
610	13	531 (X75)	
611	14	531 (X75)	
612	15	531 (X75)	
613	16	689 (X100)	Embedded
614	17	689 (X100)	Embedded
615	18	531 (X75)	Circumferential surface-breaking
616	19	531 (X75)	
617	21	466 (X65)	
618	22	466 (X65)	
619	23	466 (X65)	
620	24	496 (X70)	
621	25	496 (X70)	
622	26	496 (X70)	
623	27	441 (X60)	
624	28	466 (X65)	
625	29	470 (X65)	
626	30	470 (X65)	
627	31	470 (X65)	

628	32	532 (X75)	
629	33	532 (X75)	
630	34	532 (X75)	
631	35	532 (X75)	
632	46	460 (X65)	
633	47	460 (X65)	
634	48	460 (X65)	
635	49	472 (X65)	
636	50	472 (X65)	
637	51	472 (X65)	
638	52	470 (X65)	

Fracture toughness was measured in terms of CTOD, with characteristic values ranging from 0.03 to 0.60mm. The analyses shown below use $X=1.5$ to allow the FAD to be plotted in terms of K_r . Some of the tensile data that would normally be required to allow a full analysis are not available in the original reference. For example, yield strength and flow strength are cited, but not UTS, and some simplifying assumptions have been made in order to analyse the tests in accordance with the FITNET procedure. Residual stress has been treated in accordance with the recommendations of FITNET, ie the magnitude is assumed to reach the full yield strength of the parent pipe.

All the bend tests failed outside the FAD, however some of the specimens failed by buckling instead of fracture, and some tests were stopped, as indicated in Figure 13.20.

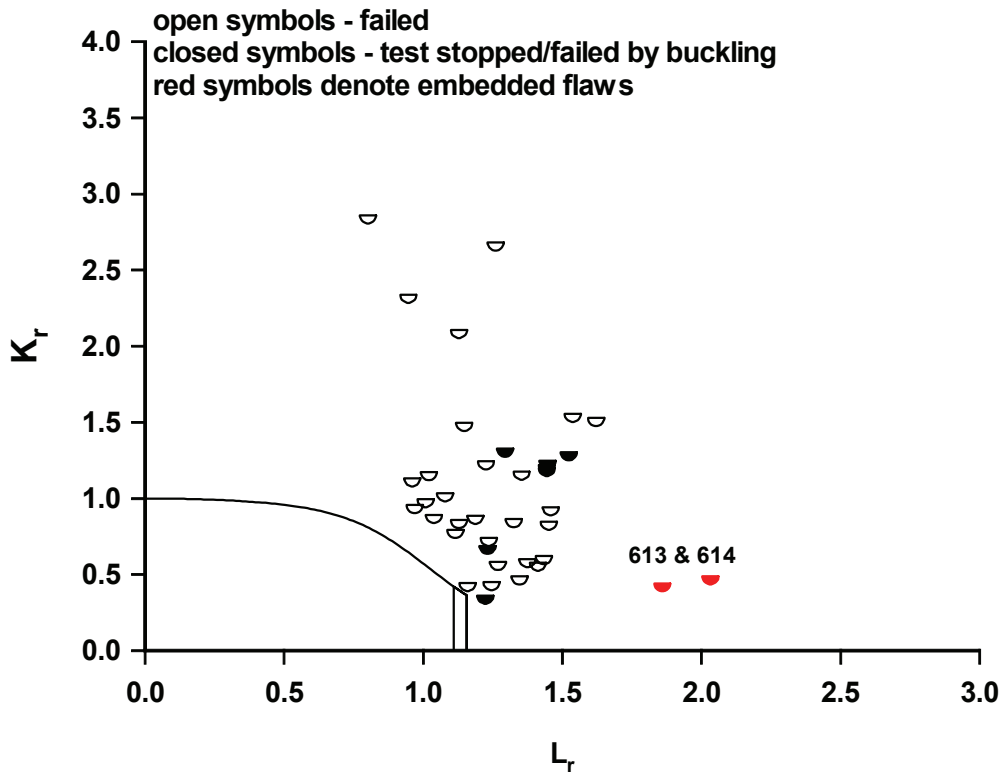


Figure 13.20 – Failure assessment diagram for ID 601-638.

Features of this case:

Very few collapse tests on embedded flaws in a cylindrical geometry have been published, presumably at least in part because of the practical difficulties of creating an artificial embedded flaw. Although only two of the datapoints above refer to embedded flaws, there is evidence from this and other studies that the reference stress solution for embedded flaws recommended by Annex P of BS 7910 (for this geometry, it is a flat plate solution) is highly conservative, incorporating a higher safety factor than that associated with collapse of surface-breaking flaws.

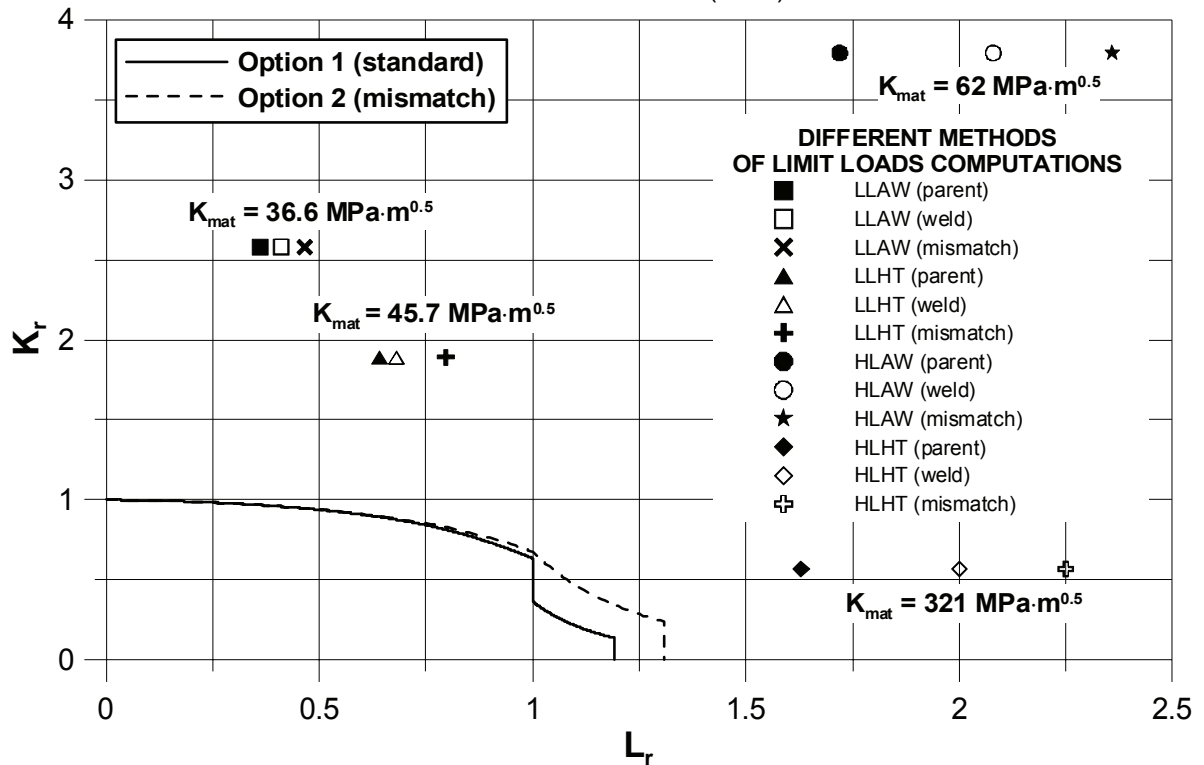
Bibliography

- [13.4] I Hadley and P Moore, Fracture case studies for validation of fitness-for-service procedures, TWI members' report 850/2006.

13.2.5 A533B-1 Steel Residual Stress Experiments

Specimen :	Plate containing a double-vee-preparation weld 2 pairs of experiments, each pair consisting of one as-welded specimen and one Post Weld Heat Treated (PWHT) specimen)
Loading :	Primary: Monotonic four-point loading (through-wall bending) Secondary: Through-wall self-balancing residual stress field produced by welding (tensile region at edges of plate, compressive region in centre of plate)
Material :	A533B-1 Steel
Defect :	Semi-elliptical surface crack in weldment
Temperature :	Specimens LLAW/LLHT -120°C (low L_r regime, as-welded)/ (low L_r regime, PWHT) Specimens HLAH/HLHT -30°C (high L_r regime, as-welded)/(high L_r regime, PWHT)

Further test details are listed below in this section and in:
C C France, J K Sharples and C Wignall, AEA Technology Report AEAT-4236, SINTAP/TASK4/AEAT18 (1998).



Specimen Details: The specimen is shown in Figure 13.21.

In-plane dimensions	600 mm x 600 mm
Thickness	70 to 72 mm
Inner span of rollers	170 mm
Outer span of rollers	560 mm

Primary Loading: Each test consisted of a monotonic, slow increase in the applied bending force which was uniformly distributed by a roller arrangement; Figure 13.21 The fracture loads were as follows:

Specimen LLAW	- 1.27 MN
Specimen LLHT	- 2.19 MN
Specimen HLAW (high L_r regime, as-welded)	- 5.10 MN
Specimen HLHT (high L_r regime, PWHT)	- 4.83 MN

Secondary Loading: Through-wall self-balancing residual stress field produced by welding; tensile region at edges of plate, compressive region in centre of plate; Figure 13.21. The through-thickness distribution of residual stresses was evaluated by a block removal and splitting technique incorporating strain gauge measurements. The measured through-thickness residual stress distributions for the direction transverse to the weld are shown in Figure 13.22 for the specimens LLAW and LLHT. The distribution is self-balancing with tension on the outside and compression in the mid-thickness region. The residual stress for the PWHT plate is reduced from the as-welded plate by at least an order of magnitude. The measured through-thickness residual stress distributions for specimens HLAW and HLHT were comparable with those for LLAW and LLHT, respectively. A comparison of the measured distributions for the two as-welded specimens is shown in Figure 13.23. The comparison gives confidence that the two pairs of large scale fracture test specimens were in very similar residual stress states when tested.

Temperature: The fracture tests were carried out in a 6.3 MN rig with the plate temperature stabilised at -120°C for specimens LLAW and LLHT and -30°C for HLAW and HLHT. The temperature of the test plates was monitored by six thermocouples.

Materials Tensile Data: Young's modulus was taken as 210 GPa and Poisson's ratio as 0.3. Yield and ultimate stress data are tabulated below.

Material	Relevant Test	Temperature [°C]	Individual Yield Stress Values [MPa]	Average Yield Stress [MPa]	Individual Ultimate Stress Values [MPa]	Average Ultimate Stress [MPa]
As welded parent	LLAW	-120	621, 615	618	798, 783	791
	HLAW	-30	-	520	-	677
As welded weld	LLAW	-120	567, 534	551	767, 757	762
	HLAW	-30	450, 412	431	638, 586	612
PWHT parent	LLHT	-120	613, 579	596	776, 768	772
	HLHT	-30	-	520	-	677
PWHT weld	LLHT	-120	546, 576	561	686, 702	694
	HLPW	-30	437, 413	425	575, 546	561

Fracture Toughness Data: Fracture toughness properties for the weld material in both the as-welded and stress relieved conditions were obtained from single edge notch bend (SENB) specimens of 67 mm thickness (B), 67 mm width (W) and an a_0/W ratio of 0.5 where a_0 is initial crack length. All the specimens failed by cleavage fracture. The measured K_{mat} values were:

Material	Temperature [°C]	Individual K_{mat} values [MPa m ^{0.5}]	Average K_{mat} [MPa m ^{0.5}]
As welded weld	-120	32.2, 41.0	36.3
	-30	59.0, 61.4, 65.6	62
PWHT weld	-120	50.4, 41.2†	45.2
	-30		321.2

† Invalid result, as a pop-in was observed in this test

Defects: Semi-elliptical surface cracks were initially machined and then fatigue pre-cracked under four-point bending at room temperature with a stress intensity factor range of approximately 20 MPa·m^{0.5} and a stress ratio just above zero. The machined crack was extended by between 2 mm and 4 mm by the fatigue loading leading to the following dimensions:

Specimen	Crack length (2c ₀) [mm]	Depth at centre of crack [mm]	Maximum crack depth [mm]
LLAW	174.8	18	19.4*
LLHT	174.2	18.4	18.6**
HLAW	175	18	18
HLHT	175	18	18

* Maximum depth occurred at distance of 23 mm from centre of crack

** Maximum depth occurred at distance of 14 mm from centre of crack

Crack extension was monitored by the ACPD (Alternating Current Potential Drop) technique using fitted probes.

As-Welded Specimen LLAW: During this experiment, a fracture event occurred at an applied load of 1.27 MN corresponding to an applied bending stress of 245 MPa. However, the applied load did not return to zero immediately following the event, but showed a constant value of 0.32 MN corresponding to an applied bending stress of 62 MPa. ACPD and visual examination of the specimen indicated that the crack had extended fully along the surface and had extended in the depth direction by approximately 40 mm and then arrested. This was confirmed by post-test examination of the fracture surface.

Following this fracture event, the specimen was again pre-fatigued at room temperature to extend the crack by approximately 3 mm (according to the ACPD measurements) and a further test was performed at a temperature of -120°C. This resulted in a complete fracture at an applied load of 0.57 MN corresponding to an applied bending stress of 110 MPa.

PWHT Specimen LLHT: This experiment resulted in a complete fracture at a load of 2.19 MN corresponding to an applied bending stress of 424 MPa. The load carrying capacity of the PWHT specimen was therefore approximately 1.7 times that of the corresponding as-welded specimen.

As-Welded Specimen HLAW: This experiment resulted in fracture at a load of 5.1 MN corresponding to an applied (elastic) stress of 1015 MPa. There was significant yielding of the specimen prior to the brittle fracture event. The load returned completely to zero immediately following the fracture event. Visual examination revealed that the crack had extended fully along the surface and almost completely through the thickness of the specimen. One complete unloading was performed from an applied load of 4.76 MN to attempt to mark the fracture surface. There was some evidence of a beach mark on the fracture surface produced by the complete unloading but no clear, continuous mark could be measured.

There was clear evidence on the fracture surface of ductile crack extension prior to the final brittle failure, confirming observations made from the ACPD crack monitoring instrumentation during the test. The maximum tearing of approximately 5 mm occurred at the centre of the defect. A small amount of sub-surface "tunnelling" crack extension was also noticeable near the surface intersection points. The tearing behaviour before cleavage fracture was not observed in the small scale materials tests, which indicates a difference in the ductile/brittle transition temperature between the structural and materials type tests on as-welded specimens of this A533B-1 material.

PWHT Specimen HLHT: This experiment resulted in fracture at an applied load of 4.83 MN corresponding to an applied (elastic) stress of 960 MPa. Again, significant yielding of the specimen occurred and the applied load returned completely to zero immediately following the fracture event. Almost complete separation of the specimen halves resulted.

Three complete unloadings were performed from applied loads of 3.295 MN, 4.395 MN and 4.71 MN. There was some evidence of a beach mark on the fracture surface produced by the complete unloadings but no clear series of marks could be measured.

Despite the much lower levels of residual stress and greater toughness measured on stress-relieved materials test specimens, the overall specimen behaviour was very similar to that of the corresponding as-welded specimen. In fact, the as-welded specimen failure load (5.1 MN) was approximately 5% higher than that (4.83 MN) for this stress-relieved specimen.

There was again clear evidence on the fracture surface of ductile crack extension prior to the final brittle failure, which confirmed observations made from the ACPD crack monitoring instrumentation during the test. The maximum tearing of approximately 4 mm occurred at the centre of the defect. A small amount of sub-surface "tunnelling" crack extension was also noticeable again near the surface intersection points. As with the corresponding as-welded case, a difference in the ductile/brittle transition temperature between the structural and materials type tests is also indicated for the welded material in the PWHT state.

Summary of Analysis and Results: Analysis details are given in Table 13.9. Results are summarized in

Table 13.10 and Figure 13.24.

Table 13.9 – Analysis Details of A533B-1 Residual Stress Experiments.

Step	Information	Data and Equation
1	Determine loads and stresses	
	Primary stresses, σ^p	$= 6M/(Wt^2)$
	M(moment), MNm	$= 0.0975P$
	P(applied load), N	As given under Primary Loading
	W(plate width), m	$= 0.6$
	t (plate thickness), m	$= 0.071$ for specimen LLAW, LLHT $= 0.070$ for specimens HLAW, HLHT
	Secondary stresses, σ^s	Curve fit for up to a through thickness Distance to plate thickness ratio (x/t) of 0.5: <i>Specimens LLAW, HLAW:</i> $\sigma^s = -108.35+3543.6(x/t)-9871.5(x/t)^2+2930.3(x/t)^3$ MPa <i>Specimens LLHT, HLHT:</i> $\sigma^s = -28.032+609.14(x/t)-1590.8(x/t)^2$ MPa
2	Establish yield and tensile strength	
	Average Yield Stress	<i>Specimen LLAW</i> - 618 MPa considering parent props. - 551 MPa considering weld props. <i>Specimen LLHT</i> - 596 MPa considering parent props. - 561 MPa considering weld props. <i>Specimen HLAW</i> -520 MPa considering parent props. - 431 MPa considering weld props. <i>Specimen HLHT</i> -520 MPa considering parent props. - 425 MPa considering weld props.
	Average Ultimate Tensile	<i>Specimen LLAW</i> - 791 MPa considering parent props. - 762 MPa considering weld props. <i>Specimen LLHT</i> -772 MPa considering parent props. - 694 MPa considering weld props. <i>Specimen HLAW</i> - 677 MPa considering parent props. - 612 MPa considering weld props. <i>Specimen HLHT</i> - 677 MPa considering parent props. - 561 MPa considering weld props.

3	FAD Selection	<p>Option 1 (Standard):</p> $f(L_r) = (1 + 0.5L_r^2)^{-1/2} [0.3 + 0.7 \exp(-\mu L_r^6)] \text{ for } L_r \leq 1$ $f(L_r) = f(1)L_r^{(N-1)/2N} \text{ for } 1 \leq L_r \leq L_{r_max}$ <p>Option 2 (Mismatch):</p> $f(L_r) = (1 + 0.5L_r^2)^{-1/2} [0.3 + 0.7 \exp(-\mu^M L_r^6)] \text{ for } L_r \leq 1$ $f(L_r) = f(1)L_r^{(NM-1)/2NM} \text{ for } 1 \leq L_r \leq L_{r_max}$
4	Flaw Characterisation	Semi-elliptical surface crack
5	Analysis	Crack Initiation
6	Fracture Toughness, K_{mat}	<p><i>Specimen</i> LLAW - 37 MPa·m^{0.5}</p> <p><i>Specimen</i> LLHT - 46 MPa·m^{0.5}</p> <p><i>Specimen</i> HLAW - 62 MPa·m^{0.5}</p> <p><i>Specimen</i> HLHT - 321 MPa·m^{0.5}</p>
Step	Information	Data and Equation
7	Flaw size	<p>Maximum crack depth, mm</p> <p><i>Specimen</i> LLAW - 19.4 mm</p> <p><i>Specimen</i> LLHT - 18.6 mm</p> <p><i>Specimen</i> HLAW - 19.0 mm</p> <p><i>Specimen</i> HLHT - 19.0 mm</p> <p>Crack length, $2c_0$, mm</p> <p><i>Specimen</i> LLAW - 175 mm</p> <p><i>Specimen</i> LLHT - 174 mm</p> <p><i>Specimen</i> HLAW - 174 mm</p> <p><i>Specimen</i> HLHT - 174 mm</p>
8	L_r^1	$= 0.667\sigma^p [1 - 20(a_0/2c_0)^{0.75}\zeta^3] / [\sigma_y(1-\zeta)^2]$
	ζ	$= 2a_0c_0 / [t(2c_0 + 2t)]$
9	K_r	$= K_I^p(a_0)/K_{mat} + K_I^s(a_0)/K_{mat} + \rho$
	K_I^p	Sharples and Clayton
	K_I^s	Sharples and Clayton

¹ In the case of uniform material the limit load was computed using the formula listed in the table. In the case of mismatch the limit load was computed numerically with the help of Finite Element code ADINA, 3D model of the specimen.

	ρ	$= \psi - \phi(K_I^S/K_p^S - 1)$
	K_p^S	Evaluated using the simple procedure given in the FITNET procedure using the plastic zone correction.
10	Plot on FAD	
11	Assess Significance	See below

Table 13.10 – Calculated K_r and L_r of A533B-1 Residual Stress Experiments.

Test	K_{mat} [MPa·m ^{0.5}]	Yield stress [MPa]	UTS [MPa]	L_r (FEM results for MIS-MATCH CASE)	L_r	K_r
LLAW	37	618 (parent)	791 (parent)	0.47	0.36	2.58
		551 (weld)	762 (weld)		0.41	2.58
LLHT	46	596 (parent)	772 (parent)	0.80	0.64	1.89
		561 (weld)	694 (weld)		0.68	1.89
HLAW	62	520 (parent)	677 (parent)	2.36	1.72	3.79
		431 (weld)	612 (weld)		2.08	3.79
HLHT	321	520 (parent)	677 (parent)	2.25	1.63	0.57
		425 (weld)	561 (weld)		2.00	0.57

Assessment of Significance of the Results: Results are plotted on the failure assessment diagram in Figure 13.24. The assessment points include an allowance for the residual stress field and refer to the deepest point of the crack since K_I at that point is higher than that at the surface for both the residual stress field and the applied bending stress field. This is consistent with the general experimental failure which was shown to occur from the deepest point of the crack. Each failure point is calculated and plotted twice. One data point uses mean parent material tensile properties and the other uses mean weld material tensile properties. The mean fracture toughness of the weld material was used in each case.

It can be seen from Figure 13.24 that all points lie significantly above the failure assessment curve. For the low L_r experiments, it may be noted that the failure points for the as-welded specimen (LLAW) lie above those for the PWHT specimen (LLHT) even though the failure load for the former was a factor of approximately 1.7 times lower than that of the latter. This mainly arises from the fact that K_I at the deepest point of the crack is calculated to be 46 MPa√m for the specimen in the as-welded state, whereas it is calculated to be only 5 MPa√m for the specimen in the PWHT state. The large difference in failure points between the as-welded specimen (HLAW) and the PWHT specimen (HLHT) for the high L_r tests is a consequence of the large difference in K_{mat} values obtained from the fracture toughness specimens in the two material states. Note that the limit load computed numerically for the 3D specimen model assumes lower values (L_r is greater) than results obtained from the analytical formula.

The assessment is therefore shown to be considerably conservative for the geometry and material properties considered here. The conservatism is greater for the as-welded specimen than for the PWHT specimen cases.

Bibliography

For L_r solutions:

- [13.5] I Sattari-Far, Finite element analysis of limit loads for surface cracks in plates, Int J Pres Ves Piping 57, 237-243 (1994).

For K_I^P and K_I^S , solution of a semi-elliptical surface crack in a plate under distributed loading

- [13.6] J K Sharples, A M Clayton et al., Assessment of fracture mechanics fatigue predictions of T-butt welded connections with complex stress fields, OTI 88 536, HMSO, (1988).

Further details of the tests are contained in:

- [13.7] C C France, J.K. Sharples and C Wignall, Experimental programme to assess the influence of residual stress on fracture behavior – summary report, AEAT Report AEAT-4236, SINTAP/TASK4/AEAT18 (1998).

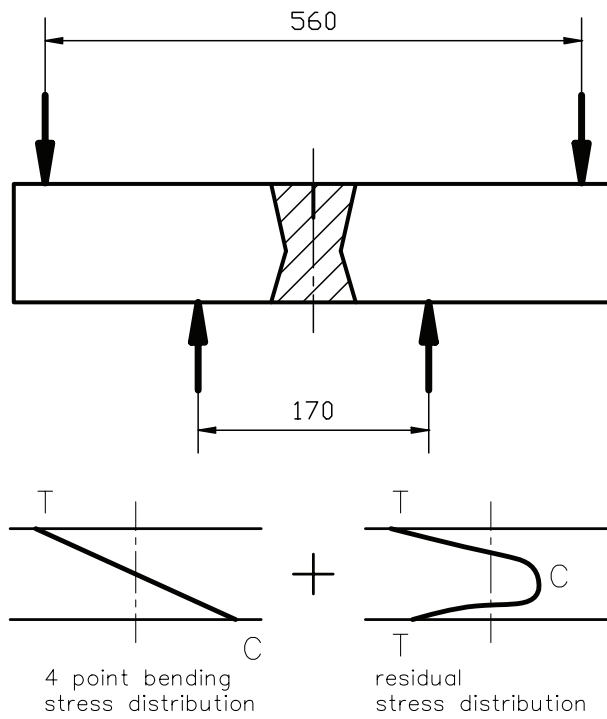
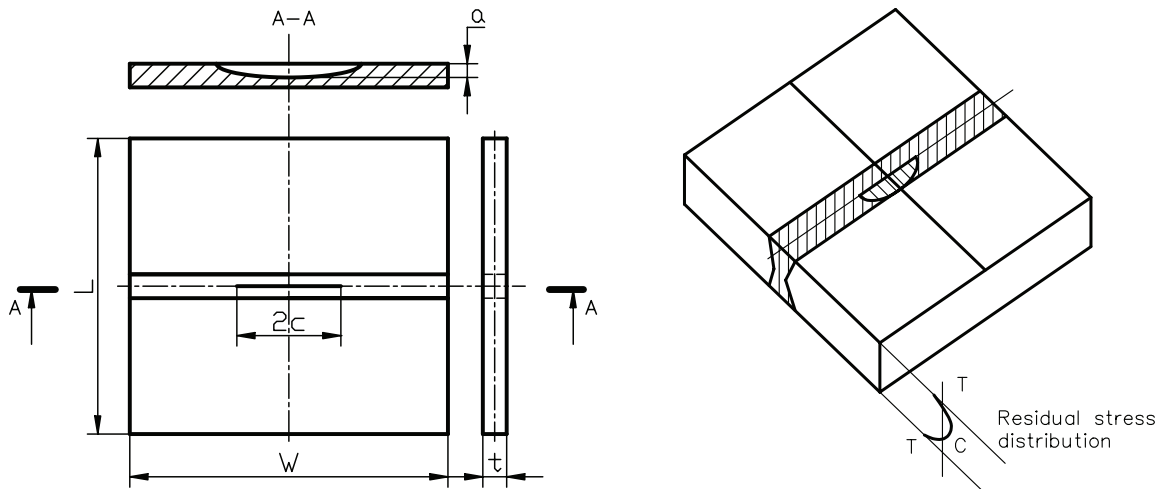


Figure 13.21 – Double-Vee-preparation weld in plate, through thickness residual stress distribution and four point bending configuration.

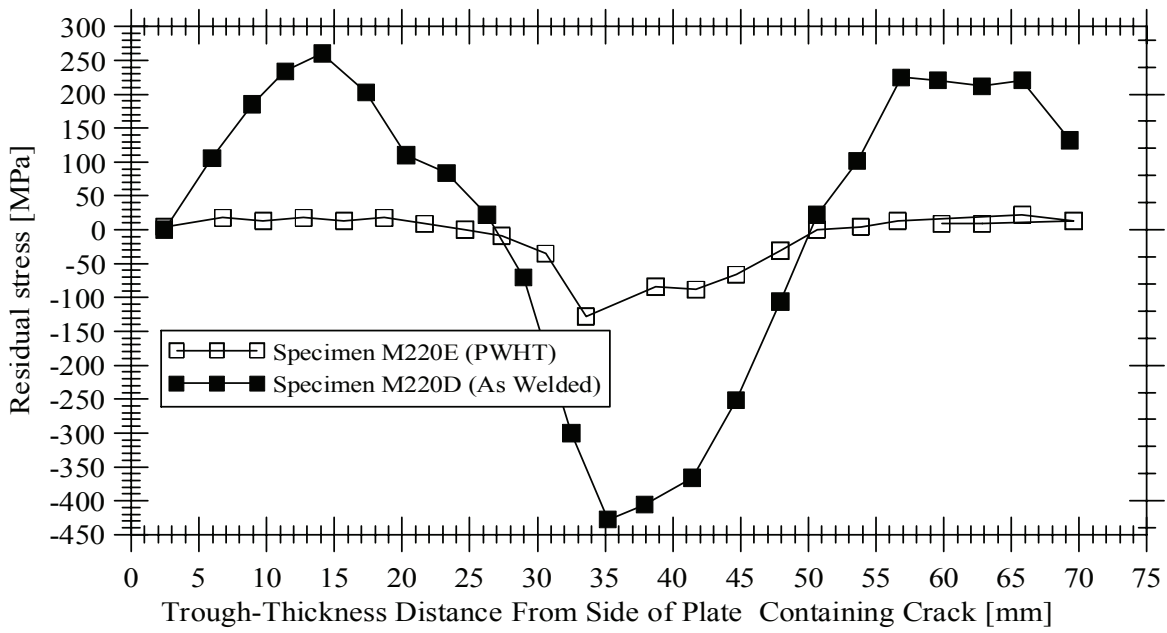


Figure 13.22 – Residual stress measured transverse to the weld for A533B-1 low L_r specimen.

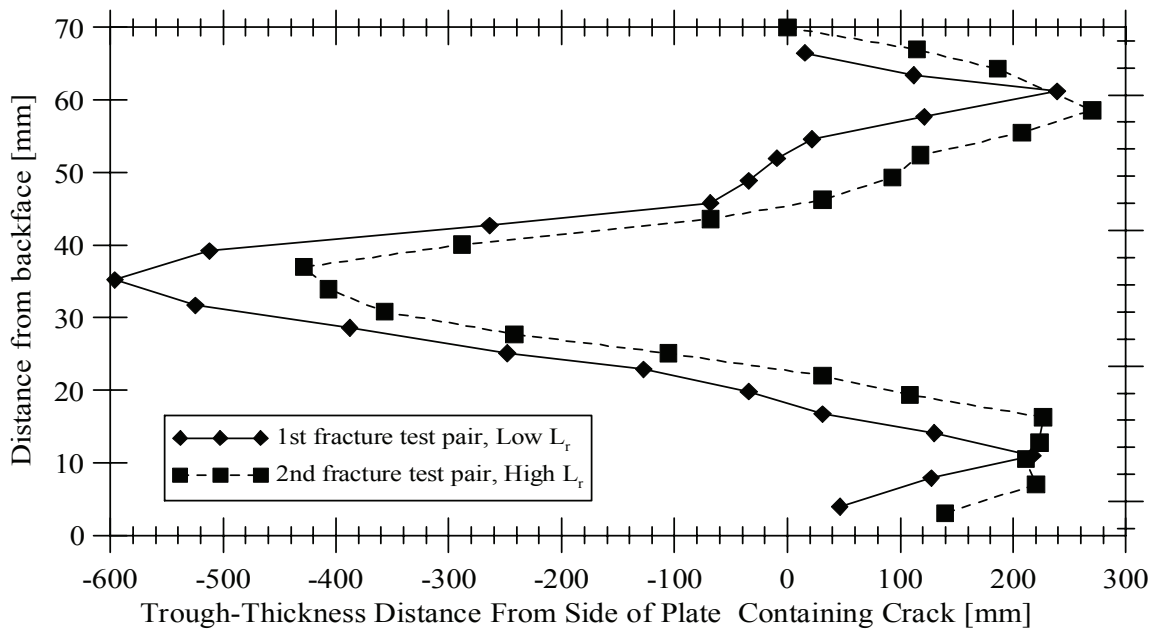


Figure 13.23 – Residual stress measured transverse to the weld for A533B-1 as-welded steel specimens – comparison of distributions for low L_r and high L_r .

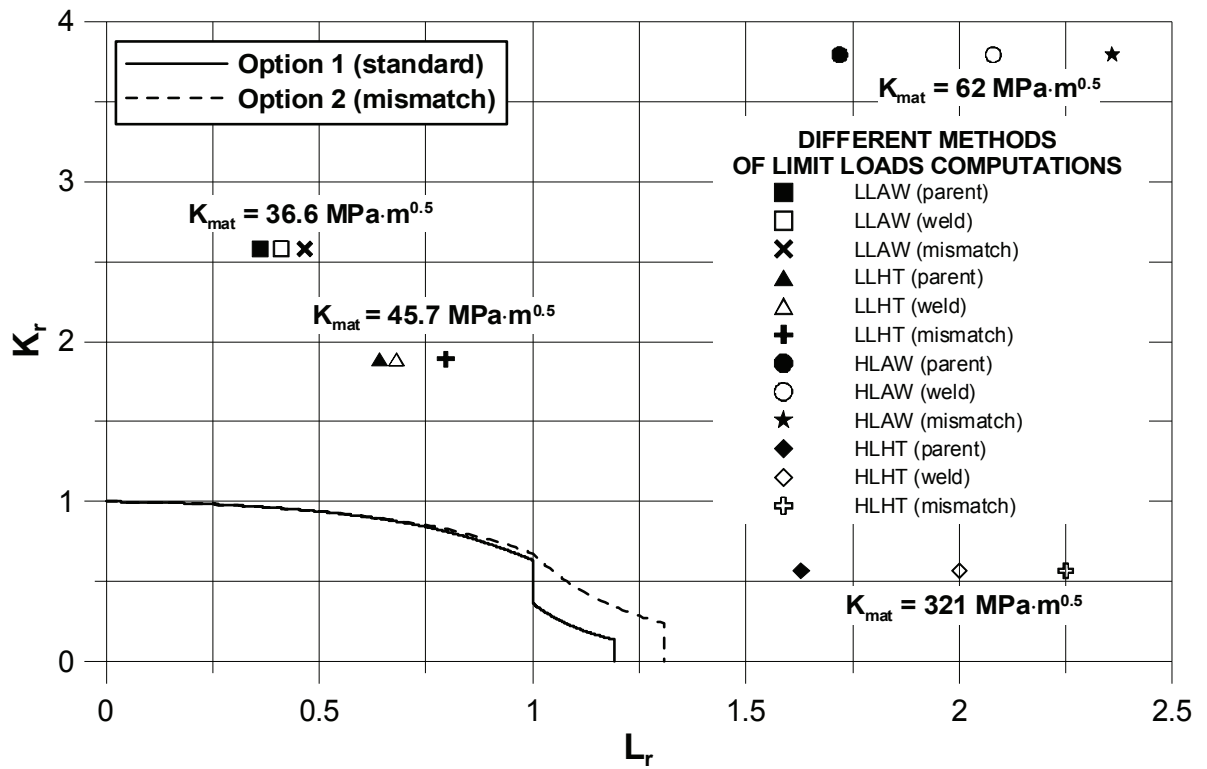
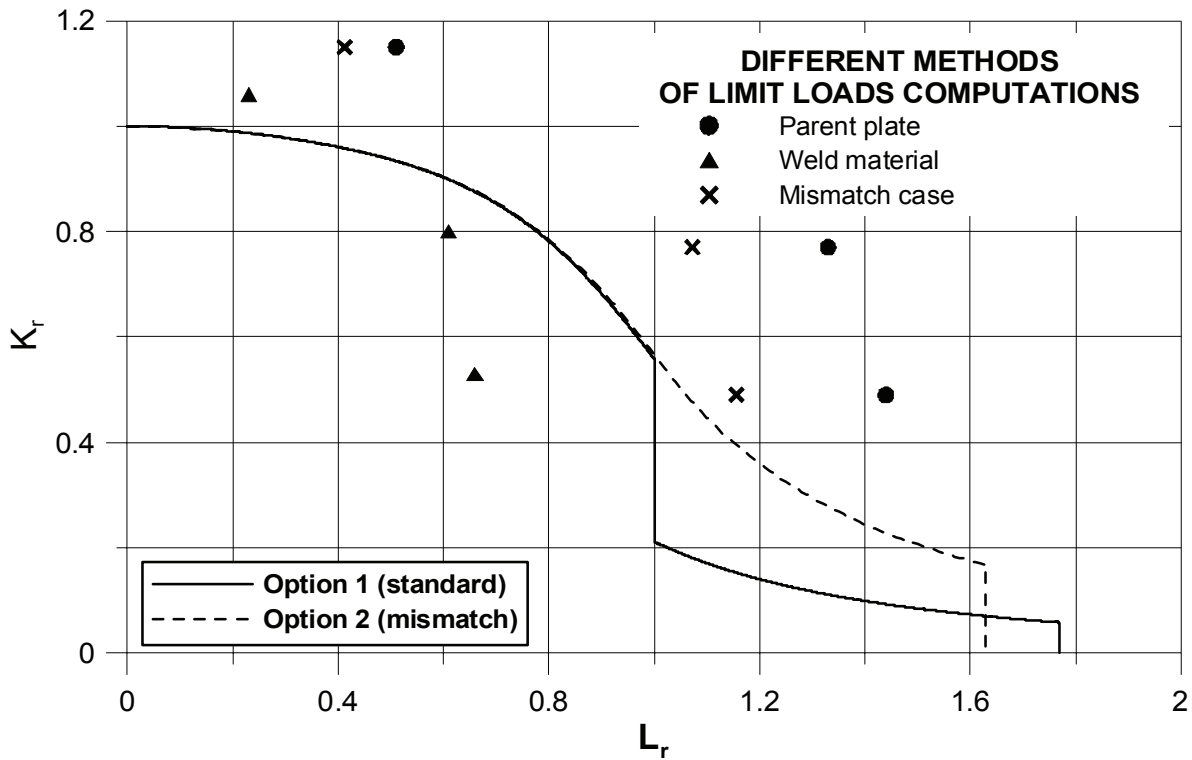


Figure 13.24 – Option 1 (standard) and option 2 (mismatch) failure assessment curves and assessment points for A533B-1 specimens.

13.2.6 Stainless Steel Large Plate Test SSTP10

Specimen : Plate with through-thickness crack in weldment under applied membrane load
 Loading : Primary: Applied membrane load
 Secondary: In-plane self-balancing residual stress field produced by weld repair (tensile region in centre of plate, compressive region at edges of plate)
 Material : Stainless Steel SSTP10
 Defect : through-thickness crack in weldment
 Temperature :

Further test details are listed below in this section and in:
 C C France, J K Sharples and C Wignall, AEA Technology Report AEAT-4236, SINTAP/TASK4/AEAT18 (1998).



Specimen Details: The specimen is shown in Figure 13.25.

Width	820 mm
Thickness	61.2 mm
Height	760 mm

Primary Loading: Monotonic membrane loading with the applied load increased until crack initiation and various amounts of stable tearing occurred. Primary load versus crack growth data are given in Table 13.12. The value of 4 MN is the lowest value of initiation load which occurred at the centre of crack tip 1, as evaluated by ACPD. The crack extension of 2.38 mm is the average of values from the centre and the surface of crack tips 1 and 2 measured from chevron marking. The load of 10.83 MN is the instability load

with the corresponding crack growth being the average of values of the centre and the surface of crack tips 1 and 2, measured from chevron marking.

Secondary Loading: In-plane self-balancing residual stress field produced by weld repair, tensile region in centre of plate, compressive region at edges of plate. The level of residual stress generated approached yield stress value.

Materials Tensile Data: Data for parent plate and weld metal were obtained at room temperature as tabulated below with Young's modulus = 173GPa and Poisson's ratio = 0.3 for both materials.

Material	Individual Yield Strength Values (MPa)	Average Yield Strength (MPa)	Individual Ultimate Strength Values (MPa)	Average Ultimate Strength (MPa)
Parent Plate	242, 229, 230	234	599, 591, 593	594
Weld Metal	489, 466, 579	511	679, 662, 711	684

Fracture Toughness Data: At room temperature for weld metal, J-resistance data according to ASTM E813-81 and corrected for crack growth were obtained on 50 mm thick compact tension specimens using the multi-specimen technique. Results are shown in Figure 13.26 inclusive of the stretch zone which varied from 0.005 mm to 0.083 mm. A power law fit to the data is given in Table 13.11. The validity requirement of the CEGB method for fracture toughness testing of ductile steels, based on J_{max} is shown in the figure. This would exclude three of the eight data points and restrict the data to a maximum crack growth of 2.46 mm.

Defects: A through-wall crack was initially machined as shown in Figure 13.29. The wide portion (6.5 mm) of the defect was machined by milling, whilst the narrower portions (1.5 mm and 0.15 mm) were cut by spark erosion. The crack tips were then grown under fatigue membrane loading to produce a sharp starter crack of length 273 mm.

Other Information and Observations: Specimen manufacture took place in four phases. The first phase was associated with making the large central slot weld in the panel. The preparation was machined out as shown in Figure 13.27 and then welded up by manual metal arc welding with Armex GT electrodes. Once welding had been completed, the amount of shrinkage across the weld was measured so that residual stresses could be evaluated by applying the shrinkage to a finite element model (see below). The second stage involved machining the defect as described above. For the third stage, the test panel was submerged arc welded, via 100 mm thick type 316 transition pieces, to two sets of mild steel loading heads (Figure 13.28). The fourth and final stage of the manufacturing process was the sharpening of the crack tips by fatigue as noted above.

The residual stress field distribution for the SSTP10 test panel was evaluated by a semi-empirical method whereby an elastic-plastic finite element analysis was used to reproduce shrinkages measured in the test panel. The residual stress field is contained in Figure 13.29 with a similar stress field evaluated by Leggatt using the same prescribed displacement data but with a much coarser finite element mesh. It may be noted that the stresses describe the through-thickness membrane contribution of residual stresses. No attempt was made to obtain the variation in the through-thickness direction since the membrane contribution was considered adequate for assessing through-thickness cracks.

The plate was slowly loaded by applying hydrostatic pressure to 10 pairs of actuators located between the loading heads. The pressure was increased until crack initiation was observed (by the ACPD technique) and then more regularly until about 2 mm of crack growth was observed at the surface. The plate was then unloaded to mark the crack front at this point and the process was repeated several times.

The fracture surface, examined after failure, showed a clear distinction between the weld metal and the more ductile surrounding plate. Even so, large scale plastic deformation was evident all the way across the plate near to the line of fracture. The amount of plate thinning across the fracture surface was measured and is

plotted in Figure 13.30. The minimum thickness recorded was 45.5 mm at a position which corresponded to 250 mm of growth from Crack Tip 1. The minimum thickness on the fracture surface of Crack Tip 2 was 59 mm at between 100 and 175 mm out from the initial crack tip. These thicknesses are in comparison to a pre-test value of 61.2 mm.

The unloading chevrons appeared very clearly on the fracture surface, the most interesting being that produced by the first unloading at an applied load of 10.35 MN. It showed a degree of asymmetry which reflected the asymmetrical nature of the weld preparation (Figure 13.31). The crack had propagated well into the weld metal on each side, being deeper on the side with the thicker weld, but it had grown much less at the location near the middle of the plate where the welds from either side had met up. In fact the growth at this point was almost as little as that at the edge of the plate. However, by the second unloading, the crack front had assumed the usual chevron shape (Figure 13.31).

The chevron marking due to the first unloading at a load of 10.35 MN was the only one available up to the maximum instability load of 10.83 MN. The crack growth data are therefore average values of the centre and the surface of Crack Tips 1 and 2, and, the lowest value of initiation load which occurred at the centre of Crack Tip 1 as evaluated by ACPD is taken.

Summary of Analysis and Results: **Analysis details are given in Table 13.11. Results are summarised in Table 13.12 and in Figure 13.32.**

Table 13.11 – Analysis Details of Stainless Steel Large Plate Test SSTP10.

Step	Information	Data and Equation
1	Determine loads and stresses	
	Primary stresses, σ^p Secondary stresses, σ^s	Loads in Table 13.12 divided by (Specimen Width multiplied by Specimen Thickness) Figure 13.29
2	Establish yield and tensile strength	
	Average Yield strength	Parent plate: 234 MPa Weld metal: 511 MPa
	Average Ultimate strength Tensile strength	Parent plate: 594 MPa Weld metal: 684 Mpa
3	FAD Selection	Option 1 (Standard): $f(L_r) = (1 + 0,5L_r^2)^{-1/2} [0,3 + 0,7 \exp(-\mu L_r^6)] \quad \text{dla } L_r \leq 1$ $f(L_r) = f(1)L_r^{(N-1)/2N} \quad \text{for } 1 \leq L_r \leq L_{r_max}$ Option 2 (Mismatch): $f(L_r) = (1 + 0,5L_r^2)^{-1/2} [0,3 + 0,7 \exp(-\mu^M L_r^6)] \quad \text{for } L_r \leq 1$ $f(L_r) = f(1)L_r^{(N^M-1)/2N^M} \quad \text{for } 1 \leq L_r \leq L_{r_max}$
4	Flaw Characterisation	Through-thickness crack
5	Analysis	Ductile tearing
6	Fracture Toughness, K_{mat}	$J(kJ / m^2) = 317.31 \Delta a^{0.6475}$, Δa in mm

Table 13.12 – Calculated K_r and L_r for Large Plate Stainless Steel Test SSTP10.

Applied Load (MN)	Crack Growth (mm)	Parent Plate Tensile Properties		Weld Metal Tensile Properties		FEM results for MIS-MATCH CASE	
		L_r	K_r	L_r	K_r	L_r	K_r
4.0	0.2 (initiation)	0.51	1.15	0.23	1.06	0.41	1.15
10.35	2.38	1.33	0.77	0.61	0.80	1.07	0.77
10.83	10.94	1.44	0.49	0.66	0.53	1.16	0.49

Assessment of Significance of the Results: Ductile tearing analyses were performed for the SSTP10 test specimen using the general Option 1 FAD. Fracture toughness values, K_{mat} , were obtained by converting from J by the conventional plane strain relationship. Table 13.11 and

Table 13.12 contain summaries of the test details, analysis details and the resulting values of L_r , K_r . These are plotted on the R6 Option 1 FAD in Figure 13.32 and are based on mean material properties as given in Table 13.11. It can be seen from Figure 13.32 that, when based on the parent tensile properties, all the data points lie above the failure assessment curve, showing the curve to be conservative. When based on the weld material properties, although the initiation point still lies above the curve, the other two points lie inside the curve. This indicates that it would generally be non-conservative for the weld tensile properties to be used in R6 assessments of this experiment.

Bibliography

- [13.8] D P Rooke and D J Cartwright, Compendium of Stress Intensity Factors, HMSO, London (1976).
- [13.9] J K Sharples, T Davenport, P R Whyatt and L Gardner, Report of Chapelcross stainless steel large plate test SSTP10, AEA Technology Report FRDCC/SIWG/FESG/P(90)24, GNSR/FMWG/P(90)113N (1990).
- [13.10] American Society for Testing and Materials, Standard test for J_{IC} , a measure of fracture toughness, ASTM E813-81 (1981).
- [13.11] B K Neale, D A Curry, G Green, J R Haigh and K N Akhurst, A procedure for the determination of the fracture resistance of ductile steels, CEGB Report CEGB/TPRD/B/0495/R84 (1984).
- [13.12] R H Leggatt, Estimation of through-wall distribution residual stresses in SSTP10 and SSTP12, Welding Institute Report 24950/3/88 (1988).

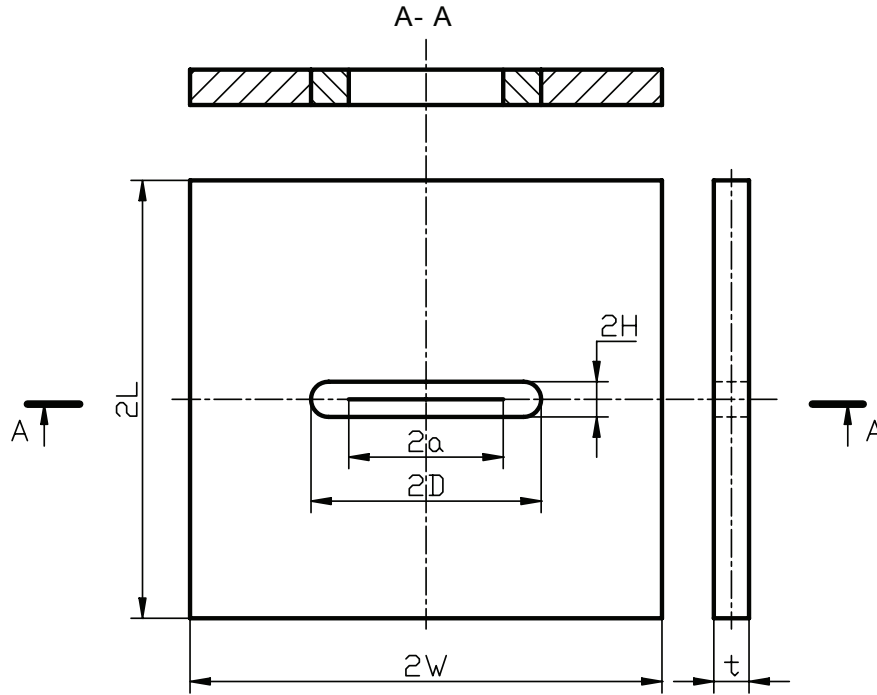


Figure 13.25 – Test Plate geometry

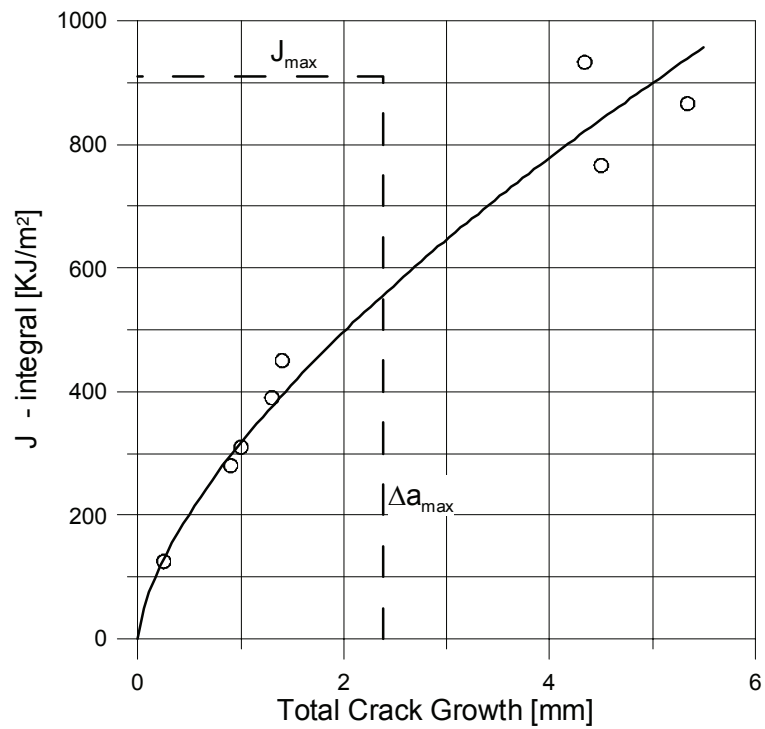
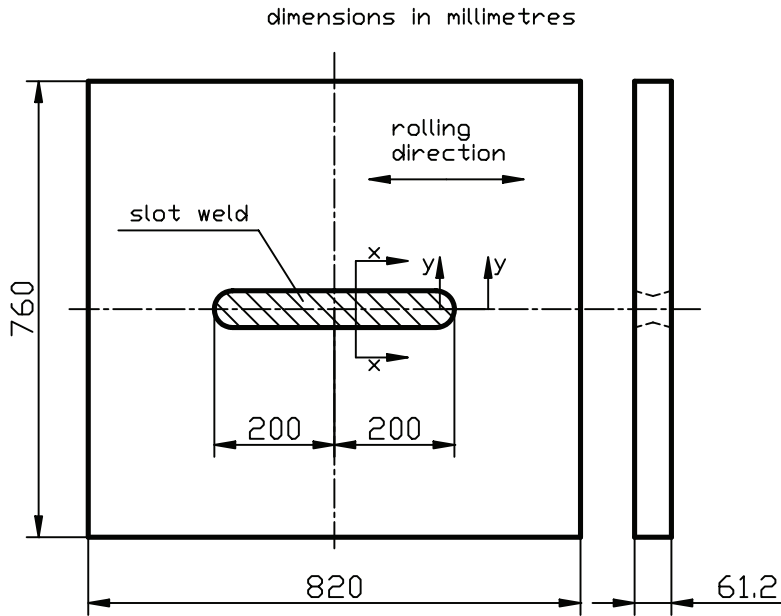
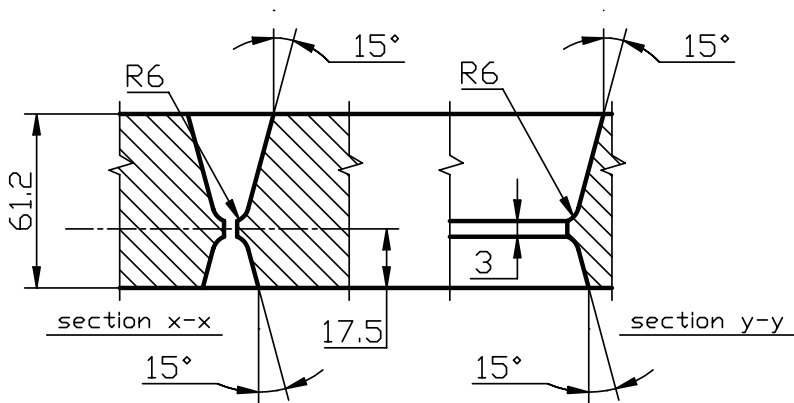


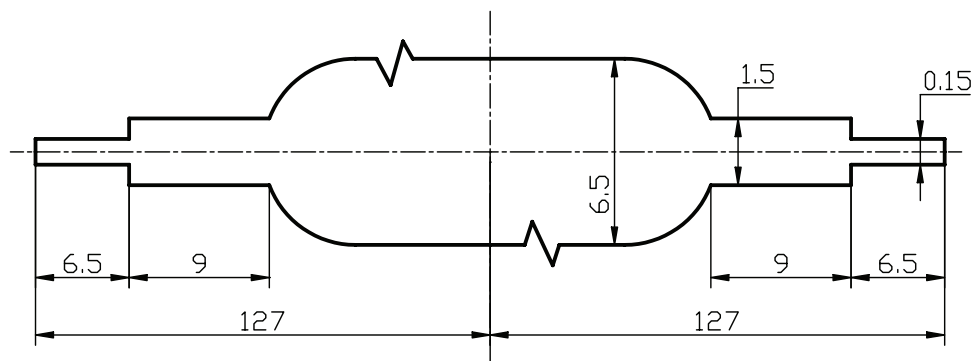
Figure 13.26 – Crack growth resistance curve for weld metal of SSTP10 test plate.



1.1 TEST PLATE GEOMETRY

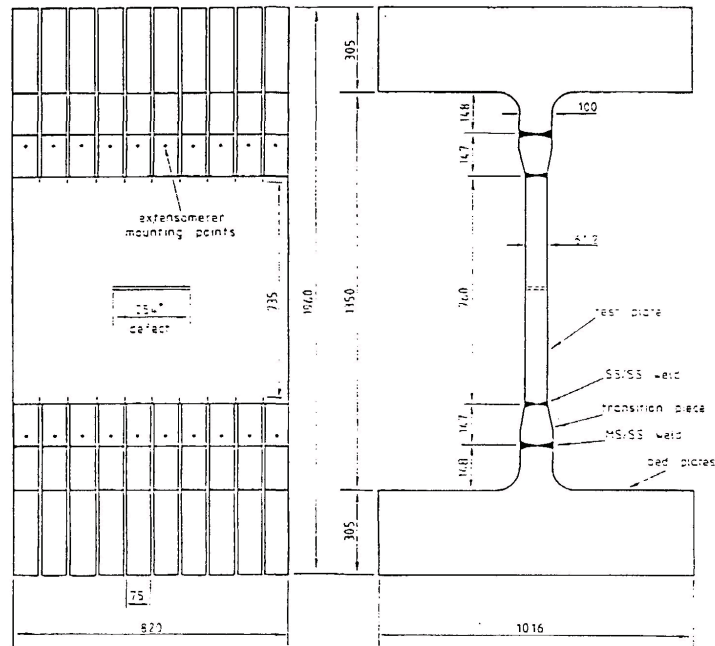


1.2. SLOT WELD PREPARATION



1.3. DEFECT (through – thickness and centrally located within the weld). Note – defect extended to 273 mm by fatigue prior to testing

Figure 13.27 – Test plate geometry, weld preparation and defect detail for SSTP10 test plate.



* 273mm after fatigue

Figure 13.28 – SSTP 10 test configuration and dimensions.

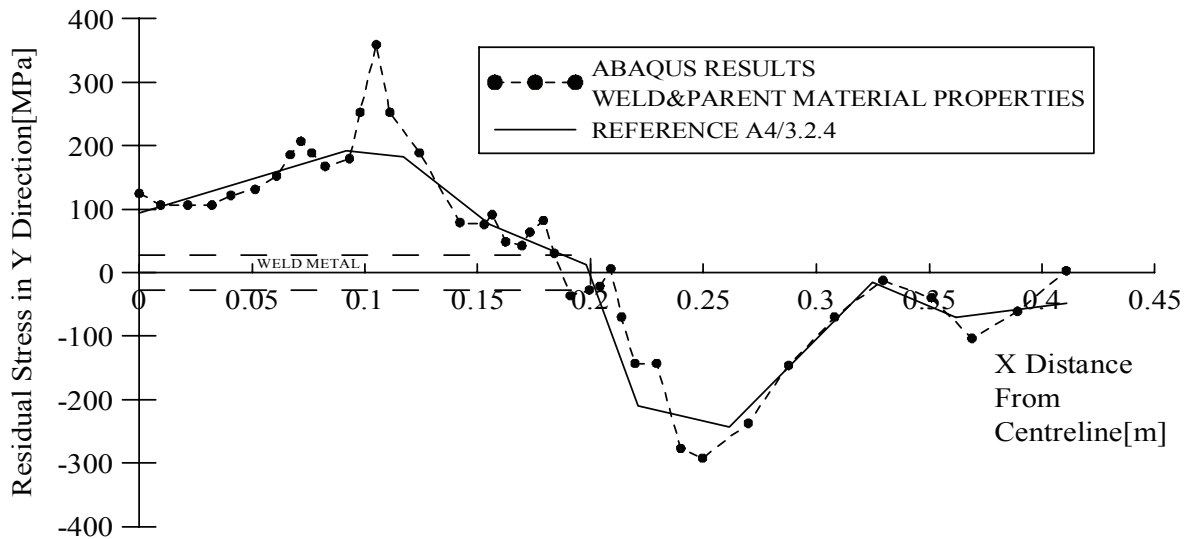


Figure 13.29 – Residual stress distribution for SSTP 10 test plate.

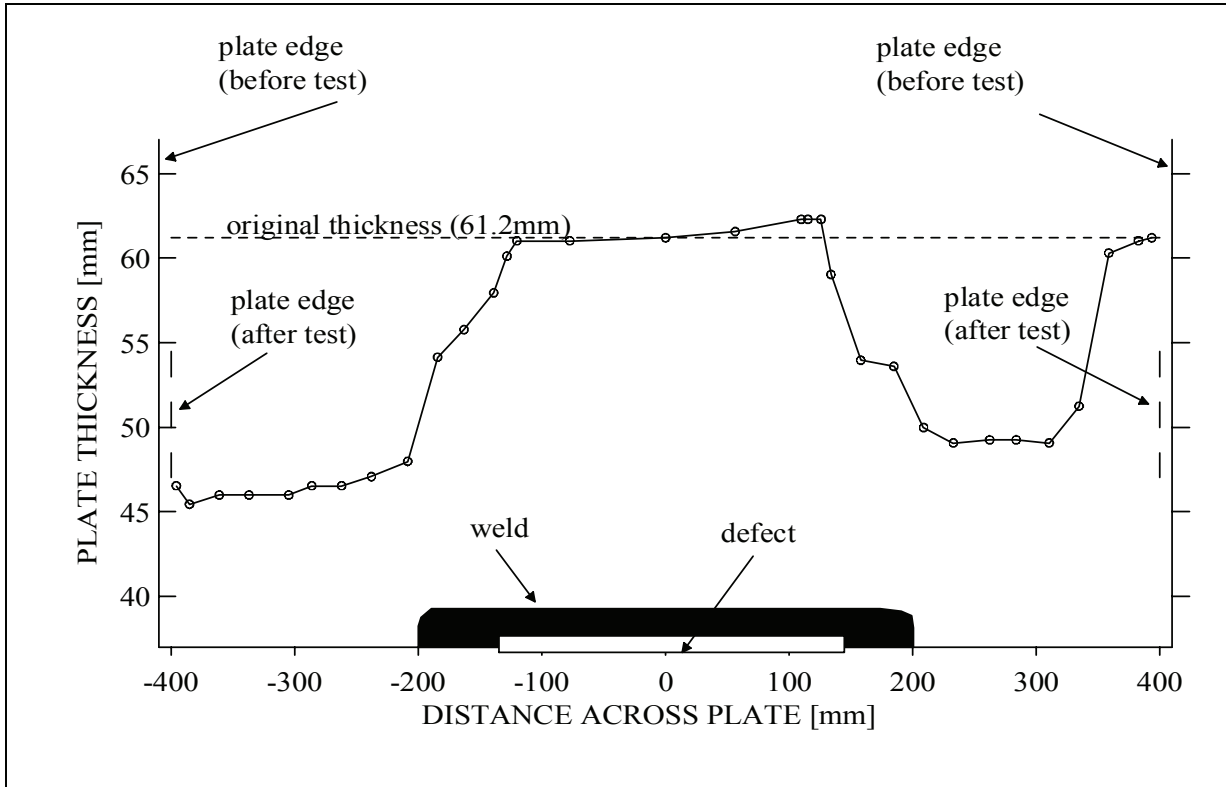


Figure 13.30 – Plate thickness along the fracture line for SSTP 10 test specimen.

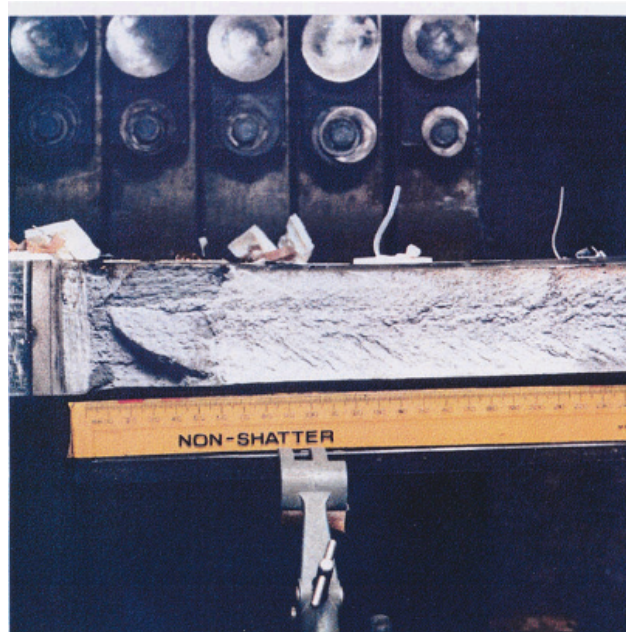


Figure 13.31 – Fracture surface detail - top face - crack tip 2.

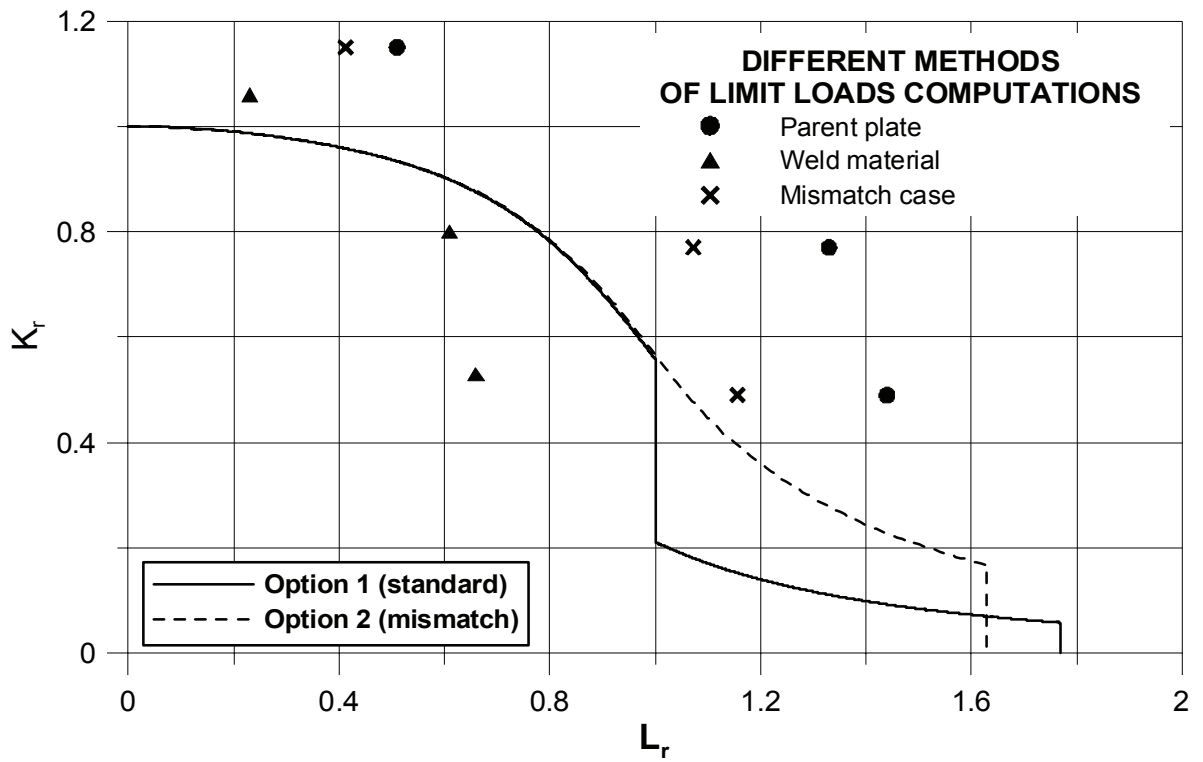
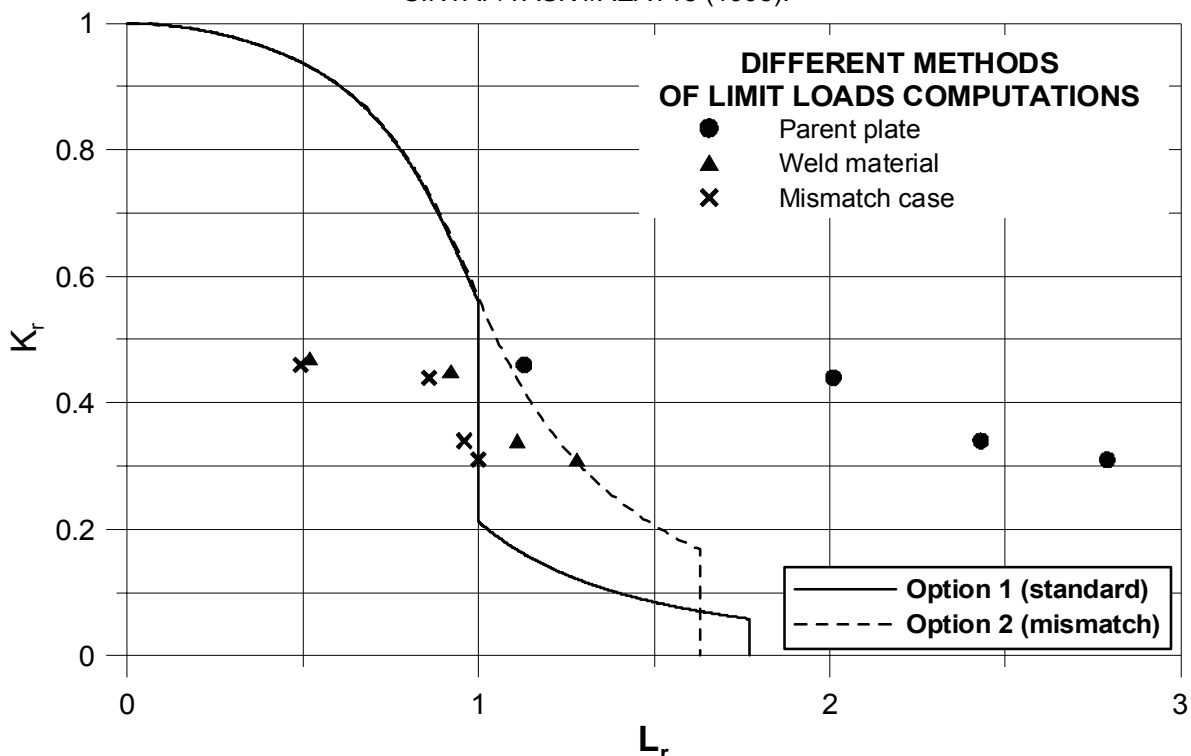


Figure 13.32 – Option 1 (standard) and Option 2 (mismatch) failure assessment curve and assessment points for SSTP 10 specimen.

13.2.7 Stainless Steel Large Plate Test SSTP12

Specimen : Plate with semi-elliptical surface crack in weldment with applied membrane load
 Loading : Primary: Applied membrane load
 Material : Stainless Steel SSTP12
 Defect : Semi-elliptical surface crack in weldment
 Temperature :

Further test details are listed below in this section and in:
 C C France, J K Sharples and C Wignall, AEA Technology Report AEAT-4236,
 SINTAP/TASK4/AEAT18 (1998).



Specimen Details: The specimen is shown in Figure 13.33.

Width	770 mm
Thickness	60 mm
Height	787 mm

Loading: Through-wall distribution with net membrane tensile component, high tensile region at edges of plate and low compressive region at mid-thickness region.

Primary Loading: Monotonic membrane loading with the applied load increased until crack initiation and various amounts of stable tearing occurred, up to and beyond breakthrough. Primary load versus crack growth data are given in Table 13.15 with initiation evaluated from ACPD, growths of 1mm and 4mm measured from chevron marks and the load of 9.81MN corresponding to crack penetration to the back surface.

Materials Tensile Data: All data were collected at room temperature as tabulated below with Young's modulus = 173 GPa and Poisson's ratio = 0.3 for both weld and parent materials.

Material	Individual Yield Stress Values (MPa)	Average Yield Stress (MPa)	Individual Ultimate Stress Values (MPa)	Average Ultimate Stress (MPa)
Parent Plate	242, 229, 230	234	599, 591, 593	594
Weld Metal	489, 466, 579	511	-	684

Fracture Toughness Data: Weld metal J-resistance data at room temperature were obtained according to ASTM E813-81 and corrected for crack growth on 50 mm thick compact tension specimen using the multi-specimen technique. Results are shown in Figure 13.34 inclusive of the stretch zone which varied from 0.005 mm to 0.083 mm. A power law fit to data is given in

Table 13.12. The validity requirement of the CEGB method for fracture toughness testing of ductile steels, based on J_{max} , is shown in Figure 13.34. This would exclude three of the eight data points and restrict the data to a maximum crack growth of 2.46 mm.

Defects: A semi-elliptical surface crack was initially machined (Figure 13.33) consisting of a wide portion (3 mm) and a narrow portion (0.2 mm) extending over a distance of 5 mm in the vicinity of the crack tip. Tensile fatigue cycling was performed prior to the fracture test. After 20,000 cycles, 2 to 3 mm of fatigue crack extension was observed at both notch tips at the surface of the specimen. Cycling was stopped at this point since it was assumed that a similar amount of growth would have occurred at the deepest point of the crack. However, post-test examination of the fracture surface indicated that the fatigue crack had extended by 7 mm at the deepest point. The starter crack size after fatigue loading was of length, $2c_0 = 255$ mm and depth, $a_0 = 52$ mm.

Other Information and Observations: Specimen manufacture took place in four phases. The first phase was production of the large central slot weld in the panel. The preparation was machined out as shown in Figure 13.33 and was then welded up by manual metal arc welding with Armex GT electrodes. After welding, the amount of shrinkage across the weld was measured so that in-plane residual stresses could be evaluated. The second stage involved machining the defect. For the third stage, the test panel was welded to extension pieces, between forged steel cross heads to form an assembly resembling a large "I" beam (Figure 13.35). The rig's four hydraulic actuators (each of 5 MN load capacity) were mounted between the cross-heads to act against the flanges of the "I" beam and produce tensile stresses in the test plate which forms the web. With this arrangement, the forces applied by the actuators were reacted by the specimen. The fourth and final stage of the manufacturing process was the sharpening of the crack tips by fatigue.

The in-plane residual stress field distribution was evaluated semi-empirically using an elastic-plastic finite element analysis to reproduce measured shrinkages. However, the through-thickness distribution of residual stresses is required when assessing a surface crack. The through-thickness residual stress profile at the centre of the slot weld was estimated by Leggatt using a block removal and splitting technique incorporating strain gauge measurements. The residual stress field is shown in Figure 13.36. The stress is estimated to vary from 260 MPa (tensile at the plate surfaces to 48 MPa (compressive) at the centre of the plate, with the distribution being symmetric about that centre.

The plate was slowly loaded in tension by increasing the pressure in the 20 MN rig's 4 actuators until crack initiation was observed (by the ACPD technique). Then several complete unloadings were performed to mark the fracture surface and allow post-test measurements of crack size and shape. Initiation at the deepest point of the crack was estimated from ACPD measurements to have occurred at an applied load of 5 MN. Initiation at the surface points of the crack occurred at an applied load of approximately 10 MN as evaluated by both ACPD measurements and visual observations. Photographs of the fracture surfaces of the SSTPP12 test plate are presented in Figure 13.37 in which the chevron markings, corresponding to each of the unloadings performed during the test, can be seen. Table 13.13 summarizes measurements from the fracture surface and Figure 13.38 contains this information in graphical form.

Table 13.13 – Results of Fracture Surface Measurements on SSTP12 Test Plate.

Surface Marking	Applied Load (MN)	Front Face Crack Length - 2c (mm)	Back Face Crack Length (mm)	Crack Depth - a (mm)
Spark Eroded Crack	-	250	-	45
Fatigue Crack	-	255	-	52
Unload 1	8.68	255	-	53
Unload 2	9.58	255	-	56
Unload 3	9.81	255	25	-
Unload 4	9.86	255	50	-
Unload 5	10.03	255	90	-
Unload 6	10.99	257	158	-
Unload 7	11.73	275	205	-
Unload 8	11.75	< 299	< 227	-

Initiation at deepest point of crack detected at 5 MN, Initiation at surface points of crack detected at 10 MN

Summary of Analysis and Results: Analysis details are given in Table 13.14. Results are summarized in Table 13.15 and in Figure 13.39.

Table 13.14 – Analysis Details of Stainless Steel Large Plate Test SSTP12

Step	Information	Data and Equation
1	Determine loads and stresses	
	Primary stresses, σ^p	Loads given in Table 13.15 divided by (Specimen Width multiplied by Specimen Thickness)
	Secondary stresses, σ^s	Figure 13.36
2	Establish yield and tensile strength	
	Average Yield strength	Parent plate: 234 MPa, Weld metal: 511 MPa
	Average Ultimate Tensile strength	Parent plate: 594 MPa, Weld metal: 684 MPa

3	FAD Selection	<p>Option 1 (Standard):</p> $f(L_r) = (1 + 0,5L_r^2)^{-1/2} [0,3 + 0,7 \exp(-\mu L_r^6)] \text{ for } L_r \leq 1$ $f(L_r) = f(1)L_r^{(N-1)/2N} \text{ for } 1 \leq L_r \leq L_{r_max}$ <p>Option 2 (Mismatch):</p> $f(L_r) = (1 + 0,5L_r^2)^{-1/2} [0,3 + 0,7 \exp(-\mu^M L_r^6)] \text{ dla } L_r \leq 1$ $f(L_r) = f(1)L_r^{(N^M-1)/2N^M} \text{ dla } 1 \leq L_r \leq L_{r_max}$
4	Flaw Characterisation	Semi-elliptical surface
5	Analysis	Ductile tearing
6	Fracture Toughness, K_{mat}	$J(kJ / m^2) = 317.31 \Delta a^{0.6475} \Delta a \text{ in mm}$

Table 13.15 – Calculated K_r and L_r at Deepest point of Crack for Stainless Steel Test SSTP12

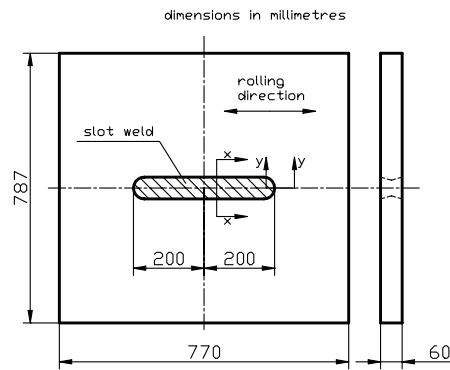
Applied Load (MN)	Crack Growth (mm)	Parent Plate Tensile Properties		Weld Metal Tensile Properties		FEM results for MIS-MATCH CASE	
		L_r	K_r	L_r	K_r	L_r	K_r
5.0	0.2 (initiation)	1.13	0.46	0.52	0.47	0.49	0.46
8.68	1.0	2.01	0.44	0.92	0.45	0.86	0.44
9.58	4.0	2.43	0.34	1.11	0.34	0.96	0.34
9.81	7.5 (penetration)	2.79	0.31	1.28	0.31	1,00	0.31

Assessment of Significance of the Test: Ductile tearing analyses were performed using the Option 1 FAD. Fracture toughness values were obtained from the J-integral equation given in Table 13.14 by the conventional plane strain relationship. Table 13.14 and Table 13.15 contain summaries of the test details, analysis details and the resulting values of L_r , K_r . These are plotted on the Option 1 FAD in Figure 13.39 and are based on mean material properties as given in Table 13.15. It can be seen from Figure 13.39 that, when based on the parent tensile properties, all the data points lie above and to the right of the failure assessment curve showing the curve to be conservative. When based on the weld material properties, all points except the last (i.e. corresponding to breakthrough) lie inside the curve. This indicates that it would be non-conservative for the weld tensile properties to be used in assessments of this experiment for the input parameters considered. Results obtained using the limit load computed numerically for the non-uniform specimen, using 3D model and FE method are non-conservative.

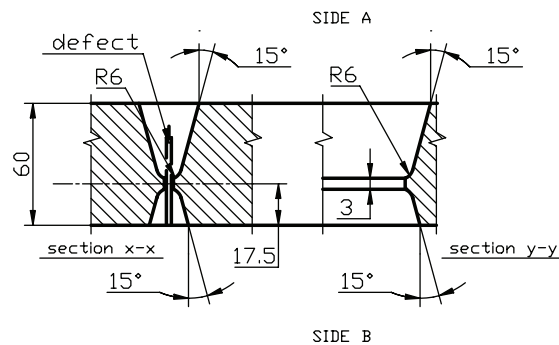
Bibliography

- [13.13] I Sattari-Far, Finite element analysis of limit loads for surface cracks in plates, Int J Pres Ves Piping 57, 237-243 (1994).
- [13.14] J K Sharples, A M Clayton, et. al., Assessment of fracture mechanics fatigue predictions of T-butt welded connections with complex stress fields, OTI 88 536, HMSO (1988).

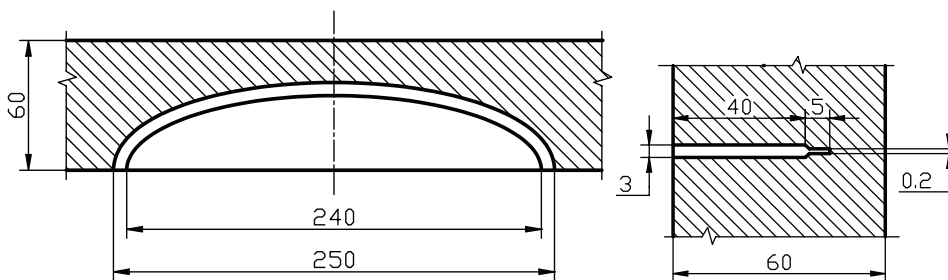
- [13.15] J K Sharples, L Gardner and A M France, Final report on wide plate test SSTP12, AEA Technology Report, FR/SIWG/FESG/P(91)29, GNSR/FMWG/P(91)120N (1991).
- [13.16] American Society for Testing and Materials, Standard test for J_{IC} , a measure of fracture toughness, ASTM E813-81 (1981).
- [13.17] B K Neale, D A Curry, G Green, J R Haigh and K N Akhurst, A procedure for the determination of the fracture resistance of ductile steels, CEBG Report CEBG/TPRD/B/0495/R84 (1984).
- [13.18] R H Leggatt, Estimation of through-wall distribution residual stresses in SSTP10 and SSTP12, Welding Institute Report 24950/3/88 (1988).



1.1. Test Plate Geometry



1.2. Slot Weld Preparation



1.3. Defect Detail (through-thickness and centrally located within the weld). Note – defect extended to 273 mm by fatigue prior to testing

Figure 13.33 – Test plate geometry, weld preparation and defect detail for SSTP12 test plate.

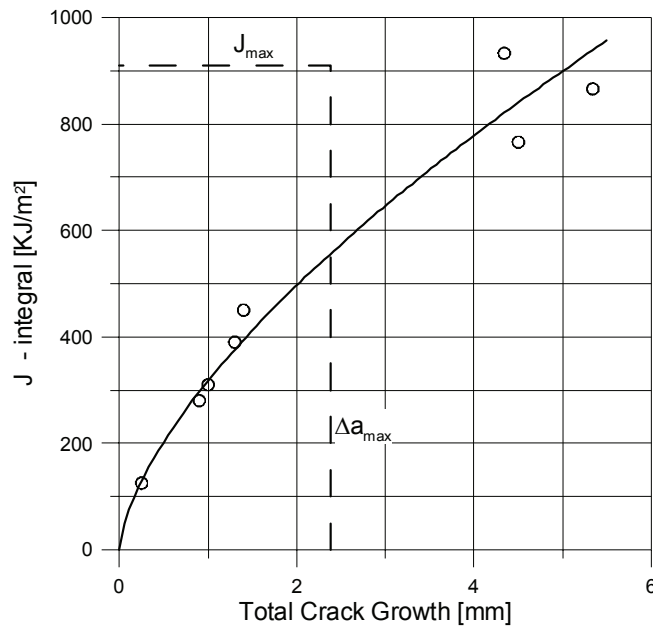


Figure 13.34 – Crack growth resistance curve for weld metal of SSTP12 test plate.

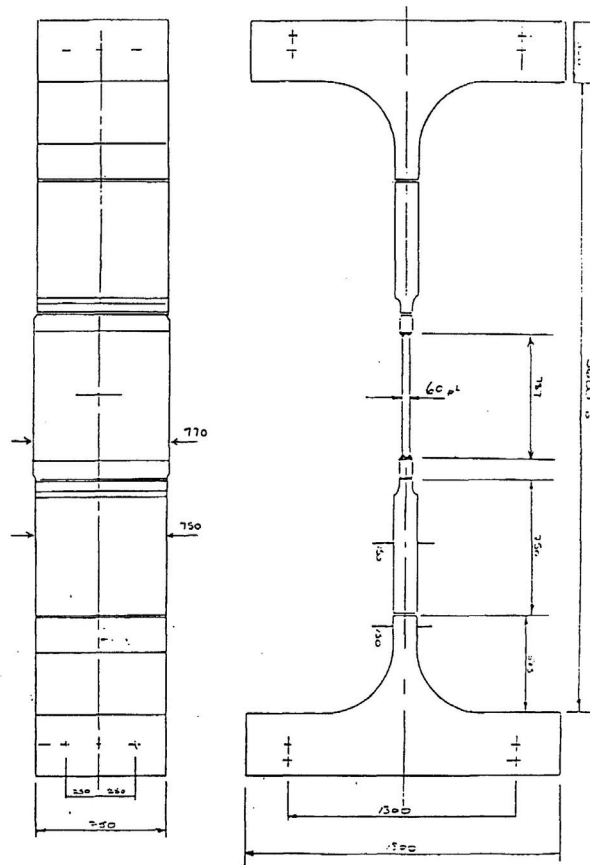


Figure 13.35 – SSTP 12 test configuration and dimensions.

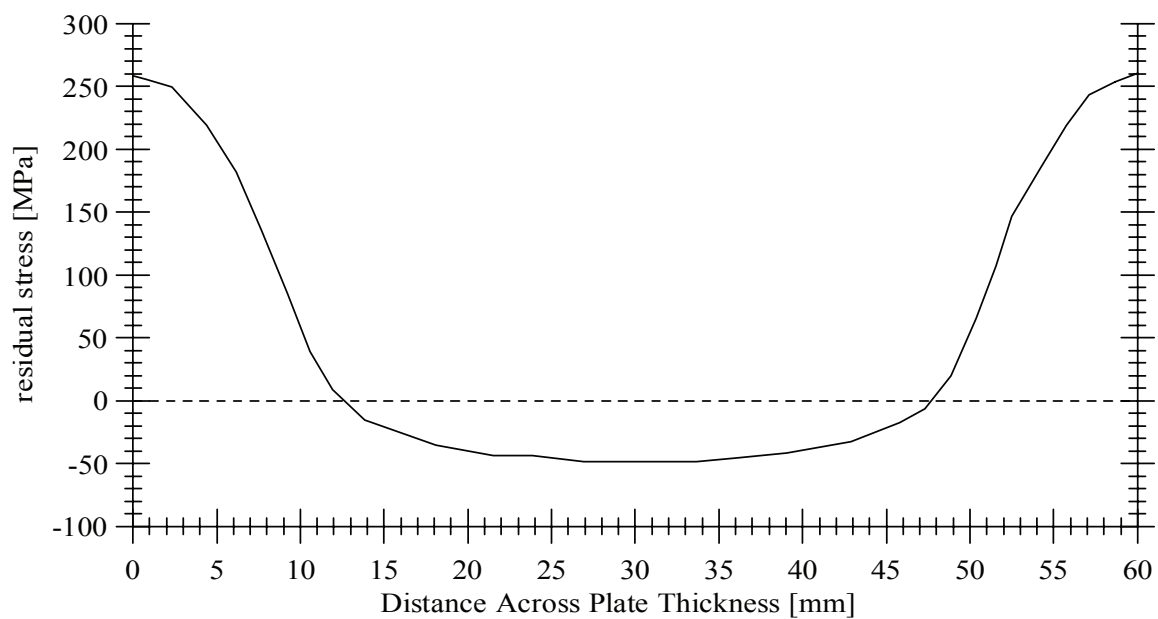


Figure 13.36 – Through-thickness residual stress distribution for SSTP 12 test plate.

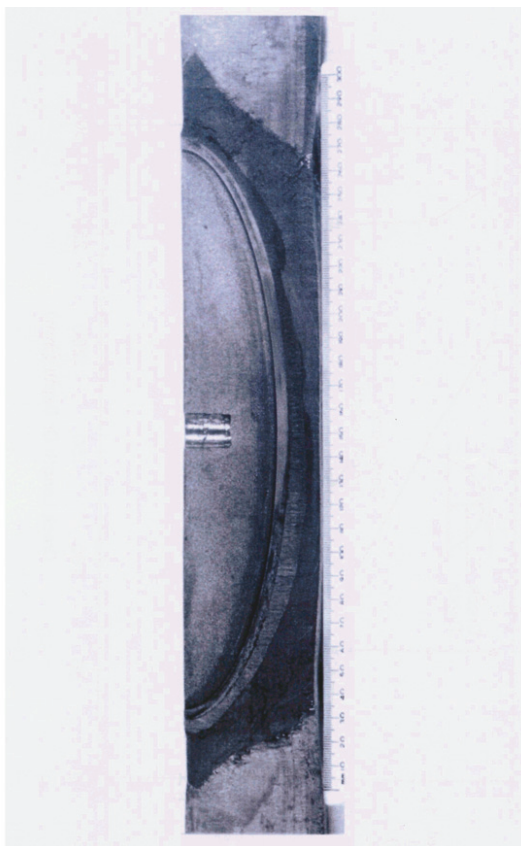


Figure 13.37 – Fracture surface of SSTP 12 test plate.

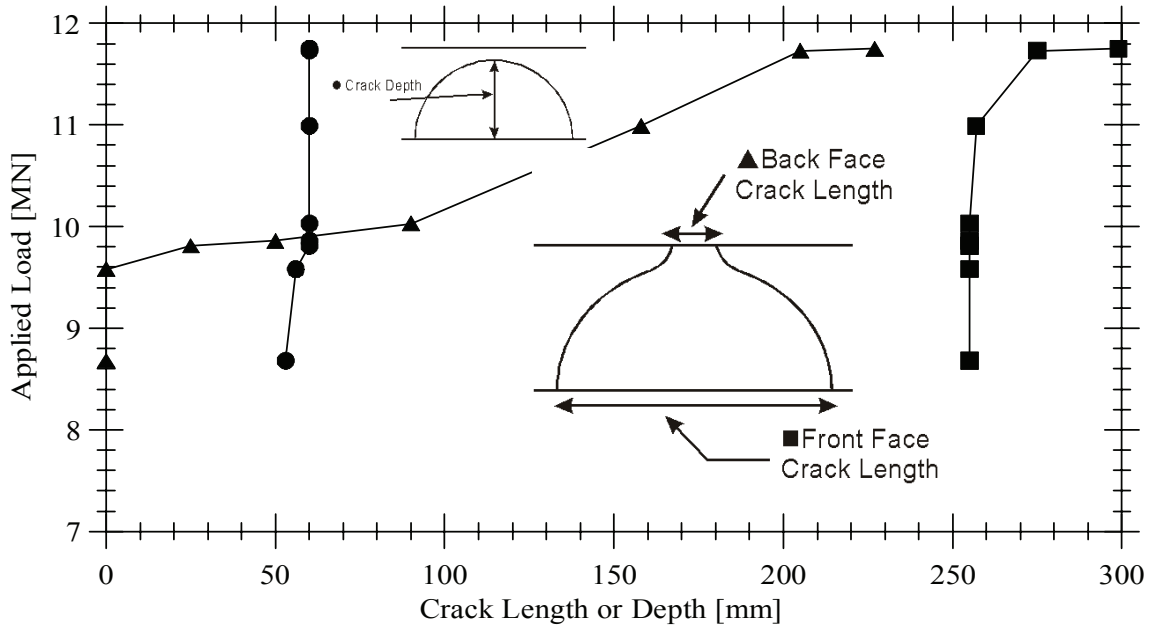


Figure 13.38 – Summary of post-test measurements taken on fracture surface of SSTP 12 test plate

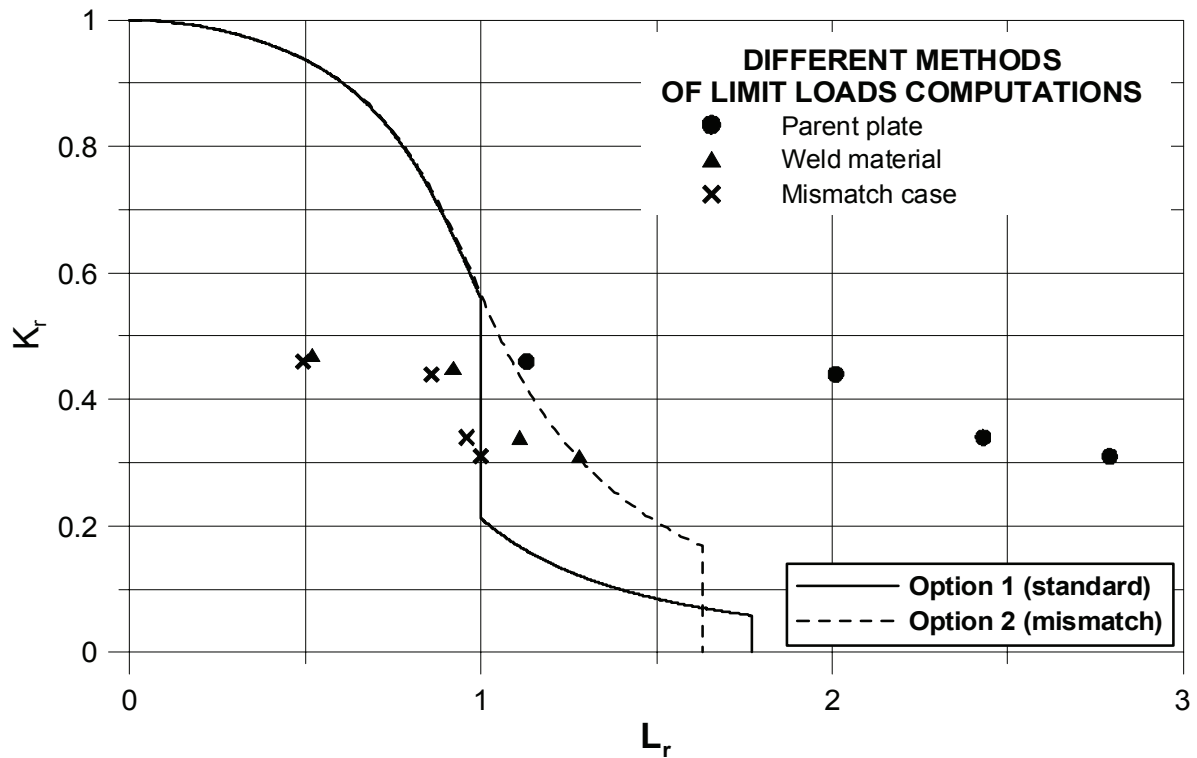
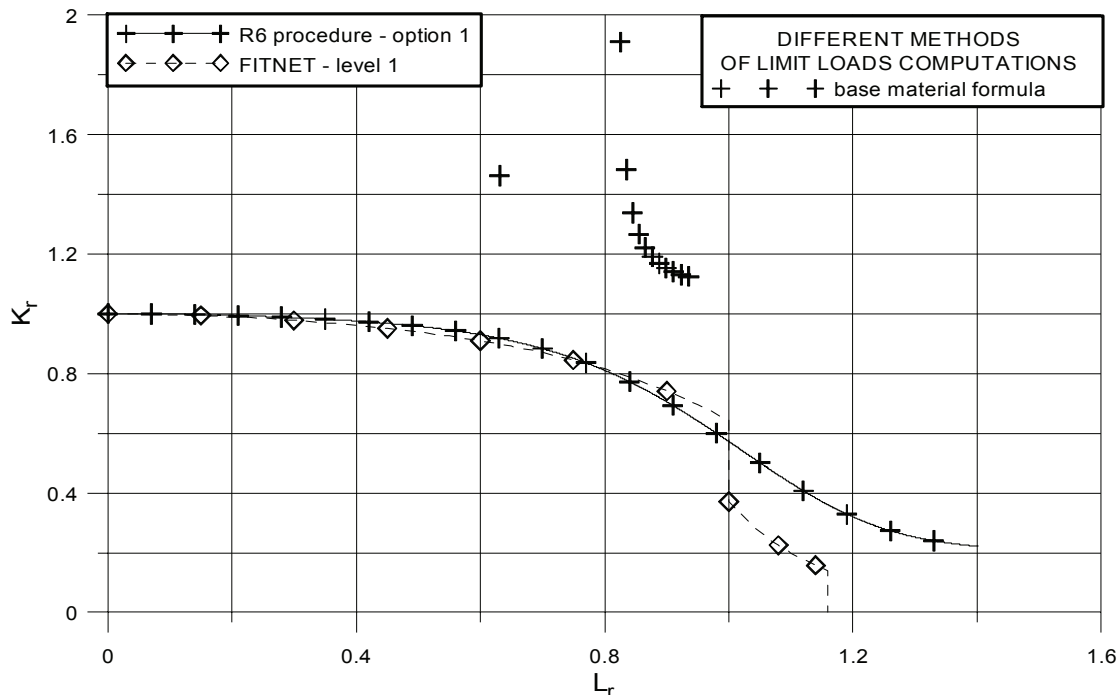


Figure 13.39 – Option 1 (standard) and Option 2 (mismatch) failure assessment curve and points for SSTP 12 experiment.

13.2.8 Spinning Cylinder Test 1

Specimen : Cylinder containing internal axial defect
 Loading : Primary: The cylinder was spun to a maximum speed of 2600rpm
 Material : SA508 Class 3 ferritic steel
 Defect : A fully extended internal axial crack
 Temperature : The cylinder was heated to a temperature of about 290°C



Specimen Details: Internal diameter = 1000mm, Wall thickness = 200mm, Mean radius = 600mm, Cylindrical length = 1300mm

Primary Loading: The cylinder was spun to a maximum speed of 2600rpm. **Secondary Loading:** None

Temperature: The cylinder was heated to a temperature of about 290°C.

Materials Tensile Data: The pressure vessel material was SA508 Class 3 ferritic steel with the data tabulated below, with Young’s modulus $E = 193.12 \text{ GPa}$ at 290°C ($E = 212.35 - 0.0663T$, where T is in $^\circ\text{C}$) and Poisson’s ratio $\nu = 0.28$ at 20°C and $\nu = 0.275$ at 290°C .

Table 13.16 – Mechanical properties of the material

Material	Mean 0.2% Proof strength (MPa)	Mean UTS (MPa)	Temperature ($^\circ\text{C}$)
SA508 / Class 3 Ferritic Steel	539	707	290

Fracture Toughness Data: A pre-test J-resistance power law curve was established at 290°C by tests on 35mm compact tension specimens. These gave:

$$J = 0.208\Delta a^{0.329} \quad \text{with } J \text{ in } \text{MJ/m}^2 \text{ and } \Delta a \text{ in mm.}$$

Defects: A fully extended internal axial defect was machined to an initial depth of 106mm. Then the cylinder was subjected to fatigue pre-cracking which extended the defect depth to about 116mm at the mid-height of the cylinder and about 107mm at the ends.

Other Information and Observations: Post-test destructive examination showed that about 2.5 to 3 mm of ductile tearing had occurred more or less uniformly along the length of the cylinder except close to each end where about 0.5 mm of tearing was measured. In the test report it was considered that the ACPD measurements indicated defect initiation at a speed of about 2275 rpm.

Summary of Analysis and Results: Analysis details are given in Table 13.17. Results are summarised in Table 13.18 and in Figure 13.40.

Table 13.17 – Analysis Details for Spinning Cylinder Test 1

Step	Information	Data and Equation
1.	σ^p loads σ^s loads	2275 rpm and 2600 rpm 0
2.	Yield strength Ultimate tensile strength	539 MPa 707 MPa
3.	FAD selection	Option 1, Option 3: derived from $a=117$ mm data in Table 18.2 of Lacey <i>et al.</i>
4.	Flaw characterisation	extended axial internal crack in cylinder
5.	Analysis categories	Initiation and tearing
6.	Fracture toughness	$J = 0.208\Delta a^{0.329}$ (J in MJm ⁻² and Δa in mm)
7.	Flaw depth a_0 Δa	116 mm 0 to 10.0mm in steps of 1.0mm
8.	L_r $\omega_{0.2}$ ω R_1 R_2 R_c ρ	$= (\omega/\omega_{0.2})^2$ $= \left[\frac{2\sigma_{0.2} \log_e(R_c/R_2)/\sqrt{3}}{\left(\frac{1}{3R_c}(R_1^3 - R_c^3) + \frac{1}{2}(R_c^2 - R_2^2) \right) \rho} \right]^{1/2}$ <p>= rotational speed = inner radius = outer radius = radius at crack tip = density</p>
9.	K_r	from Ductile Fracture Handbook of Zahoor, Chapter 7, Section 1.3.
10.	Plot on FAD	Figure 13.40
11.	Assess significance	See below

Table 13.18 – Values of K_r and L_r for Spinning Cylinder Test 1

Rotational Speed (rpm)	Crack Depth (mm)	Crack Extension (mm)	L_r	K_r
2275	116	0.0	0.631	1.462
2600	116	0.0	0.825	1.910
2600	117	1.0	0.835	1.483
2600	118	2.0	0.845	1.338
2600	119	3.0	0.855	1.266
2600	120	4.0	0.866	1.221
2600	121	5.0	0.877	1.191
2600	122	6.0	0.888	1.169
2600	123	7.0	0.899	1.153
2600	124	8.0	0.911	1.141
2600	125	9.0	0.923	1.131
2600	126	10.0	0.935	1.125

Assessment of Significance of the Test: Both initiation and ductile tearing analyses were carried out using the general Option 1 both for R6, Rev.3 and FITNET failure assessment diagram. Numerical results for the assessment parameters are given in Table 13.18. Figure 13.40 shows the Option 1 both for R6, Rev.3 and FITNET derived from tensile tests on the material at 290°C.

An assessment point is shown in Figure 13.40 for the measured crack initiation speed of 2275 rpm. This point lies outside each of the assessment diagrams, demonstrating that the R6 procedure would conservatively predict initiation at a lower speed than observed in the test. Table 13.18 gives the co-ordinates of the assessment points. On the basis of this assessment, initiation would be predicted to occur at a rotational speed of 1893 rpm. The power law fit to the J-resistance curve measured using 35 mm thick compact tension specimens was limited to 4.5 mm of ductile tearing. Despite this, the assessment considered up to 10 mm of ductile tearing. The locus of assessment points at the maximum test speed of 2600 rpm is also shown in Figure 13.40. These assessment points lie outside the various assessment curves which again demonstrate that R6 provides a conservative prediction of ductile tearing at the maximum test speed. Table 13.18 gives the co-ordinates of the assessment points of the tearing locus.

Bibliography

[13.19] M R Goldthorpe and C J Gardner, R6 validation: an assessment of spinning cylinder tests 1 to 6 carried out at AEA Technology, Risley, Nuclear Electric Report EPD/GEN/REP/0127/97 (1997).

[13.20] D J Lacey et al. Spinning cylinder tests 1 to 3: an investigation of upper shelf fracture behaviour in thick section steel specimens, AEA Technology Report AEA-TRS-4080, in three parts)(1991).

[13.21] A Zahoor, Ductile Fracture Handbook, EPRI Report No. NP-6301-D, Electrical Power Research Institute, Palo Alto, California (1989).

Failure Assessment Diagram showing test and analysis results:

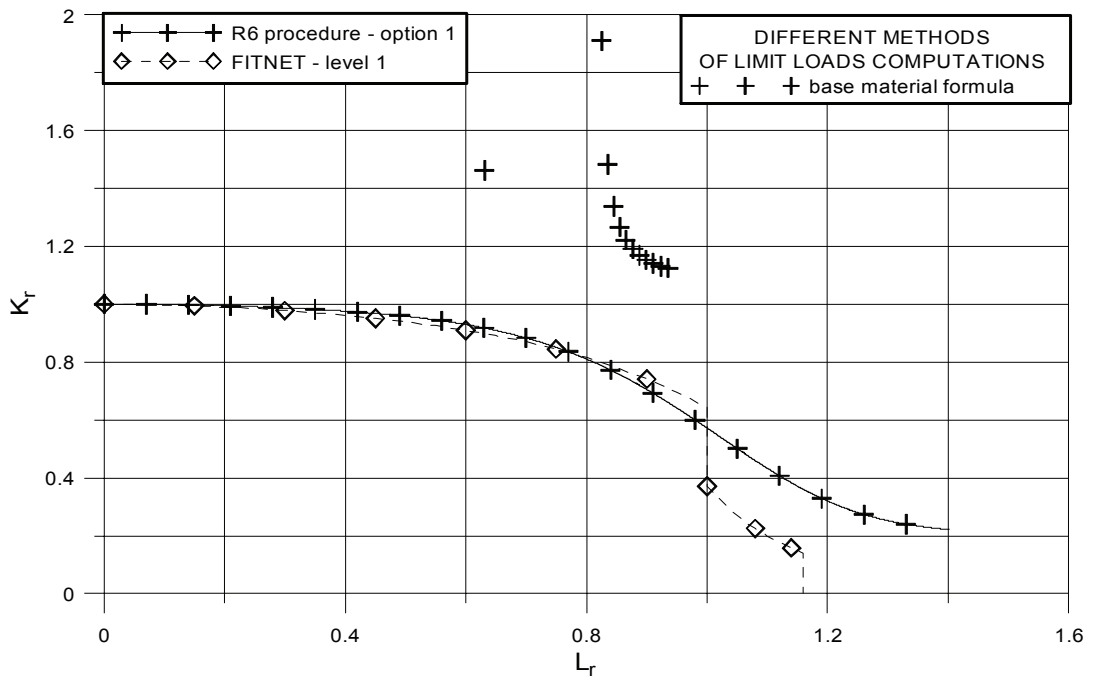


Figure 13.40 – R6 Rev. 3 Option 1 and Option 1 FITNET failure assessment diagram for spinning cylinder. Test 1 showing an assessment point for the measured speed at the initiation of tearing and a locus of points for up to 10 mm tearing at the measured maximum test speed.

13.2.9 Master Curve Analysis of the Point Pleasant Bridge Failure

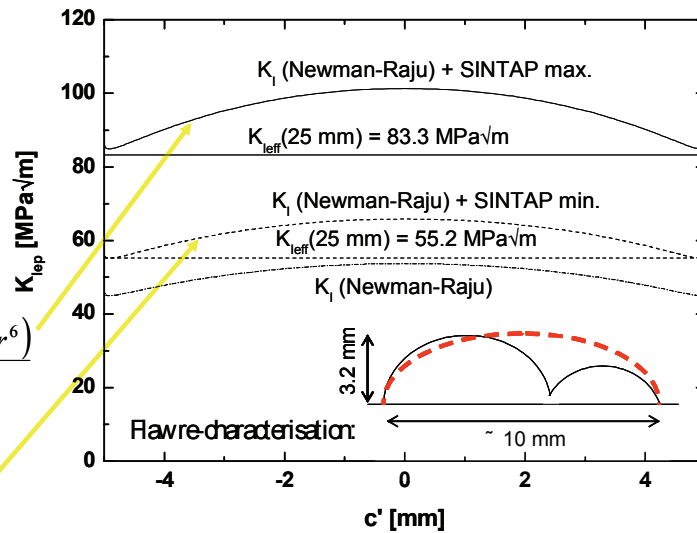
Specimen : Bridge eye-bar structure
 Loading : Primary: Tension loading
 Material : 1060 carbon steel
 Defect : Semi-elliptical surface cracks
 Temperature : Ambient temperature at the time of failure -1°C

$T_0 = +77^\circ\text{C}$
 $\sigma = 585\text{ MPa}$
 $T = -1^\circ\text{C}$
 $\sigma_Y = 540\text{ MPa}$

$$f(L_r) = \frac{0.3 + 0.7 \cdot \exp(-0.4 \cdot L_r^6)}{(1 + 0.5 \cdot L_r^2)^{0.5}}$$

SINTAP plasticity correction

$$f(L_r) = [1 + 0.5 \cdot L_r^2]^{-1/2}$$



Specimen Details:

The bridge was located at Point Pleasant, West Virginia over the Ohio River. It was originally built in 1928. The bridge floor was renovated in 1941.

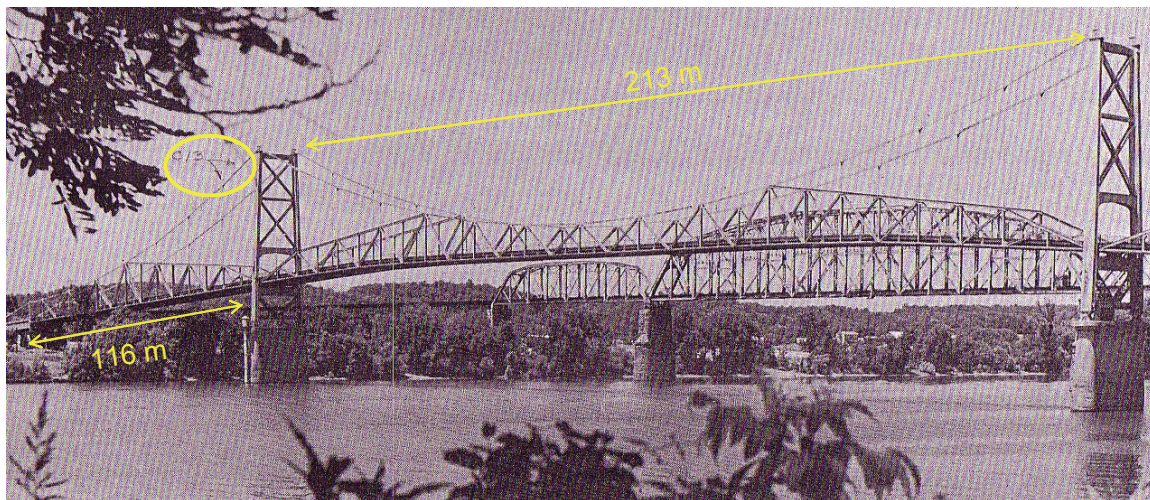


Figure 13.41 – Overview of bridge showing location of fracture initiation.

The bridge failed on Dec.15, 1967 at 5:10 PM during evening traffic and 46 lives were lost. The temperature at fracture was -1°C. “Cracking” started 30 min prior to final collapse. The cause of failure was identified to be brittle fracture of eye-bar 330 in joint C13N of the north eye-bar suspension chain in the Ohio side span. The fracture was caused by the development of a critical size flaw over the 40-year life of the structure as the result of the joint action of stress corrosion cracking and corrosion fatigue.

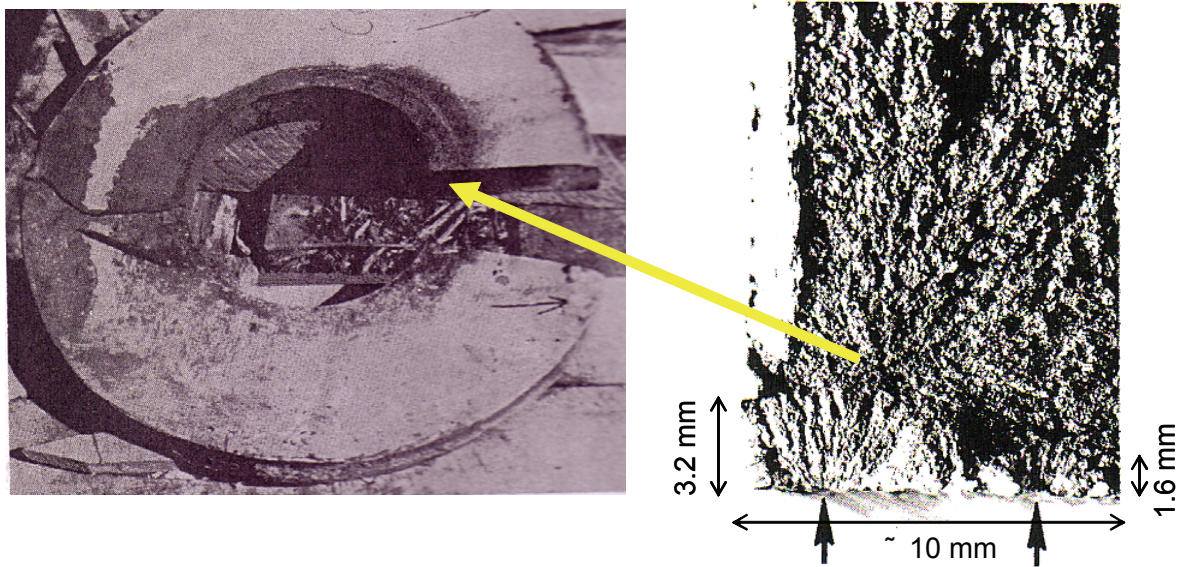


Figure 13.42 – The failure initiated from a semielliptical stress corrosion crack in eye-bar 330. Based on stress analysis and post-measurements the stress at the edge of the eye-bar hole was estimated to be 585 MPa.

Material: The eye-bar material was heat-treated rolled carbon steel with forged heads. Nominally it was a heat treated “1060” carbon steel. The specified yield strength was 517 MPa and ultimate strength 724 MPa. The average measured room temperature yield strength (σ_y) was 520 MPa. The measured yield strength values varied between 457 MPa and 620 MPa. The measured ultimate strength varied between 809 MPa and 854 MPa. The material had a low upper shelf toughness measured by Charpy-V (Figure 13.43).

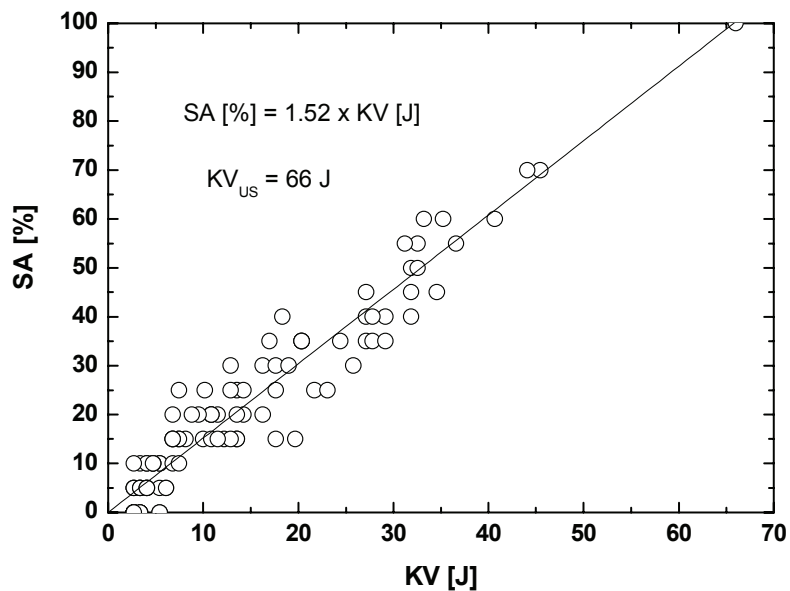


Figure 13.43 – Dependence of Charpy-V impact energy and fracture appearance (SA denotes % shear on fracture surface) used to estimate the materials upper shelf energy.

The 28J transition temperature for the material was very high (Figure 13.44). At 28J energy, there is already more than 40 % ductile fracture on the specimens fracture surface. This low upper shelf energy affects the transition temperatures, making them more conservative than if they corresponded to brittle fracture alone. Thus, for this material, the fracture toughness estimate based on Charpy-V is highly conservative. For such low upper shelf materials, a direct measurement of the materials fracture toughness is more appropriate. The materials fracture toughness was determined with 50 mm thick SE(B) specimens tested under linear-elastic loading conditions. The former three step SINTAP Master Curve analysis of the data is shown in Figure 13.45. The fracture toughness transition temperature T_0 was for the material +77°C, a value clearly less conservative than the Charpy-V tests indicate.

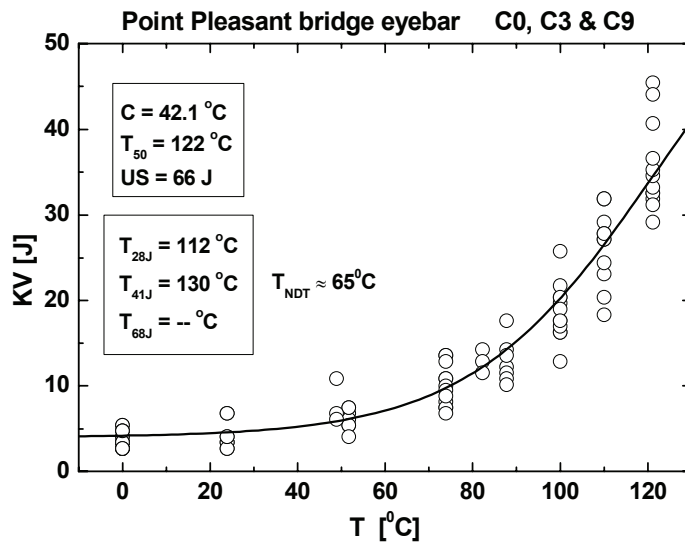


Figure 13.44 – Charpy-V impact energy results for eye-bar material.

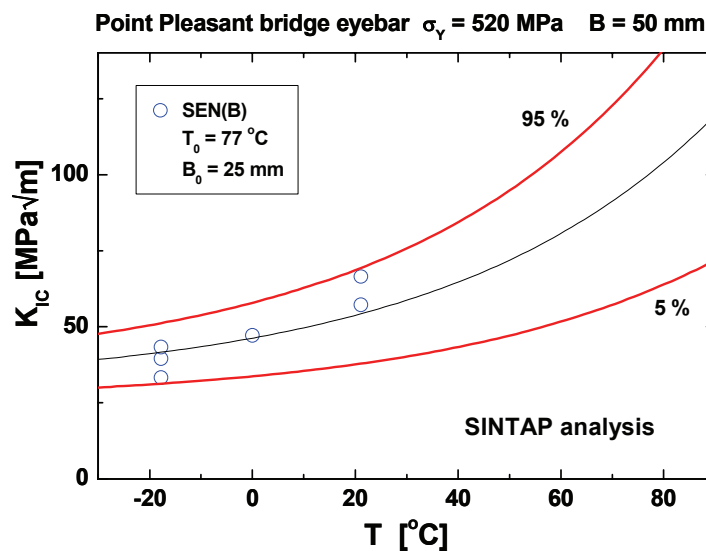


Figure 13.45 – Master Curve (SINTAP) analysis of eye-bar material.

Fracture Toughness Constraint Assessment: Besides SE(B) specimens, the material was also characterized with SEN(T) specimens. These specimens have a negative T-stress of about -130 MPa. The SINTAP three step analysis of the data gave T_0 value of +57°C (Figure 13.46). Since the SE(B) specimens have a positive T-stress of about +50 MPa, it means that the eye-bar materials constraint response is approximately $\Delta T_0 [^\circ\text{C}] \approx \Delta T\text{-stress}[\text{MPa}]/10$.

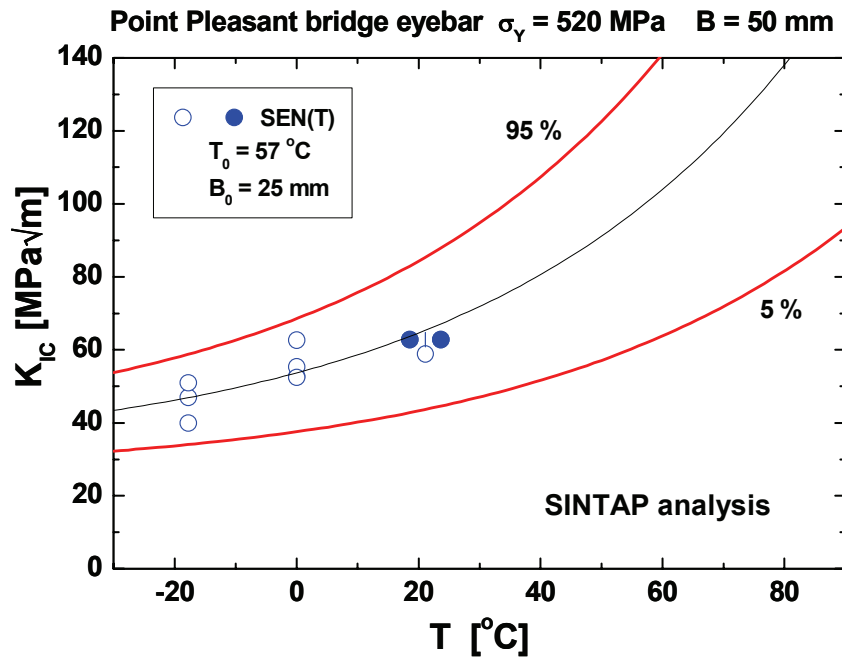


Figure 13.46 – Master Curve analysis of SEN(T) specimens from eye-bar material.

Constraint Corrected Integrity Assessment: Normally, the Master Curve parameters are determined using test specimens with "straight" crack fronts and comparatively uniform stress state along the crack front. This enables the use of a single K_I value and single constraint value to describe the whole specimen

$$P_f = 1 - \exp \left\{ \frac{B}{B_0} \cdot \left(\frac{K_f - K_{\min}}{K_0 - K_{\min}} \right)^4 \right\}$$

For a real crack in a structure, this is usually not the case. Normally, both K_I and constraint varies along the crack front and in the case of a thermal shock, even the temperature will vary along the crack front (Figure 13.47). This necessitates the use of a more complicated formulation.

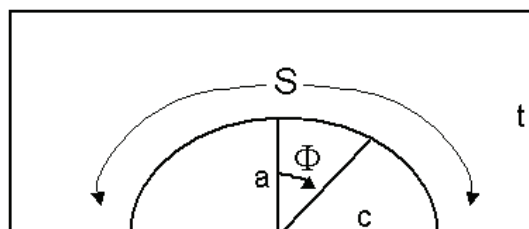


Figure 13.47 – Definitions for an elliptic surface flaw.

$$P_f = 1 - \exp\left\{ \int_0^s \left(\frac{K_{I\Phi} - K_{\min}}{K_{0\Phi} - K_{\min}} \right)^4 \cdot \frac{ds}{B_0} \right\}$$

A visualisation that is in line with standard FITNET practice can be achieved by defining an effective stress intensity factor K_{Ieff} corresponding to a specific reference temperature. The reference temperature can be chosen as, e.g., the minimum temperature along the crack front. The procedure is to determine an effective driving force, which would give the same failure probability as a standard Master Curve presentation

$$K_{\text{Ieff}T_{\text{ref}}} = \left\{ \int_0^s \left(\frac{K_{I\Phi} - K_{\min}}{K_{0\Phi} - K_{\min}} \right)^4 \cdot \frac{ds}{B_0} \right\}^{1/4} \cdot (K_{0T_{\text{ref}}} - K_{\min}) + K_{\min}$$

$K_{I\Phi}$ is obtained from the stress analysis as a function of location (Φ). $K_{0T_{\text{ref}}}$ is the standard, high constraint, Master Curve K_0 , corresponding to a reference temperature along the crack front

$$K_{0T_{\text{ref}}} = 31 + 77 \cdot \exp[0.019 \cdot (T_{\text{ref}} - T_0)]$$

The constraint correction for this material becomes

$$K_{0\Phi} = K_{0T, T-stress} = 31 + 77 \cdot \exp\left[0.019 \cdot \left(T - T_{0\text{deep}} - \frac{T - stress}{10 \text{MPa}/^\circ\text{C}} \right) \right]$$

Integrity Assessment

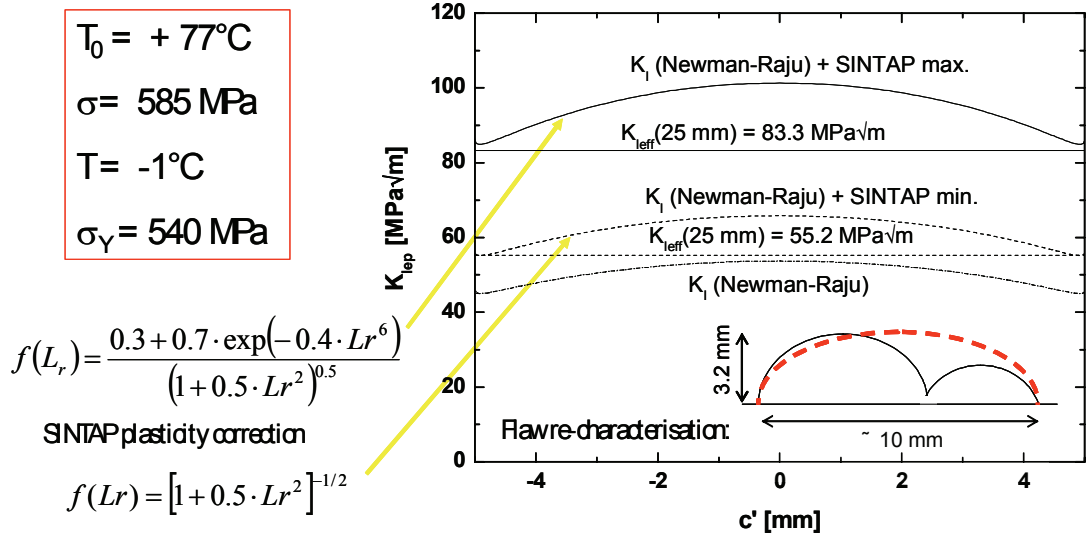


Figure 13.48 – Principle of engineering assessment performed using two limiting FITNET FAD equations.

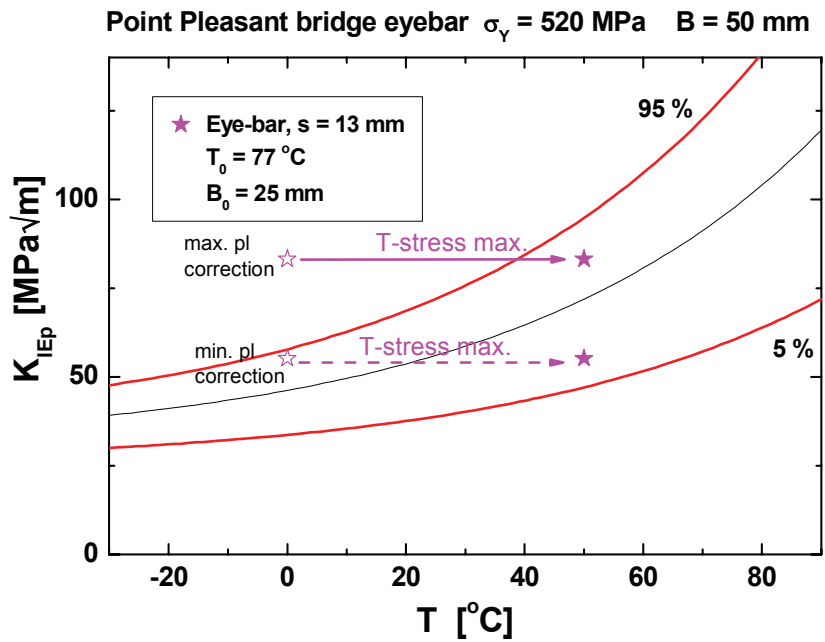


Figure 13.49 – Outcome of engineering assessment predicting failure in eye-bar, even when considering constraint loss in eye-bar.

The FITNET Fracture Module Option 1 analysis produces a viable analysis result, and use of the constraint corrected Master Curve method leads to a realistic estimate of the limiting conditions.

13.2.10 Crack Arrest Evaluation

Specimen :	Two wide plates with secondary loading tabs
Loading :	Uniaxial tension applied in main plate and uniaxial tension in secondary loading tab
Material :	plate 1 : C-Mn, , plate 2 : SAW in C-Mn plate (temper embrittled)
Defect :	Through thickness cracks in secondary loading tab, fnal defects partly penetrating
Temperature :	plate 1 - 20°C, plate 2 - 38°C

Specimen Details: The specimen is shown in Figure 13.50 with the dimensions given in the overview above.

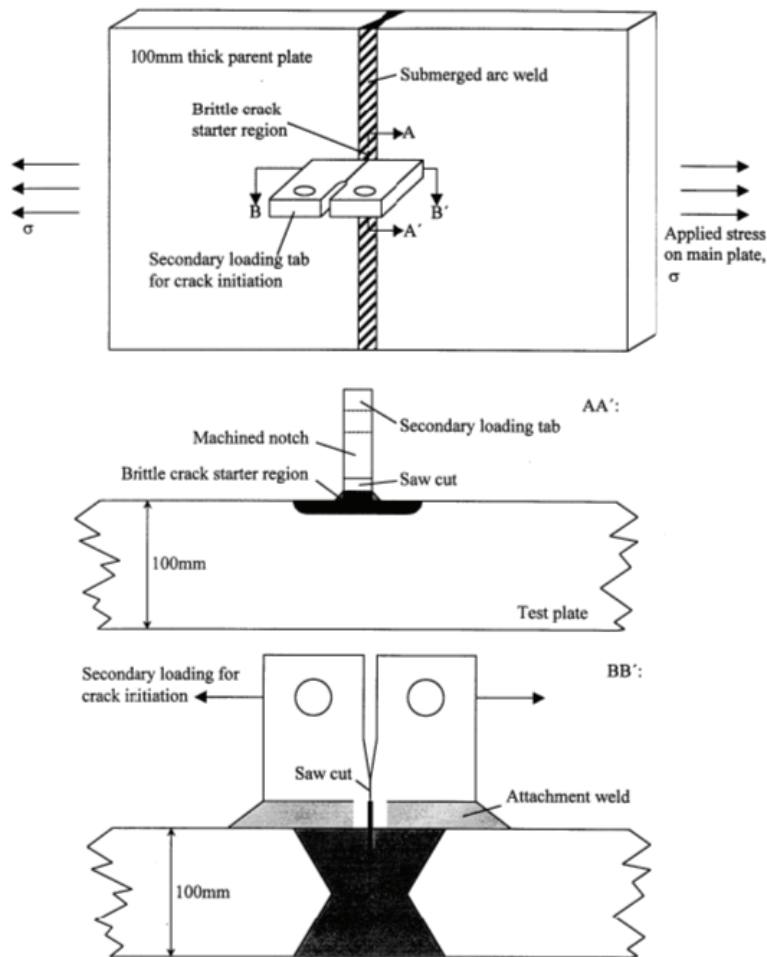


Figure 13.50 – Schematic diagram of test plates.

Material: Plate (1): C-Mn steel plate (as-received conditions)

Plate (2): SAW in C-Mn plate (temper embrittled)

Plates 1 and 2 were both assumed to have a Young's modulus, $E=206$ GPa and a Poisson's ratio, $\nu=0.3$, for the finite element analysis described below.

Loading: Plate 1 was loaded in tension to 1.57 MN and this was maintained throughout the test. The stress in the plate from this load was 203MPa (approximately 0.66 times the yield stress of the as-received plate material). A load was then applied to the loading pins of the secondary loading device and steadily increased until the crack propagated rapidly when this load was 700kN. The crack arrested in the main test plate. After this, the specimen was loaded in fatigue to create a contrasting fracture surface and to separate the two halves of the specimen. The resulting fracture surface is shown in Figure 13.51.



Figure 13.51 – Plate 1 fracture surface.

For plate 2 the secondary loading device was a development of that shown in Figure 13.50 but had a closed outer region to reduce the bending stress in the ligament below the starter crack. The ligament had a side groove to increase the local stress, and was cooled by liquid nitrogen vapour in order to promote brittle crack initiation. The main plate was loaded to 18.32MN which provided a uniform plate stress of 201MPa. The load in the secondary loading device was increased to the value 2.31MN when crack initiation and propagation occurred. The crack tip entered the main plate and then the crack arrested. The temperature of the plate near the crack tip was 38°C.

Defect: For plate 1, a three dimensional finite element linear elastic stress analysis of a representation of the arrested crack configuration was carried out. The dimensions of this deep crack were: depth=34 mm, full surface length=70 mm. In addition, the analysis was repeated for a shallower crack of depth=8 mm and surface length=70 mm.

For plate 2, a three dimensional finite element linear elastic stress analysis was carried out for the cracked configuration. The dimensions of this crack were: depth=5 mm, full length=33 mm. Metallographic investigation showed that the tip had arrested in material of the target microstructure, i.e. temper-embrittled SAW weld material.

Other information and observations: These tests examined crack arrest in 100mm thick plates made of parent plate and submerged arc weld (SAW) materials representative of the materials used in Magnox reactor

steel pressure vessels, including the effects of in-service degradation. Various heat treatments were investigated to produce suitably embrittled materials, which were characterized by tensile, Charpy, drop weight (Pellini) tests, and compact crack arrest toughness tests. The secondary loading tab welded on to the side of the plate provided a starter notch from which a rapidly propagating crack would be initiated when a tensile load was applied to it. The tests would investigate the subsequent propagation and possible arrest after the crack tip had entered the test material of the main plate.

A large experimental and analytical programme of work was carried out, some of which was necessary to quantify the heat treatments. An initial test was carried out on an intermediate sized plate (plate 1) made of the as-received material. The purpose of this test, regarded as a trial for the full size tests, was to investigate the effectiveness of the overall design, especially the method of brittle crack initiation, and to develop the analytical procedures to be employed in the large scale tests.

Summary of analysis and results

Details of plate 1 test:

The loads in the main plate and the secondary loading tab were used to evaluate the variation of the total Mode 1 stress intensity factor along the crack fronts, as shown in Figure 13.52. Also shown is the range of crack arrest toughness values obtained from a number of specimens. The shallow crack has values of stress intensity factor greater than the toughness estimates for a significant part of its length, whereas the deep crack has stress intensity factor values below the range of arrest toughness for most of its length.

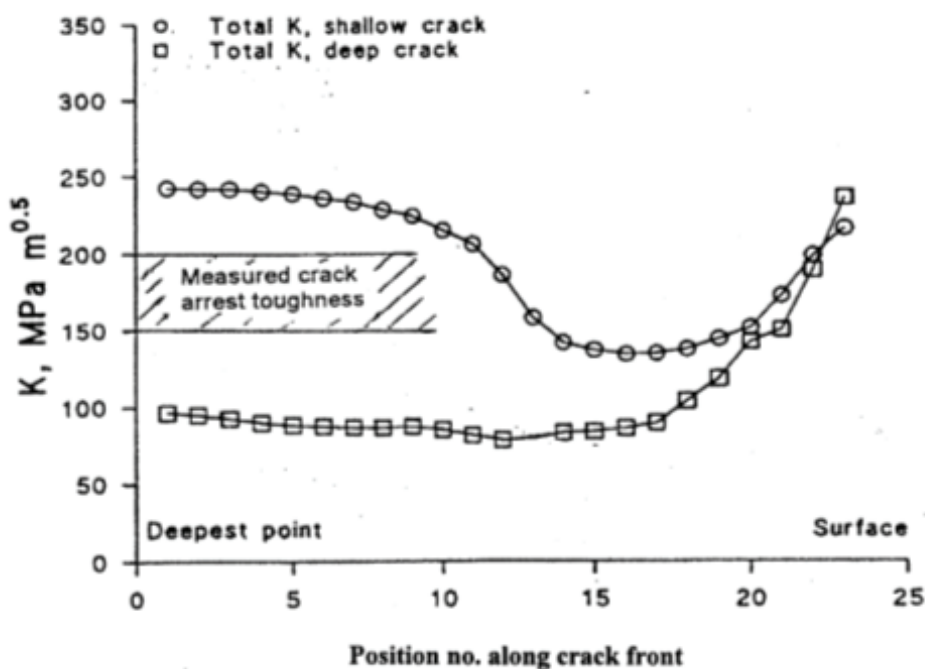


Figure 13.52 – Stress intensity factor around arrested crack fronts in plate 1.

Crack arrest analysis of plate 1 test using section 11.3

1. Toughness approach

Arrest of a propagating crack is predicted by the quasi-static analyses of section 11.3 if the static stress intensity factor, K_I , of the crack multiplied by an enhancement factor, f_s , to account for dynamic effects is smaller than the crack arrest toughness. The value $f_s=1.5$ is recommended when dynamic structural analysis is not available. It can be seen from Figure 13.52 that when the enhancement factor is applied to the shallow

crack no part of it would fulfill the condition for arrest. Crack arrest is, therefore, not predicted. For the deep crack, after multiplying by $f_s=1.5$, about one quarter of the crack front has an enhanced stress intensity factor greater than the lower bound arrest toughness, so again crack arrest is not predicted.

2. Crack arrest temperature approach

Section 11.3 provides for crack arrest predictions based on the material's crack arrest temperature (CAT). This quantity has not been directly measured for the plate material, but estimates can be obtained from Charpy and Pellini test results by means of correlations. Using the Charpy data of Figure 13.54, a value of -16°C is obtained for the Charpy FATT (corresponding to the temperature of the occurrence of 50% crystallinity in the Charpy specimen fracture surface), and using this value with parameters $\alpha=0.84$ and $\beta=3$ in Equation (5) an estimate of -10°C is obtained for the CAT.

Another estimate of the CAT can be obtained from the nil-ductility transition temperature (NDTT) obtained in Pellini drop weight tests. This has been estimated as -30°C for the as-received plate material used in this test. This can be used in Equation (6) of Section 11.3 which relates the CAT to the material NDTT, the applied stress and the plate thickness. This results in the estimated $\text{CAT}=2.5^{\circ}\text{C}$. These two estimates of CAT are reasonably close and are both below the test temperature, so that crack arrest would be predicted.

Details of plate 2 test:

The dimensions of the arrested crack were full length of 33 mm \times depth of 5 mm. Metallographic investigation showed that the tip had arrested in material of the target microstructure, i.e. temper-embrittled SAW weld material. The variation of the stress intensity factor at positions along the crack front is shown in Figure 13.54, which also shows the range of arrest toughness values measured from weld specimens.

Crack arrest analysis of plate 2 using FITNET section 11.3

1. Toughness approach

It is clear from the comparison shown in Figure 13.54 that the static stress intensity factor of the arrested crack is greater than the measured toughness for the temper embrittled weld material even before multiplication by an enhancement factor, so that crack arrest would not have been predicted.

2. Crack arrest temperature approach

Estimates of the CAT based on the measured Charpy FATT values for the weld cap and the weld root using Equation (5) of the section 11 of the FITNET procedure give the following estimates:

$$\text{CAT}(\text{weld cap})=74^{\circ}\text{C} \text{ and } \text{CAT}(\text{weld root})=32^{\circ}\text{C}$$

Estimates of the CAT based on the measured NDTT values for the temper embrittled weld material using equation (6) give the following results for the weld cap and the weld root:

$$\text{CAT}(\text{weld cap})=52^{\circ}\text{C} \text{ and } \text{CAT}(\text{weld root})=22^{\circ}\text{C}$$

Thus both estimates of CAT for the weld cap region are greater than the temperature of the plate during the test (38°C) and so crack arrest would not be predicted. However, the CAT estimates for the weld root are both lower than the test temperature and in this case crack arrest would be predicted.

Assessment of significance of the tests:

Using the analysis for plate 1, the arrest of the propagating crack in the as-received plate material can be reconciled with the material data, since the CAT estimates are both lower than the test temperature. The calculated stress intensity factors for positions along the crack front are mostly below the measured crack arrest toughness. However, strict applications of the Section 11.3 procedure would pessimistically lead to the prediction that the crack would not arrest at the observed crack size because the analysis indicated that part of the crack front had a stress intensity factor such that, after multiplication by the enhancement factor, f_s , the value was greater than the lower bound crack arrest toughness. For plate 2, the calculated stress intensity

factor for the arrested crack was much higher than the measured crack arrest toughness. Also, CAT estimates for a significant component of the weld (the weld cap) were greater than the test temperature. It is clear that the section 11.3 procedure would not result in the prediction of crack arrest.

There is so large a discrepancy between the toughness estimates and the stress intensity factors that it may be considered that improvement is necessary in some aspects of the analysis. It would be worth considering whether the thermal gradient caused by cooling the secondary loading tab in order to promote brittle crack propagation could induce a significant compressive stress component in the propagation path of the crack and thereby reduce the stress intensity factor. Despite various shortcomings in the analysis and the material characterization for these tests, it is apparent that the procedure of section 11.3, given the data available, would have led to conservative predictions for the crack arrest behaviour of the plates.

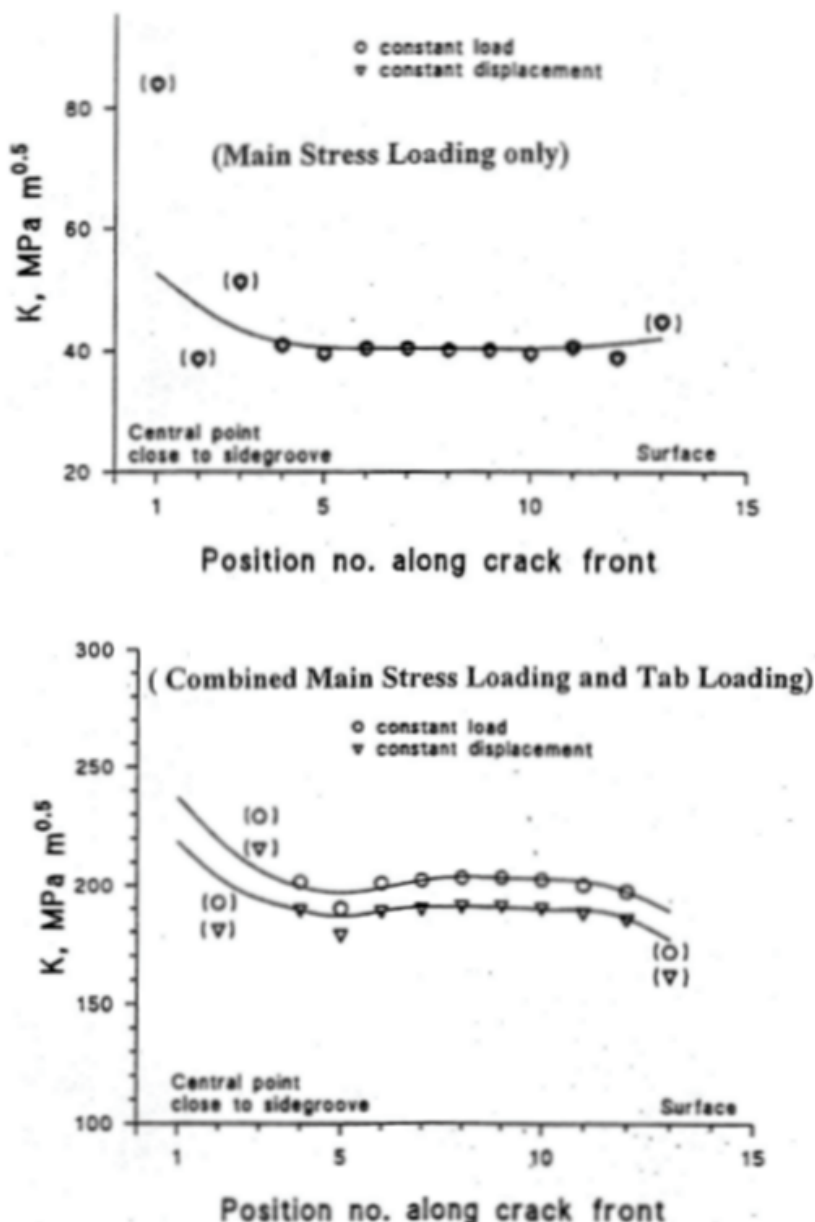


Figure 13.53 – Stress intensity factor along arrested crack front in plate 2.

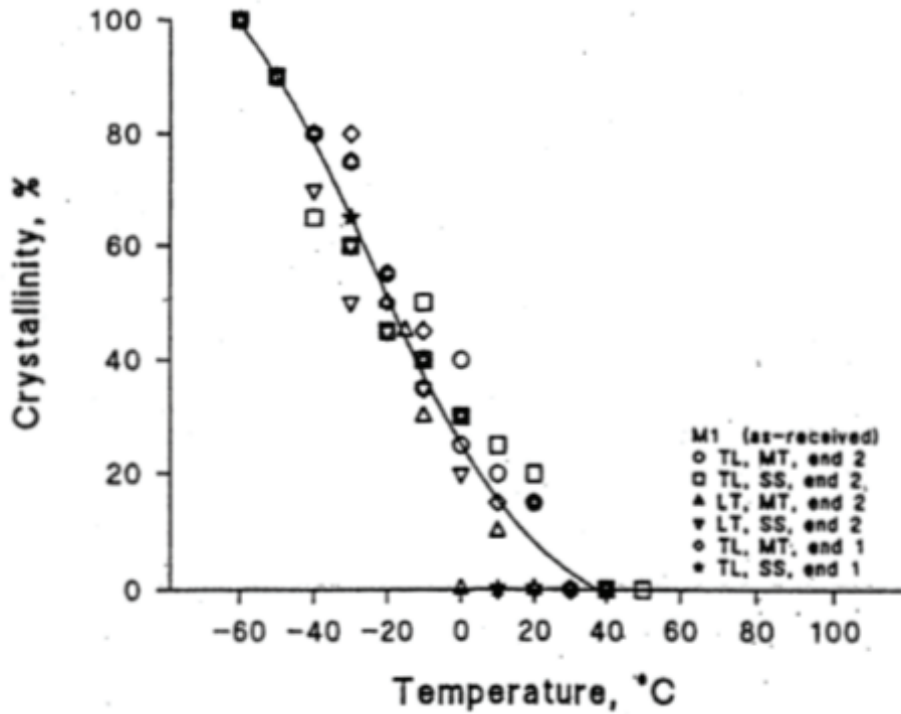
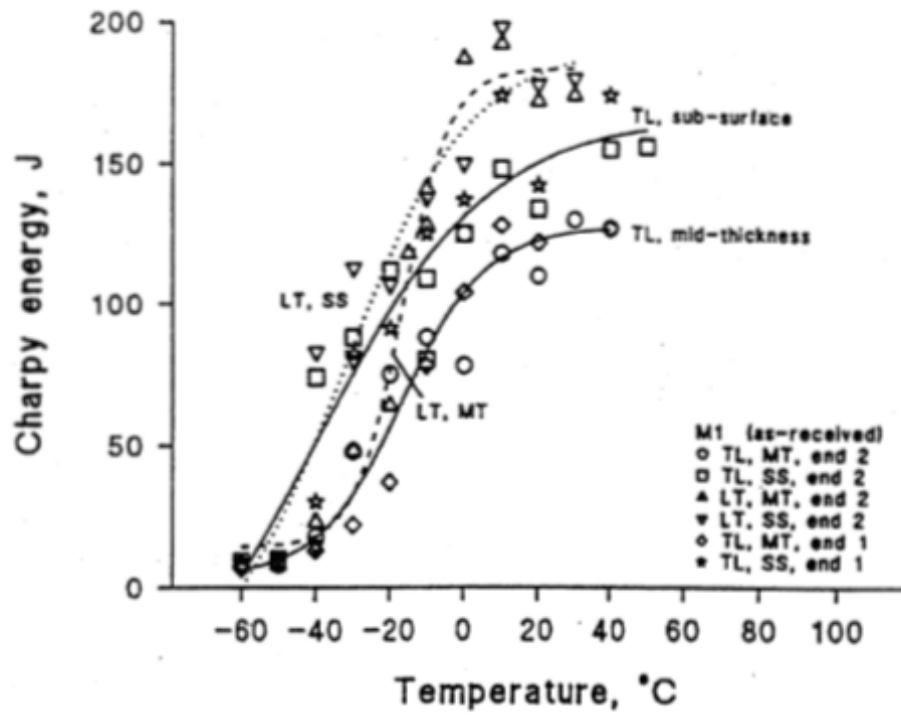


Figure 13.54 – Charpy impact test data from plate 1 material.

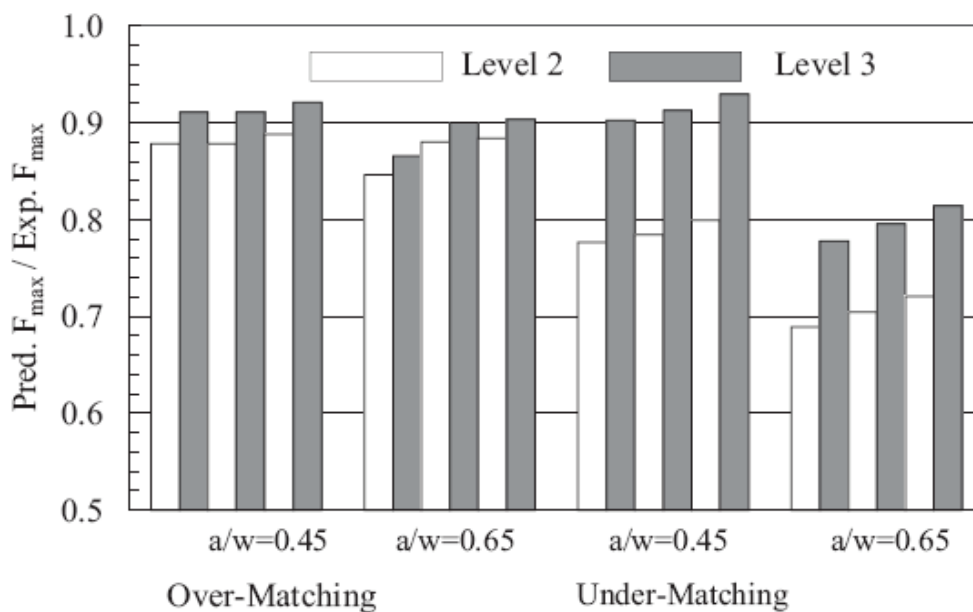
13.2.11 Weld Strength Mismatched Steel Specimens

NOTE: This case study presents the case originally used for the validation of SINTAP procedure. FITNET FFS has overtaken the SINTAP Procedure with some changes and improvements but keeping the main analysis procedure identical. The term “Level” of the analysis corresponds to the FITNET term of “Option”.

Specimen : CCT and SENB specimens
 Loading : Tension and bending loading
 Material : Under and overmatching A533B-1
 Defect : Straight through cracks
 Temperature : Ambient

Further test details are listed in:

Y J Kim, M Koçak, R A Ainsworth and U Zerbst, Engineering Fracture Mechanics, vol. 67, 2002, pp. 529-546.

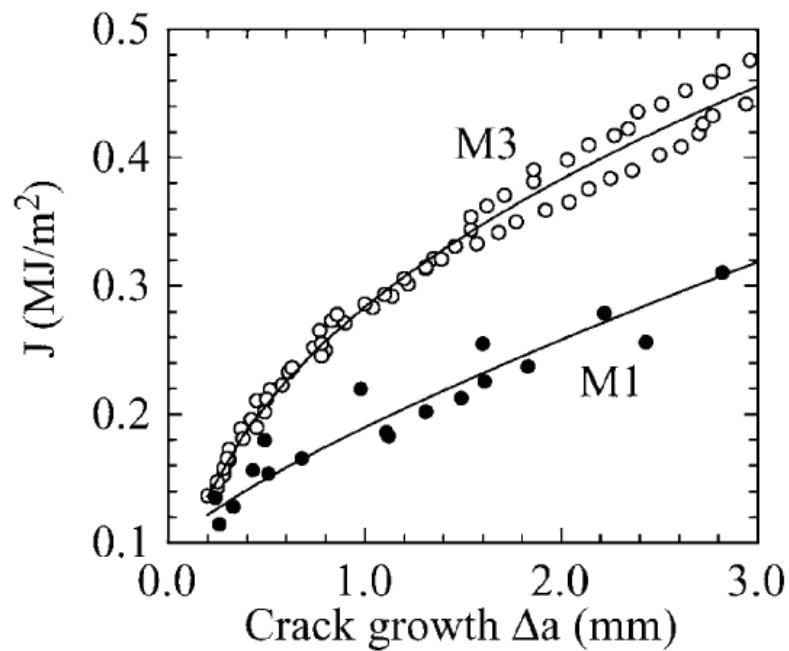


Specimen Details and Materials: An A533B-1 steel was heat treated to produce two material types with different yield and ultimate strength values. Mean tensile strength data for these materials are presented in Table 13.19. The yield strength of the higher strength material (M1 material) is about 50% higher than that of the lower strength material (M3 material). For both materials fracture resistance testing of homogeneous materials was carried out using compact tension, C(T), specimens with initial crack length to specimen width, a/W, ratio of 0.65. Two specimens were tested for each material. The resulting fracture resistance curves are presented in Figure 13.55 and the tabulated toughness data in Table 13.20.

Weld strength mismatched specimens with idealized weldments, single-edge notched bend (SENB) specimens, were produced by electron-beam (EB) welding. The specimens were stress relief heat treated to minimize residual stress effects. Two different configurations were produced, one highly overmatching (strength mismatch ratio of approximately 1.48) and highly undermatching (mismatch ratio of approximately 0.67). Cracks were placed at the centre of the weld metal with two different initial crack length to specimen width ratios, 0.45 and 0.65.

Table 13.19 – Mean tensile properties.

Material	Yield strength [MPa]	Tensile strength [MPa]
M1	738	849
M3	497	647
HAZ (EB)	880	920

**Figure 13.55 – Fracture resistance curves of M1 and M3 materials.****Table 13.20 – Fracture toughness data used in the analyses. $J(\Delta a) = c_1 + c_2(\Delta a)^m$.**

Material	c_1	c_2	m	$J_{0.2}$ [MJ/m ²]
M1	0.094	0.095	0.779	0.122
M3	0.0	0.283	0.438	0.140

Summary of Analysis and Results: Analysis was carried out using Options (levels) 2 and 3, incorporating the effects of Lüders strain. The limit load and stress intensity factor solutions were attained from the FITNET compendium. The overmatching results are presented in Figure 13.56 and the undermatching results in Figure 13.57.

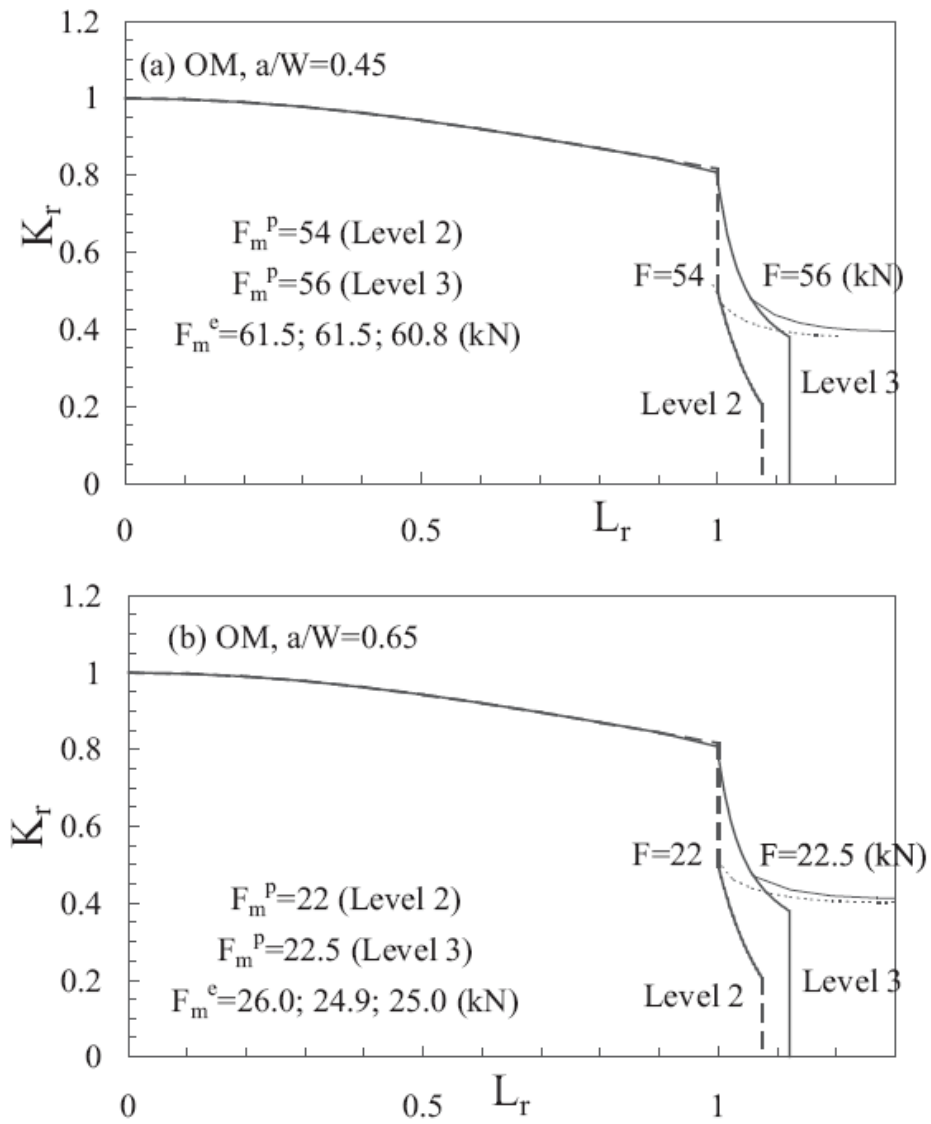


Figure 13.56 – Ductile tearing analysis results for the overmatching specimens, a) $a/W=0.45$ and b) $a/W=0.65$. Experimental and predicted maximum loads are shown

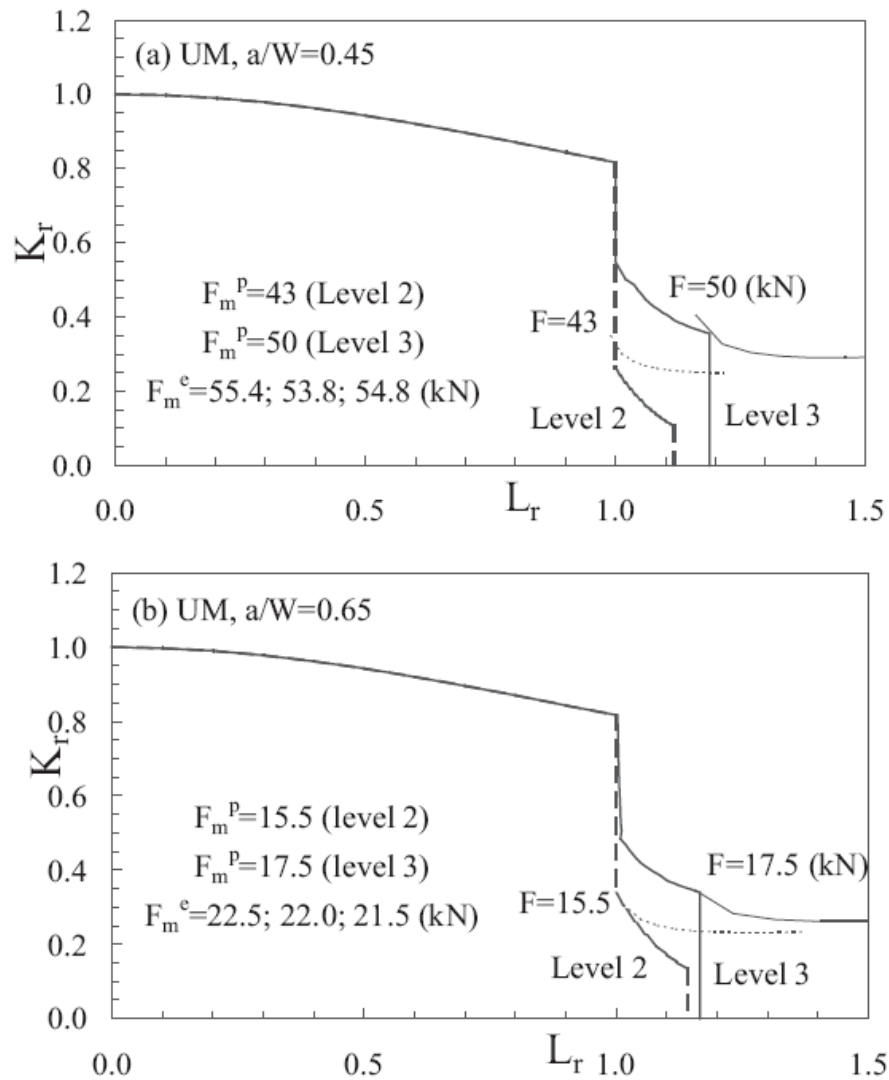


Figure 13.57 – Ductile tearing analysis results for the undermatching specimens, a) $a/W=0.45$ and b) $a/W=0.65$. Displayed are experimental and predicted maximum loads.

Assessment of Significance of Results: Comparison of analysis results using different analysis “Options” (formerly called “Levels”) is presented in Figure 13.58. Option 3 analysis is conservative only by 10% for overmatching specimens, Option 2 analysis being slightly more conservative. For undermatching (UM) specimens the results imply that the failure occurs by plastic collapse. The conservatism for Option 3 analysis for such cases increases up to 20%. Option 2 analysis yield results approximately 30% conservative.

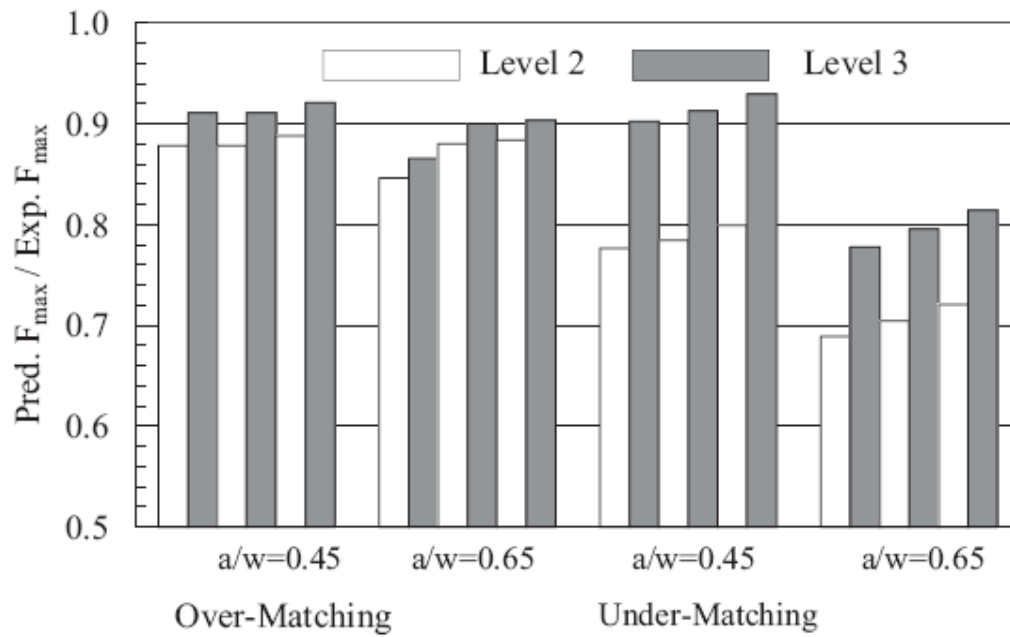


Figure 13.58 – Comparison of predicted maximum load to experimentally measured maximum load, for the option (level) 2 and 3 analyses.

NOTE: Former SINTAP Level 2 and Level 3 correspond to Option 2 and Option 3 of the FITNET FFS Procedure respectively.

Bibliography

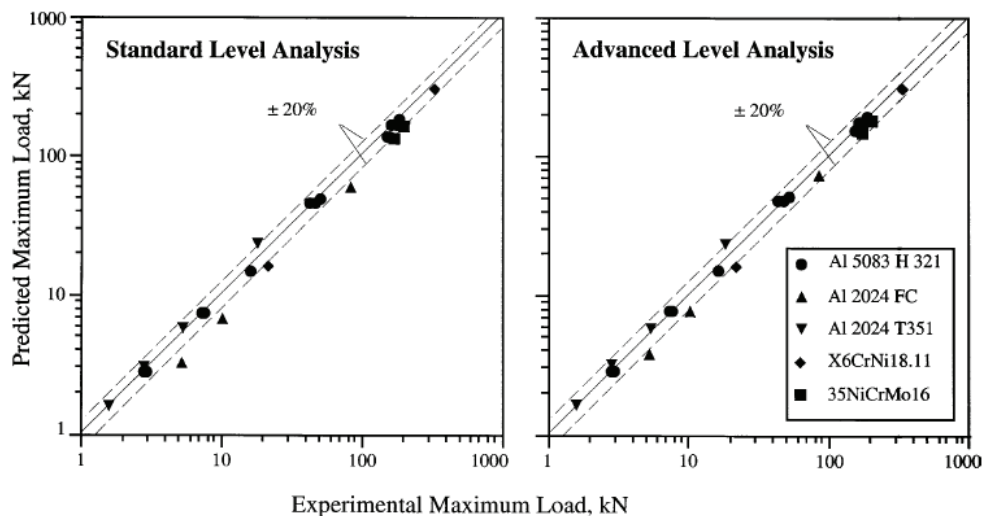
[13.22] Y J Kim, M Koçak, R A Ainsworth and U Zerbst, Engineering Fracture Mechanics, vol. 67, 2002, pp. 529-546.

13.2.12 Thin-Walled Specimens Tests

Specimen :	C(T), M(T), biaxial tension specimens
Loading :	Primary: Tension, bending, biaxial tension
Material :	Aluminium alloys, X6CrNi18-11 stainless steel, 35NiCrMo16 ferritic steel
Defect :	Central through thickness crack
Temperature :	Ambient

Further test details are listed in:

M Schödel and U Zerbst, Engineering Fracture Mechanics, 71, 2004, pp. 1035-1058.



Specimen Details and Materials: The specimen and material details are presented in Table 13.21. The materials investigated were

- Al 5083 H 321 – a strain hardening aluminium alloy with a magnesium content of 4.5% which is mainly applied for vessels and light weight structures in automotive industry and shipbuilding. A major advantage is its weldability.
- Al 2024 T 351 – an aluminium alloy subjected to precipitation heat treatment which is mainly applied in the aerospace industry.
- Al 2024 FC – an aluminium alloy which was annealed for research purposes. FC stands for “furnace cooling”
- X6CrNi18.11 – an austenitic stainless steel
- 35NiCrMo16 – a ferritic steel mainly used in power generation applications

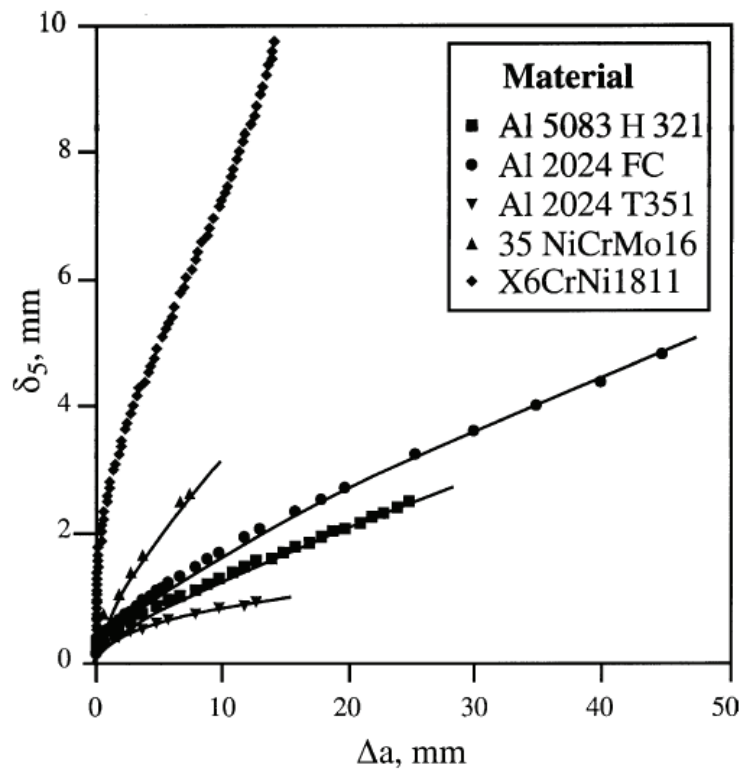
The mechanical properties of the materials are presented in Table 13.22 and CTOD- δ_5 resistance curves in Figure 13.59.

Table 13.21 – Tested materials and specimen types.

Material	Specimen Type	Thickness [mm]	Width [mm]	Initial crack length [mm]	Ligament / thickness ratio	Remarks
Al 5083 H 321	C(T)	3	50	25	8.33	Two specimens
			150	75	25	Three specimens
			300	150	50	Two specimens
			1000	500	166.67	Two specimens
	M(T)	3	50	15	11.67	Two specimens
	M(T)		150	30	40	Two specimens
	Biax	3	150	30	40	Biax. ratio -0.5, 2 spec.
						Biax. ratio 0
						Biax. ratio 0.5
						Biax. ratio 1
Al 2024 FC	C(T)	5	100	50	10	
			200	100	20	
	M(T)	5	127	63.8	12.64	
Al 2024 T351	C(T)	1.6	50	25	15.63	
			100	50	31.25	
			200	100	62.5	
			1000	500	312.5	
X6CrNi18.11	C(T)	10	100	61	3.9	
	M(T)	10	100	56.6	4.34	
35NiCrMo16	M(T)	5	50	25	5	
				20	6	

Table 13.22 – Tensile properties of the materials

Material	Yield strength [MPa]	Tensile strength [MPa]	Young's modulus [GPa]	Strain hardening exponent
Al 5083 H 321	242	345	70	0.09
Al 2024 T 351	300	427	66	0.09
Al 2024 FC	82	224	72	0.19
X6CrNi18.11	239	617	195	0.18
35NiCrMo16	510	726	215	0.09

**Figure 13.59 – Fracture resistance curves.**

Summary of Analysis and Results: The analysis results are presented in Table 13.23 and in Figure 13.60. The analyses were performed using Option 1 and 3 FADs in order to compare the differences in conservatism between a basic level analysis and an advanced level analysis. The effect of ligament on the conservatism of the analysis is presented in Figure 13.61.

Table 13.23 – Compilation of experimental and predicted results. Conservatism= $(F_{\text{predicted}}/F_{\text{experimental}} - 1)$.

Material	Type	B	W	a ₀	Exp. Failure load [kN]	Option 1 [%]	Option 3 [%]	Remarks
Al 5083	C(T)	3	50	25	2.9	-3.79	-1.93	
					3.1	-10	-8.26	
			150	75	7.7	-1.17	+1.23	
					7.8	-2.44	-0.06	
					7.7	-1.17	+1.23	
			300	150	17.3	-15.72	-13.29	V-shear
					17.0	-14.24	-11.76	V-shear
			1000	150	51.0	+3.11	+6.06	V-shear
					45.4	-8.22	-5.59	
	M(T)	3	50	15	53.5	-7.57	-3.23	
					54.0	-8.43	-4.13	
			150	30	172	-3.72	+0.37	
					172	-3.72	+0.37	
	Biax., -0.5	3	150	30	167	-16.31	-9.96	V-shear
					167	-16.31	-9.96	V-shear
	Biax, 0	3	150	30	189	-11.85	-7.58	
	Biax, 0.5	3	150	30	196	-4.88	-1.7	
	Biax 1	3	150	30	197	-7.94	-3.94	V-shear
Al 2024 FC	C(T)	5	100	50	5.38	-39.39	-28.7	
			200	100	10.71	-35.62	-26.41	
	M(T)	5	127	63.8	89.17	-33.0	-17.03	
Al2024 T 351	C(T)	1.6	50	25	1.693	-2.03	+0.76	
			100	50	3.009	+3.06	+5.95	
			200	100	5.63	+2.22	+5.01	
			1000	500	18.69	+25.47	+27.45	
X6NiCr18.11	C(T)	10	100	61	22.62	-29.35	-29.20	
	M(T)	10	100	56.6	345.9	-12.02	-11.3	
35NiCrMo16	M(T)	5	50	25	174.9	-22.27	-15.78	
				20	206.9	-20.56	-13.07	

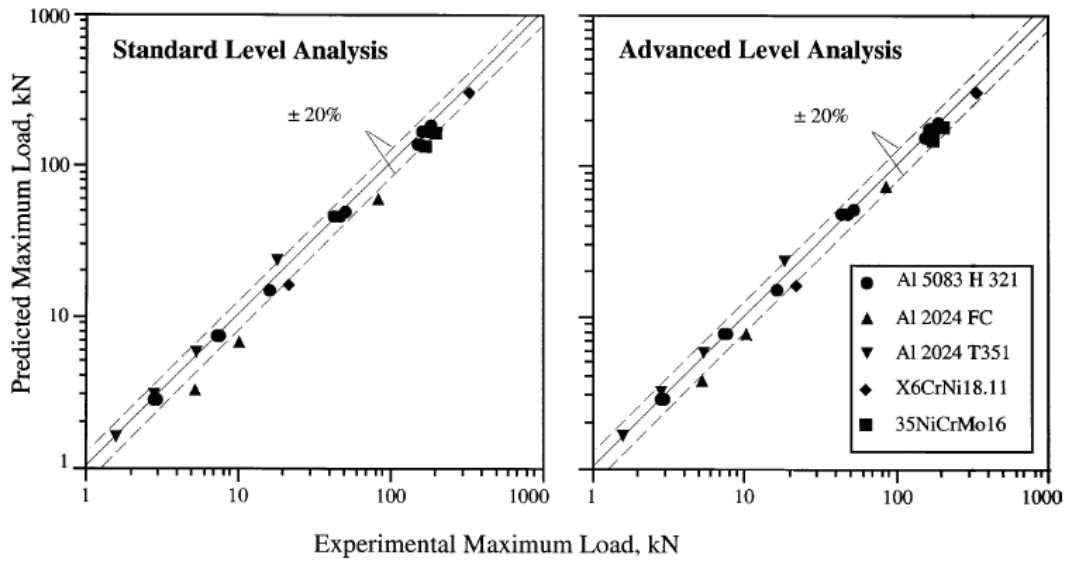


Figure 13.60 – Comparison of experimental and predicted results for maximum load.

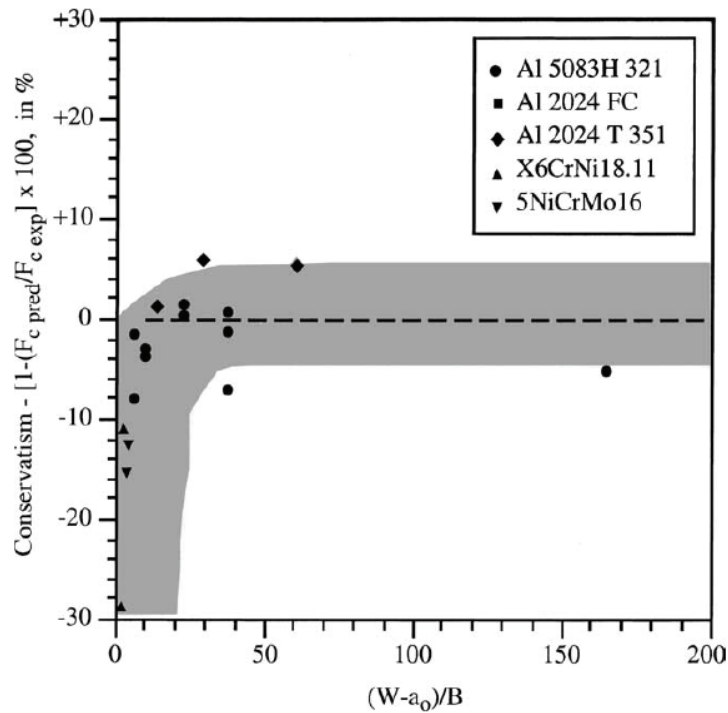


Figure 13.61 – Effect of ligament on conservatism of prediction.

Bibliography

[13.23] M Schödel and U Zerbst, Engineering Fracture Mechanics, 71, 2004, pp. 1035-1058.

13.3 Case Studies for FATIGUE

13.3.1 Fatigue Routes 1 and 2 for Welded Structures, Nominal and Notch Stress Approaches

Specimen :	Scallop in a longitudinal stiffener of a tanker ship deck
Loading :	Tension - compression
Material :	Steel 350 MPa – grade B
Defect :	End weld in the scallop
Temperature :	Ambient

The current case study is presented in more detail in the FITNET Tutorials, Chapter 14.5.

During a ship design the following detail of a tanker ship deck, a scallop in a welded longitudinal stiffener, has to be assessed in fatigue. Two Routes; **ROUTE 1** (Nominal Stress) and **ROUTE 2** (Notch Stress) are applied.

General data: The midship transverse section, the location of the detail to be assessed and the local geometry of the detail are given in Figure 13-62.

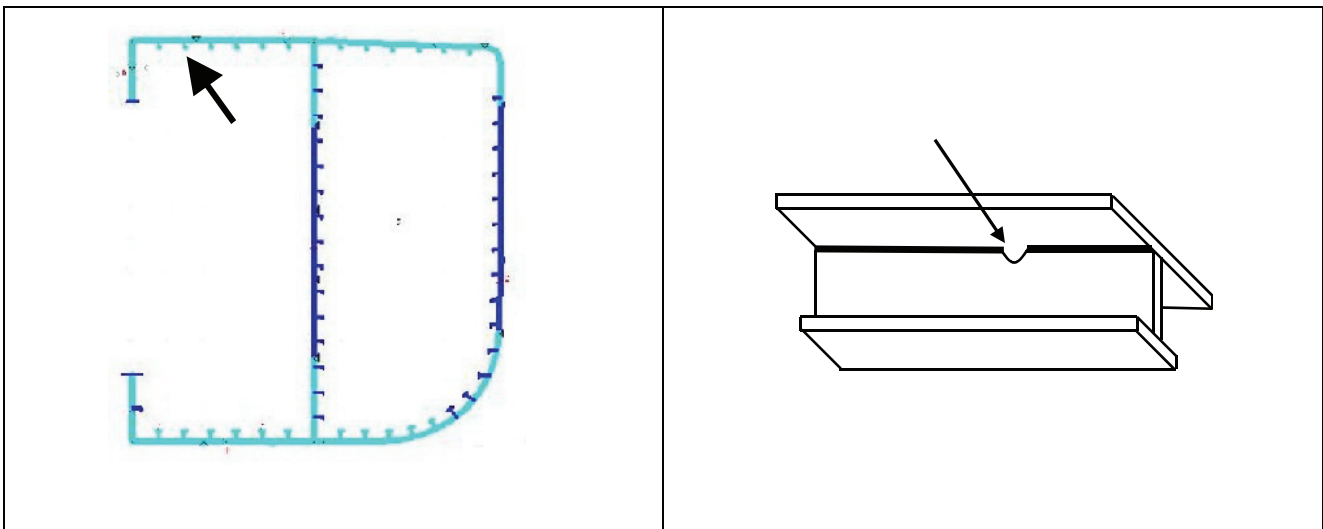


Figure 13-62 – Ship transverse section and welded detail assessed

The ship has the following dimensions:

Length $L = 300$ m, Breadth $B = 57$ m, Depth $D = 30$ m, Draught $d = 21$ m

Block coefficient $C_b = 0.85$ (ratio of the loaded ship mass to 1.025 LBT)

The ship is built with normal steel of $\sigma_Y = 235$ MPa and the plate thickness is 20 mm for the deck and 15 mm for the stiffener components. The structure scantling (dimensions) fulfils the classification rules which means that the midship vertical transverse modulus is equal to:

$$W_m = L^2 B (C_b + 0.7) 10^{-6} \dots \text{in m}^3$$

The maximum midship vertical wave bending moments during the ship life are given by the classification rules as:

$$\text{Hogging: } M_{wH} = 190 L^2 B C_b 10^{-3} \text{ in kN.m and Sagging: } M_{wS} = -110 L^2 B (C_b + 0.7) 10^{-3} \text{ in kN.m}$$

The design ship life is 25 years. The classification society rules provide a long term cumulative distribution of the vertical wave bending moment range, and therefore of the stress range, in the deck. The distribution can be represented by a stair curve (see section 7.2.1) with 16 steps as given in Table 13.24.

Table 13.24 – Long term vertical wave bending relative stress distribution.

$\Delta S_i/S_{\max}$	n_i
1	5
0.88	68
0.74	342
0.63	1 895
0.51	8 160
0.44	13 160
0.40	47 370
0.35	47 370
0.32	92 105
0.30	131 580
0.28	265 260
0.22	568 420
0.16	1 684 210
0.13	2 736 840
0.09	26 315 790
0.05	68 421 055
Σ	9055

ROUTE 1: Fatigue damage assessment using nominal stresses

Step 1: Detected flaws: The assessment concerns a new build, therefore the structure is assumed free of flaws.

Step 2: Service condition, Nominal stress range: The nominal stress is the longitudinal stress range in the deck induced by the wave vertical bending moment. The bending moment range is given by:

$$\Delta M = M_{WH} - M_{WS} = L^2 B 10^{-3} [190C_b + 110(C_b + 0.7)] \quad \text{in kN.m}$$

The maximum stress range is:

$$\Delta S_{nom} = \frac{\Delta M}{W_m} = \frac{190C_b + 110(C_b + 0.7)}{C_b + 0.7} 10^3 = 214 \text{ MPa}$$

The stress range is lower than $2 S_y$.

Step 3: Environmental issues: The structure is protected against corrosion by an efficient coating.

Step 4: Threshold for fatigue assessment: The ship loads are induced by waves and so are random. In such conditions, there is no threshold below which no fatigue damage occurs.

Step 5: Reference tables of classified components or structural details: The S-N curve can be found in the classification rule book catalogue. An extract is given in Table 13.25. This table shows that the S-N curve to be considered is the F curve. The rule design curve is the two-slope curve without a cut-off, with the change of slope fixed at 10^7 cycles (see 7.2.1.3):

$$m = 3 \quad K_{D1} = 6.316 \cdot 10^{11}$$

The slope change stress range is: $\Delta S_1 = (K_1 / 10^7)^{1/3} = 39.8 \text{ MPa}$ and

the second part of the S-N curve is: $m = 5 \quad K_{D2} = \Delta S_1^5 \times 10^7 = 9.987 \cdot 10^{14}$

Table 13.25 – Extract from the ship classification rules catalogue of details.

Welded Joint Classification (cont'd)		
Joint Classification	Description	Examples
Category 6		
E	2) Intermittent fillet welds	
F	3) As (2) but adjacent to cut-outs.	

Step 6: R-ratio effects: Ship structures are built in the as-welded condition, so, due to welding residual stresses, no correction with respect to R ratio is needed.

Step 7: Thickness reduction factor effects : The thickness being less than 25 mm, no correction is required.

Step 8: Fatigue assessment using S-N Curves: The Miner sum is given by:

$$D = \sum n_i / N_i \quad \text{where} \quad N_i = K_{D1} / \Delta S^3 \quad \text{or} \quad N_i = K_{D2} / \Delta S^5$$

The Miner sum calculation details are given in Table 13.26. The value is: D = 0.61

Table 13.26 – Miner sum calculation for nominal stress range.

$\Delta S_i / S_{max}$	ΔS nom	n_i	n_i / N_i nom
1	214	5	0
0.88	188	68	0
0.74	158	342	0.002
0.63	135	1 895	0.007
0.51	109	8 160	0.017
0.44	94	13 160	0.017
0.40	86	47 370	0.048
0.35	75	47 370	0.032
0.32	69	92 105	0.048
0.30	64	131 580	0.054
0.28	60	265 260	0.091
0.22	47	568 420	0.093
0.16	34	1 684 210	0.077
0.13	28	2 736 840	0.047
0.09	19	26 315 790	0.063
0.05	11	68 421 055	0.011
Σ		9055	0.61

italic → $m = 5$

Route 2: Fatigue damage assessment using structural or notch stresses

Step 1: Detected flaws: The assessment concerns a new build, therefore the structure is assumed free of flaws.

Step 2: Service condition: The notch stress approach requires two stress concentration factors (see 7.3.2.1): the structural hot spot stress SCF_{HS} and the notch effect SCF_{notch} . The hot spot stress concentration factor has been determined by a finite element model of the detail subjected to tension. The value found is: $SCF_{HS} = 1.1$

The notch effect factor is given in 7.3.2.1.2.3: $SCF_{notch} = \lambda (\theta / 30)^{1/2}$

with the following values: fillet weld: $\theta = 45$; well contoured end, perpendicular: $\lambda = 2.15$ and so

$$SCF_{notch} = 2.15 (45 / 30)^{1/2} = 2.63$$

The notch stress range is: $\Delta S = SCF_{HS} SCF_{notch} \Delta S_{nom} = 619 \text{ MPa}$

The hot spot stress range (235.4 MPa) is lower than $2 S_y$.

Step 3: Environmental issues: The structure is protected against corrosion by an efficient coating.

Step 4: Threshold for fatigue assessment: The ship loads are induced by waves and so are random. In such conditions, there is no threshold below which no fatigue damage occurs.

Step 5: Fatigue Data Specifications: The rule book S-N curve associated with the notch stress is the following:

mean curve $m = 3$ and $K_{mean} = 3.913 \cdot 10^{13}$

standard deviation in $\log(C) = 0.1821$

and the parameters of the design curve at minus 2 standard-deviations are: $m = 3$ $K_{D1} = 1.692 \cdot 10^{13}$

The slope change stress range is: $\Delta S_1 = (K_1 / 10^7)^{1/3} = 119.2 \text{ MPa}$

and the second part of the S-N curve is: $m = 5$ $K_{D2} = \Delta S_1^5 \times 10^7 = 2.406 \cdot 10^{17}$

Step 6: R-ratio effects: Ship structures are built as welded, so, due to welding residual stresses, no correction has to be done with respect to R ratio.

Step 7: Thickness reduction factor effects: The thickness being less than 25 mm, no correction is required.

Step 8: Fatigue assessment using S-N Curves: The Miner sum is given by:

$$D = \sum n_i / N_i \quad \text{where} \quad N_i = K_{D1} / \Delta S^3 \quad \text{or} \quad N_i = K_{D2} / \Delta S^5$$

The Miner sum calculation details are given in Table 13.27. The value is: $D = 0.54$

Table 13.27 – Miner sum calculation for notch stress range.

$\Delta S / S_{max}$	ΔS notch	n_i	n_i / N_i notch
1	619	5	0.000

0.88	544	68	0.001
0.74	457	342	0.002
0.63	391	1 895	0.007
0.51	315	8 160	0.015
0.44	272	13 160	0.016
0.40	249	47 370	0.043
0.35	217	47 370	0.029
0.32	200	92 105	0.043
0.30	185	131 580	0.049
0.28	174	265 260	0.082
0.22	136	568 420	0.084
0.16	98	1 684 210	<i>0.064</i>
0.13	81	2 736 840	<i>0.040</i>
0.09	55	26 315 790	<i>0.055</i>
0.05	32	68 421 055	<i>0.009</i>
Σ		9055	0.54

italic → m = 5

13.3.2 Fatigue Route 2, for Non Welded Components on Compressor Flange Made of Grey Iron

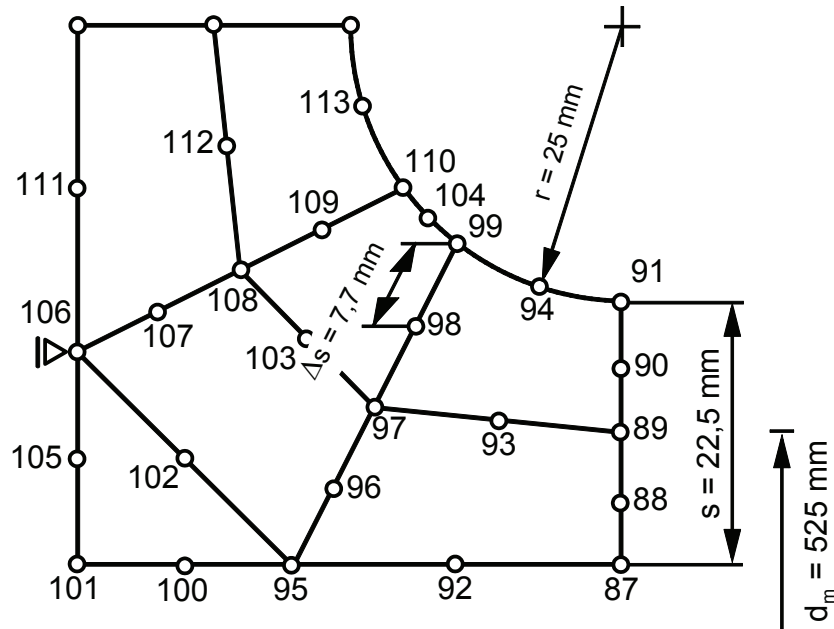


Figure 13.63 – Compressor flange made of grey cast iron

Inputs for Analysis

Stresses: Proportional, constant amplitude loading, locally elastic stresses in the directions 1 (longitudinal) and 2 (circumferential) at the reference point (node 99) of a block-shaped (3D) component, Figure 13.63.

$$\sigma_1 = \sigma_{1,m} \pm \sigma_{1,a} = 15.0 \text{ MPa} \pm 18.6 \text{ MPa}$$

$$\sigma_2 = \sigma_{2,m} \pm \sigma_{2,a} = 5.0 \text{ MPa} \pm 6.2 \text{ MPa}$$

$$\sigma_3 = 0.$$

Stress amplitudes at the neighbouring point (node 98) in a distance $s = 7.7 \text{ mm}$ below the surface

$$\sigma_{1,a} = \pm 10.0 \text{ MPa},$$

$$\sigma_{2,a} = \pm 5.3 \text{ MPa}.$$

Material: GG-30 according to DIN 1691 or DIN EN 1561.

Geometry and Dimensions: Effective wall thickness at the reference point (node 99) $s \approx 32 \text{ mm}$.

Surface: Skin, $R_z = 200 \mu\text{m}$

Task: Assessment of the fatigue limit

Method of calculation: Route 2, non welded

Analysis

Step 1: No defect

Step 2: Service condition: Constant amplitude cyclic stresses

$$\begin{aligned} \sigma_{1,a} &= 18.6 \text{ MPa}, \sigma_{1,m} = 15.0 \text{ MPa}. \\ \sigma_{2,a} &= 6.2 \text{ MPa}, \sigma_{2,m} = 5.0 \text{ MPa} \\ \sigma_{3,a} &= 0, \quad \sigma_{3,m} = 0. \end{aligned}$$

Step 3: No corrosion, no high temperature

Step 4: To be solved as part of the next steps

Step 5: Fatigue resistance data specification

Material Properties: Tensile strength for the standard dimension is $R_m = 300 \text{ MPa}$.

Technological size factor: $d_{\text{eff}} = 2s = 2 \cdot 32 \text{ mm} = 64 \text{ mm} \dots (\text{Tab. 7.6})$

$$K_{d,m} = 0.80 \tag{7.20}$$

Tensile strength of the component: $R_m = 0.80 \cdot 300 \text{ MPa} = 240 \text{ MPa}$.

Material fatigue limit for completely reversed normal stress, σ_w

$$\begin{aligned} R_m &= 240 \text{ MPa}, \\ f_{w,\sigma} &= 0.30, \end{aligned} \dots (\text{Tab. 7.5})$$

$$\sigma_{w,zd} = 0.30 \cdot 240 \text{ MPa} = 72.0 \tag{7.19}$$

$$\chi_{\sigma 1} = \frac{1}{7.7 \text{ mm}} \cdot \left(1 - \frac{10.0}{18.6} \right) = 0.0600 \text{ mm}^{-1} \tag{7.24}$$

$$\chi_{\sigma 2} = \frac{1}{7.7 \text{ mm}} \cdot \left(1 - \frac{5.3}{6.2} \right) = 0.0189 \text{ mm}^{-1}$$

$$a_G = -0.05, \quad b_G = 3200, \dots (\text{Tab. 7.7})$$

$$n_{\sigma 1} = 1.179, \quad n_{\sigma 2} = 1.056 \tag{7.26}$$

Surface roughness factor

$$\begin{aligned} R_m &= 240 \text{ MPa}, \\ R_z &= 200 \mu\text{m}, \end{aligned}$$

$$a_{R,\sigma} = 0.06, \quad R_{m,N,\min} = 100 \text{ MPa} \dots (\text{Tab. 7.8})$$

$$K_{S,\sigma} = 0.906 \tag{7.27}$$

Combined effect of technological size, notch, and roughness effect

$$\begin{aligned}\sigma_{1,WK} &= 240\text{MPa} \cdot 0.3 \cdot 1.179 \cdot 0.906 = 76.9 \\ \sigma_{2,WK} &= 240\text{MPa} \cdot 0.3 \cdot 1.056 \cdot 0.906 = 68.9\end{aligned}\quad (7.28)$$

Mean stress effect

$$\begin{aligned}a_M &= 0, \quad b_M = 0.5, \dots (\text{Tab. 7.9=}) \\ M_\sigma &= 0.5.\end{aligned}\quad (7.31)$$

Mean stress factor for direction 1

$$\begin{aligned}\sigma_{1,\min} &= 15\text{MPa} - 18.6\text{MPa} = -3.6\text{MPa} \\ \sigma_{1,\max} &= 15\text{MPa} + 18.6\text{MPa} = 33.6\text{MPa} \\ R_{\sigma 1} &= -3.6/33.6 = -0.107.\end{aligned}$$

Because of $-\infty < -0.107 \leq 0$ field II applies:

$$K_{AK,\sigma 1} = \frac{1}{1 + 0.5 \cdot 15/18.6} = 0.713. \dots \text{Fig. 7.27}$$

Mean stress factor for direction 2

The stress ratios of both directions agree:

$$\begin{aligned}R_{\sigma 2} &= R_{\sigma 1} = -0.107, \\ K_{AK,\sigma 2} &= 0.713.\end{aligned}$$

The amplitude of the component fatigue limit results from the mean stress factor and the component fatigue limit for completely reversed normal stress:

$$\begin{aligned}\sigma_{1,AK} &= 0.713 \cdot 1\text{MPa} = 55\text{MPa}, \\ \sigma_{2,AK} &= 0.713 \cdot 1\text{MPa} = 49\text{MPa}\end{aligned}\quad (7.32)$$

Step 6: Fatigue assessment:

For constant amplitude loading

$$K_{BK,\sigma 1} = K_{BK,\sigma 2} = 1.$$

The amplitude of the component variable amplitude fatigue strength results from the variable amplitude fatigue strength factor and from the amplitude of the component fatigue limit for normal stress.

$$\begin{aligned}\sigma_{1,BK} &= 1 \cdot 55 \text{ MPa} = 55\text{MPa}, \\ \sigma_{2,BK} &= 1 \cdot 49 \text{ MPa} = 49\text{MPa}.\end{aligned}\quad (7.33)$$

For severe consequence of failure, for no regular inspection and for castings tested non-destructively

$$\gamma = 1.9.$$

chosen by experience. Refer to Annex H.

Degrees of utilisation

Individual types of stress, direction 1 and 2

$$\begin{aligned} a_{BK,\sigma1} &= \frac{18.6}{55/1.9} = 0.64 < 1 \\ a_{BK,\sigma2} &= \frac{6.2}{49/1.9} = 0.24 < 1 \end{aligned} \tag{7.34}$$

Combined type of stress: $a_{BK} = 0.64 + 0.24 = 0.88 < 1$

The assessment limit is achieved.

13.3.3 Fatigue Route 3, for Non-Welded Components: Local Stress-Strain Approach

Specimen :	Tension compression sample
Loading :	Cyclic, constant and variable amplitude loading
Material :	20MV6 steel tube
Defect :	Nominal and notch stresses
Temperature :	Ambient

The purpose is to compare the assessed fatigue life time using **ROUTE 3** with test results.

General data: The sample is a 20MV6 steel tube tested in tension-compression at mid length of which an axisymmetric notch has been cut (Figure 13-64).

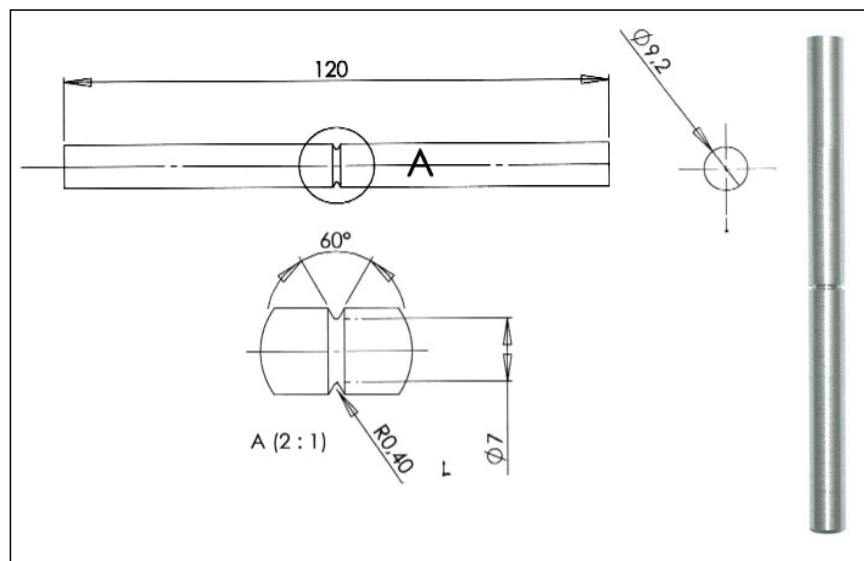


Figure 13-64: Notched cylindrical sample geometry in 20MV6 steel

Material: The mechanical properties are the following:

$R_{e0,2\%}$ (MPa)	R_m (MPa)	E (MPa)	RA(%)	$\sigma_D^{R=-1}$ (MPa)
525	735	210 000	23	362

The chemical composition is given as following:

Element	C	Mn	V	Si	S	P
Max percentage (in mass)	0,22	1,7	0,15	0,5	0,04	0,04

Loading - I: Constant Amplitude: A first series of tests were performed at constant amplitude.

Step 1: Detected flaws: The assessment concerns a laboratory sample, so the structure is free of flaws.

Step 2: Service condition, Stress - Strain Range: Table 13.28 shows the applied nominal stress (pure alternating tension-compression loading, $R=-1$).

Table 13.28 – Tested sample and nominal applied loads with R=-1.

Sample Reference	σ_{max} (MPa)
1	160
2	
3	
4	
5	
6	
7	180
8	200
9	
10	

The stress coefficient factor of the notch is: $K_t = 2,95$

Step 3: Environmental issues: The structure is not subjected to corrosion effects.

Step 4: Threshold for fatigue assessment: Not applicable.

Step 5: Elasto plastic fatigue resistance data: The cyclic hardening curve has been determined by tests and is given in Figure 13-65.

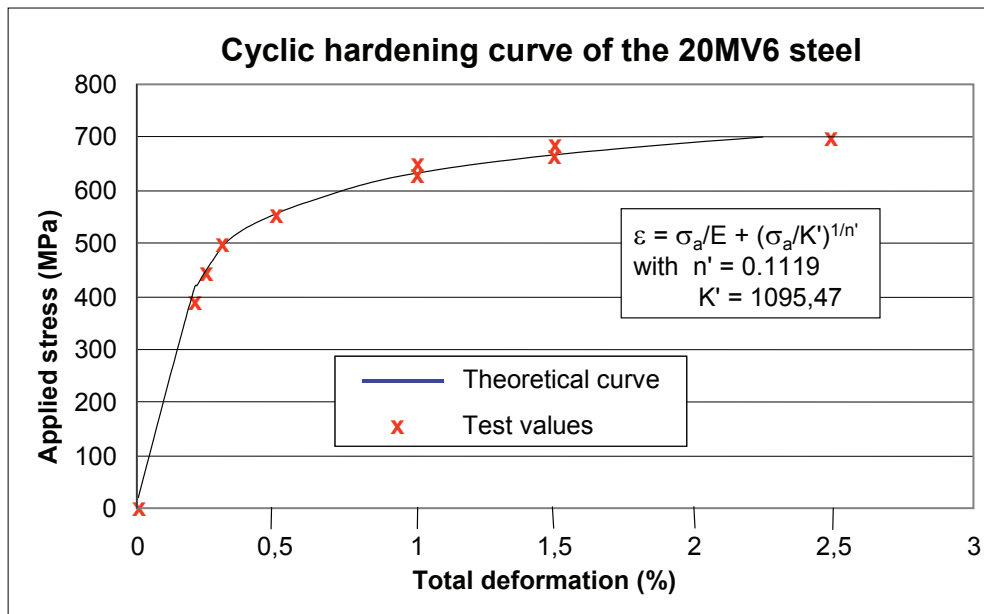


Figure 13-65: Cyclic hardening curve of the 20MV6 steel

The Manson-Coffin curve has been determined by formula and tests. The results are given in Figure 13-66.

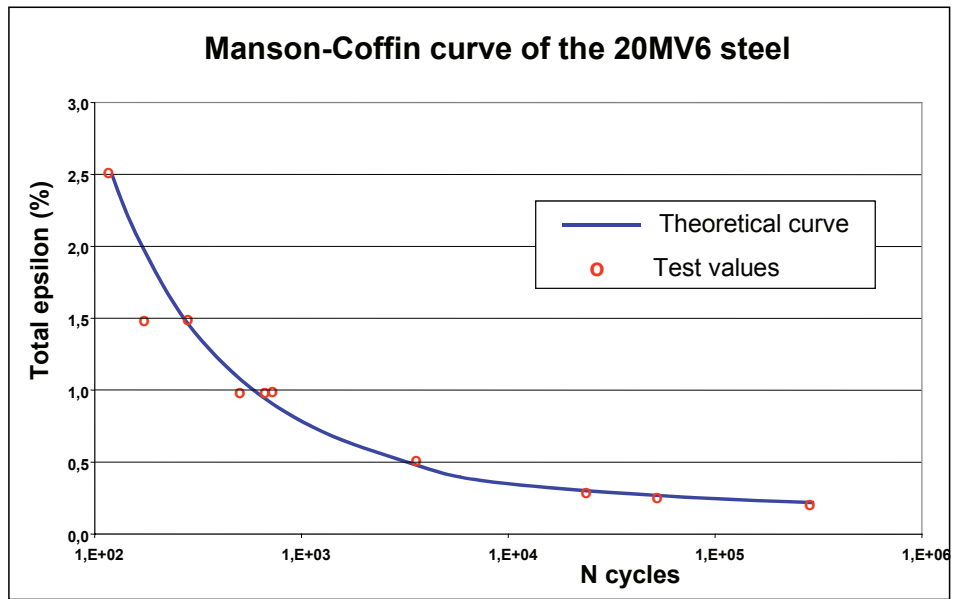


Figure 13-66: MANSON-COFFIN curve of the 20MV6 steel

From those data, the MANSON-COFFIN equation coefficients, i.e., ϵ'_f , b, c, can be calculated:

$$\epsilon_a = \frac{\sigma'_f}{E} (2N)^b + \epsilon'_f (2N)^c \quad \text{which provides the following values:}$$

σ'_f (MPa)	ϵ'_f	b	c
1036	0.5962	-0.07	-0.63

Step 5 Cumulative fatigue life calculation: The calculations have been performed using the software n'Soft (Neuber method) applicable to constant amplitude loadings. The resulting life time curve is given in Figure 13-67.

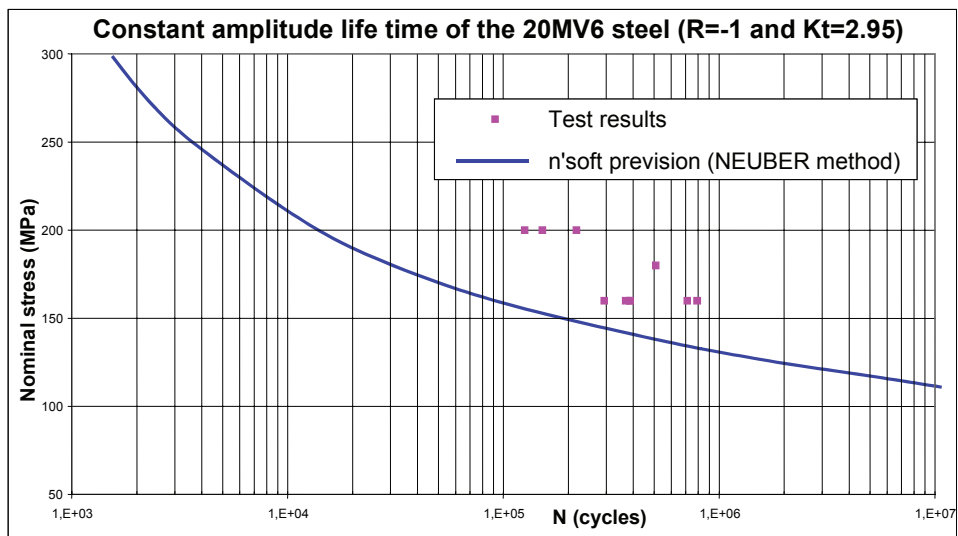


Figure 13-67: Life prediction curve and fatigue test results

Significance of Results: The fatigue test results obtained in a pure alternating tension-compression loading test ($R = -1$) are given in Table 13.29 and Figure 13-67. The values obtained from the Neuber local approach appear very conservative compared with the test results. At 160 MPa, the calculation gives 72 280 cycles, whereas the mean of the test is 456 959 cycles: the ratio is 6.3 with respect to calculation.

If at this level we take into account the dispersion, the life time can be calculated at 10% probability of failure and a confidence interval of 95%. The life time obtained is then of the order of 75 000 to 77 000 cycles. With respect to this value, the calculated value becomes "slightly" conservative.

At 200 MPa, the ratio versus the calculated value is greater: a mean of 160 826 cycles versus 10 834 cycles calculated, i.e., a ratio of 14.8. But this ratio has to be considered with great care: the small number of tests performed at 200 MPa may provide results whose distribution is not representative of reality at this level.

Higher numbers of tests would have allowed comparison of the modelling versus a "reliable" experimental life time. However it can be concluded from these tests that the local approach looks conservative in terms of predicted life time.

Table 13.29 – Measured life time at failure.

Sample Reference	σ_{max} (MPa)	Number of cycles
1	160	293 244
2		791 386
3		368 818
4		385 559
5		712 001
6		387 493
7	180	508 255
8	200	151 628
9		125 553
10		218 507

Loading - II: Variable amplitude loading: A second series of tests was performed at random amplitude.

Step 1: Detected flaws: The assessment concerns a laboratory sample, so the structure is free of flaws.

Step 2: Service condition:, Stress - Strain range

The tests have been performed applying a typical distribution (lateral CARLOS from the automotive industry) to the notched sample. A block comprises 95 180 cycles. The selected main maximum loading level corresponds to a nominal stress of 400 MPa plus one test at 450 MPa (σ_{max} of the distribution). The stress coefficient factor of the notch is: $K_t = 2.95$

Step 3: Environmental issues: The structure is not subjected to corrosion effects.

Step 4: Threshold for fatigue assessment: Not applicable.

Step 5: Elasto Plastic fatigue resistance data: The cyclic hardening curve and Masson-Coffin curves are the same as those given in Figure 13-65 and Figure 13-66.

Step 5: Cumulative Fatigue life calculation: The calculations have been performed using the software n'Soft (Neuber method) applicable to variable amplitude loadings. Two corrections, S.W.T and Morrow, have been applied. The resulting life time curves are given in Figure 13-68.

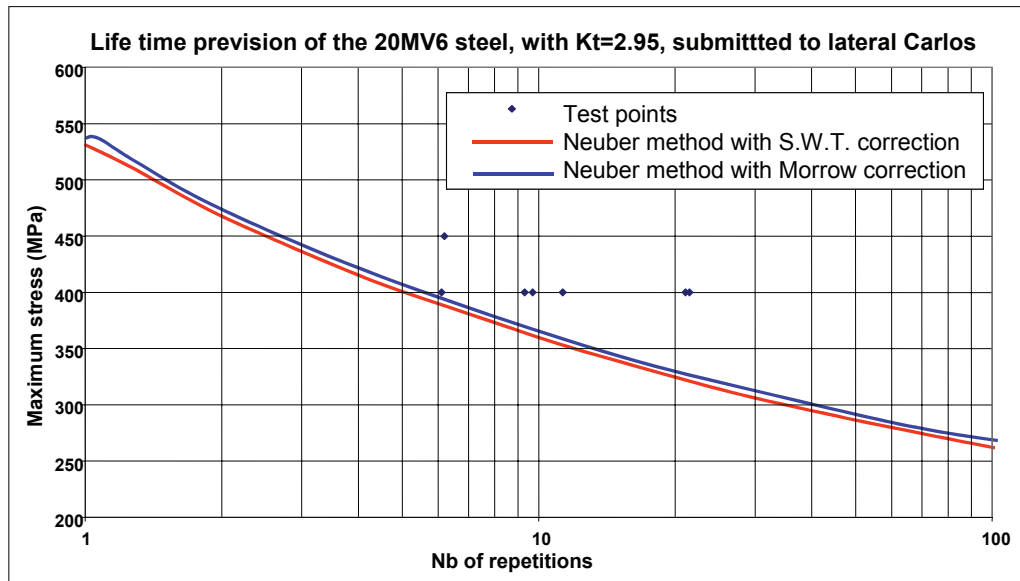


Figure 13-68: Fatigue test results with the CARLOS distribution

Significance of Results: The fatigue test results obtained in a pure alternate tension-compression loading test ($R = -1$) are given in Table 13.30 and in Figure 13-68.

Table 13.30 – Test results at failure with CARLOS distribution (a block includes 95 180 cycles).

σ_{\max} (MPa)	Sample reference	No. of half cycles	No. of blocks	Duration
400	1AV	2 153 136	11,31	49h33
	2AV	4 015 566	21,09	112h43
	4AV	1 846 459	9,70	54h22
	5AV	1 162 973	6,11	36h06
	6AV	1 775 011	9,32	50h27
	7AV	4 095 823	21,52	141h20
450	3AV	1 180 288	6,20	36h49

The local approach associated with the NEUBER rule provides a conservative evaluation of the life time of the 20MV6 steel notched samples, whatever the stress level. At 400 MPa, the estimation provides a life time of about four blocks, whereas the mean test value is 11.9 blocks. The estimation is therefore conservative by a ratio of about 3 versus the test mean. If the life time is calculated for a failure probability of 10% with a confidence interval of 95%, the number of blocks is 7.9, i.e., a ratio of 2 between the estimated and the real life time. The prediction method remains conservative by a ratio of 2 in terms of life time.

Bibliography

- [1] I. HUTHER – Comportement en fatigue des assemblages vissés Rapport CETIM 1C0230, Dec. 1999
- [2] J.F. FLAVENOT, I. HUTHER, V. BLONDEL – Assemblages vissés sollicités en fatigue, application aux fonds de vérins haute pression Rapport CETIM 1C0231, Oct. 200

13.3.4 Specific Applications: Structural Stress Approach on Welded Structures

The mesh-insensitive structural stress method (see Section 7.1 in FITNET FFS Procedure Fatigue Module) can be applied for performing fatigue evaluation of welded components. For a given engineering component, the fatigue evaluation procedure can be divided into two steps: 1) Calculation of the structural stresses (σ_s) under a given unit load condition using a typical finite element model; 2) Obtaining the fatigue life from the master S-N curve by converting the structural stress range to the corresponding equivalent structural stress range ΔS_s .

Specimen :

Yagi's component tests

Further details are contained in

- 1) SR202 of Shipbuilding Research Association of Japan, Fatigue Design and Quality Control for Offshore Structures, 1991 (in Japanese), also published as International Institute of Welding (IIW) Document: IIW XIII-1414-91, 1991 and
- 2) Dong, P., "A Robust Structural Stress Method for Fatigue Analysis of Ship Structures," Proceedings of the 22nd International Conference on Offshore Mechanics and Arctic Engineering, June 8-13, 2003, Cancun, Mexico

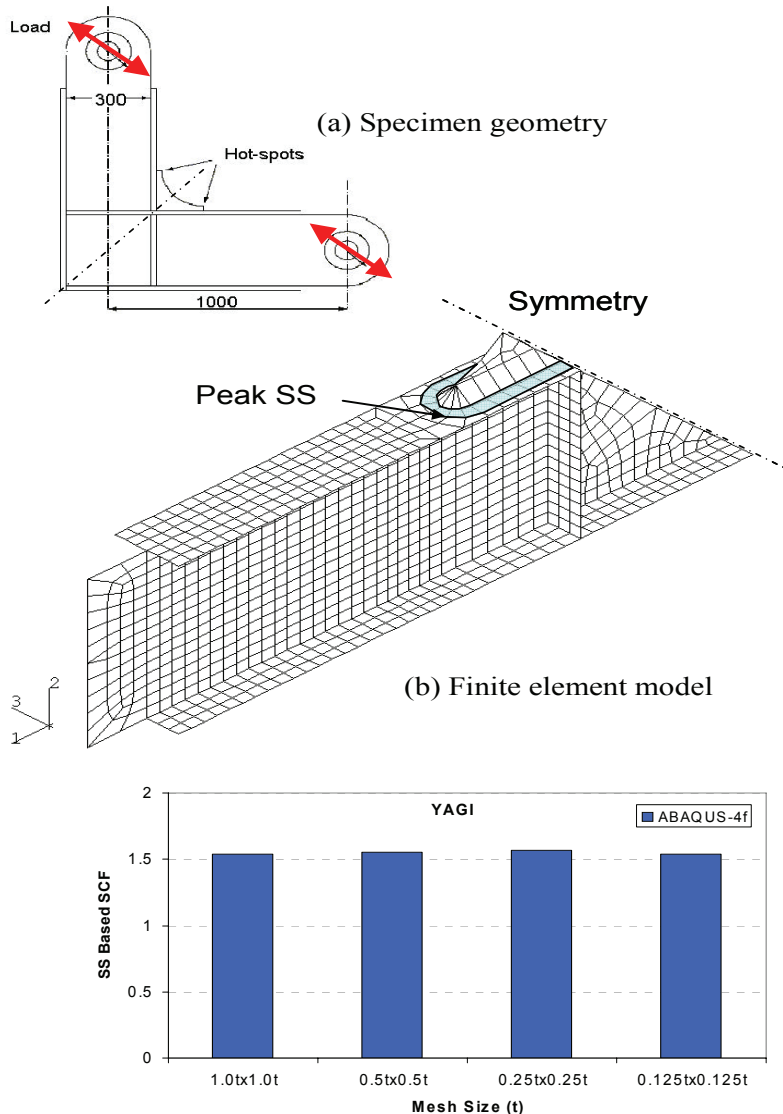


Figure 13.69 Structural Stress Calculation on Yagi's tests.

Inputs: To perform fatigue evaluation of a welded component using the mesh-insensitive structural stress method, the information required is essentially same as that in using other FEA based method, except that in performing FEA, balanced nodal forces are requested, instead of nodal stresses.

Geometry: The details are demonstrated by using an example called Yagi's component tests, Figure 13.69.

Analysis: The structural stress method and the master S-N curve will be used to evaluate fatigue lives:

1) A plate finite element model is shown in Figure 13.69, where the fillet weld between the attachment and I beam flange is represented with a row of 45 degree angle inclined elements. Under the given loading conditions, the element nodal forces surrounding the entire weld toe line are extracted from a finite element analysis.

2) The structural stresses for all the nodes describing the curve formed by the weld toe are then calculated using a JIP structural stress post-processor. The definition of the structural stresses is shown in equation:.

$$\sigma_s = \sigma_m + \sigma_b = \frac{f}{t} + \frac{6m}{t^2}$$

where t is the plate thickness, σ_m is the membrane stress and σ_b is the bending stress components being calculated from line force (f) and line moment (m). In the post-processor, coordinate rotation, construction of the system of simultaneous equations relating nodal forces and moments to line force and moments are automatically carried out. Then, the structural stresses along the weld line are searched for the maximum value, as shown in Figure 13.69c. (Note: for element sizes less than $1 \times 0.1t$, the effects of the discontinuity at the intersection between the I beam web plate and the weld line on the structural stress becomes noticeable. A weld line ending at the hot spot should be used, instead of the entire weld line as shown.)

3) With the structural stress calculated under the given constant amplitude loading conditions, the loading ratio is then used to obtain the structural stress range needed to enter following equation;

$$r = \frac{|\sigma_b|}{|\sigma_m| + |\sigma_b|}$$

At the peak structural stress range location shown in Figure 13.70, the plate thickness t is the flange thickness. At the bending ratio $r = \Delta\sigma_b / \Delta\sigma_s = \sigma_b / \sigma_s$, $I(r)$ is then determined from under load controlled conditions. Then, the equivalent structural stress range ΔS_s is fully determined.

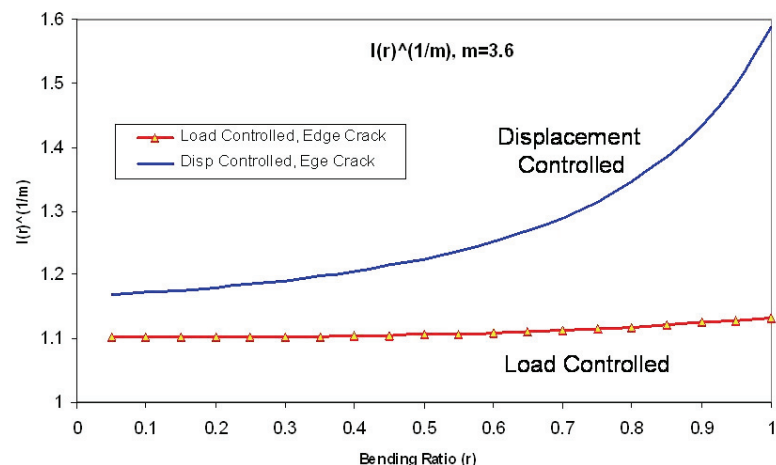


Figure 13.70 $I(r)$ functions assumed an edge crack ($a/t = 0.7$, $m = 3.6$).

The equivalent structural stress range is determined by:

$$\Delta S_s = \frac{\Delta \sigma_s}{t^{2m} \cdot I(r)^{\frac{1}{m}}}$$

- 4) With the given equivalent structural stress range ΔS_s , The master S-N curve in Figure 13.71 can be used to estimate the mean life under constant amplitude loading conditions.

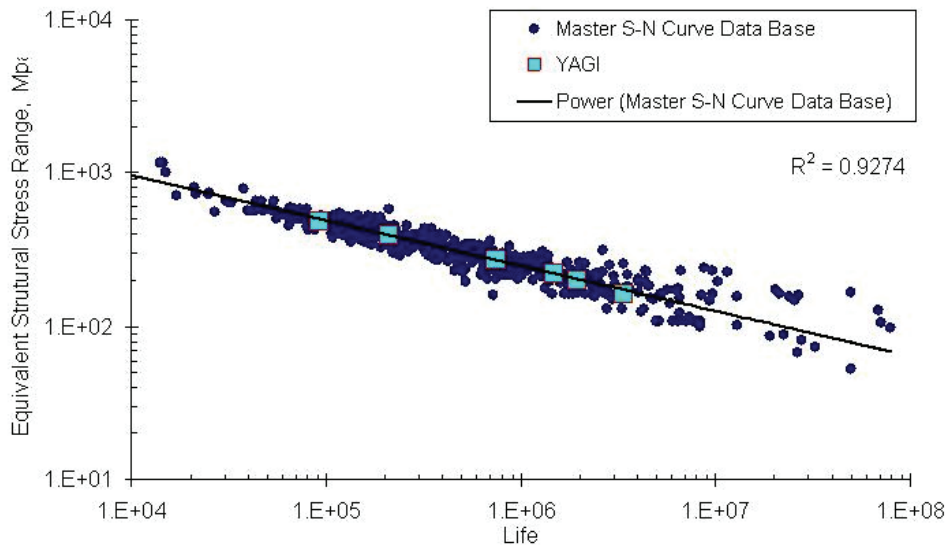
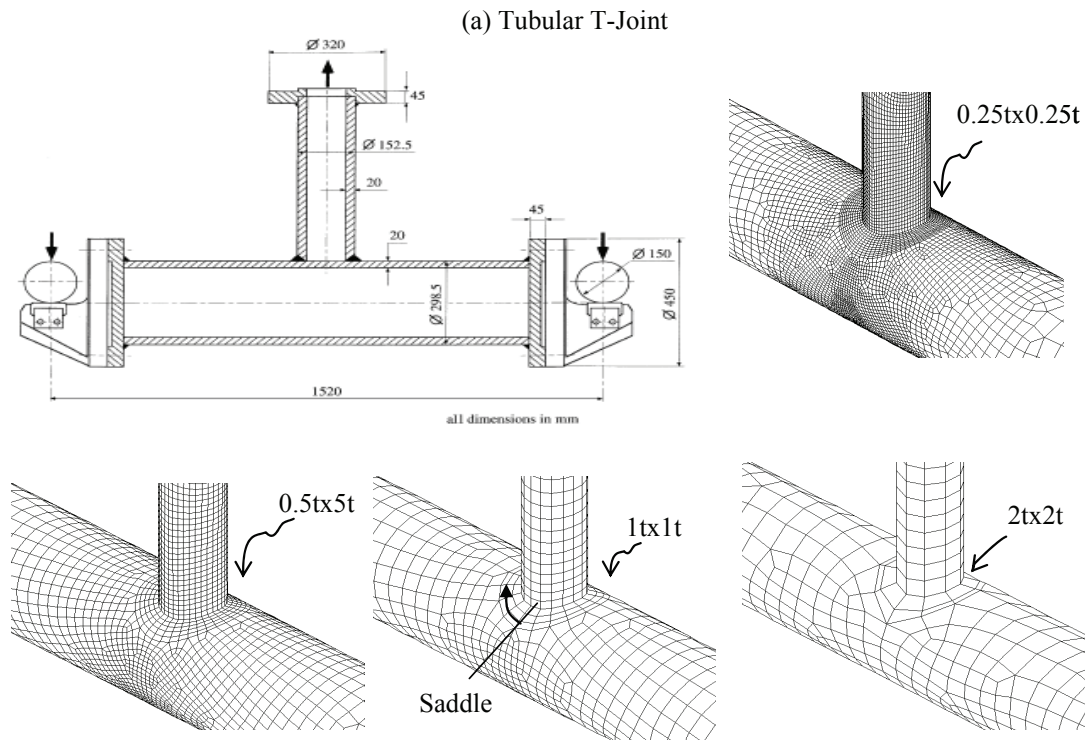


Figure 13.71 – Fatigue life evaluation of Yagi’s specimens using the structural stress based master S-N curve approach (note that the equivalent structural stress range has a reference thickness of 1mm).

5) For known test results, such as the Yagi’s tests shown in Figure 13.71, the test results can be alternatively plotted against the master S-N curve for each pair of ΔS_s -N corresponding to each test condition. The actual test data for the component shown in Figure 13.69a are approximately located within the mean line of the master S-N curve, indicating that the life estimation using the mesh-insensitive structural stress method shows a good agreement with the actual test data. If the structural stress ranges versus tested lives are plotted and if the new structural stress approach is valid, the S-N data by Yagi should be located within the scatter band in the S-N curves proposed in the FITNET Fatigue Module. Indeed, Figure 13.71 summarizes such a comparison. The five square symbols are the actual S-N data from Yagi’s tests and all small circle symbols are the S-N data same as those used to derive the mean master S-N proposed curves.

Further Reference and Case Studies for Structural Stress:

Dong, P., “Mesh-Insensitive Structural Stress Method and Master S-N Curve Development for FPSOs,” Proceedings of this conference, OMAE-FPSO’04-0021, Houston, TX, Aug 30-Sept. 2, 2004.



(b) Four FE models with different elements sizes at weld location ($t=20\text{mm}$)

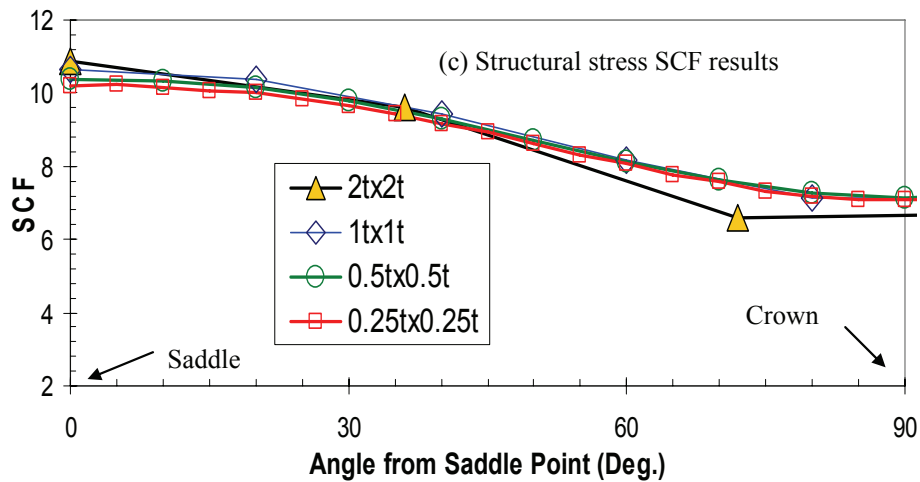


Fig. 2: Structural stress calculations for a tubular T joint (a) T-joint geometry and loading conditions; (b) Four FE models with different element sizes; (c) Comparison of the current structural stress results along weld toe at chord

Figure 13.72 – Structural stress calculations for a tubular T joint. a) T-joint geometry and loading conditions, b) four FE models with different element sizes and c) comparison of the current structural stress results along weld toe at chord

13.3.5 Application of Fatigue Improvement Techniques to Welded Structures

The two following case studies illustrate the main uses of fatigue improvement methods: a) to repair ageing structures that experience fatigue cracking, b) to upgrade and reinforce new structures that have been found to have inadequate fatigue strength due to structural changes or increased loads.

Case 1: Veslefrikk B platform: *Veslefrikk* is a floating platform originally designed for exploration drilling. Fatigue cracking started after only 6 years of service and a major retrofitting program was implemented to increase the production capability of the platform and to repair and strengthen the structure to meet an objective of additional 20 years service life. It was built as an exploration vessel and later converted to a production platform and moored to a fixed platform. When moored the structure is exposed to waves from all directions in contrast to exploration platforms that are operated more as ships and are headed into the wave direction. Waves hitting in a sideways direction give particularly high local loads in the platform structure. After six years of service fatigue cracks were detected in submerged parts of the structure. The cracks were repaired from the inside while the platform was in operation, using habitats on the outside. More cracks were found later and several repairs were made to the hull plate structure while the platform was raised in the sea to enable dry welding repairs to be made inside protective enclosures. In the summer of 1999 a major retrofitting program was implemented to increase the production capability of the platform and to repair and strengthen the structure to meet an objective of an additional 20 years service life.

The platform highly stressed areas are at the intersections between the horizontal brace and column and pontoon. Structural modifications and several weld improvement techniques were used to extend the fatigue life of the platform structure. A fatigue test program was implemented to verify the high levels of fatigue strength that were required to ensure adequate life for critical welded details.

The transitions between the vertical columns and the pontoons were particularly highly stressed as shown in the results of a finite element (FE) analysis of this area (Figure 13.72). The stresses were so high that the corners were cut out and replaced by steel inserts. The butt welds between the steel castings then became fatigue critical and had to be flush ground. Structural modifications and several weld improvement techniques were used to extend the fatigue life of the platform structure. A fatigue test program was implemented to verify the high levels of fatigue strength that were required to ensure adequate life for critical welded details.

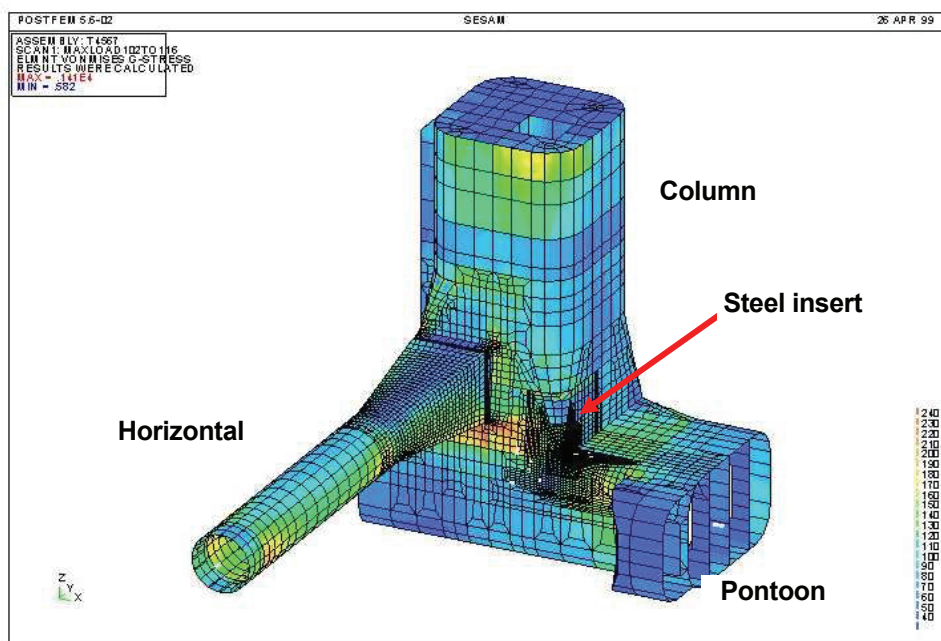


Figure 13.72 – Finite element analysis results for highly stressed areas.

As a result of extensive FE analyses the structural details listed in Table 13.31 were signaled out for repair and upgrading. For the most critical details fatigue testing programs were set up to verify the improvements.

Table 13.31 – Repair of the Veslefrikk B platform

Part of structure	Type of detail	Improvement methods
Columns and pontoons	Corners at column-pontoon intersection	Cast steel inserts; grinding of butt welds
	Selected inside fillet welds in columns	Weld toe grinding
Horizontal brace	Girth welds, inside and outside	Weld toe grinding
	Ends of longitudinal stiffeners	Weld toe grinding and needle peening
	Cope holes	Weld toe grinding and needle peening
	Cover plates	Removal and toe grinding
	Attachments for cable ladders etc.	Removal and toe grinding.

Types of improvement methods used: Generally burr grinding was used to improve fatigue strength; however, for some details with short calculated fatigue lives grinding was followed by needle peening to minimize the risk for fatigue cracking. The choice of improvement method was determined by the level of improvement needed, i.e. the type of detail and the magnitude of stresses it would be subjected to.

Equipment for repair and life improvement: Standard pneumatic rotary burr grinders as shown in Figure 13.70 were used. Two basic types of tools were used, a cylindrical burr with a hemispherical tip, and a spherical tool. The choice of burr type was left to the operator, following practice runs on different types of welds. In the trials it was generally found that using a small diameter spherical burr was useful in establishing a groove to the required depth, positioned directly at the weld toe, especially for fillet welds with steep flank angles. A cylindrical burr with the required diameter was then used to finish a smooth groove with a radius that was equal to or larger than the specified radius. This groove was easy to inspect for depth and for any remaining traces of undercuts or embedded defects.

Standard arc gouging equipment was used to remove the major part of the cover plate fillet welds. The remaining parts of the welds were ground flush with disk grinders, while the toes of the welds were burr ground. The disk grinders used for removing weld material were also standard tools that are available in fabrication yards. The procedure for anode plate removal is described in more detail in the next section.

Examples of treated details are shown in Figure 13.69 and Figure 13.70.

Procedures: Grinding and peening was performed in accordance with the IIW recommendations. The burr diameter is scaled to the plate thickness to ensure that an adequate toe radius is obtained. Grinding has to be performed to a minimum depth of 0.5 mm in order to remove all weld toe defects.

A depth gauge was used by operators and inspectors to ensure that the minimum groove depth was obtained. This gauge worked well on flat surfaces but is more difficult to use on curved plates. Details treated by needle peening were inspected for complete coverage.

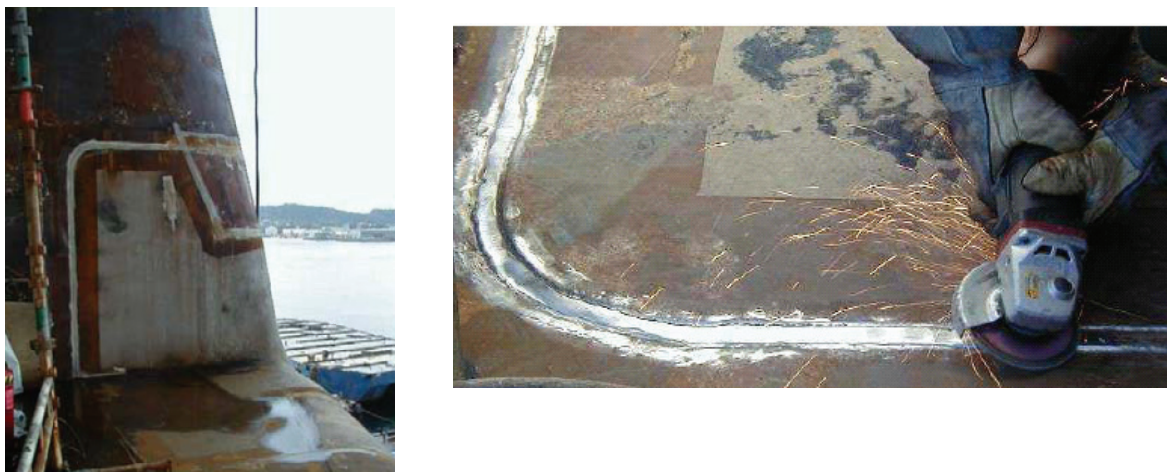


Figure 13.69 – Steel casting used at corners of columns and pontoons. a) Welded in place, b) grinding of butt welds.



Figure 13.70 – Attachment for cable ladder inside brace: toe ground and needle peened.

Operator training and quality control: The skills required to perform the types of grinding and peening operation that were planned in the *Veslefrikk B* project are not normally available in fabrication yards; a training program for operators and inspectors was therefore set up. Since improvement work is noisy and tedious, and attention to details in the procedure is crucial, a high priority was given to ensure that the operators and inspectors would understand the basic principles and purpose of the repair and upgrading project. The content of the one-day course included the following:

- Motivation and understanding of importance of improvement work.
- Overview of platform history and fatigue criticality in project
- Effect of local weld geometry on fatigue strength, and importance of good workmanship and quality control
- Explanation of procedures for specific weld details by specially trained welding engineers.
- Practice various treatments in welding shop.

Fatigue tests: The effectiveness of the weld improvement methods that were applied to the simple types of plate welds in the horizontal brace is well documented in the literature for rolled steel plate material. However, similar data for double sided butt welds of the type used for the cast steel inserts were not available. A fatigue-testing program on as-welded and improved welds was therefore implemented. The main objectives of the program were a) to verify that the fatigue strength of as-welded joints would satisfy the D-curve in the DnV rules (FAT 90), and b) to determine the increase in fatigue strength that could be obtained by using two types of post-weld improvement methods. The D curve is the S-N curve that applies to this type of butt weld welded from two sides. The specimen and the test rig are shown in Figure 13.71.

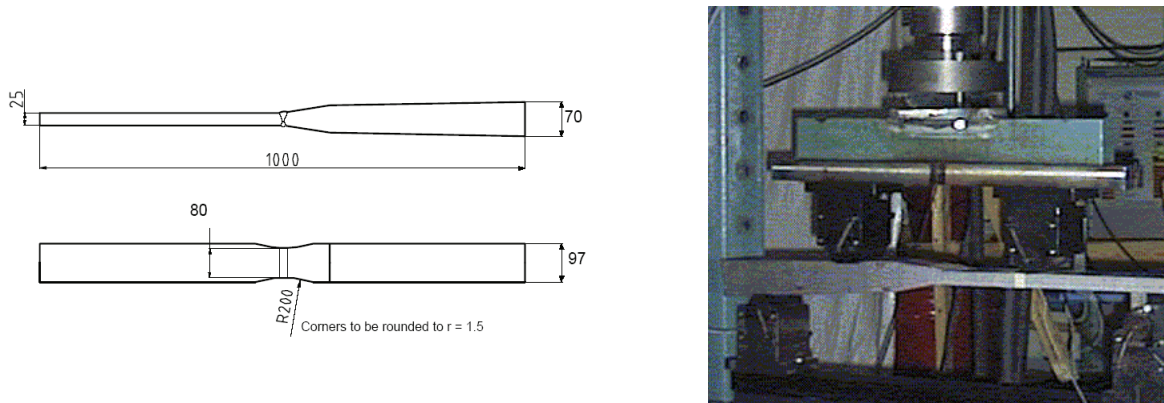


Figure 13.71 – Specimen and fatigue test rig.

The results in **Fehler! Verweisquelle konnte nicht gefunden werden.** clearly indicate that the data support the D design curve, also the untreated weld.

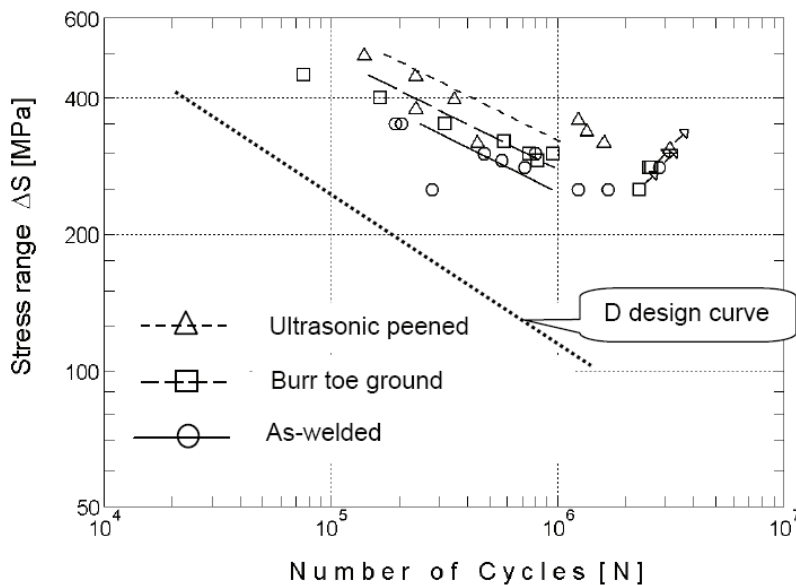


Figure 13.80– Fatigue test results.

Case 2: Troll C platform

This case concerns the upgrading of a platform during the late stages of construction. The modifications were necessitated by the inadequate fatigue strengths that were calculated after detailed FE analyses were performed to check for the effects of added weight.

Details requiring improvement: Two generic types of details needed fatigue strengthening: bellmouths and attachments for pipes.

Bellmouths, are large bell-shaped penetrations in the lower part of the hull through which risers (production pipes for oil and gas) are pulled from the sea floor. These penetrations create high stresses in the hull plates and in the weld itself. Figure 13.72 shows critical areas of the bellmouths. Stress analyses showed that not only the weld toes, but the entire weld face was highly stressed, implying that a weld toe treatment might produce only a limited increase in fatigue life since fatigue cracks would initiate at inter-pass notches. Traditional weld toe treatments such as burr grinding, TIG dressing or hammer peening were thus ruled out. It was decided to use a combination of grinding and peening techniques, involving grinding the weld face and weld toes, and then needle peen the ground area.



Figure 13.72 – a) Bellmouths with highly stressed regions that have been examined by magnetic particle inspection (MPI) in preparation for weld improvement by grinding and needle peening and b) needle peening of bellmouth weld.

The following procedure was adopted:

1. Grind weld face and toes, finishing with a cylindrical abrasive wheel.
2. Check for defects by Magnetic Particle Inspection.
3. Needle peen until surface completely covered, using the equipment shown in Figure 14. Use the quality control criterion of 200% coverage as used for shot peening.
4. Document result by high resolution photographs.

The peening procedure, and an improvement factor of 4 on life was approved by the classification company DNV, giving acceptable calculated fatigue lives for all details treated.

Pipe support attachments. Extra attachments are sometimes added late during of the construction periods and might therefore escape the initial fatigue calculations. Additionally, attachments are often placed in the worst possible places, e.g. on the flanges of beams that are subjected to bending. The fatigue classification may therefore change from one of the highest to one of the lowest.

Two types of pipe supports were welded to deck beams, flat bars attached to the top of the bulb and angle profiles welded to the sides of the beam. Following trials with grinding and needle peening, hammer peening was chosen because of ease of application in confined areas where large tools could not be used. Exploratory fatigue test also indicated that very large improvements in fatigue could be obtained by hammer peening. To facilitate the peening process a steering groove was established, using a small burr with a diameter of 5 mm.

The peening tool, is small, the weight is only about 0.5 kg.



Figure 13.73 – Pipe attachments, flat bar welded to top of beam and angle profile welded to side of beam.

Fatigue testing programme: In order to verify the improvements resulting from the hammer peening procedure established for the pipe support welds, a testing program for deck beams with attachments was carried out. The detail in Fig. has a higher stress concentration factor and a lower fatigue strength than the flat bar in Figure 13.73. Testing was performed on this detail. Full scale beams of 300 mm depth were welded with the two types of attachments. The material was the same as specified for the platform; with a minimum yield strength of 355 MPa. Beams with attachments in the as-welded condition were tested for reference. The majority of the test specimens were strain gaged to monitor applied loads.

All fatigue tests were made in air under constant amplitude, three point bending loading, at a stress ratio of $R = 0.1$, using a servo-hydraulic fatigue testing machine. The tests were conducted under load control conditions, at frequencies between 3 and 5 Hz. Failure was defined to have taken place when the deflection of the specimen became large enough to exceed the actuator stroke limits; generally this would occur when the crack was approximately 50 mm long. Test data for as-welded angle bracket data are shown in Figure 13.74. The design line estimated from the test results is also shown.

Test data for hammer peened angle attachment welds are shown in Figure 13.74, with the mean regression line from tests on as-welded beams and the design for AW and improved welds.

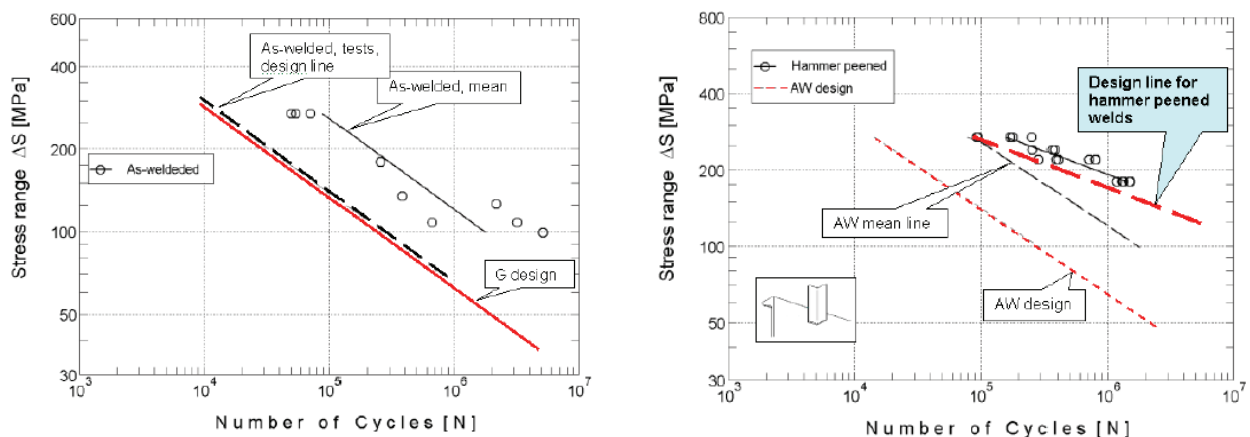


Figure 13.74 – Fatigue test results for beams with angle attachment welded to side of beam, a) as welded and b) weld hammer peened.

The S-N curve for the as-welded beams has a FAT of 50 MPa whereas the FAT for beams with hammer peened welds is 149 MPa, i.e. an improvement of nearly 200%. This is in line with other tests results for hammer peened welds reported in the literature.

Based on the procedures for the execution and quality control and quality assurance, DNV accepted needle peening and hammer peening for upgrading the fatigue strength of bellmouth and attachment welds in the Troll C project, thus avoiding costly structural changes and serious delays. These procedures are now part of NORSOK as an informative guidance.

13.4 Case Studies for CREEP

13.4.1 Flat Plate under Constant Tensile Load

Specimen :	Flat plate
Loading :	Constant tensile load
Material :	C-Mn steel
Defect :	Single edge crack
Temperature :	380°C

The current case study is presented in more details in the FITNET Tutorials, chapter 14.5.

A8.2 Example 1 - Flat plate with a Single Edge Crack Under Constant Load

A8.2.1 Establish cause of cracking and characterise initial defect (Step 1)

The first example is a C-Mn steel plate of width 100 mm with a single edge notch of depth 20mm. The defect is assumed to have been present from the start of high temperature operation.

A8.2.2 Define service conditions (Step 2)

The plate operates at 380°C under a constant tension, P, corresponding to a nominal stress

$$P/Bw = 100 \text{ MPa.}$$

A8.2.3 Collect materials data (Step 3)

Creep strain and creep rupture properties are related by an equation [A8.5] given by

$$\varepsilon_c(\sigma, t) = A' \{ \sigma / (\sigma_R + B') \}^{C'} \quad (\text{A8.1})$$

where A', B' and C' are constants and σ_R is obtained from rupture data as the stress to give failure in time t. These data are fitted by a polynomial relationship between failure time, t_r , and $x = \log_{10}\sigma$:

$$\log_{10} t_r = 10.68 + 153.2(a + bx + cx^2 + dx^3 + ex^4) \quad (\text{A8.2})$$

where a, b, c, d and e are constants. The constants in the equations (A8.1) and (A8.2) are given in Table A8.1 along with all other material properties required.

A8.2.4 Perform basic stress analysis (Step 4)

For steady creep loading, the following data are required:

Categorised (primary or secondary) stresses

Reference stresses for appropriate crack lengths

Stress intensity factors for appropriate crack lengths

In this case, the load is a primary membrane stress of 100 MPa.

The reference stress is calculated according to the limit load for this geometry [A8.6] given by

$$P_L = 1.155\sigma_y Bw \{1 - a/w - 1.232(a/w)^2 + (a/w)^3\} \quad (\text{A8.3})$$

where the plane strain Mises solution has been adopted. For component applications, the appropriate limit load (plane stress or strain, Tresca or Mises) must be chosen on the basis of geometrical constraint and the multiaxial creep rupture surface (see Section A2.3). From equation (A2.1) the reference stress is then

$$\sigma_{\text{ref}} = 0.866(P/Bw) / \{1 - a/w - 1.232(a/w)^2 + (a/w)^3\} \quad (\text{A8.4})$$

which has a value

$$\sigma_{\text{ref}}(a_0) = 114 \text{ MPa} \quad (\text{A8.5})$$

for the applied loading $P/Bw = 100 \text{ MPa}$ and initial crack size $a_0 = 20 \text{ mm}$.

For the single edge notch plate the handbook of Tada, Paris and Irwin [A8.7] gives a solution for K

$$K = \sigma(\pi a)^{1/2} F(a/w) \quad (\text{A8.6})$$

where $\sigma = P/Bw$

$$F = \left\{ \frac{\tan \theta}{\theta} \right\}^{1/2} \frac{0.752 + 2.02(a/w) + 0.37(1 - \sin \theta)^3}{\cos \theta} \quad (\text{A8.7})$$

where $\theta = \pi a/2w$. For the nominal stress of 100 MPa and $a/w = 0.2$, this gives

$$K = 34.3 \text{ MPa} \sqrt{\text{m}} \quad (\text{A8.8})$$

A8.2.5 Check stability under time-independent loads (Step 5)

This step is not considered in detail for this example. The check on time-independent failure would normally be based on short-term fault loadings rather than on the steady operating loadings. Reference may be made to R6 [A8.8] for examples of such calculations.

A8.2.6 Check significance of creep and fatigue (Step 6)

In this case, the load is constant and so fatigue is not a consideration. For the purpose of this example, it is assumed that creep is significant. Example 7 gives details of the tests that can be applied at this stage to determine whether creep, fatigue or creep-fatigue interactions are insignificant. In some cases, this may render further calculations unnecessary.

A8.2.7 Calculate rupture life (Step 7)

The rupture life for failure by continuum damage mechanisms, t_{CD} , is evaluated from equation (10.1) knowing the reference stress of equation (A8.5), and creep rupture data of equation (A8.2).

Hence, the time for failure by continuum damage

$$t_{\text{CD}} = 2.17 \times 10^6 \text{ h} \quad (\text{A8.9})$$

follows from equation (A2.19) and the creep rupture data, as depicted in Figure A8.1.

A8.2.8 Calculate incubation time (Step 8)

Creep crack incubation occurs when the creep strain accumulation, ε_c , at the reference stress of equation (A8.5) after a time t_i produces a critical crack opening displacement (Sections 10.4 and A2.6). Provided widespread creep conditions have been established, these terms are related by equation (A2.14) as:

$$\varepsilon_c = 0.5(\delta_i / R')^{n/(n+1)} \quad (\text{A8.10})$$

The length parameter R' is defined by equation (10.6), which requires the reference stress of equation (A8.5) and the elastic stress intensity factor K . Thus

$$R' = (34.3/114)^2 \text{ m} = 90\text{mm} \quad (\text{A8.11})$$

which is comparable to the section width. This is generally the case, although for small cracks R' is comparable to crack size and for deep cracks R' is proportional to the remaining ligament. From equation (A8.10), the creep strain for incubation is

$$\varepsilon_c = 0.5(0.06/90)^{n/(n+1)}$$

using the data in Table A8.1. As the creep data for this material are not in the form of a power law, a value of n is not available and hence $n/(n+1)$ is set equal to the exponent q in the creep crack growth law ($q = 0.85$ in Table A8.1), as suggested in Section A2.6. Whence

$$\varepsilon_c = 0.001 \quad (\text{A8.12})$$

This may be substituted into equation (A8.1) for $\sigma = 114$ MPa from equation (A8.5) to give $\sigma_R = 260$ MPa. From equation (A8.2), this corresponds to a rupture time of 20000 hours and hence the creep strain of 0.001 is accumulated in this time, i.e.

$$t_i = 20000 \text{ h} \quad (\text{A8.13})$$

as depicted in Figure A8.2. It may be noted that the elastic strain at the reference stress is

$$\sigma_{\text{ref}}(a_0) / E = 114 / 185000 = 0.0006 \quad (\text{A8.14})$$

which is less than the creep strain at incubation. Thus, the incubation time exceeds the redistribution time of equation (10.9) and the conservative expression of equation (A2.14) is valid. The more general case of incubation preceding the attainment of widespread creep conditions is illustrated by Example 2.

A8.2.9 Calculate crack size after growth (**Step 9**)

The procedure specifies that the extent of crack growth occurring during the desired additional service life should be calculated at this stage. As an additional life has not been specified in the present example, the crack growth calculations are carried out until the calculated crack growth rate is high and failure is essentially reached. Crack growth is calculated according to the methods of Section 10.7 using the C^* parameter as defined in Section 10.3:

$$C^* = \sigma_{\text{ref}} \dot{\varepsilon}_c (\sigma_{\text{ref}}, \varepsilon_c) R' \quad (\text{A8.15})$$

The reference stress and length parameter R' have already been calculated for the initial crack size in Sections A8.2.4 and A8.2.8. From Figure A8.2, the creep strain rate at the incubation time is:

$$\dot{\varepsilon}_c = 3 \times 10^{-8} / \text{hour} \quad (\text{A8.16})$$

Thus

$$C^* = 3 \times 10^{-7} \text{ MPa m h}^{-1} \quad (\text{A8.17})$$

at the incubation time. The corresponding crack growth rate using the crack growth law in Table A8.1 is:

$$\dot{a} = 1.8 \times 10^{-5} \text{ mm h}^{-1} \quad (\text{A8.18})$$

The non-dimensional parameter λ of equation (A2.27) is easily obtained from the calculations performed above as:

$$\lambda = 0.004 \quad (\text{A8.19})$$

so that equation (A2.28) indicates that correlations of crack growth rate with C^* can validly be used.

By assuming that the crack growth and creep strain rates are constant for a short time, Δt , the crack size and accumulated creep strain can be updated, and new values for reference stress and creep strain rate can be obtained from equation (A8.4) and equation (A8.1) assuming a strain hardening rule. The value of C^* can then be obtained with R' evaluated for the new crack size, leading to a new value for \dot{a} . In practice it is more convenient to implement these calculations by incrementing crack size or creep strain using R-Code [A8.9] or special purpose computer programs or spreadsheet calculations. R-Code will also calculate rupture life using a life fraction approach and incubation time. A special purpose computer program was used here to predict the crack size as a function of time shown in Figure A8.3.

A8.2.10 Recalculate rupture life after growth (**Step 10**)

As the reference stress is calculated at each stage of the crack growth calculations of Section A8.2.9, it is straightforward to recalculate t_{CD} from equation (A2.20). Even when the crack has grown to a depth of 35 mm, the reference stress of equation (A8.4) is only 160 MPa and this corresponds to a remaining life of 650000 hours. It is then clear from the timescale in Figure A8.3 that in this example creep crack growth rather than creep rupture is the dominant failure mechanism.

A8.2.11 Check stability of time-independent loads after growth (**Step 11**)

Again, these calculations are not considered in detail for this example.

A8.2.12 Assess significance of results (**Step 12**)

The following conclusions can be drawn for this example:

- The remaining creep rupture life was found to be high at all stages of the assessment, showing that creep crack growth, rather than creep rupture, is the dominant failure mechanism.
- Widespread creep conditions are achieved prior to the incubation time.
- An incubation time of $t_i = 20000$ hrs is predicted.
- The crack is predicted to grow by 15mm over 380000hrs.

Some aspects of the sensitivity of the analysis to crack incubation and growth data are illustrated for Example 3. The sensitivity of the calculated rupture life, t_{CD} , for the present example may be examined simply from equation (A8.2). This shows that the rupture life is reduced by a factor of 2 for a 25 per cent increase in the reference stress.

Table A8.1 - Material Properties for Examples 1-3

	Example 1 C-Mn	Example 2 C-Mn Weld	Example 3 $\frac{1}{2}\text{Cr}\frac{1}{2}\text{Mo}\frac{1}{4}\text{V}$
Young's modulus (MPa)	185 000	185 000	165 000
Creep Strain (σ in MPa)	Equation (A8.1) with $A' = 0.526$ $B' = 23.0$ $C' = 6.9$	θ - parameter fit of Fig A9.2.1-1	Equation (A8.33) with $\varepsilon_p = 0$ $\gamma = 6.4$ $D = 5.8 \times 10^{-29}$ $n = 10.6$
Creep Rupture (σ in MPa, t_r in hours)	Equation (A8.2) with $a = -1.26$ $b = 2.62$ $c = -2.06$ $d = 0.72$ $e = -0.094$	Time for creep strain to reach a ductility of 25%	Equation (A8.34) with $D' = 5 \times 10^{18}$ $v = 7$
Incubation COD (mm)	0.06	0.06	0.11
Crack Growth Rate in equation (7.2) A (\dot{a} in mh^{-1} , q C^* in MPa mh^{-1})	0.006 0.85	0.006 0.85	$0.003/\varepsilon_f$ 0.85

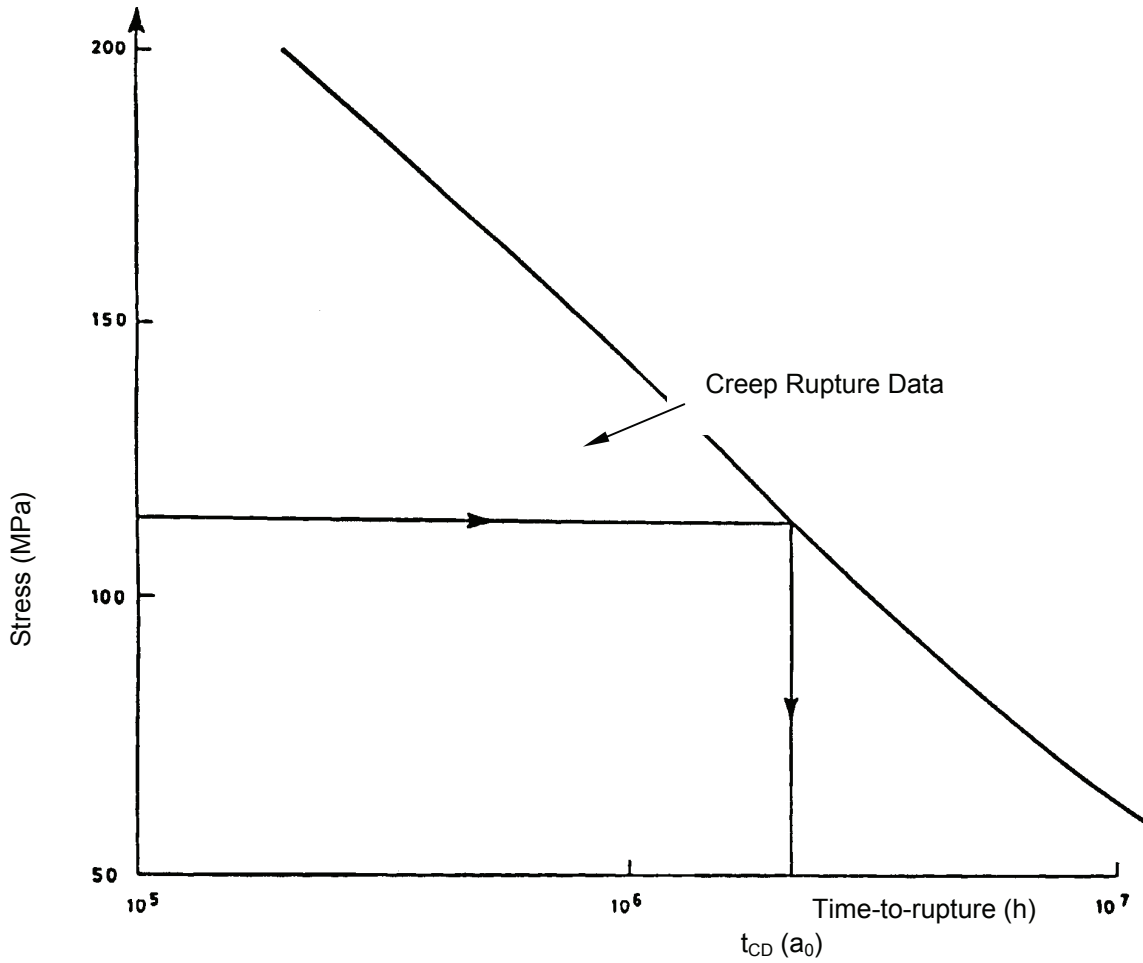


Figure A8.1 - Uniaxial stress/time-to-rupture data for Example 1, illustrating calculation of t

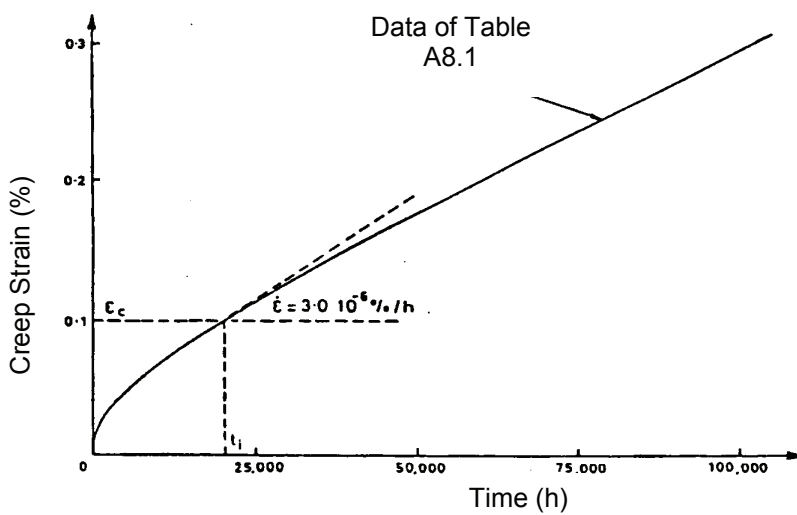


Figure A8.2 Creep strain/time data for Example 1, illustrating calculation of t_i

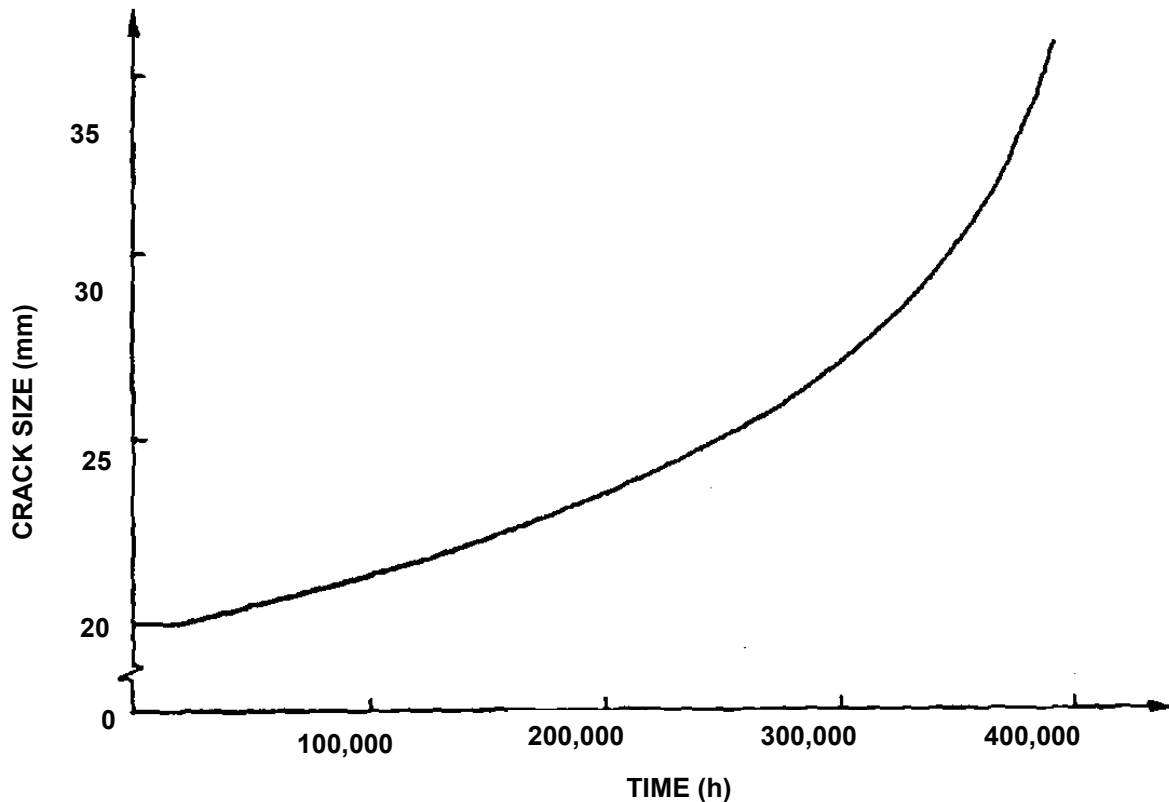


Figure A8.3 Calculation of crack growth stage for Example 1

A8.3 Example 2 – Flat plate With a Single Edge Crack Under Constant Load

This example is used to illustrate crack incubation occurring prior to widespread creep conditions and how this affects the calculation of incubation time and the early stages of crack growth. Therefore the calculation of rupture life is only considered briefly and, as in Example 1, Steps 5, 11 and 12 of the procedure are not explicitly addressed.

A8.3.1 Establish cause of cracking and characterise initial defect (Step 1)

The geometry is identical to that of Example 1. A plate of width 100mm contains an edge defect of depth 20mm. The defect is located within C-Mn weld metal and is present from the start of high temperature operation.

A8.3.2 Define service conditions (Step 2)

The plate operates at 360°C under a constant nominal stress $P/Bw = 300$ MPa.

A8.3.3 Collect materials data (Step 3)

The weld is assumed to occupy a significant portion of the plate. A separate assessment of creep rupture of the surrounding parent plate is not considered so that only material properties of the weld metal are required; these are summarised in Table A8.1.

A8.3.4 Perform basic stress analysis (Step 4)

As mentioned above, the geometry of this example is identical to that of Example 1. Therefore, the stress analysis follows the same procedure as Section A8.2.4. From equation (A8.4) and the applied load $P/Bw = 300$ MPa, the initial reference stress is:

$$\sigma_{\text{ref}}(a_0) = 342 \text{ MPa} \quad (\text{A8.20})$$

A8.3.5 Check stability under time-independent loads (Step 5)

This step is not considered in detail for this example. The check on time-independent failure would normally be based on short-term fault loadings rather than on the steady operating loadings. Reference may be made to R6 [A8.8] for examples of such calculations.

A8.3.6 Check significance of creep and fatigue (Step 6)

As for Example 1, the loading is constant and so fatigue is not an issue. Creep is assumed to be significant for the purposes of this example. See Example 7 for a more detailed account of the checks for insignificant creep, fatigue and creep-fatigue interactions.

A8.3.7 Calculate rupture life (Step 7)

The reference stress is given in equation (A8.20) above. The corresponding rupture life is obtained from the θ – parameter_{fit} of Figure A9.2.1-1, assuming a rupture ductility of 25 per cent (see Table A8.1).

$$t_{\text{CD}} = 5.4 \times 10^4 \text{ h} \quad (\text{A8.21})$$

A8.3.8 Calculate incubation time (Step 8)

At incubation, the creep strain accumulation, ε_c , at the reference stress is related to the critical crack opening displacement, δ_i , by equation (10.8):

$$\varepsilon_c = (\delta_i / R')^{n/(n+1)} - \sigma_{\text{ref}} / E \quad (\text{A8.22})$$

As the initial crack size is the same as for Example 1, R' is given by equation (A8.11) as $R' = 90\text{mm}$ (although the load differs from Example 1 this does not influence equation (10.6) since K and σ_{ref} are both directly proportional to load). As in Example 1, $n/(n+1)$ is set equal to 0.85 from the creep crack growth data, and hence:

$$\varepsilon_c = 0.00014 \quad (\text{A8.23})$$

Consequently, from the creep strain data at the reference stress level of equation (A8.20), the incubation time is:

$$t_i = 11.0 \text{ h} \quad (\text{A8.24})$$

It may be noted that this is less than the redistribution time of equation (10.9) since the creep strain of equation (A8.22) is less than the elastic strain at the reference stress:

$$\sigma_{\text{ref}}(a_0) / E = 0.00185 \quad (\text{A8.25})$$

By entering the creep curve at the reference stress of equation (A8.20) at this value of strain, the redistribution time is obtained from equation (10.9) as:

$$t_{\text{red}} = 144 \text{ h} \quad (\text{A8.26})$$

A8.3.9 Calculate crack size after growth (Step 9)

As for Example 1, crack growth is based on the parameter C^* (see Section A8.2.9). At the incubation time, the creep strain rate is:

$$\dot{\epsilon}_c = 1.3 \times 10^{-5} / \text{hour} \quad (\text{A8.27})$$

and the corresponding value of C^* at incubation is:

$$C^* = 4 \times 10^{-4} \text{MPa m h}^{-1} \quad (\text{A8.28})$$

As $t_i < t_{red}$, the corresponding crack growth rate is given in equation (10.13) as:

$$\dot{a} = 2\dot{a}(C^*) \quad (\text{A8.29})$$

where $\dot{a}(C^*)$ is the crack growth law in Table A8.1. Hence,

$$\dot{a} = 1.6 \times 10^{-2} \text{mm h}^{-1} \quad (\text{A8.30})$$

The non-dimensional parameter λ of equation (A2.27) is obtained as

$$\lambda = 0.01 \quad (\text{A8.31})$$

(including the effect of the factor of 2 on crack growth rate as described in Section A2.8) so that correlations of crack growth rate with C^* are valid as in Section A8.2.9. The calculations of crack growth are performed in an iterative manner, as for Example 1, with a change in crack growth rate from

$$\dot{a} = 2\dot{a}(C^*) \quad \text{for } t < t_{red} \quad (\text{A8.32a})$$

$$\dot{a} = \dot{a}(C^*) \quad \text{for } t \geq t_{red} \quad (\text{A8.32b})$$

The results of these iterative calculations are shown in Figure A8.4.

A8.3.10 Re-calculate rupture life after growth (**Step 10**)

It is straightforward to recalculate t_{CD} from equation (A2.20). The results are shown in Figure A8.4. When the crack has grown to a depth of, say, 35 mm the reference stress is 479 MPa, corresponding to a remaining life of only 63 hours.

A8.3.11 Check stability of time-independent loads after growth (**Step 11**)

Again, these calculations are not considered in detail here.

A8.3.12 Assess significance of results (**Step 12**)

The following conclusions can be drawn for this example:

- The incubation time is lower than the redistribution time for this example. Therefore, creep crack growth occurs before widespread creep conditions have been achieved. This is accounted for by a modification to the creep crack growth law.
- At a depth of, say, 35mm the reference stress is calculated as 479 MPa, corresponding to a remaining life of only 63 hours. Assuming that the critical crack size is greater than 35mm then the dominant failure mechanism would be creep rupture.

- In practice, a sensitivity study would also be undertaken to assess the sensitivity of the results to potential variations in input parameters.

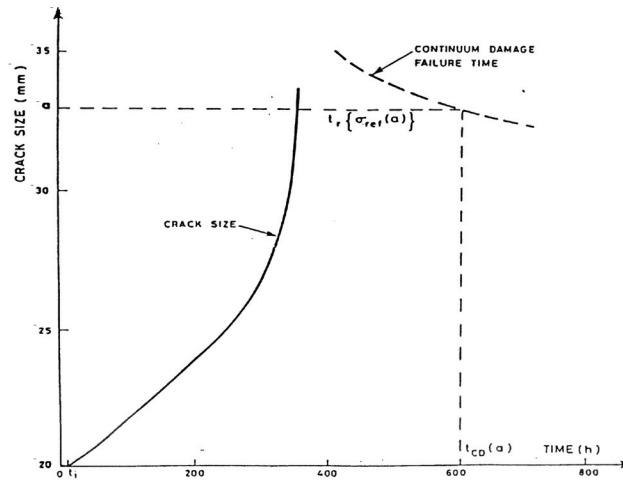


Figure A8.4 - Calculation of crack growth stage for Example 2, illustrating calculation of rupture life

13.4.2 Cylindrical Pipe With an External Crack under Constant Load

Specimen :	Cylindrical pipe
Loading :	Constant load
Material :	½Cr½Mo¼V steel
Defect :	External, part-penetrating, part-circumferential crack
Temperature :	565°C

A8.5 Example 4 - Cylindrical Pipe With an External, Part-Penetrating, Part-Circumferential Defect Under Constant Load

The next example is a **test vessel with a defect in a weld joint** and is presented to illustrate the way in which the calculations, described for the first three examples, are modified to account for the presence of a weldment (see Appendix A4). Further details of this assessment and assessments of other defects in the same test vessel are contained in [A8.3].

A8.5.1 Establish cause of cracking and characterise initial defect (Step 1)

This example is a similar basic geometry to Example 3, being a ½Cr½Mo¼V steam pipe of wall thickness 60 mm and outer diameter 350 mm. The associated test vessel contained a number of welds and defects. The particular defect analysed here is an external part circumferential defect machined into the HAZ adjacent to a post-weld-heat-treated 2CrMo manual metal arc weld (see Figure A8.7). The crack had an initial depth of 16 mm and total length 160 mm.

A8.5.2 Define service conditions (Step 2)

As for Example 3, the pipe operates at 565°C. For consistency with the experimental test programme, the loading consists of an initial period of 2000 h at an internal pressure of 25 MPa and subsequent operation at 35 MPa.

A8.5.3 Collect materials data (**Step 3**)

It is necessary to have creep strain and rupture data for the parent pipe, HAZ and weld metal. These are assumed to obey equations (A8.33) and (A8.34) with the constants given in Table A8.3 for each material. As the HAZ is predominantly coarse grained, creep deformation and rupture data for coarse grained material have been used for conservatism throughout the analysis. The initial defect was such that the crack tip was located in a coarse grained region of the HAZ and the crack incubation data for this material are listed in Table A8.3. As subsequent crack growth occurs through both coarse and fine grained HAZ, crack growth rate data for material in both these conditions are given in Table A8.3.

A8.5.4 Perform basic stress analysis (**Step 4**)

In order to calculate the rupture life, it is first necessary to calculate the reference stress for each material region within the welded joint. This can be performed using the general approach of Section A4.3.2 with the reference stress for each region given by equation (A4.1); this requires the homogeneous cracked-body limit load and the factor k in equation (A4.1) for the uncracked weldment. A lower bound to the Mises limit load for cracks less than 70% through the wall is the uncracked Tresca limit pressure [A8.3] given by

$$p_L = \sigma_y \ln(r_o / r_i) \quad (\text{A8.43})$$

For deeper cracks the limit pressure is given by a modification of equation (A8.35) in terms of the fraction of the circumference which is cracked. However, this is not considered here but reference may be made to [A8.3] for further details. The reference stress is therefore simply given by equation (A4.1),

$$\sigma_{\text{ref}} = kp / \ln(r_o / r_i) \quad (\text{A8.44})$$

where the factor $k=1$ for the parent pipe, 1.4 for the HAZ and 0.7 for the weld metal (see Table A4.4).

The stress intensity factor is given in [A8.3] as

$$K = \frac{p\sqrt{\pi a}}{[(r_o^2 / r_i^2) - 1]} \{0.78715 + 2.0349(a/w) - 4.2635(a/w)^2 + 3.7245(a/w)^3\} \quad (\text{A8.45})$$

A8.5.5 Check stability under time-independent loads (**Step 5**)

This step is not considered in detail for this example. The check on time-independent failure would normally be based on short-term fault loadings rather than on the steady operating loadings. Reference may be made to R6 [A8.8] for examples of such calculations.

A8.5.6 Check significance of creep and fatigue (**Step 6**)

As for Example 1, the loading is essentially constant and so fatigue is not an issue. Creep is assumed to be significant for the purposes of this example. See Example 7 for a more detailed account of the checks for insignificant creep, fatigue and creep-fatigue interactions.

A8.5.7 Calculate rupture life (**Step 7**)

As the pressure was increased after 2000 h, a life fraction rule is adopted for the calculation of t_{CD} .

$$\frac{t_1}{t_r[\sigma_{\text{ref}}(p_1)]} + \frac{t_{CD} - t_1}{t_r[\sigma_{\text{ref}}(p_2)]} = 1 \quad (\text{A8.46})$$

where $t_1 = 2000$ h, $p_1 = 25$ MPa and $p_2 = 35$ MPa. Using the data in Table A8.3, the rupture life is found to be limited by the (coarse grained) HAZ giving

$$t_{CD} = 46399 \text{ h} \quad (\text{A8.47})$$

As the HAZ is not all coarse grained, the rupture life would be somewhat greater than calculated in equation (A8.47). If the initial period at the lower pressure is ignored, then $t_{CD} = 44900 \text{ h}$ indicating that there is little creep damage at the lower pressure. This period is therefore ignored in calculating t_i in Section A8.5.8 but a method for its inclusion using a strain fraction method is described in [A8.3].

A8.5.8 Calculate incubation time (Step 8)

As for Example 2, the incubation time is obtained from the critical strain of equation (A8.22). The length parameter, R' , is then given as the ratio of K_2 to the square of the reference stress for the homogeneous pipe (Section A4.7.7), i.e.

$$R' = K^2 \ln^2(r_o / r_i) / p^2 \quad (\text{A8.48})$$

For $a_0 = 16 \text{ mm}$, $w = 60 \text{ mm}$,

$$R' = 6.2 \text{ mm} \quad (\text{A8.49})$$

The corresponding incubation strain from equation (A8.22) is

$$\varepsilon_c = 0.005 \quad (\text{A8.50})$$

using the reference stress of equation (A8.44) and the data in Table A8.3. The incubation time is then obtained in a similar manner to Figure A8.2 using the reference stress of equation (A8.44) and the creep strain data for the parent material (Table A8.3) as

$$t_i = 28007 \text{ h} \quad (\text{A8.51})$$

The creep strain of equation (A8.50) is in excess of the elastic strain at the reference stress, so that widespread creep conditions are established prior to incubation (i.e. $t_i > t_{red}$). It should also be noted that similar calculations using equation (A4.2) show that welding residual stresses may be neglected provided the peak value is less than 108 MPa. The defect considered here was in a stress relieved weld (Figure A8.7) for which the measured residual stresses were below this value, and therefore residual stresses are not considered in the assessment.

A8.5.9 Calculate crack size after growth (Step 9)

Crack growth is calculated in a similar manner to the previous examples by iterative calculations in terms of the parameter C^* . The crack growth rate is determined in terms of C^* for the material in which the crack tip is positioned. The relevant crack growth law changes as the crack moves from coarse to fine-grained microstructure (Table A8.3). However, alternatively an average crack growth law may be used as described in Appendix A6 of Volume 7. In this case

$$\dot{a} = A_m (C^*)^q \quad (\text{A8.52})$$

with

$$A_m = \frac{A_c (1 + \alpha)}{(A_c / A_R) + \alpha} \quad (\text{A8.53})$$

where A_c and A_R are the coefficients in Table A8.3 for the coarse and refined HAZ material, respectively, and α is the ratio of coarse to refined microstructure in the direction of crack growth. For the weldment in this example $\alpha = 9$, and hence from the coefficients in Table A8.3

$$A_m = 0.071 \quad (A8.54)$$

The results of the calculations using either instantaneous crack growth rates as the crack traverses different microstructures, or using the weighted average growth rate are shown in Figure A8.8. In both cases, $k = 1.4$ has been assumed in estimating C^* values in the HAZ. Results calculated by R-Code [A8.9] for the weighted average growth law are given in Section A8.5.13.

A8.5.10 Re-calculate rupture life after growth (**Step 10**)

Figure A8.8 also shows the rupture time t_{CD} of Section A8.5.7. It may be noted that this rupture time is unaltered as the crack grows because the reference stress is unchanged for cracks less than 70 per cent through the wall thickness, and the rupture time rather than crack growth is life-limiting for this particular initial defect size.

A8.5.11 Check stability of time-independent loads after growth (**Step 11**)

These calculations are not considered in detail here.

A8.5.12 Assess significance of results (**Step 12**)

Appropriate sensitivity analyses are given in [A8.3], which also includes a comparison of the analysis with experimental data, some of which are shown in Figure A8.8. Failure of the test vessel occurred after 46085 hours as a result of creep crack incubation and growth at the location of another defect in a HAZ adjacent to an end-cap. Validation aspects of this vessel test analysis are considered in Appendix A9.

A8.5.13 R-Code results

Properties Data number 1 geometry Property 1

RunTime Formula given by:

$-r.membrane (r.total, r.total) * (0.78715 + r.length * 0.033915)$

$-r.length^2 * 0.0011843 + r.length^3 * 1.7243e-5 * \sqrt{0.001 * \pi * r.length}$

Geometric Data

Code number = 416

(Circumferential Elliptic Surface Crack Outside Cylinder

Arbitrary Radial Symmetric Stress and Bending)

Section size = 60.00000 mm

Mean radius = 145.0000 mm

Stress Intensity Factor given by property 1

Stress Intensity Factor = 1.0000E+00

Load Data load-1

Stress polynomial

$$= a_0 + a_1 * x + a_2 * x^{**2} + a_3 * x^{**3} + \dots + a_8 * x^{**8}$$

Where x=Independent variable and

Term Value

a0 3.8000

a1 0.0000

Materials Data mats-1

Lower bound yield = 1.5000E+02 MPa

Mean yield = 1.5000E+02 MPa

Ultimate Tensile Stress = 5.0000E+02 MPa

Youngs Modulus = 1.6500E+05 MPa

Poissons Ratio = 3.0000E-01

Fracture Toughness = 2.0000E+02 MPa m**1/2

Material is 0.5CrMoV HAZ

Ductility = 0.0000E+00

Formula strain method will be adopted

Factor on Strain = 1.0000000000000000 Creep strain given by property 2

Creep Strain at t=0 = 0.0000000000000000E+000

R5 Volume 4 method used to calculate creep crack growth during redistribution period

Continuum damage failure determined using life fraction rule

Coarse factor, Kc = 1.4000000000000000 Refined factor, Kr = 1.4000000000000000

Microstructural factor, a = 9.0000000000000000

Weld constituent factor, Km = (a+1)/(a+Kc/Kr)*Kc = 1.4000000000000000

Parent creep deformation law used as hoop stress dominates

The standard (Lonsdale) rupture equation is to be used.

R66 creep rupture equation : Lonsdale

$$(\log_{10}(S.t)-F)/(T-G)**H=a+b\log_{10}(rs)+c(\log_{10}(rs)**2) +d(\log_{10}(rs)**3)+e(\log_{10}(rs)**4)+i(rs)+j(\ln(rs))+k(rs**2)$$

Where (as appropriate):-

E = Creep strain s = Reference stress (MPa)

T = Temperature (deg. K) t = Time (hrs) rs = Rupture stress (MPa)

S = Mean to lower bound adjustment on time M = Mean to lower bound adjustment on stress

Lonsdale coefficients for above equation

Term Value

F = 0.0000 G = 0.0000 H = 0.0000

a = 12.920 b = -4.0000 c = 0.0000 d = 0.0000 e = 0.0000 i = 0.0000

j = 0.0000 k = 0.0000 S = 1.0000 M = 1.0000

Minimum valid stress = 0.000000000000000E+000 MPa

Maximum valid stress = 1000000.00000000 MPa

Minimum valid temperature = 0.000000000000000E+000 C

Maximum valid temperature = 600.000000000000 C

Coarse factor, Ac = 252.000000000000 Refined factor, Ar = 9.50000000000000

Microstructural factor, a = 9.00000000000000 Creep constant, Am = (a+1)/(a+Ac/Ar)*Ac

Creep crack growth equation

da/dt=A*(Cstar**m)

Where da/dt = Creep crack growth rate (mm/h) & Cstar = C* (MN/mh)

Creep crack growth const= 7.0933E+01 Creep crack growth expon= 8.0000E-01

Incubation COD = 1.000000000000000E-002 mm

Assessment Results

Prob-1

Assessment at semi-minor varying minor and aspect , fixed major, Crack length is semi-minor

Incubation time = 2.94 yrs (25741.2 hrs)

Continuum damage failure predicted after 5.31 yrs

in material mats-1

Crack depth at failure = 22.204 mm Redistribution time = 0.00 yrs (0.0 hrs)

Integrated creep crack growth in redistribution time = 0.000 mm

Code no=416, Reference/Lr eqn=usrp

R6 Toughness= 200 MPa m**1/2 R6 Yield Stress= 150 MPa C. Defect Size Information

Time	Time Assn.	Tran Crack	Creep	Total	Creep	None
(hrs)	(hrs)	No.	No.	Length	Increment	Creep
(mm)	(mm)	Crack	Growth			Crack
			Growth	Rate		
			(mm)	(mm/h)		

2000.0	2000	1	1	16.0000	0.000E+000	0.000E+000	0.000E+000		
4000.0	4000	1	2	16.0000	0.000E+000	0.000E+000	0.000E+000		
6000.0	6000	1	2	16.0000	0.000E+000	0.000E+000	0.000E+000		
8000.0	8000	1	2	16.0000	0.000E+000	0.000E+000	0.000E+000		
10000.0	10000	1	2	16.0000	0.000E+000	0.000E+000	0.000E+000		
12000.0	12000	1	2	16.0000	0.000E+000	0.000E+000	0.000E+000		
14000.0	14000	1	2	16.0000	0.000E+000	0.000E+000	0.000E+000		
16000.0	16000	1	2	16.0000	0.000E+000	0.000E+000	0.000E+000		
18000.0	18000	1	2	16.0000	0.000E+000	0.000E+000	0.000E+000		
20000.0	20000	1	2	16.0000	0.000E+000	0.000E+000	0.000E+000		
22000.0	22000	1	2	16.0000	0.000E+000	0.000E+000	0.000E+000		
24000.0	24000	1	2	16.0000	0.000E+000	0.000E+000	0.000E+000		
26000.0	26000	1	2	16.0596	5.965E-002	5.965E-002	2.310E-004		
28000.0	28000	1	2	16.5323	4.727E-001	5.323E-001	2.418E-004		
30000.0	30000	1	2	17.0273	4.949E-001	1.027E+000	2.533E-004		
32000.0	32000	1	2	17.5460	5.187E-001	1.546E+000	2.655E-004		
34000.0	34000	1	2	18.0900	5.441E-001	2.090E+000	2.787E-004		
36000.0	36000	1	2	18.6612	5.712E-001	2.661E+000	2.927E-004		
38000.0	38000	1	2	19.2615	6.003E-001	3.261E+000	3.078E-004		
40000.0	40000	1	2	19.8930	6.315E-001	3.893E+000	3.240E-004		
42000.0	42000	1	2	20.5581	6.651E-001	4.558E+000	3.414E-004		
44000.0	44000	1	2	21.2596	7.014E-001	5.260E+000	3.603E-004		
46000.0	46000	1	2	22.0002	7.407E-001	6.000E+000	3.807E-004		
46530.5	46531	1	2	22.2037	2.035E-001	6.204E+000	3.864E-004		

J. Stress and C* Information with Weld Factor

Time	Tran	Temp	Ref.	K*	Primary	Secondary	Total	C*	C(t)
(hrs)	No.	R5	Stress	Ref.	SIF R5	SIF R5	SIF	(MN/mh)	(MN/mh)
(C)	(MPa)	Stress	(MPa/~m)	(MPa/~m)	(MPa/~m)	(MPa)			

2000.0	1	565.0	59.536	83.351	4.674	0.000	4.674	2.074E-008	2.074E-008
4000.0	2	565.0	83.351	116.691	6.544	0.000	6.544	1.133E-007	1.133E-007
6000.0	2	565.0	83.351	116.691	6.544	0.000	6.544	1.151E-007	1.151E-007
8000.0	2	565.0	83.351	116.691	6.544	0.000	6.544	1.170E-007	1.170E-007
10000.0	2	565.0	83.351	116.691	6.544	0.000	6.544	1.190E-007	1.190E-007
12000.0	2	565.0	83.351	116.691	6.544	0.000	6.544	1.210E-007	1.210E-007
14000.0	2	565.0	83.351	116.691	6.544	0.000	6.544	1.231E-007	1.231E-007
16000.0	2	565.0	83.351	116.691	6.544	0.000	6.544	1.253E-007	1.253E-007
18000.0	2	565.0	83.351	116.691	6.544	0.000	6.544	1.276E-007	1.276E-007
20000.0	2	565.0	83.351	116.691	6.544	0.000	6.544	1.300E-007	1.300E-007
22000.0	2	565.0	83.351	116.691	6.544	0.000	6.544	1.324E-007	1.324E-007
24000.0	2	565.0	83.351	116.691	6.544	0.000	6.544	1.350E-007	1.350E-007
26000.0	2	565.0	83.351	116.691	6.559	0.000	6.559	1.384E-007	1.384E-007
28000.0	2	565.0	83.351	116.691	6.681	0.000	6.681	1.465E-007	1.465E-007
30000.0	2	565.0	83.351	116.691	6.807	0.000	6.807	1.552E-007	1.552E-007
32000.0	2	565.0	83.351	116.691	6.937	0.000	6.937	1.647E-007	1.647E-007
34000.0	2	565.0	83.351	116.691	7.072	0.000	7.072	1.749E-007	1.749E-007
36000.0	2	565.0	83.351	116.691	7.211	0.000	7.211	1.860E-007	1.860E-007
38000.0	2	565.0	83.351	116.691	7.356	0.000	7.356	1.980E-007	1.980E-007
40000.0	2	565.0	83.351	116.691	7.507	0.000	7.507	2.111E-007	2.111E-007
42000.0	2	565.0	83.351	116.691	7.664	0.000	7.664	2.254E-007	2.254E-007
44000.0	2	565.0	83.351	116.691	7.827	0.000	7.827	2.411E-007	2.411E-007
46000.0	2	565.0	83.351	116.691	7.998	0.000	7.998	2.583E-007	2.583E-007
46530.5	2	565.0	83.351	116.691	8.045	0.000	8.045	2.583E-007	2.583E-007

E. Strain Information

Time	Total	Creep	Creep	Creep/	Lambda	l(nit)
(hrs)	Creep	Strain	Life	Elastic		R(edis)
	Strain	Rate	Fraction	Strain		(1/hr)

2000.0	1.081E-003	4.037E-008	0.01161	2.139E+000	0.0000	#R
4000.0	1.393E-003	1.575E-007	0.05619	1.970E+000	0.0000	
6000.0	1.711E-003	1.601E-007	0.10077	2.419E+000	0.0000	
8000.0	2.034E-003	1.627E-007	0.14536	2.875E+000	0.0000	
10000.0	2.362E-003	1.654E-007	0.18994	3.339E+000	0.0000	
12000.0	2.695E-003	1.682E-007	0.23453	3.811E+000	0.0000	
14000.0	3.035E-003	1.712E-007	0.27911	4.291E+000	0.0000	
16000.0	3.380E-003	1.742E-007	0.32369	4.779E+000	0.0000	
18000.0	3.732E-003	1.774E-007	0.36828	5.277E+000	0.0000	
20000.0	4.090E-003	1.807E-007	0.41286	5.783E+000	0.0000	
22000.0	4.455E-003	1.841E-007	0.45745	6.299E+000	0.0000	
24000.0	4.826E-003	1.877E-007	0.50203	6.825E+000	0.0000	
26000.0	5.206E-003	1.915E-007	0.54661	7.361E+000	0.1378	# I
28000.0	5.592E-003	1.954E-007	0.59120	7.908E+000	0.1362	
30000.0	5.987E-003	1.995E-007	0.63578	8.466E+000	0.1347	
32000.0	6.390E-003	2.037E-007	0.68037	9.036E+000	0.1331	
34000.0	6.802E-003	2.082E-007	0.72495	9.618E+000	0.1315	
36000.0	7.223E-003	2.129E-007	0.76954	1.021E+001	0.1299	
38000.0	7.654E-003	2.178E-007	0.81412	1.082E+001	0.1283	
40000.0	8.095E-003	2.230E-007	0.85870	1.145E+001	0.1266	
42000.0	8.546E-003	2.285E-007	0.90329	1.208E+001	0.1250	
44000.0	9.009E-003	2.343E-007	0.94787	1.274E+001	0.1233	
46000.0	9.484E-003	2.404E-007	0.99246	1.341E+001	0.1216	
46530.5	9.612E-003	2.421E-007	1.00428	1.359E+001	0.1216	# F

Notes: #I is initiation time, # R is redistribution time

Table A8.3 - Material Properties for Example 4

	Parent Pipe	Weld Metal	HAZ	
			Coarse	Fine
Young's modulus (MPa)	165 000	165 000	165 000	
Creep Strain Equation (A8.33) with σ in MPa				
ϵ_p	0.001	0.001	0.001	N/A
γ	6.38	5.63	1.5	N/A
D	3.2×10^{-15}	1.6×10^{-14}	6.9×10^{-16}	N/A
n	4	4	4	N/A
Creep Rupture Equation (A8.34) with t_r in hours, σ in MPa				
D'	5.26×10^{12}	9.09×10^{11}	8.33×10^{12}	N/A
ν	4	4	4	N/A
Incubation COD (mm)	N/A	N/A	0.01	N/A
Crack Growth Rate Equation (7.2) A	N/A	N/A	0.252	0.0095
(\dot{a} in mh ⁻¹ , q C* in MPa mh ⁻¹)	N/A	N/A	0.8	0.8

Note: N/A = Not Applicable

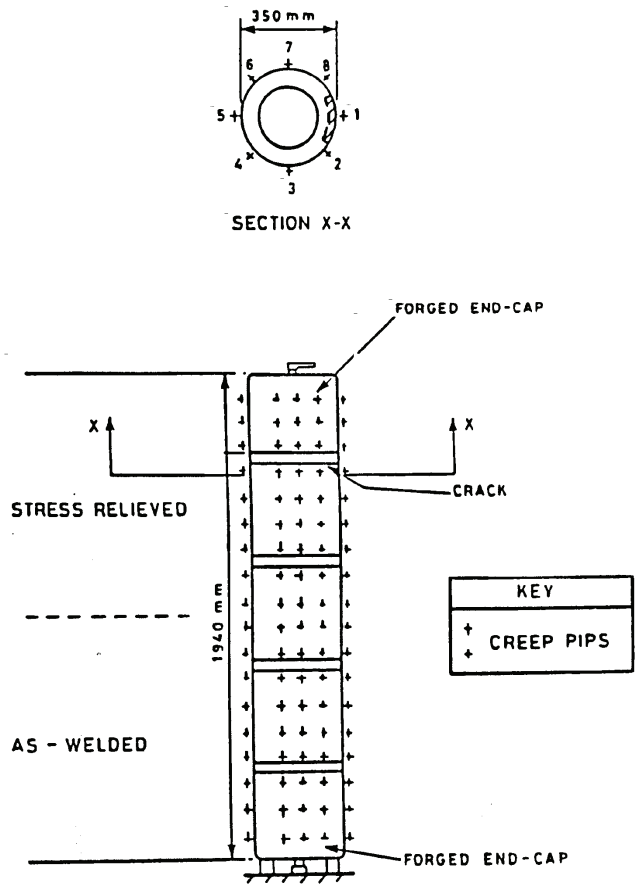


Figure A8.7 - Example 4; schematic of pressure vessel showing welds and location of HAZ defect and strain monitoring positions

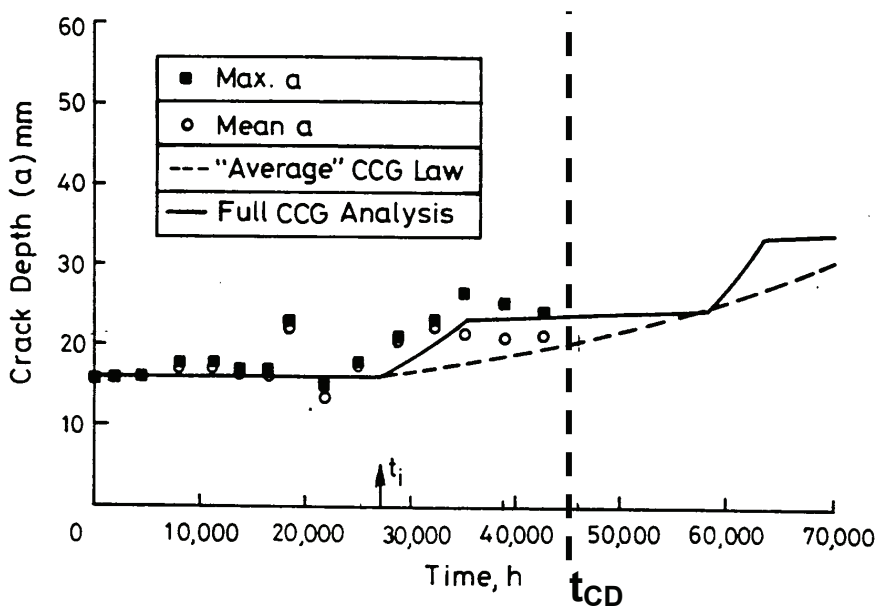


Figure A8.8 - Calculations of crack growth stage for Example 4, using both instantaneous and average growth laws

13.4.3 Cylindrical Pipe With an Internal Crack under Cyclic Loading

Specimen :	Cylindrical pipe
Loading :	Cyclic loading
Material :	½Cr½Mo¼V steel
Defect :	External, part-penetrating, part-circumferential crack
Temperature :	565°C

The current case study is presented in more detail in the FITNET Tutorials, chapter 14.6.

A8.6 Example 5 - Cylindrical Pipe With an Internal, Part-Penetrating, Fully Circumferential Defect Under Cyclic Loading

Examples 5 and 6 demonstrate **how the procedure may be applied to components subjected to creep-fatigue loading**. The two examples are based on the same geometry, temperature history and initial crack depths but with different loading histories. Loads are chosen so that the structure is operating within strict shakedown for Example 5, and within global shakedown with the defect embedded within the cyclic plastic zone for Example 6. The two worked examples therefore demonstrate application of assessment Methods I and II to an idealised structural geometry. The details given in these examples are therefore limited mainly to the crack growth calculations.

A8.6.1 Establish cause of cracking and characterise initial defect (**Step 1**)

The idealised structural geometry is shown in Figure A8.9. It comprises a homogeneous Type 316 Stainless Steel pipe of internal radius, $R_i=300$ mm and wall thickness, $w=100$ mm. A defect is assumed to be present at the start of high temperature operation so that the life to date is taken as zero. The defect is assumed to be fully circumferential on the inside of the pipe with the initial depth, a_0 , taken as 3mm.

A8.6.2 Define service conditions (**Step 2**)

The pipe is subjected to repeated cyclic loading from an initially unstressed shutdown condition at ambient temperature (20°C) to an operating condition at 600°C, comprising an internal pressure of 16 MPa together with through wall axial and hoop thermal bending stresses of 200 MPa. The bending stresses are such that tensile stresses arise on the inside surface of the pipe (Figure A8.10). In the present examples 500 equal cycles, with 3000 hour dwells at operating conditions, are assumed to occur during the desired future service life of 1.5×10^6 hours.

A8.6.3 Collect materials data (**Step 3**)

Creep strain data are described by the following parametric expression proposed by White [A8.13].

$$\varepsilon = \varepsilon_p [1 - \exp(-rt^\mu)] + \dot{\varepsilon}_s t \quad (\text{A8.55})$$

with the maximum primary strain, ε_p , given by

$$\varepsilon_p = A' \sigma^{m(\theta)} \exp[-P/(\theta + 273)] \quad (\text{A8.56})$$

where $m(\theta) = \alpha - \gamma\theta$ and the secondary creep strain rate is given by

$$\dot{\varepsilon}_s = B \sigma^n \exp[-P/(\theta + 273)] \quad (\text{A8.57})$$

where θ is the temperature (in °C) and σ is the reference stress. The constants in equations (A8.55) to (A8.57) are given in Table A8.4 together with other required material properties. The creep strain rate may be obtained by differentiating equation (A8.55) with respect to time as

$$\dot{\epsilon} = \epsilon_p r \mu t^{\mu-1} \exp(-rt^\mu) + \dot{\epsilon}_s \tag{A8.58}$$

However, as $\mu < 1$, the creep strain rate given by the above analytical expression becomes infinite at time zero. For short times and low strains (<10⁻⁴), the creep strain rate is approximated by dividing the strain of 10⁻⁴ by the time to reach this strain (obtained from equation (A8.55)).

As the stresses acting during the dwell periods are treated as load controlled (as described in Section A8.6.9), forward creep data are appropriate for calculating creep strains and strain rates.

A8.6.4 Perform basic stress analysis (Step 4)

For cyclic loading, the following are required:

- A shakedown analysis.
- The depth of the cyclic plastic zone on the surface of the defective section.
- The elastic follow-up factor.
- The stress intensity factors, Kmin and Kmax and the associated R ratio, which permit the effective stress intensity factor range, ΔK_{eff} , to be calculated.
- The reference stress for the creep dwell.

A8.6.4.1 Shakedown analysis

Details of shakedown analysis methods are given in Volume 2/3. Uncracked body elastic stresses are required as the starting point for the analyses. In this example, the pressure stresses are given by the Lamé thick cylinder equations with the thermal stresses taken as through wall bending stresses of equal magnitude in the hoop and axial directions (see Figure A8.10); k in this figure is the ratio of outer to inner radius, r_o / r_i . The initial total operating elastic stresses are then the sum of the pressure and thermal contributions.

In order to determine if the structure is operating within shakedown it is necessary to generate a residual stress field. For this example, it is convenient to select a residual stress field which is a factor, α , times the thermal stress field (i.e. axial and hoop bending stresses of 200α MPa). The shakedown stress field, $\tilde{\sigma}_s$, is then obtained by adding the residual stress field $\tilde{\rho}$ to the elastically calculated stress field, $\tilde{\sigma}_{el}$. Thus,

$$\tilde{\sigma}_s = \tilde{\sigma}_{el} + \tilde{\rho} \tag{A8.59}$$

Shakedown stress fields are thereby determined for the cold (non-creep) and hot (creep) extremes of the loading cycle, denoted $(\tilde{\sigma}_s)_{nc}$ and $(\tilde{\sigma}_s)_c$ for shutdown and operating conditions, respectively. For the structure to attain strict shakedown, the shakedown stress fields at the cold and hot extremes of the loading cycle must satisfy the following criteria

$$(\bar{\sigma}_s)_{nc} \leq (K_s S_y)_{nc} \tag{A8.60a}$$

and

$$(\bar{\sigma}_s)_c \leq (K_s S_y)_c \quad (\text{A8.60b})$$

where S_y is the minimum 0.2% proof stress, K_s is applied to S_y to obtain the material ratchet limit factor (see Volume 2/3) with the values $(K_s)_{nc}$ and $(K_s)_c$ at shutdown and operating conditions respectively, and $(\bar{\sigma}_s)_{nc}$ and $(\bar{\sigma}_s)_c$ are the shakedown equivalent stresses at shutdown and operating conditions respectively. Volume 2/3 permits limited regions of a structure to be exempted from strict shakedown requirements. The structure is then deemed to be within global shakedown if at least 80% of every section consists of a ligament over which the shakedown criteria are satisfied at the two extremes of the loading cycle. For the current examples 5 and 6, which involve shutdown at 20°C, values of $(K_s)_{nc} = 0.752$ and $(S_y)_{nc} = 245 \text{ MPa}$ are assumed for the Type 316 Stainless Steel, leading to a shakedown criterion at shutdown of

$$(\bar{\sigma}_s)_{nc} \leq 184.2 \text{ MPa} \quad (\text{A8.61})$$

For operation at 600°C, assumed values of $(K_s)_c = 1.15$ and $(S_y)_c = 109.6 \text{ MPa}$ give a shakedown criterion at operation of

$$(\bar{\sigma}_s)_c \leq 126.0 \text{ MPa} \quad (\text{A8.62})$$

For this example, strict shakedown can be demonstrated for the pipe. Creep relaxation during early loading cycles reduces the stress at the hot extreme of the cycle until the cold extreme of the cycle reaches the limit of the shakedown criterion at shutdown (equation (A8.61)). This situation is achieved using a residual stress field obtained by scaling the thermal stress field by $\alpha = -0.921$. Resulting steady cyclic stress profiles for the uncracked pipe are shown in Figures A8.11 and A8.12 for shutdown and operating conditions, respectively.

In order to take account of early cycles prior to attainment of the steady cyclic state, it is also necessary to determine the initial stress state. For this example, the initial stress state is obtained using a Neuber construction for the most highly stressed inside surface point as described in Volume 2/3. The initial elastic operating stress profiles shown in Figure A8.13 give an initial elastic equivalent stress at the inner surface of 256.8 MPa. This elastic equivalent stress has then been used, together with monotonic isochronous data for Type 316 Stainless Steel at 600°C, to estimate the initial equivalent stress at the inner surface as shown in Figure A8.14. This initial equivalent stress at the inner surface (141.8 MPa) has then been used to infer an initial residual stress field, which when combined with the initial elastic stresses, gives the correct value of inner surface equivalent stress. The required initial residual stress field is obtained by scaling the thermal stress field by $\alpha = -0.583$. Resulting initial stress profiles are shown in Figures A8.15 and A8.16 for shutdown and operating conditions, respectively.

A8.6.4.2 Surface cyclic plastic zone size

Strict shakedown has been demonstrated for this example. There is therefore no cyclic plastic deformation at the inner surface of the defective pipe section and the cyclic plastic zone size, r_p , is set equal to zero.

A8.6.4.3 Stress intensity factors

The effective stress intensity factor range, ΔK_{eff} , is required as a function of crack depth. For this example, where the cyclic structural response is elastic, ΔK_{eff} is calculated using the stress intensity factors, K_{max} and K_{min} , corresponding to the maximum (i.e. operation) and minimum (i.e. shutdown) load conditions, respectively, of the cycle. As the axial stresses vary linearly through the pipe wall at both extremes of the cycle, the stresses can be represented by membrane and bending components, denoted σ_m and σ_b respectively. Membrane and bending stresses appropriate to both initial and shakedown conditions are given in Table A8.5. Stress intensity factor solutions are therefore required for a cylinder with $R_i/w=3$ subjected to combined axial membrane and bending stresses, with the total stress intensity factor given by

$$K = (F_m \sigma_m + F_b \sigma_b) \sqrt{\pi a} \tag{A8.63}$$

where the membrane and bending compliance functions, F_m and F_b respectively, are functions

of R_i/w and a/w . The handbook of Tada, Paris and Irwin [A8.7] gives graphical membrane compliance solutions for a range of R_i/w values, thereby permitting the solution for $R_i/w=3$ to be approximated in polynomial form as

$$F_m = 1.123 - 0.103x + 2.030x^2 - 1.373x^3 + 0.790x^4 \tag{A8.64}$$

for $0 < x < 0.6$ where $x = a/w$.

The corresponding bending compliance function has been derived using the computer program R-Code [A8.9]), with the above membrane compliance function used as the Reference State Solution (RSS). The derived bending compliance function may be approximated in polynomial form as

$$F_b = 1.126 - 1.543x + 2.613x^2 - 3.986x^3 + 2.123x^4 \tag{A8.65}$$

where the range of validity is the same as for the membrane compliance function. The effective stress intensity factor range, ΔK_{eff} , has been evaluated as a function of crack depth from equations (10.2) to (10.5) for both initial and shakedown conditions using the compliance functions given in equations (A8.64) and (A8.65) together with the axial stresses given in Table A8.5. The effective stress intensity factor ranges (together with associated values of K_{max}) are shown as functions of crack depth in Figure A8.17 for both the initial and shakedown conditions. Note that for the current example $R < 0$ and hence $q_0 < 1$ for both initial and shakedown conditions (for all crack depths).

For the period prior to the attainment of the steady cyclic state (i.e. $t < t_{cyc}$), the effective stress intensity factor range has been taken as the mean of the initial and shakedown values.

A8.6.4.4 Reference stresses

The reference stress during the dwell periods has been calculated by determining the forces and moments acting across the section of interest. The forces and moments (per unit thickness), F and M respectively, acting across the section in the axial (superscript a) and hoop (superscript h) directions have been evaluated for both steady cyclic and initial conditions (based on Neuber) using the stress profiles shown in Figures A8.12 and A8.16, respectively. In both cases, the axial and hoop stresses may be well represented by membrane and bending stresses, σ_m and σ_b , respectively. Table A8.6 gives axial and hoop stresses appropriate to initial and shakedown conditions and associated forces and moments (per unit thickness) evaluated using

$$F = \sigma_m w \tag{A8.66}$$

and

$$M = \frac{\sigma_b w^2}{6} \tag{A8.67}$$

Equation (A8.67) provides a conservative estimate of the moment by ignoring the effect of radius on the integration of the linear stress distribution. The reference stress has been determined using lower bound limit load theory treating the secondary (thermal) wall bending stress as primary, for a pipe containing an internal fully circumferential crack subjected to both axial and hoop forces and moments based on a Tresca yield criterion. The reference stress, σ_{ref} , may be calculated using

$$\sigma_{\text{ref}} = \frac{F}{F_L} \sigma_y \quad (\text{A8.68})$$

where σ_y is an arbitrary yield stress and F_L is the limit load. If proportional loading is assumed the limit loads can be determined from

$$\frac{F_L}{M_L} = \frac{F}{M} \quad (\text{A8.69})$$

where F and M are the forces and moments, respectively, from Table A8.6.

The limit loads for axially dominated collapse have the form

$$F_L^a = (2y - a) \sigma_y \quad (\text{A8.70})$$

and

$$M_L^a = \left[\frac{w^2}{4} + \frac{a^2}{2} - \frac{at}{2} - x^2 \right] \sigma_y \quad (\text{A8.71})$$

where w is the pipe wall thickness and y is the distance between the plastic neutral axis and the mid-wall thickness. The value of y is found from equation (A8.69) based on values of F and M from Table A8.6, and the expressions involving y (equations (A8.70) and (A8.71)) for F_L^a and M_L^a . The resulting quadratic equation can then be easily solved.

For hoop dominated collapse the limit loads are

$$F_L^h = 2y \sigma_y \quad (\text{A8.72})$$

and

$$M_L^h = \left(\frac{w^2}{4} - y^2 \right) \sigma_y \quad (\text{A8.73})$$

The value of y is again calculated using these expressions in equation (A8.69) together with values of F and M from Table A8.6. The maximum of the axial and hoop reference stress is then chosen. For both the initial and shakedown conditions the reference stress is hoop dominated, and is therefore independent of crack depth. For initial conditions the reference stress is

$$\sigma_{\text{ref}}^{\text{cyc}=1} = 88.1 \text{ MPa} \quad (\text{A8.74})$$

while for steady cyclic conditions

$$\sigma_{\text{ref}} = 57.6 \text{ MPa} \quad (\text{A8.75})$$

is obtained.

A8.6.4.5 C* parameter

The parameter C* is calculated according to the methods of Section 10.3.2, with C* given by equation (10.7) as

$$C^* = \sigma_{ref} \dot{\epsilon}_{ref} R' \tag{A8.76}$$

where σ_{ref} is the reference stress described in Section A8.6.4.4. R' is defined by

$$R' = (K / \sigma_{ref})^2 \tag{A8.77}$$

A8.6.5 Check stability under time-independent loads (Step 5)

This step is not considered in detail for this example. The check on time-independent failure would normally be based on short-term fault loadings rather than on the steady operating loadings. Reference may be made to R6 [A8.8] for examples of such calculations.

A8.6.6 Check significance of creep and fatigue (Step 6)

For the purpose of this example, it is assumed that both creep and fatigue are significant. Example 7 gives details of the tests that can be applied at this stage to determine whether creep, fatigue or creep-fatigue interactions are insignificant. In some cases, this may render further calculations unnecessary.

A8.6.7 Calculate rupture life (Step 7)

Not considered in this example.

A8.6.8 Calculate incubation time (Step 8)

Not considered in this example, although a conservative incubation time of zero is often assumed when creep and fatigue are significant.

A8.6.9 Calculate crack size after growth (Step 9)

Strict shakedown of the uncracked structure has been demonstrated for this example and so a Method I crack growth calculation is appropriate. The creep and fatigue crack growth contributions are separately calculated and added for each cycle. The creep crack growth rate law takes the form given in equation (7.2), with the creep crack growth rate, da/dt, given by

$$\frac{da}{dt} = A(C^*)^q \tag{A8.78}$$

Values of the coefficients A and q used in the current example are given in Table A8.4. In general, the parameter C* is calculated by the reference stress approach of Section A8.6.4.5. It is also necessary to calculate a mean value of C* for use in calculating creep crack growth occurring in the dwell periods prior to the attainment of the steady cyclic state (i.e. t<tcyc as given by equation (10.10)). This is given in equation (10.17) as

$$\bar{C}^* = (\sigma_{ref}^{cyc=1} + \sigma_{ref}) \dot{\epsilon} R' / 2 \tag{A8.79}$$

where $\dot{\epsilon}$ is evaluated as $\dot{\epsilon} [(\sigma_{ref}^{cyc=1} + \sigma_{ref}) / 2]$. For the current example, the stresses acting during the dwell periods after the steady cyclic state is reached are predominantly primary. Therefore, the small amount of stress relaxation that would occur during the dwell has been neglected and load-controlled loading has been assumed in calculating creep strain accumulation and crack growth during the dwell.

The stress intensity factor used in the calculation of R' in equation (A8.77) is evaluated using the stresses at the beginning of the dwell and is therefore equal to K_{\max} (see Figure A8.17). Prior to attainment of the steady cyclic state, a mean value of K_{\max} has been used in the calculation of R' .

This is given by

$$\bar{K}_{\max} = (K_{\max}^{\text{cyc}=1} + K_{\max})/2 \quad (\text{A8.80})$$

where $K_{\max}^{\text{cyc}=1}$ and K_{\max} are the maximum stress intensity factors at the start of the first cycle (using a Neuber construction) and the cycle in the steady cyclic state, respectively. The cyclic crack growth rate law takes the form given in equation (7.3), with the cyclic crack growth rate, $(da/dN)_f$, given by

$$\left(\frac{da}{dN} \right)_f = C(\Delta K_{\text{eff}})^\ell \quad (\text{A8.81})$$

where the coefficients C and ℓ may be temperature dependent. Values of the coefficients C and ℓ used in the current example are given in Table A8.4. The calculation of ΔK_{eff} is described in Section A8.6.4.3. The total crack growth per cycle is obtained by summing the cyclic and creep contributions as described in Section 10.7.3. The crack extension over the desired future service life of 1.5×10^6 hours is then calculated iteratively using a computer program. The main features of the iterative procedure are as follows:

(i) Calculate creep crack growth for the dwell period in the first cycle. It should be noted that this itself involves an iterative procedure in which the creep crack growth and strain rates are assumed constant for a short time, Δt . The crack depth and accumulated creep strain are then updated and new values of reference stress and creep strain rate obtained assuming a strain hardening rule. The value of C^* can then be obtained with R' evaluated for the new crack depth, leading to a new value of creep crack growth rate. For the current example, these calculations have actually been implemented by incrementing crack depth, although details of the numerical procedures are not discussed here.

(ii) Calculate cyclic crack growth for the first cycle and increment crack depth.

(iii) Repeat calculations for subsequent cycles.

For the current example it is also necessary to determine t_{cyc} , the time to redistribute to the steady cyclic state using equation (10.10). A value of elastic follow up factor $Z=3$ is arbitrarily assumed. With this assumption, the steady cyclic state is achieved after 1 cycle. Prior to attainment of the steady cyclic state, mean values of ΔK_{eff} and C^* are used to calculate cyclic and creep components of crack growth as described above. After the steady cyclic state has been established (i.e. $t > t_{\text{cyc}}$), values of ΔK_{eff} and C^* appropriate to steady state conditions are used in the crack growth calculations. The results of these iterative calculations lead to the crack depth as a function of time shown in Figure A8.18.

A8.6.10 Recalculate rupture life after growth (**Step 10**)

Not considered in this example.

A8.6.11 Check stability of time-independent loads after growth (**Step 11**)

Not considered in this example.

A8.6.12 Assess significance of results (**Step 12**)

In practice, studies would be performed to examine the sensitivity of the results to the assumed input data. However, as the main purpose of this example is to illustrate the use of the Volume 4/5 procedure for creep-fatigue crack growth, sensitivity studies have not been considered in this example.

Table A8.4 - Material Properties for Example 5

Elastic Modulus (MPa)	155 000
Creep Strain	Equations (A8.55) to (A8.57) with $r=2.42 \times 10^{-2}$ $\mu=0.64$ $A'=1.632 \times 10^{35}$ $P=9.292 \times 10^4$ $\alpha = 16.32$ $\gamma=0.02044$ $B=1.065 \times 10^{-5}$ $Q=1.97 \times 10^4$ $n=4$
Cyclic Crack Growth Rate (m/cycle)	Equation (7.3) with $C=2.0 \times 10^{-9}$ $\ell = 3$
Creep Crack Growth Rate (m/h)	Equation (7.2) with $A=0.0197$ $q=0.89$

Table A8.5 - Axial Stresses for Example 5 (Used in Calculation of Stress Intensity Factors including Effective Stress Intensity Factor Range)

Loading Conditions	Operation		Shutdown	
	Membrane Stress (MPa)	Bending Stress# (MPa)	Membrane Stress (MPa)	Bending Stress# (MPa)
Initial (Start of first cycle)	20.6	83.4	0	-116.6
Shakedown (Steady cyclic state)	20.6	15.8	0	-184.2

Positive values indicate tensile stress on the inside surface of the pipe

Table A8.6 - Axial and Hoop Stresses, Forces and Moments for Example 5 (Used in the Calculation of Reference Stress)

Loading Conditions	Axial				Hoop			
	Membrane Stress σ_{am} (MPa)	Bending Stress σ_{ab} (MPa)	Force per Unit Thickness F_a (N/m)	Moment per Unit Thickness M_a (Nm/m)	Membrane Stress σ_{hm} (MPa)	Bending Stress σ_{hb} (MPa)	Force Per Unit Thickness F_h (N/m)	Moment Per Unit Thickness M_h (Nm/m)
Initial (Start of First Cycle)	20.6	83.4	2.06×10^6	1.39×10^5	49.1	91.4	4.91×10^6	1.52×10^5
Shake down (Steady cyclic state)	20.6	15.8	2.06×10^6	2.63×10^4	49.1	23.8	4.91×10^6	3.97×10^4

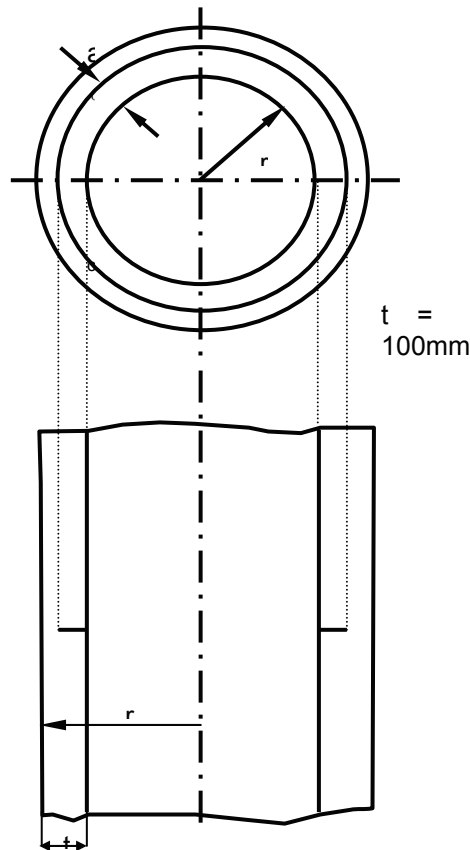
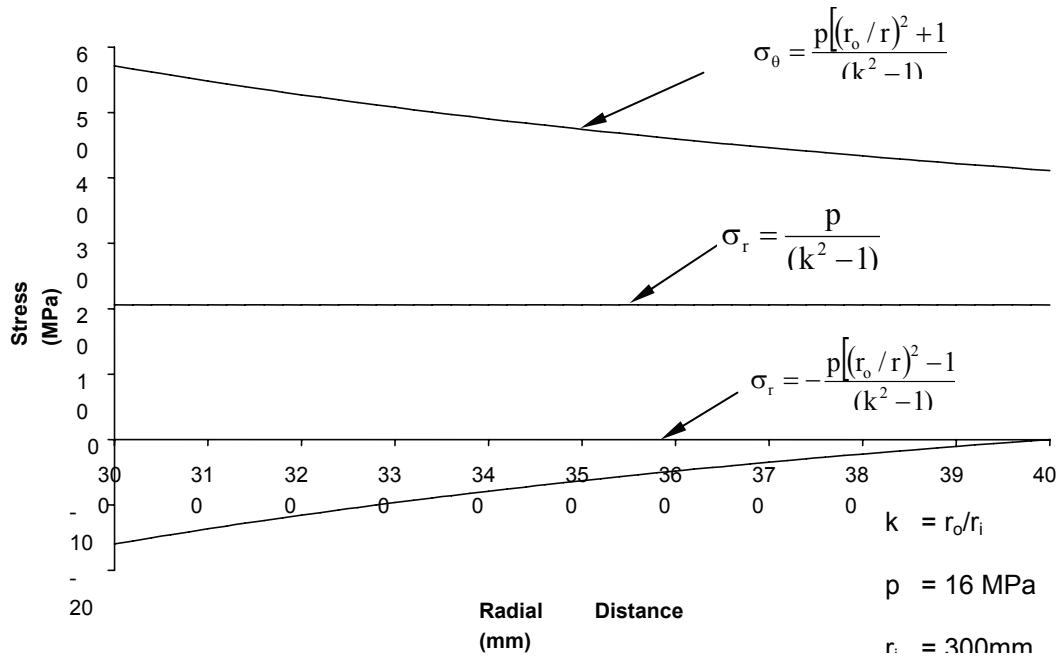
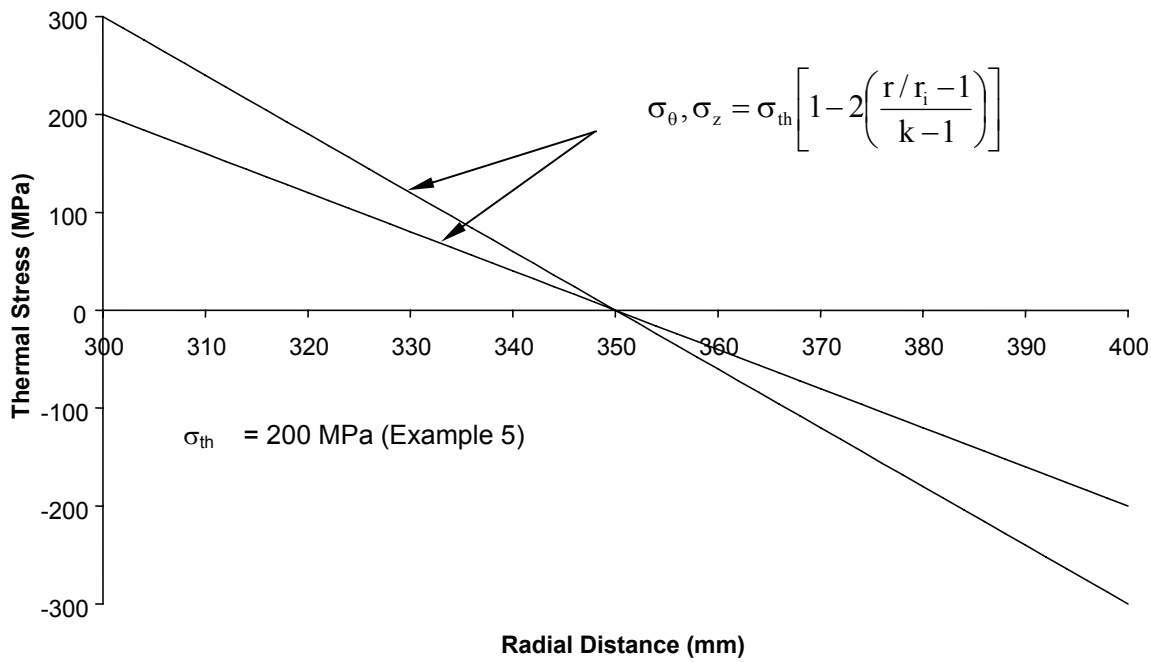


Figure A8.9 Idealised structural geometry for Examples 5 and 6



a) Pressure stresses



b) Thermal Stresses

Figure A8.10 - Initial operating elastic stresses (Examples 5 and 6)

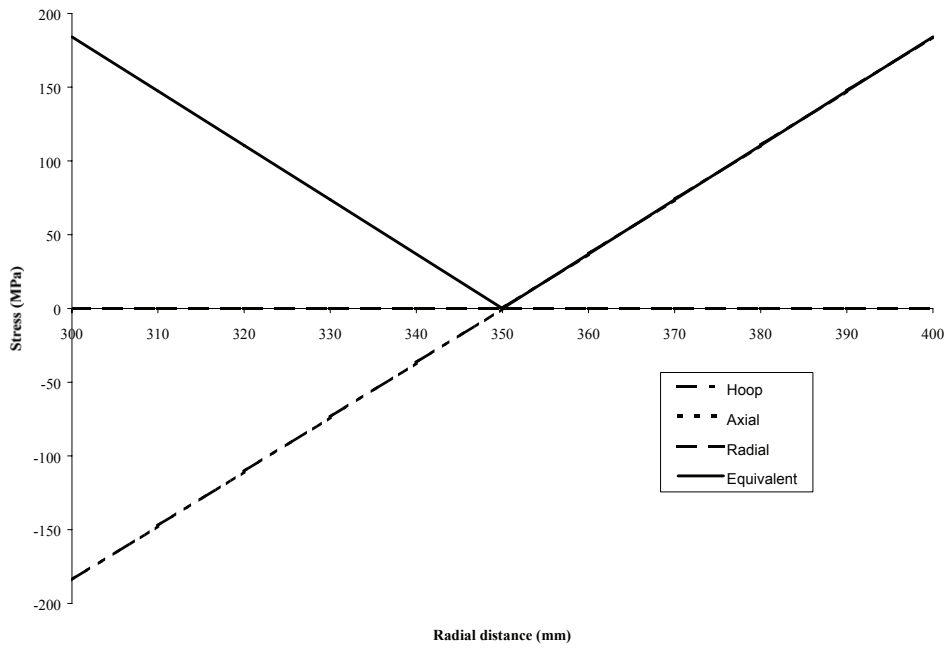


Figure A8.11 Shutdown shakedown elastic stresses (Example 5)

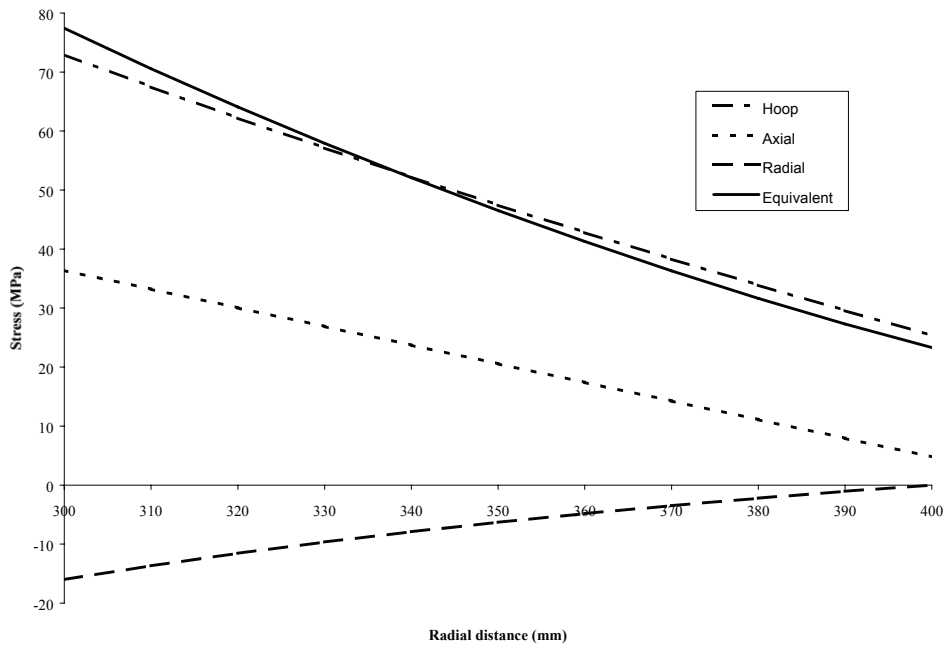


Figure A8.12 - Operating shakedown elastic stresses (Example 5)

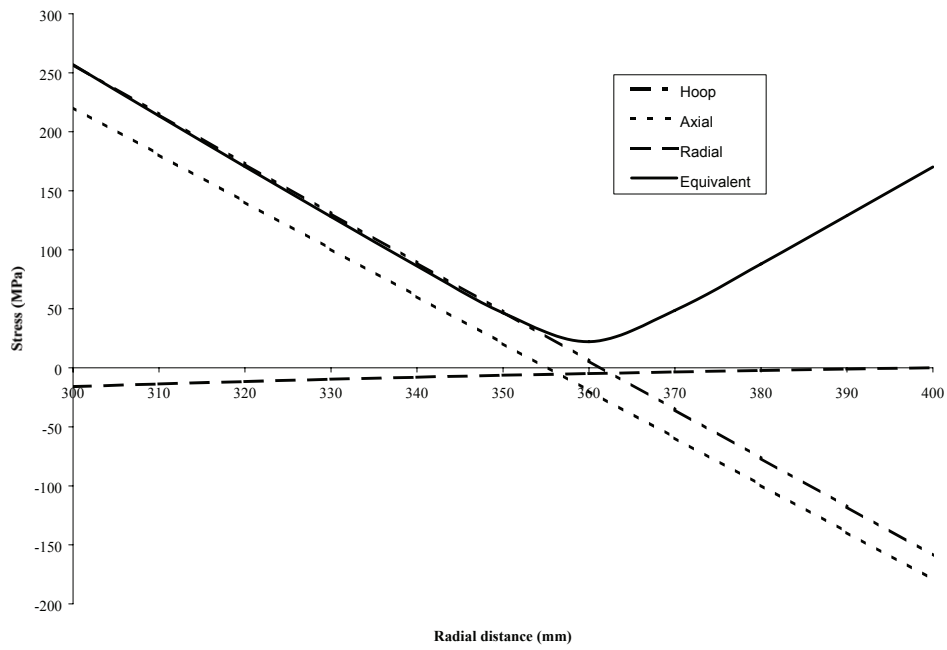


Figure A8.13 - Initial operating elastic stresses (Example 5)

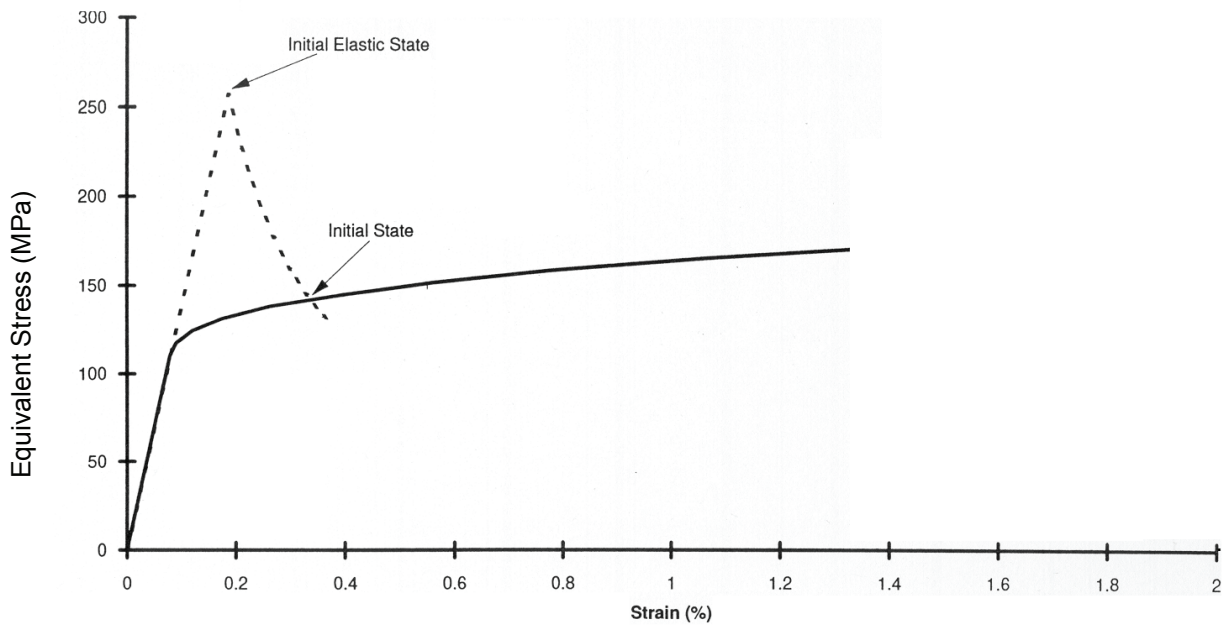


Figure A8.14 - Neuber construction for initial stresses at inner surface (Example 5)

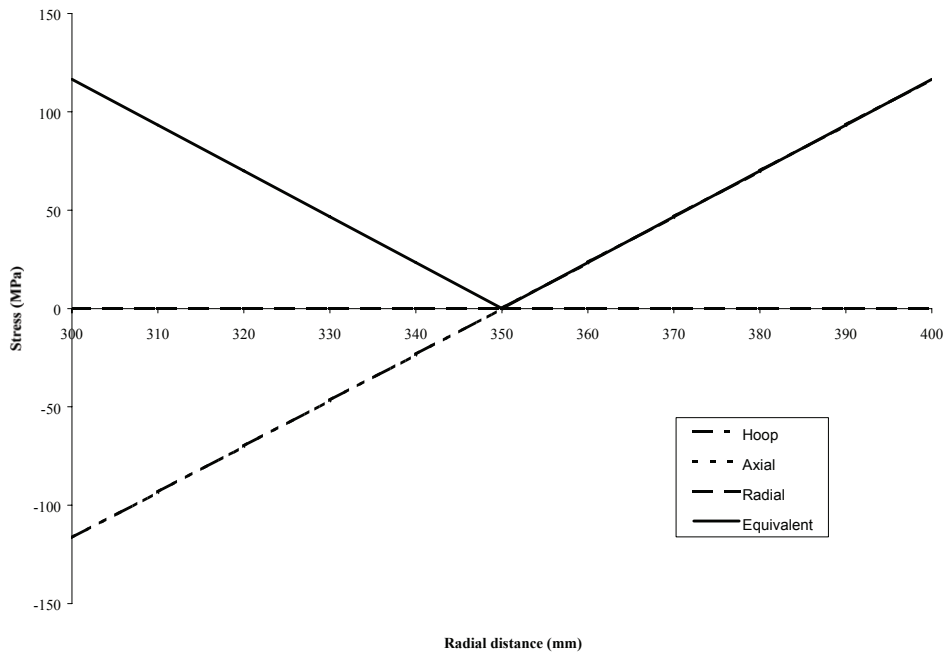


Figure A8.15 - Initial shutdown stresses for Example 5 (based on Neuber)

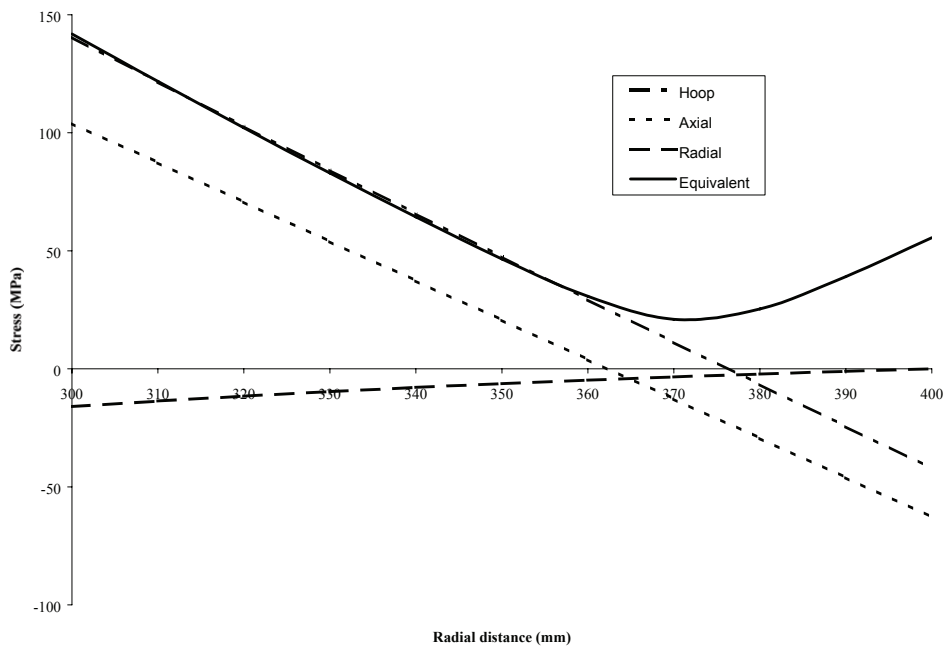


Figure A8.16- Initial operating stresses for Example 5 (based on Neuber)

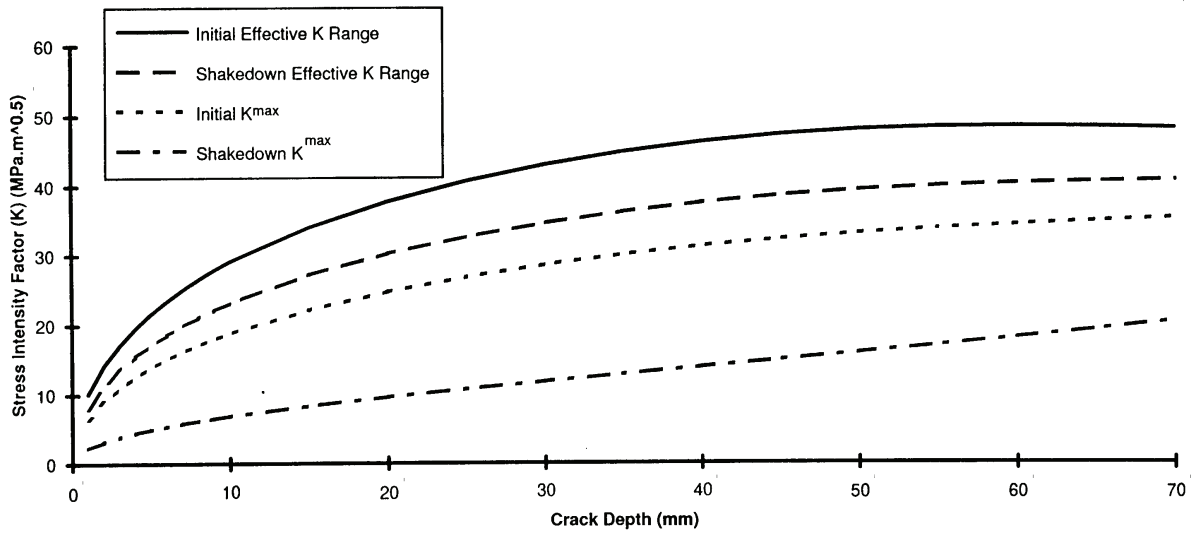


Figure A8.17 - Stress intensity factors for Example 5

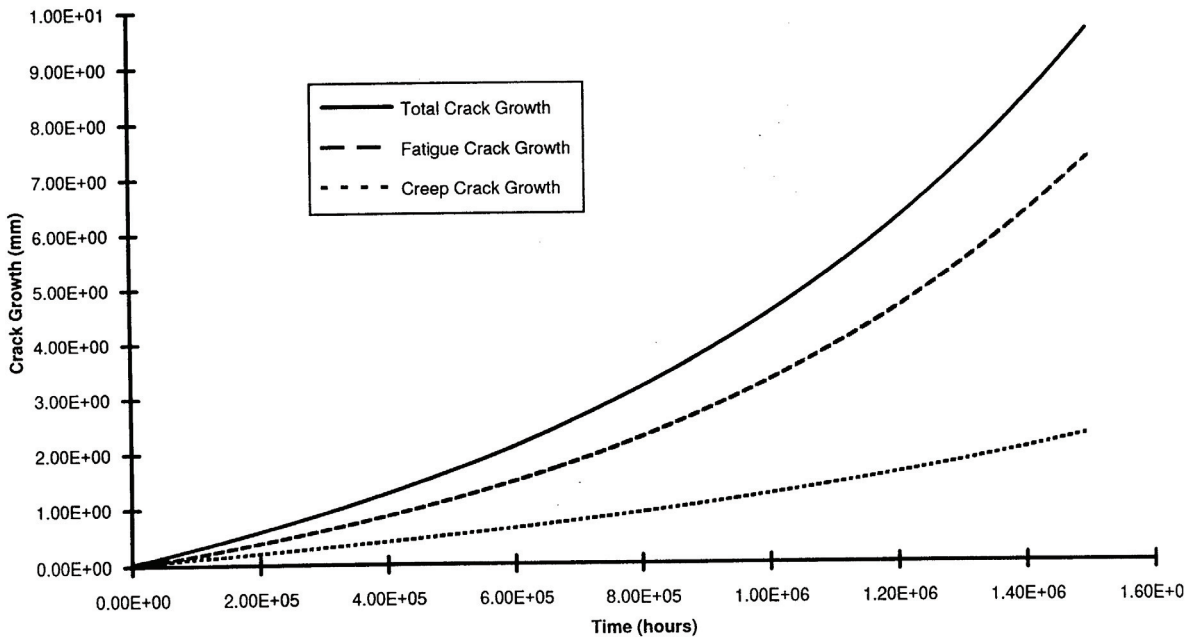


Figure A8.18- Calculation of crack growth in Example 5

13.4.4 Flat Plate With a Part-Penetrating Defect under Cyclic Loading

Specimen :	Flat plate
Loading :	Cycling bending
Material :	316L(N)
Defect :	Part-penetrating, semi-elliptical defect
Temperature :	650°C

A8.8 Example 7 - Flat Plate With a Part-Penetrating, Semi-Elliptical Defect Under Cyclic Loading

This example is a 316L(N) wide plate containing a semi-elliptical defect, which was subjected to cyclic bending at 650°C with 1 hour dwells at peak stress [A8.14, A8.15]. An assessment of the plate has been carried out [A8.4] as part of the validation of this volume (see Appendix A9) and it is presented here to illustrate application of the steps in this procedure and also relevant steps in the Volume 2/3 procedure (which are italicised so they can be distinguished from steps in this procedure).

A8.8.1 Establish cause of cracking and characterise initial defect (**Step 1**)

Cracking was caused by intentional machining and fatigue pre-cracking of a defect into the plate. This defect was present from the beginning of the test. Prior to the start of testing, the plate material had not undergone any creep damage. The defect is a semi-elliptical surface defect of depth, $a = 7.9\text{mm}$, and surface length, $2c = 87.2\text{mm}$, in a plate of thickness, $t = 24.5\text{mm}$, and width, $w = 350\text{mm}$. Since the initial defect profile is known fairly accurately, it is not necessary to simplify or bound the defect shape. The initial defect is shown schematically in Figure A8.24. The position of this defect within the plate component is shown in Figure A8.25.

A8.8.2 Define service conditions (**Step 2**)

The plate was subjected to bending loads and small membrane loads by loading on the arms connected to the top and bottom of the plate (see Figure A8.25). Note that a positive, tensile load on the loading arms produces a negative, compressive stress on the cracked side of the plate and vice versa. The temperature was held at 650°C throughout the test. The test conditions are shown in Figure A8.26 and Table A8.10. Triangular waveforms were used to cycle the load under load control. At the tensile peak of each creep fatigue cycle there was a one hour dwell period. Some pure fatigue cycles were also performed for beachmarking. These were carried out at a lower stress range.

A8.8.3 Collect materials data (**Step 3**)

For Type 316L(N) steel at 650°C, the following material properties have been obtained. For the purposes of this example representative rather than bounding data have been assumed.

A8.8.3.1 Elastic and physical constants

Young's modulus at 650°C was taken as 151GPa.

A8.8.3.2 Monotonic tensile data

The monotonic 0.2% proof stress is taken as 170MPa.

A8.8.3.3 Fracture toughness data

The initiation fracture toughness is taken as $K_{mat} = 170 \text{ MPa}\cdot\text{m}^{1/2}$.

A8.8.3.4 The shakedown factor, K_s

From R5 Volume 2/3 Figure 5.1, $K_s = 1.05$ at 650°C for Type 316 steel.

A8.8.3.4 Cyclic stress / strain data: Not required in this assessment.

A8.8.3.5 Creep rupture data: Creep rupture data are described by:

$$t_r = 10^{\left(\frac{13.72 - \frac{[\sigma + 353.1][\theta - 227]}{21.13 \times 10^3}}{\theta} \right)} \quad (\text{A8.94})$$

where σ is stress in MPa, θ is temperature in $^\circ\text{C}$ and t_r is the rupture life in hours.

A8.8.3.6 Creep deformation data: Creep deformation data follow the RCC-MR [A8.16] type equation given by

$$t_{fp} = C_3 \sigma^{n_3} \quad (\text{A8.95a})$$

$$\varepsilon = C_1 t^{C_2} \sigma^{n_1} \quad \text{for time, } t \leq t_{fp} \quad (\text{A8.95b})$$

$$\varepsilon = C_1 t_{fp}^{C_2} \sigma^{n_1} + 100 C \sigma^n (t - t_{fp}) \quad \text{for time, } t > t_{fp} \quad (\text{A8.95c})$$

where t is time in hours, σ is stress in MPa, ε is creep strain in percent and $C, C_1, C_2, C_3, n, n_1, n_3$ are temperature dependant constants. The values of these constants used in this example are given below.

C	C1	C2	C3	n	n1	n3
1.018E-25	5.863x10-11	0.565	5.8101x1028	9.407	4.233	-11.8943

A8.8.3.7 Creep ductility data: Not required in this assessment.

A8.8.3.8 Creep crack incubation data: Not required in this assessment as the incubation time has been pessimistically assumed to be zero.

A8.8.3.9 Creep crack growth data: Creep crack growth is estimated using equation (7.2) as:

$$\dot{a} = 0.001224 C^{*0.6728} \quad (\text{A8.96})$$

where \dot{a} is in m/h and C^* is in MPa.mh-1.

A8.8.3.10 Cyclic crack growth data: Fatigue crack growth per cycle is estimated using equation (7.3) as:

$$\left(\frac{da}{dN_f} \right) = 4.662 \times 10^{-2} \Delta K_{eff}^{2.339} \quad (\text{A8.97})$$

where da/dN is in m/cycle and ΔK_{eff} is in $\text{MPa}\sqrt{\text{m}}$.

A8.8.4 Perform basic stress analysis (Step 4)

For cyclic loading, the following are required:

A shakedown analysis (Section A8.8.4.1)

The elastic follow-up factor (Section A8.8.4.2)

The depth of the cyclic plastic zone on the surface of the defective section (Section A8.8.4.3)

The stress intensity factors, K_{min} and K_{max} and corresponding ranges and ratios (Section A8.8.4.4)

The reference stress for the creep dwell (Section A8.8.4.5)

A8.8.4.1 Shakedown analysis

An uncracked body stress analysis should be used for the shakedown calculations. The effect of the crack on the compliance of the structure should be small. For this assessment, the change in compliance is small, and can be neglected. Reference to Volume 2/3 needs to be made for the shakedown calculations. For the purposes of this assessment, the Volume 2/3 procedure has been joined at Section 6 (Perform Basic Analysis), and this part of the assessment is set out in terms of Volume 2/3 section headings.

Volume 2/3 Shakedown Analysis

Perform Basic Analysis

6.1 Resolve Load History Into Different Service Cycles (**Step 1**)

Two different cycle types exist (Section A8.8.2). These are the creep fatigue cycles and the beachmarking. Both were carried out at a temperature of 650°C.

6.2 Perform Elastic Stress Analysis (**Step 2**)

6.2.1 Perform stress analysis

As required by Volume 4/5, Section 8.2, the shakedown analysis should be performed for an uncracked body. For the plate test, all stresses are uniaxial and consist of a membrane and a bending component.

The membrane stresses can be calculated from:

$$\sigma_m = \frac{P}{wt} \quad (\text{A8.98})$$

where P is the load applied to the loading arms, w is the width of the plate (350mm) and t is the thickness (24.5mm). Peak values of σ_m for the creep-fatigue and beachmarking cycles are given below:

Creep-fatigue:

$$\sigma_m = \pm 1.63 \text{ MPa} \quad (\text{A8.99})$$

Beachmarking:

$$\sigma_m = \pm 1.17 \text{ MPa}$$

Maximum surface bending stresses are determined from the expression below. Note that the elastic bending stress distribution throughout the plate thickness is linear, varying from \pm the values determined below from one side of the plate to the other.

$$\sigma_b = \frac{3Pl}{2w\left(\frac{t}{2}\right)^2} \quad (\text{A8.100})$$

where P is the load applied to the loading arms, l is the loading arm length (350mm), w is the plate width (350mm) and t is the thickness (24.5mm). Peak values of the bending stress at the surface are given below:

$$\text{Creep-fatigue: } \sigma_b = \pm 139.9 \text{ MPa} \quad (\text{A8.101})$$

$$\text{Beachmarking: } \sigma_b = \pm 100.0 \text{ MPa}$$

It should be noted that the bending stress on the surface of the plate containing the defect has the opposite sign to the membrane stress, thus the total peak stress at the surface of the plate varies during the cycle as:

$$\text{Creep fatigue: } \sigma = \pm 138.3 \text{ MPa} \quad (\text{A8.102})$$

$$\text{Beachmarking: } \sigma = \pm 98.8 \text{ MPa}$$

6.2.2 Select critical locations

For the plate test, the most critical location is the plate surface which contains the defect. The stresses are at their highest on the surfaces.

6.2.3 Calculate equivalent stress and strain ranges

Reference is made to Volume 2/3, Appendix A2.

A2.3.4 Equivalent stress and strain ranges

For the plate test, all stresses are uniaxial and are fully reversed in the cycle, so equivalent stress and strain ranges can be calculated easily for the surface position:

$$\text{Creep fatigue: } \Delta\bar{\sigma} = 2 \times 138.3 = 276.6 \text{ MPa} \quad (\text{A8.103})$$

$$\text{Beachmarking: } \Delta\bar{\sigma} = 2 \times 98.8 = 197.6 \text{ MPa}$$

Elastic strain ranges of 0.183% and 0.131% have been calculated for the creep-fatigue and beachmarking cycles, respectively.

6.2.4 Calculate P_m, P_L, P_B, Q and F

For both creep-fatigue and beachmarking cycles, a convenient stress classification line is a through thickness line from the surface containing the defect to the back surface of the plate. For the purposes of this assessment, it is assumed that P_m = P_L. Since all the elastic stresses in the plate are uniaxial and have linear distributions across the wall thickness, P_L and P_B can simply be equated with σ_m and σ_b respectively, as given above. There are no thermal stresses, so Q = 0. In addition, since all elastic stresses are linear across the section, F stresses are zero.

6.3 Demonstrate sufficient margins against plastic collapse (**Step 3**)

For the purposes of this example, S'_y is taken as the 0.2% proof stress of 170MPa. The simple checks for margins against collapse are shown below for the various material properties at the extremes of the creep fatigue cycle (the beachmarking is under less onerous conditions and will therefore have sufficient margins against collapse if the creep fatigue cycles do).

$$P_m \leq 0.67 S'_y \quad (\text{equation (6.1) of Volume 2/3})$$

$$1.633 \leq 0.67 \times 170 = 113.9 \text{ PASSED}$$

$$PL + PB \leq S'_y \quad (\text{equation (6.2) of Volume 2/3})$$

$$138.3 \leq 170 \quad \text{PASSED}$$

$$(PL + PB + Q) \leq 2.7 S'_y \quad (\text{equation (6.4) of Volume 2/3})$$

$$276.6 \leq 2.7 \times 170 = 459 \quad \text{PASSED}$$

It can be seen that the margins against plastic collapse are demonstrated for the uncracked structure.

6.4 Determine Whether Creep is Significant (Step 4)

Note that the following check has been applied to the uncracked body. A further check on the significance of creep is carried out in Step 6 of Volume 4/5. Creep can be neglected if:

$$\sum_j n_j \left[\frac{t}{t_m(T_{ref})} \right]_j \leq 1 \quad (\text{equation (6.5) of Volume 2/3}) \quad (\text{A8.104})$$

where t is the hold time, n_j is the number of cycles of type j and t_m is determined from Volume 2/3 Figure 5.3(a) at a temperature of 650°C as approximately 1.25 hours. Only the creep-fatigue cycles need be considered, of which there are 3129 at 1 hour each, and therefore creep is significant for the uncracked body.

Demonstrate that Creep Rupture Endurance is Satisfactory (Step 5)

Demonstration that creep rupture endurance is satisfactory is not necessary at this stage as calculations performed in Step 7 of Volume 4/5 cover this area.

6.5 Perform Simple Test for Shakedown and Check for Insignificant Cyclic Loading (Step 6)

6.5.1 Simple test for global shakedown

It must be shown that elastic linearised stresses are lower than the modified yield limit ($K_s S_y$) for all times and positions. From Section A8.8.34, $K_s = 1.05$. Taking the most onerous position at the plate surface at the peak of the creep-fatigue cycle gives:

$$\Delta \bar{\sigma}_{lin}(x, t) \leq K_s S_y \quad (\text{equation (6.11) of Volume 2/3}) \quad (\text{A8.105})$$

$$138.3 \leq 1.05 \times 170 = 178.5 \text{ PASSED}$$

Thus, the simple test for global shakedown has been satisfied for the uncracked plate.

6.5.2 Check for insignificant cyclic loading

The following check has been made to determine whether the plate is in strict shakedown:

$$\Delta \bar{\sigma}_{el,max} \leq (K_s S_y)_c + (K_s S_y)_{nc} \quad (\text{equation (6.14) of Volume 2/3}) \quad (\text{A8.106})$$

$$276.6 \leq 2(1.05 \times 170) = 357 \quad \text{PASSED}$$

Since the cycle is performed at a uniform temperature, K_{sSy} is the same for both extremes of the cycle. Thus, the creep fatigue cycles are in strict shakedown. At this stage, further checks on whether fatigue is insignificant have been neglected and the assessment can return to R5 Volume 4/5 Section 8.3.

End of Volume 2/3 Shakedown Analysis

A8.8.4.2 Elastic follow-up factor

Since the wide plate tests were performed under load control, the elastic follow-up factor is not required as stress relaxation does not occur.

A8.8.4.3 Surface cyclic plastic zone parameters

It was determined in Volume 2/3 Section 6.6 above, that the plate test is in strict shakedown. There are therefore no surface plastic zones and the Method I crack growth laws can be applied.

A8.8.4.4 Stress intensity factors

The stress intensity factor solutions used for this assessment were the Newman and Raju solutions for a semi-elliptical surface defect under bending and tension [A8.17]. For the initial crack size, the stress intensity factors at the deepest point, K_a , and at the surface points, K_c are:

$$\text{Creep Fatigue: } K_a = \pm 17.1 \text{ MPa.m}^{1/2} \quad (\text{A8.107})$$

$$K_c = \pm 11.7 \text{ MPa.m}^{1/2}$$

$$\text{Beachmarking: } K_a = \pm 12.2 \text{ MPa.m}^{1/2}$$

$$K_c = \pm 8.3 \text{ MPa.m}^{1/2}$$

The cycles are in strict shakedown and are fully reversed, i.e. $R = -1$. The stress intensity factor ranges for the initial conditions are:

$$\text{Creep Fatigue: } K_a = \pm 34.3 \text{ MPa.m}^{1/2} \quad (\text{A8.108})$$

$$K_c = \pm 23.4 \text{ MPa.m}^{1/2}$$

$$\text{Beachmarking: } K_a = \pm 16.7 \text{ MPa.m}^{1/2}$$

$$K_c = \pm 24.5 \text{ MPa.m}^{1/2}$$

For the purposes of this assessment, the stress intensity factors were recalculated after each increment of crack growth.

A8.8.4.5 Reference stress and C^* parameter

The reference stress used in this assessment was determined using the solution given in [A8.18]. The reference stress during dwell for the initial crack size is:

$$\sigma_{\text{ref}} = 105.2 \text{ MPa} \quad (\text{A8.109})$$

The reference stress was recalculated for each increment of crack growth. C^* was estimated using reference stress techniques as discussed in Section A8.8.9.1.

A8.8.5 Check stability under time-independent loads (**Step 5**)

The procedure requires an R6 assessment [A8.8] to preclude failure by time-independent mechanisms. For the purposes of this example, the crack was assessed for the initial conditions and for the final crack size of a

= 13.35 mm and $c/2 = 54.98$ mm. For brevity, details of the calculations performed are not repeated here. Both deepest and surface points fall well within the R6 Option 1 FAD, as shown in Figure A8.27.

A8.8.6 Check significance of creep and fatigue (**Step 6**)

Note that the checks carried out in this section supersede those carried out as part of the Volume 2/3 analysis.

A8.8.6.1 Test for Insignificant Creep

This test is not necessary as creep was shown to be significant for the uncracked structure, and will, therefore, also be significant for the cracked structure.

A8.8.6.2 Test for insignificant fatigue

Reference is made to Volume 2/3 Section 6.6.2 to check the overall structural response.

Volume 2/3 Overall Structural Test for Insignificant Cyclic Loading

6.6.2 Check for insignificant cyclic loading

It has been shown previously that the inequality of equation (6.14) of Volume 2/3 has been satisfied. It is then necessary to check whether the creep behaviour is unperturbed by cyclic loading. For creep dwell at peak tensile stress, as in this case, it should be demonstrated that the inequality of equation (6.17) of Volume 2/3 is satisfied. Firstly, the steady state creep stress, σ_{ss} , is calculated from equation (6.7) of Volume 2/3 as 109.493MPa.

$$\Delta\bar{\sigma}_{el,max} \leq \sigma_{ss} + (K_s S_y)_{nc} \quad (A8.110)$$

Creep Fatigue: $276.6 \leq 109.5 + (170 \times 1.05) = 288.0$ PASSED

End of Volume 2/3 Test for Insignificant Cyclic Loading

In addition to the overall structural response, it is also necessary to demonstrate that the cyclic plastic zone at the crack tip is small for cyclic loading to be considered insignificant. An estimate of the plastic zone size is calculated from:

$$r_p^{crack} = \beta \left(\Delta K / 2\sigma_y \right)^2 \quad (A8.111)$$

where β is $1/2\pi$ for plane stress and $1/6\pi$ for plane strain. Using the plane stress value for conservatism, gives:

$$r_p^{crack} = \frac{1}{2\pi} \left(\frac{34.3}{2 \times 170} \right)^2 = 1.6 \text{ mm} \quad (A8.112)$$

This value is small compared with the crack depth and other structural dimensions so that cyclic loading can be considered to be insignificant. Both the overall structural response and the local behaviour confirm that cyclic loading is insignificant. It is also necessary to check whether fatigue is insignificant; fatigue is deemed to be insignificant if the total fatigue crack growth does not exceed 1/10 of the creep crack growth. Values shown here have been calculated for the 250th creep fatigue cycle and the 2612th creep fatigue cycle. The first cycles were neglected since creep crack growth rates are predicted to be higher during the redistribution period. However, redistribution occurs relatively quickly, so the overall effect is limited.

Cycle 250 Creep Crack Growth: 1.14×10^{-3} mm

Cycle 250 Fatigue Crack Growth:	9.28 x 10 ⁻⁴ mm	
Ratio of Fatigue/Creep Growth:	0.81 > 1/10	FAILED
Cycle 2612 Creep Crack Growth:	5.20 x 10 ⁻⁴ mm	
Cycle 2612 Fatigue Crack Growth:	6.01 x 10 ⁻⁴ mm	
Ratio of Fatigue/Creep Growth:	1.15 > 1/10	FAILED

It can be seen that the ratio of fatigue to creep crack growth increases such that towards the end of the test the fatigue crack growth is greater than the creep crack growth. Therefore, fatigue crack growth is significant for this example.

A8.8.6.3 Test for insignificant creep-fatigue interaction

Creep-fatigue interaction can be considered to be insignificant as cyclic loading is insignificant and fatigue crack growth is a significant proportion of the total crack growth per cycle

A8.8.7 Calculate rupture life based on the initial defect size (Step 7)

Calculation of the rupture life using equation (10.1) requires the initial reference stress, as calculated in Section A8.8.4.5 (105.2 MPa), and the rupture expression given in Section A8.8.3.5. From these data, the time, t_{CD} is calculated as 35122 hours. This is significantly greater than the assessment time of 3129 hours, so failure by creep of the remaining ligament is avoided.

A8.8.8 Calculate incubation time (Step 8)

Where fatigue is significant, it is conservative to assume that the incubation time is zero.

A8.8.9 Calculate crack size after growth (Step 9)

R5 Volume 4/5 calculations of crack growth take account of incremental changes in the crack length on creep and fatigue crack growth as well as on the stress intensity factors and reference stress. The crack growth calculations have been implemented numerically in a spreadsheet. Crack growth in the through thickness direction and along the plate surface have been considered separately. It is assumed that the crack maintains a semi-elliptical shape throughout, although the aspect ratio is allowed to change as a result of different crack growth rates at the deepest and surface points. Blocks of creep-fatigue cycles and beachmarking cycles were assessed in the order in which they were applied in the test. These calculations were also carried out using R-Code [A8.9] and the results are given in Section A8.8.13.

A8.8.9.1 Calculate the crack tip parameters

Calculation of K_{eff} for cyclic crack growth

For the load controlled current assessment, R is always -1. Thus, q_o is always 0.75 and $\Delta K_{eff} = 0.75\Delta K$.

Calculation of R' and C* for creep crack growth

For the calculation of R' in equation (10.6), K_p is equal to K_{max} for the creep-fatigue cycles and σ_{ref}^p is equal to σ_{ref} . R' was recalculated for every increment of crack growth. Equation (10.7) was used to estimate C* with a strain hardening law applied to the calculation of the creep strain rate. C* was recalculated for every increment of crack growth considered. Equation (A1.14) was used to demonstrate that crack growth can be characterised by C* as $\lambda \ll 0.5$.

A8.8.9.2 Calculate the redistribution time, t_{red}

Calculation of the redistribution time is required when cyclic loading is insignificant, as in the current example. Equation (10.9) has been solved within the Visual Basic code by comparing the accumulated creep strain (required for calculation of C^*) with the elastic strain at the reference stress. The redistribution time is relatively short for this example.

A8.8.9.3 Calculate Crack Growth, Δa_g

Steady state creep crack growth

Equation (10.11) has been solved numerically in a spreadsheet by splitting the creep dwell into 10 equal increments of time. To ascertain whether more increments would affect the results, the code was re-run using 1000 increments for each creep dwell and the difference in the two predicted final crack sizes was only 0.001%. The small dependence on the number of increments is probably due to the fact that the dwells are under load control and there is no stress drop to model.

Non steady state creep crack growth, $t < t_{red}$

Since the total assessment time was significantly greater than the redistribution time, it was possible to estimate the creep crack growth during the redistribution period by doubling the steady state crack growth rate in accordance with equation (10.13).

Fatigue Crack Growth per cycle, $(da/dN)_f$

Fatigue crack growth was calculated using equation (10.20).

Combined creep and fatigue crack growth per cycle, da/dN

Since there is no cyclic plasticity for the uncracked structure, it is clear that the Method 1 crack growth rate law of equation (10.20) can be used. For each creep fatigue cycle, the creep crack growth was calculated first for the creep dwell. Fatigue crack growth was then calculated based on the current crack size (including creep crack growth) and added to the total crack size.

A8.8.10 Re-calculate rupture life after growth (**Step 10**)

At each increment of crack growth during the creep-fatigue cycles, the rupture life check of Section A8.8.7 was repeated for the current crack size.

A8.8.11 Check stability of time-independent loads after growth (**Step 11**)

The calculations carried out in Step 5 (Section A8.5.5) show that the crack is stable under time-independent loads for all crack sizes encountered in the test. This check was therefore not repeated as a part of the spreadsheet calculations.

A8.8.12 Assess significance of results (**Step 12**)

The results of the analysis are shown in Figure A8.28 for crack growth through the plate thickness and in Figure A8.29 for crack growth along the surface. Both predictions were determined using cast-specific mean material properties. These figures also show crack growth measurements from the test, although no further discussion of the comparison between measured and predicted crack sizes is given here; these aspects are discussed for this test in Appendix A9, which also considers the sensitivity of the predictions to various input parameters.

A8.8.13 R-Code results

Properties Data number 1 geometry Property 1

RunTime Formula given by:-

sif(r.membrane(r.total,r.total),-r.bending(r.total,r.total),
r.sminor,r.smajor,24.5,175,90)

Properties Data number 2 geometry Property 2

RunTime Formula given by:-

SIF(r.membrane(r.total,r.total),-r.bending(r.total,r.total),
r.sminor,r.smajor,24.5,175,0)

Geometric Data

Code number= 25

(Finite Width Plate Containing Surface Elliptic Flaw

Arbitrary Stress)

Section size = 24.50000 mm

Stress Intensity Factor given by property 1 Stress Intensity Factor given by property 2

Load Data load-1

Stress polynomial

$$=a_0+a_1*x+a_2*x^{**2}+a_3*x^{**3}+ \dots +a_8*x^{**8}$$

Where x=Independent variable and

Term Value

a0 138.31

a1 -11.424

Properties Data number 3 mats-1 Property 1

RunTime Formula given by:-

CreepStrain(r.ref,r.straintime)

Properties Data number 4 mats-1 Property 2

RunTime Formula given by:-

$$10^{(13.72-((r.ref+353.1)*(r.temp-227))/21.13e3)}$$

Materials Data mats-1

Lower bound yield = 1.7000E+02 MPa

Mean yield = 1.7000E+02 MPa

Ultimate Tensile Stress = 4.0000E+02 MPa

Youngs Modulus = 1.5850E+05 MPa

Poissons Ratio = 3.0000E-01

Fracture Toughness = 1.7000E+02 MPa m**1/2

Material is Non volume 7 material

Ductility = 0.0000E+00

Formula strain method will be adopted

Factor on Strain = 1.00000000000000

Creep strain given by property 3

Creep Strain at t=0 = 0.00000000000000E+000

R5 Volume 4 method used to calculate creep crack growth during redistribution period

Continuum damage failure determined using life fraction rule

A user supplied equation for rupture is to be used:

$$S = 1.0000$$

$$M = 1.0000$$

Minimum valid stress = 0.00000000000000E+000 Mpa

Maximum valid stress = 1000000.00000000 Mpa

Minimum valid temperature = 0.00000000000000E+000 C

Maximum valid temperature = 1000000.00000000 C

Rupture time given by property 4

Creep crack growth equation

$$da/dt=A*(Cstar**m)$$

Where da/dt = Creep crack growth rate (mm/h) & Cstar = C* (MN/mh)

Creep crack growth const= 1.2240E+00

Creep crack growth expon= 6.7280E-01

No allowance for incubation

Assessment Results

prob-3

Assessment at both crack tips, Crack length is semi-minor, Incubation has not occurred after 0.36 yrs (3171.1 hrs)

After 0.36 years (3171.1 hrs) -

Final predicted crack depth = 14.401 mm

2nd crack dim (s-major or offset) = 51.074 mm

Final creep strain (1st tip) = 2.3552E-02 (2nd tip) = 2.3552E-02

Creep crack growth (1st tip) = 2.388 mm (2nd tip) = 2.527 mm

Creep life fraction (1st tip) = 0.11 (2nd tip) = 0.11

Redistribution time at 2nd tip = 0.00 yrs (7.5 hrs)

Integrated creep crack growth in redistribution time at 2nd tip = 0.040 mm

Code no= 25, Reference/Lr eqn=usrp

R6 Toughness= 170 MPa m^{1/2}, R6 Yield Stress= 170 MPa

A. Defect Size Information

Time (hrs)	Semi- Minor Crack Length (mm)	Semi- Major Crack Length (mm)	Creep Increment (mm)	Total Creep Growth (mm)	Creep Crack Growth Rate (mm/h)	Creep Increment Tip 2 (mm)	Total Creep Grwth Tip2 (mm)	Creep Crack Growth Rate Tip2 (mm/h)
87.60	8.20281	43.7706	2.221E-001	2.221E-001	1.537E-003	1.358E-001	1.358E-001	9.651E-004
175.20	8.40526	43.8851	1.207E-001	3.429E-001	1.264E-003	7.706E-002	2.129E-001	8.198E-004
262.80	8.59018	43.9928	1.042E-001	4.471E-001	1.128E-003	6.861E-002	2.815E-001	7.543E-004
350.40	8.76653	44.0986	9.480E-002	5.418E-001	1.042E-003	6.428E-002	3.458E-001	7.168E-004
438.00	8.93629	44.2037	8.841E-002	6.303E-001	9.801E-004	6.164E-002	4.074E-001	6.926E-004
525.60	9.93561	44.8441	6.700E-002	6.973E-001	9.575E-004	5.135E-002	4.588E-001	7.957E-004
613.20	10.09466	44.9702	8.176E-002	7.790E-001	9.114E-004	6.883E-002	5.276E-001	7.770E-004
700.80	10.25029	45.0978	7.810E-002	8.571E-001	8.733E-004	6.744E-002	5.950E-001	7.636E-004
788.40	10.40218	45.2264	7.503E-002	9.322E-001	8.410E-004	6.642E-002	6.614E-001	7.535E-004
876.00	10.54986	45.3556	7.240E-002	1.005E+000	8.129E-004	6.566E-002	7.271E-001	7.461E-004
963.60	10.69537	45.4870	7.009E-002	1.075E+000	7.880E-004	6.510E-002	7.922E-001	7.406E-004
1051.20	10.83722	45.6193	6.803E-002	1.143E+000	7.657E-004	6.469E-002	8.569E-001	7.366E-004
1138.80	10.97729	45.7542	6.617E-002	1.209E+000	7.455E-004	6.439E-002	9.213E-001	7.337E-004
1226.40	11.11487	45.8909	6.448E-002	1.273E+000	7.270E-004	6.418E-002	9.855E-001	7.318E-004
1314.00	11.77541	46.6245	5.343E-002	1.327E+000	7.067E-004	5.618E-002	1.042E+000	7.937E-004
1401.60	11.90460	46.7788	6.114E-002	1.388E+000	6.895E-004	6.941E-002	1.111E+000	7.913E-004

1489.20 12.03067 46.9340 5.968E-002 1.448E+000 6.734E-004 6.923E-002 1.180E+000 7.895E-004
1576.80 12.15526 47.0921 5.832E-002 1.506E+000 6.584E-004 6.910E-002 1.249E+000 7.883E-004
1664.40 12.27693 47.2511 5.704E-002 1.563E+000 6.443E-004 6.901E-002 1.318E+000 7.875E-004
1752.00 12.39725 47.4131 5.584E-002 1.619E+000 6.310E-004 6.897E-002 1.387E+000 7.873E-004
1839.60 12.51555 47.5772 5.471E-002 1.673E+000 6.183E-004 6.896E-002 1.456E+000 7.873E-004
1927.20 12.63117 47.7421 5.363E-002 1.727E+000 6.064E-004 6.898E-002 1.525E+000 7.876E-004
2014.80 12.74559 47.9102 5.261E-002 1.780E+000 5.950E-004 6.902E-002 1.594E+000 7.882E-004
2102.40 12.85747 48.0792 5.163E-002 1.831E+000 5.841E-004 6.908E-002 1.663E+000 7.890E-004
2190.00 12.96823 48.2514 5.070E-002 1.882E+000 5.737E-004 6.916E-002 1.733E+000 7.901E-004
2277.60 13.07724 48.4257 4.981E-002 1.932E+000 5.637E-004 6.926E-002 1.802E+000 7.913E-004
2365.20 13.18386 48.6008 4.895E-002 1.981E+000 5.541E-004 6.937E-002 1.871E+000 7.926E-004
2452.80 13.28948 48.7791 4.813E-002 2.029E+000 5.449E-004 6.949E-002 1.941E+000 7.941E-004
2540.40 13.39282 48.9583 4.733E-002 2.076E+000 5.360E-004 6.962E-002 2.010E+000 7.956E-004
2628.00 13.49520 49.1407 4.657E-002 2.123E+000 5.274E-004 6.977E-002 2.080E+000 7.973E-004
2715.60 13.91648 50.0362 3.997E-002 2.163E+000 5.136E-004 6.387E-002 2.144E+000 8.363E-004
2803.20 14.01283 50.2321 4.463E-002 2.207E+000 5.055E-004 7.331E-002 2.217E+000 8.376E-004
2890.80 14.10711 50.4285 4.393E-002 2.251E+000 4.976E-004 7.343E-002 2.291E+000 8.390E-004
2978.40 14.20054 50.6283 4.325E-002 2.295E+000 4.901E-004 7.356E-002 2.364E+000 8.406E-004
3066.00 14.29200 50.8287 4.261E-002 2.337E+000 4.828E-004 7.371E-002 2.438E+000 8.423E-004
3153.60 14.38266 51.0325 4.199E-002 2.379E+000 4.759E-004 7.388E-002 2.512E+000 8.443E-004
3166.74 14.39603 51.0629 6.247E-003 2.385E+000 4.749E-004 1.110E-002 2.523E+000 8.447E-004

B. Fatigue Information

Time (hrs)	Semi- Minor Crack Length (mm)	Semi- Major Crack Length (mm)	Fatigue SIF Max. (MPa/~m)	Fatigue SIF Min. (MPa/~m)	Effective Fatigue SIF Range (MPa/~m)	Fatigue Increment (mm)	Fat Cyc	Total Fatigue Crack Growth (mm)
87.60	8.20281	43.7706	17.155	-17.155	25.732	8.069E-002	87	8.069E-002
175.20	8.40526	43.8851	17.156	-17.156	25.734	8.170E-002	175	1.624E-001
262.80	8.59018	43.9928	17.149	-17.149	25.723	8.074E-002	262	2.431E-001
350.40	8.76653	44.0986	17.135	-17.135	25.702	8.155E-002	350	3.247E-001
438.00	8.93629	44.2037	17.114	-17.114	25.672	8.135E-002	438	4.060E-001
525.60	9.93561	44.8441	16.864	-16.864	25.296	9.323E-001	2607	1.338E+000
613.20	10.09466	44.9702	16.807	-16.807	25.210	7.729E-002	2694	1.416E+000
700.80	10.25029	45.0978	16.745	-16.745	25.118	7.753E-002	2782	1.493E+000
788.40	10.40218	45.2264	16.681	-16.681	25.022	7.685E-002	2870	1.570E+000
876.00	10.54986	45.3556	16.615	-16.615	24.922	7.529E-002	2957	1.645E+000
963.60	10.69537	45.4870	16.545	-16.545	24.817	7.542E-002	3045	1.721E+000
1051.20	10.83722	45.6193	16.473	-16.473	24.710	7.382E-002	3132	1.795E+000
1138.80	10.97729	45.7542	16.398	-16.398	24.598	7.390E-002	3220	1.868E+000
1226.40	11.11487	45.8909	16.322	-16.322	24.483	7.311E-002	3308	1.942E+000
1314.00	11.77541	46.6245	15.911	-15.911	23.867	6.071E-001	4882	2.549E+000
1401.60	11.90460	46.7788	15.822	-15.822	23.733	6.805E-002	4970	2.617E+000
1489.20	12.03067	46.9340	15.733	-15.733	23.599	6.640E-002	5057	2.683E+000
1576.80	12.15526	47.0921	15.642	-15.642	23.463	6.627E-002	5145	2.749E+000
1664.40	12.27693	47.2511	15.551	-15.551	23.327	6.463E-002	5232	2.814E+000
1752.00	12.39725	47.4131	15.459	-15.459	23.189	6.448E-002	5320	2.878E+000
1839.60	12.51555	47.5772	15.366	-15.366	23.050	6.358E-002	5408	2.942E+000
1927.20	12.63117	47.7421	15.274	-15.274	22.912	6.199E-002	5495	3.004E+000
2014.80	12.74559	47.9102	15.181	-15.181	22.772	6.181E-002	5583	3.066E+000
2102.40	12.85747	48.0792	15.089	-15.089	22.633	6.024E-002	5670	3.126E+000

2190.00	12.96823	48.2514	14.995	-14.995	22.493	6.007E-002	5758	3.186E+000
2277.60	13.07724	48.4257	14.902	-14.902	22.353	5.920E-002	5846	3.245E+000
2365.20	13.18386	48.6008	14.809	-14.809	22.214	5.768E-002	5933	3.303E+000
2452.80	13.28948	48.7791	14.716	-14.716	22.074	5.749E-002	6021	3.361E+000
2540.40	13.39282	48.9583	14.624	-14.624	21.936	5.600E-002	6108	3.417E+000
2628.00	13.49520	49.1407	14.531	-14.531	21.797	5.582E-002	6196	3.472E+000
2715.60	13.91648	50.0362	14.156	-14.156	21.235	3.813E-001	7473	3.854E+000
2803.20	14.01283	50.2321	14.064	-14.064	21.096	5.172E-002	7561	3.905E+000
2890.80	14.10711	50.4285	13.973	-13.973	20.960	5.036E-002	7648	3.956E+000
2978.40	14.20054	50.6283	13.882	-13.882	20.824	5.017E-002	7736	4.006E+000
3066.00	14.29200	50.8287	13.793	-13.793	20.690	4.885E-002	7823	4.055E+000
3153.60	14.38266	51.0325	13.704	-13.704	20.555	4.867E-002	7911	4.103E+000
3166.74	14.39603	51.0629	13.690	-13.690	20.536	7.127E-003	7924	4.111E+000

B2. Fatigue Information - Second Crack Tip

Time (hrs)	Semi- Minor Crack Length (mm)	Semi- Major Crack Length (mm)	SIF Pos 2 (Max) (MPa/~m)	SIF Pos 2 (Min) (MPa/~m)	Effective Fatigue SIF Range Tip 2 (MPa/~m)	Fatigue Increment Tip 2 (mm)	Fat Cyc	Total Fatigue Crack Grwth Tip2 (mm)
87.60	8.20281	43.7706	12.136	-12.136	18.205	3.475E-002	87	3.475E-002
175.20	8.40526	43.8851	12.438	-12.438	18.657	3.746E-002	175	7.221E-002
262.80	8.59018	43.9928	12.711	-12.711	19.066	3.908E-002	262	1.113E-001
350.40	8.76653	44.0986	12.973	-12.973	19.459	4.152E-002	350	1.528E-001
438.00	8.93629	44.2037	13.224	-13.224	19.836	4.348E-002	438	1.963E-001
525.60	9.93561	44.8441	14.696	-14.696	22.044	5.891E-001	2607	7.854E-001
613.20	10.09466	44.9702	14.927	-14.927	22.391	5.730E-002	2694	8.427E-001
700.80	10.25029	45.0978	15.154	-15.154	22.731	6.007E-002	2782	9.027E-001
788.40	10.40218	45.2264	15.375	-15.375	23.062	6.218E-002	2870	9.649E-001
876.00	10.54986	45.3556	15.588	-15.588	23.382	6.354E-002	2957	1.028E+000
963.60	10.69537	45.4870	15.799	-15.799	23.698	6.635E-002	3045	1.095E+000
1051.20	10.83722	45.6193	16.003	-16.003	24.004	6.764E-002	3132	1.162E+000
1138.80	10.97729	45.7542	16.204	-16.204	24.307	7.047E-002	3220	1.233E+000
1226.40	11.11487	45.8909	16.402	-16.402	24.604	7.254E-002	3308	1.305E+000
1314.00	11.77541	46.6245	17.343	-17.343	26.015	6.774E-001	4882	1.983E+000
1401.60	11.90460	46.7788	17.527	-17.527	26.290	8.486E-002	4970	2.068E+000
1489.20	12.03067	46.9340	17.705	-17.705	26.557	8.594E-002	5057	2.154E+000
1576.80	12.15526	47.0921	17.881	-17.881	26.821	8.899E-002	5145	2.243E+000
1664.40	12.27693	47.2511	18.052	-18.052	27.078	9.000E-002	5232	2.333E+000
1752.00	12.39725	47.4131	18.222	-18.222	27.332	9.306E-002	5320	2.426E+000
1839.60	12.51555	47.5772	18.388	-18.388	27.582	9.509E-002	5408	2.521E+000
1927.20	12.63117	47.7421	18.550	-18.550	27.824	9.599E-002	5495	2.617E+000
2014.80	12.74559	47.9102	18.710	-18.710	28.065	9.909E-002	5583	2.716E+000
2102.40	12.85747	48.0792	18.866	-18.866	28.299	9.992E-002	5670	2.816E+000

2190.00	12.96823	48.2514	19.021	-19.021	28.531	1.030E-001	5758	2.919E+000
2277.60	13.07724	48.4257	19.173	-19.173	28.760	1.050E-001	5846	3.024E+000
2365.20	13.18386	48.6008	19.321	-19.321	28.982	1.057E-001	5933	3.130E+000
2452.80	13.28948	48.7791	19.468	-19.468	29.203	1.089E-001	6021	3.238E+000
2540.40	13.39282	48.9583	19.612	-19.612	29.417	1.095E-001	6108	3.348E+000
2628.00	13.49520	49.1407	19.754	-19.754	29.631	1.127E-001	6196	3.461E+000
2715.60	13.91648	50.0362	20.336	-20.336	30.503	8.316E-001	7473	4.292E+000
2803.20	14.01283	50.2321	20.469	-20.469	30.704	1.226E-001	7561	4.415E+000
2890.80	14.10711	50.4285	20.600	-20.600	30.899	1.230E-001	7648	4.538E+000
2978.40	14.20054	50.6283	20.729	-20.729	31.094	1.263E-001	7736	4.664E+000
3066.00	14.29200	50.8287	20.856	-20.856	31.283	1.266E-001	7823	4.791E+000
3153.60	14.38266	51.0325	20.982	-20.982	31.472	1.299E-001	7911	4.921E+000
3166.74	14.39603	51.0629	21.000	-21.000	31.500	1.935E-002	7924	4.940E+000

D. Stress and C* Information

Time (hrs)	Tran No.	Temp R5	Ref. Stress (MPa)	Primary SIF R5 (MPa/~m)	Secondary SIF R5 (MPa/~m)	Total SIF (MPa/~m)	C* (MN/mh)	C(t) (MN/mh)
87.60	2	650.0	105.545	17.155	0.000	17.155	4.877E-005	4.877E-005
175.20	2	650.0	105.778	17.156	0.000	17.156	3.644E-005	3.644E-005
262.80	2	650.0	105.988	17.148	0.000	17.148	3.080E-005	3.080E-005
350.40	2	650.0	106.186	17.134	0.000	17.134	2.737E-005	2.737E-005
438.00	2	650.0	106.372	17.114	0.000	17.114	2.498E-005	2.498E-005
525.60	2	650.0	107.411	16.864	0.000	16.864	2.413E-005	2.413E-005
613.20	2	650.0	107.573	16.806	0.000	16.806	2.242E-005	2.242E-005
700.80	2	650.0	107.731	16.745	0.000	16.745	2.104E-005	2.104E-005
788.40	2	650.0	107.882	16.681	0.000	16.681	1.990E-005	1.990E-005
876.00	2	650.0	108.030	16.614	0.000	16.614	1.892E-005	1.892E-005
963.60	2	650.0	108.174	16.544	0.000	16.544	1.806E-005	1.806E-005
1051.20	2	650.0	108.313	16.472	0.000	16.472	1.731E-005	1.731E-005
1138.80	2	650.0	108.449	16.398	0.000	16.398	1.663E-005	1.663E-005
1226.40	2	650.0	108.581	16.321	0.000	16.321	1.602E-005	1.602E-005
1314.00	2	650.0	109.219	15.911	0.000	15.911	1.536E-005	1.536E-005
1401.60	2	650.0	109.342	15.821	0.000	15.821	1.481E-005	1.481E-005
1489.20	2	650.0	109.461	15.732	0.000	15.732	1.430E-005	1.430E-005
1576.80	2	650.0	109.579	15.641	0.000	15.641	1.383E-005	1.383E-005
1664.40	2	650.0	109.694	15.550	0.000	15.550	1.339E-005	1.339E-005
1752.00	2	650.0	109.808	15.458	0.000	15.458	1.298E-005	1.298E-005
1839.60	2	650.0	109.920	15.366	0.000	15.366	1.260E-005	1.260E-005
1927.20	2	650.0	110.031	15.274	0.000	15.274	1.224E-005	1.224E-005
2014.80	2	650.0	110.140	15.181	0.000	15.181	1.190E-005	1.190E-005
2102.40	2	650.0	110.247	15.088	0.000	15.088	1.157E-005	1.157E-005
2190.00	2	650.0	110.354	14.995	0.000	14.995	1.127E-005	1.127E-005
2277.60	2	650.0	110.460	14.901	0.000	14.901	1.098E-005	1.098E-005

2365.20	2	650.0	110.564	14.809	0.000	14.809	1.070E-005	1.070E-005
2452.80	2	650.0	110.667	14.715	0.000	14.715	1.044E-005	1.044E-005
2540.40	2	650.0	110.770	14.623	0.000	14.623	1.019E-005	1.019E-005
2628.00	2	650.0	110.872	14.531	0.000	14.531	9.945E-006	9.945E-006
2715.60	2	650.0	111.349	14.156	0.000	14.156	9.560E-006	9.560E-006
2803.20	2	650.0	111.450	14.063	0.000	14.063	9.335E-006	9.335E-006
2890.80	2	650.0	111.551	13.973	0.000	13.973	9.121E-006	9.121E-006
2978.40	2	650.0	111.654	13.882	0.000	13.882	8.916E-006	8.916E-006
3066.00	2	650.0	111.759	13.792	0.000	13.792	8.721E-006	8.721E-006
3153.60	2	650.0	111.869	13.703	0.000	13.703	8.536E-006	8.536E-006
3166.74	2	650.0	111.885	13.690	0.000	13.690	8.509E-006	8.509E-006

D2. Stress and C* Information - Second Crack Tip

Time (hrs)	Tran No.	Temp R5 (C)	Ref. Stress Tip 2 (MPa)	Primary SIF R5 Tip 2 (MPa/~m)	Secondary SIF R5 Tip 2 (MPa/~m)	Total SIF Tip 2 (MPa/~m)	C* (MN/mh) Tip 2	C(t) (MN/mh) Tip 2
87.60	2	650.0	105.545	12.138	0.000	12.138	2.441E-005	2.441E-005
175.20	2	650.0	105.778	12.438	0.000	12.438	1.916E-005	1.916E-005
262.80	2	650.0	105.988	12.712	0.000	12.712	1.693E-005	1.693E-005
350.40	2	650.0	106.186	12.973	0.000	12.973	1.569E-005	1.569E-005
438.00	2	650.0	106.372	13.224	0.000	13.224	1.491E-005	1.491E-005
525.60	2	650.0	107.411	14.696	0.000	14.696	1.832E-005	1.832E-005
613.20	2	650.0	107.573	14.928	0.000	14.928	1.769E-005	1.769E-005
700.80	2	650.0	107.731	15.154	0.000	15.154	1.724E-005	1.724E-005
788.40	2	650.0	107.882	15.375	0.000	15.375	1.690E-005	1.690E-005
876.00	2	650.0	108.030	15.589	0.000	15.589	1.665E-005	1.665E-005
963.60	2	650.0	108.174	15.799	0.000	15.799	1.647E-005	1.647E-005
1051.20	2	650.0	108.313	16.003	0.000	16.003	1.634E-005	1.634E-005
1138.80	2	650.0	108.449	16.205	0.000	16.205	1.624E-005	1.624E-005
1226.40	2	650.0	108.581	16.402	0.000	16.402	1.618E-005	1.618E-005
1314.00	2	650.0	109.219	17.344	0.000	17.344	1.826E-005	1.826E-005
1401.60	2	650.0	109.342	17.527	0.000	17.527	1.817E-005	1.817E-005
1489.20	2	650.0	109.461	17.705	0.000	17.705	1.811E-005	1.811E-005
1576.80	2	650.0	109.579	17.881	0.000	17.881	1.807E-005	1.807E-005
1664.40	2	650.0	109.694	18.053	0.000	18.053	1.805E-005	1.805E-005
1752.00	2	650.0	109.808	18.222	0.000	18.222	1.804E-005	1.804E-005
1839.60	2	650.0	109.920	18.388	0.000	18.388	1.804E-005	1.804E-005
1927.20	2	650.0	110.031	18.550	0.000	18.550	1.805E-005	1.805E-005
2014.80	2	650.0	110.140	18.710	0.000	18.710	1.807E-005	1.807E-005
2102.40	2	650.0	110.247	18.867	0.000	18.867	1.810E-005	1.810E-005
2190.00	2	650.0	110.354	19.021	0.000	19.021	1.813E-005	1.813E-005

2277.60	2	650.0	110.460	19.173	0.000	19.173	1.817E-005	1.817E-005
2365.20	2	650.0	110.564	19.322	0.000	19.322	1.822E-005	1.822E-005
2452.80	2	650.0	110.667	19.469	0.000	19.469	1.827E-005	1.827E-005
2540.40	2	650.0	110.770	19.612	0.000	19.612	1.832E-005	1.832E-005
2628.00	2	650.0	110.872	19.754	0.000	19.754	1.838E-005	1.838E-005
2715.60	2	650.0	111.349	20.336	0.000	20.336	1.973E-005	1.973E-005
2803.20	2	650.0	111.450	20.469	0.000	20.469	1.978E-005	1.978E-005
2890.80	2	650.0	111.551	20.600	0.000	20.600	1.982E-005	1.982E-005
2978.40	2	650.0	111.654	20.730	0.000	20.730	1.988E-005	1.988E-005
3066.00	2	650.0	111.759	20.856	0.000	20.856	1.994E-005	1.994E-005
3153.60	2	650.0	111.869	20.982	0.000	20.982	2.001E-005	2.001E-005
3166.74	2	650.0	111.885	21.000	0.000	21.000	2.003E-005	2.003E-005

E. Strain Information

Time (hrs)	Total Creep Strain Rate	Creep Strain	Creep Life Fraction	Creep/ Elastic Strain	Lambda R(edis) (1/hr)	I(nit)
87.60	2.678E-003	1.749E-005	0.00252	4.021E+000	0.0022	
175.20	3.983E-003	1.310E-005	0.00507	5.968E+000	0.0024	
262.80	5.033E-003	1.110E-005	0.00764	7.527E+000	0.0026	
350.40	5.949E-003	9.898E-006	0.01024	8.880E+000	0.0027	
438.00	6.777E-003	9.071E-006	0.01287	1.010E+001	0.0028	
525.60	7.405E-003	9.113E-006	0.01500	1.093E+001	0.0029	
613.20	8.177E-003	8.539E-006	0.01777	1.205E+001	0.0030	
700.80	8.904E-003	8.085E-006	0.02057	1.310E+001	0.0030	
788.40	9.596E-003	7.714E-006	0.02338	1.410E+001	0.0031	
876.00	1.026E-002	7.403E-006	0.02621	1.505E+001	0.0032	
963.60	1.089E-002	7.139E-006	0.02907	1.596E+001	0.0032	
1051.20	1.151E-002	6.909E-006	0.03194	1.684E+001	0.0033	
1138.80	1.210E-002	6.709E-006	0.03483	1.769E+001	0.0033	
1226.40	1.268E-002	6.531E-006	0.03774	1.852E+001	0.0034	
1314.00	1.317E-002	6.629E-006	0.04024	1.912E+001	0.0035	
1401.60	1.375E-002	6.469E-006	0.04326	1.993E+001	0.0035	
1489.20	1.431E-002	6.324E-006	0.04629	2.071E+001	0.0036	
1576.80	1.485E-002	6.194E-006	0.04933	2.148E+001	0.0036	
1664.40	1.539E-002	6.074E-006	0.05239	2.224E+001	0.0037	
1752.00	1.592E-002	5.965E-006	0.05547	2.298E+001	0.0037	
1839.60	1.644E-002	5.864E-006	0.05857	2.370E+001	0.0037	
1927.20	1.695E-002	5.771E-006	0.06168	2.441E+001	0.0038	
2014.80	1.745E-002	5.685E-006	0.06480	2.511E+001	0.0038	
2102.40	1.794E-002	5.605E-006	0.06794	2.579E+001	0.0039	
2190.00	1.843E-002	5.530E-006	0.07110	2.647E+001	0.0039	

2277.60 1.891E-002 5.461E-006 0.07427 2.713E+001 0.0040
 2365.20 1.939E-002 5.395E-006 0.07746 2.779E+001 0.0040
 2452.80 1.986E-002 5.334E-006 0.08066 2.844E+001 0.0040
 2540.40 2.032E-002 5.276E-006 0.08388 2.908E+001 0.0041
 2628.00 2.078E-002 5.222E-006 0.08712 2.971E+001 0.0041
 2715.60 2.119E-002 5.312E-006 0.09002 3.016E+001 0.0042
 2803.20 2.165E-002 5.260E-006 0.09334 3.079E+001 0.0042
 2890.80 2.211E-002 5.211E-006 0.09668 3.142E+001 0.0043
 2978.40 2.257E-002 5.166E-006 0.10003 3.203E+001 0.0043
 3066.00 2.302E-002 5.124E-006 0.10340 3.264E+001 0.0044
 3153.60 2.346E-002 5.086E-006 0.10678 3.324E+001 0.0044
 3166.74 2.353E-002 5.080E-006 0.10729 3.333E+001 0.0044 # 2

Table A8.10 - Loading History for Example 7

Action	Number of Cycles	Cumulated Creep Fatigue Cycles	Max Load (kN)	Min Load (kN)
Fatigue pre-cracking at 650°C	68271	-	-13.5	3.5
Creep-fatigue cycles	474	474	-14	14
1st Beachmarking	2100	-	-10	10
Creep-fatigue cycles	781	1255	-14	14
2nd Beachmarking	1500	-	-10	10
Creep-fatigue cycles	1356	2611	-14	14
3rd Beachmarking	1200	-	-10	10
Creep-fatigue cycles	518	3129	-14	14
Fatigue post cracking at room temperature	8578	-	-	-

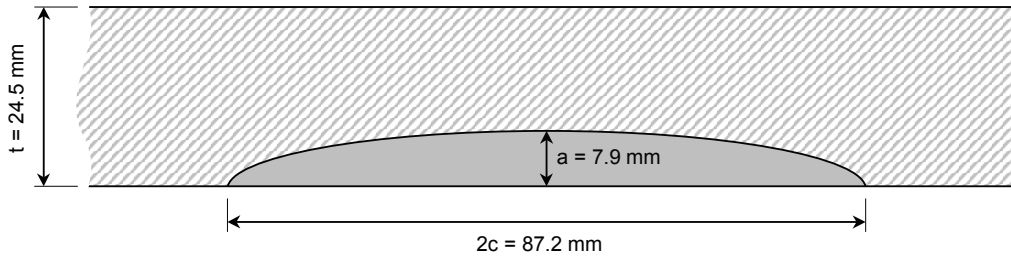


Figure A8.24- Defect shape and dimensions (Example 7)

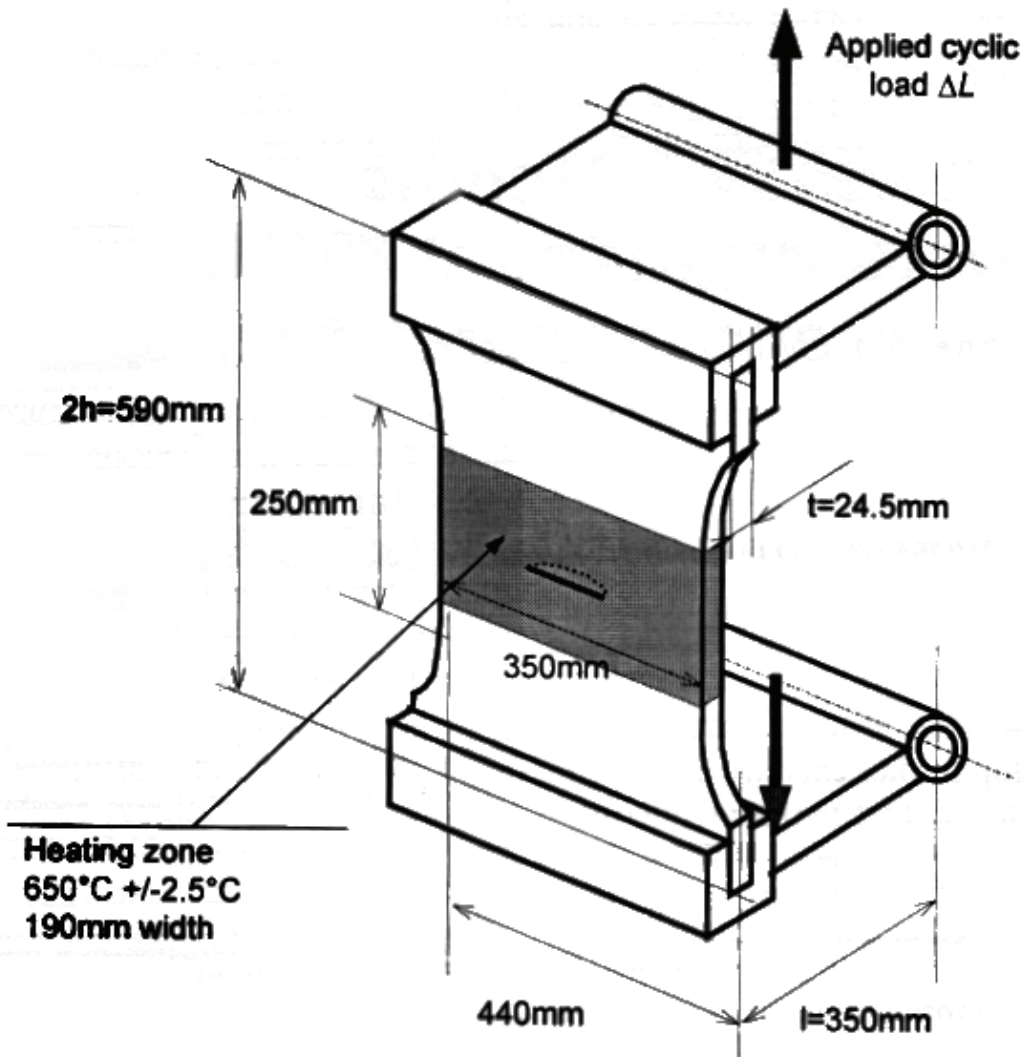


Figure A8.25- Plate dimensions, test set-up and location of defect (Example 7)

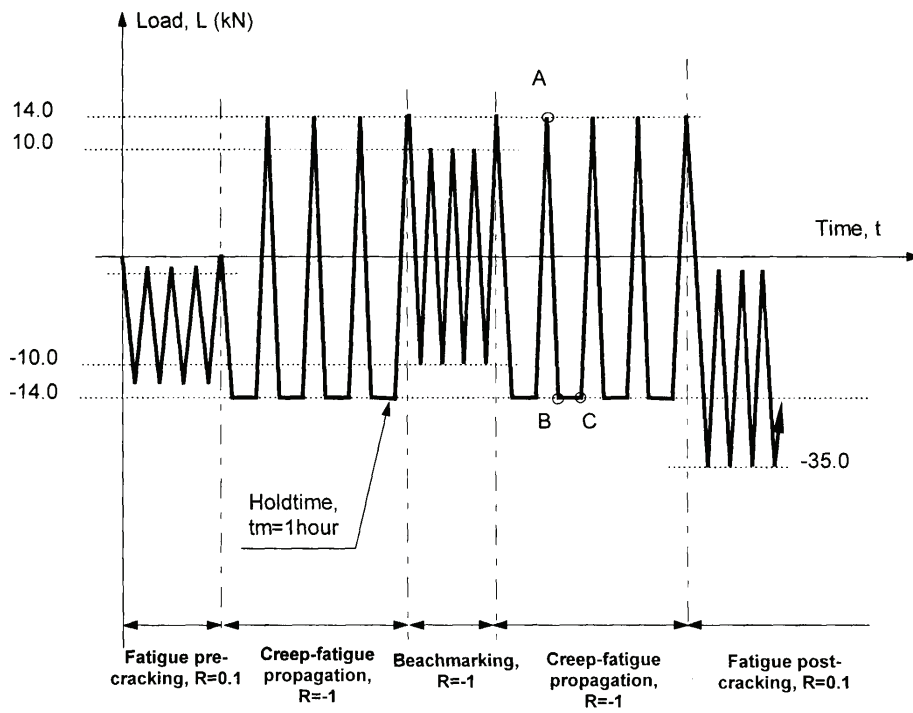


Figure A8.26 - Loading cycles for plate test (A = compressive peak; B = start of tensile dwell; C = end of dwell period)

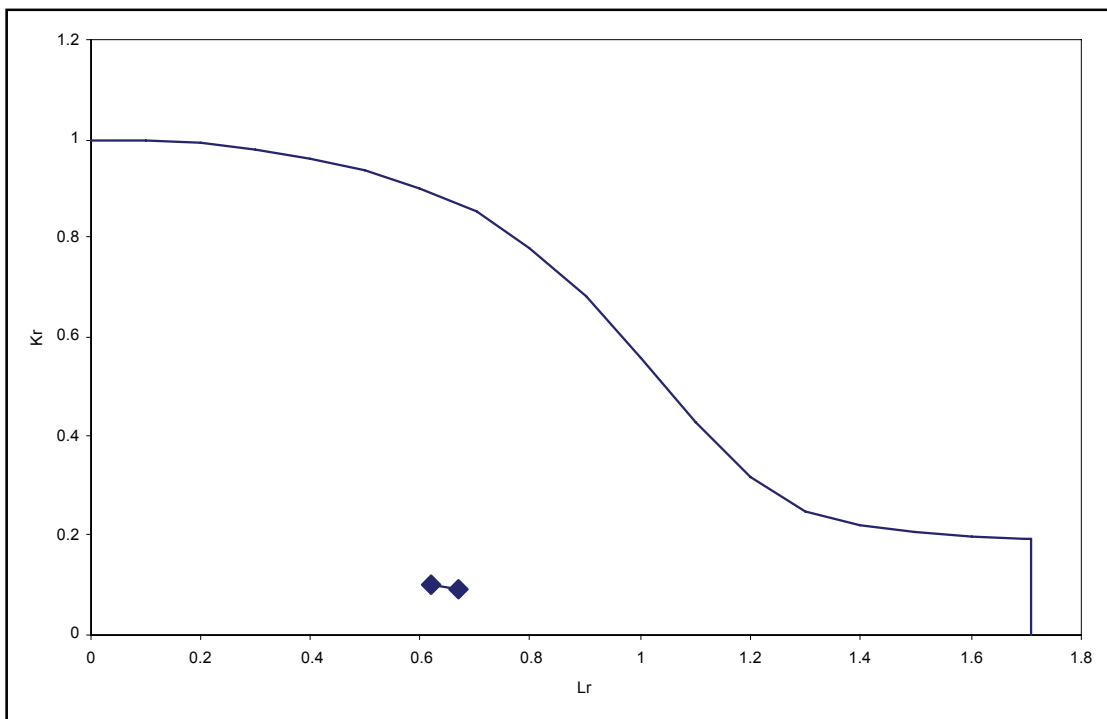


Figure A8.27 - Option 1 FAD for initial and final crack sizes (Example 7)

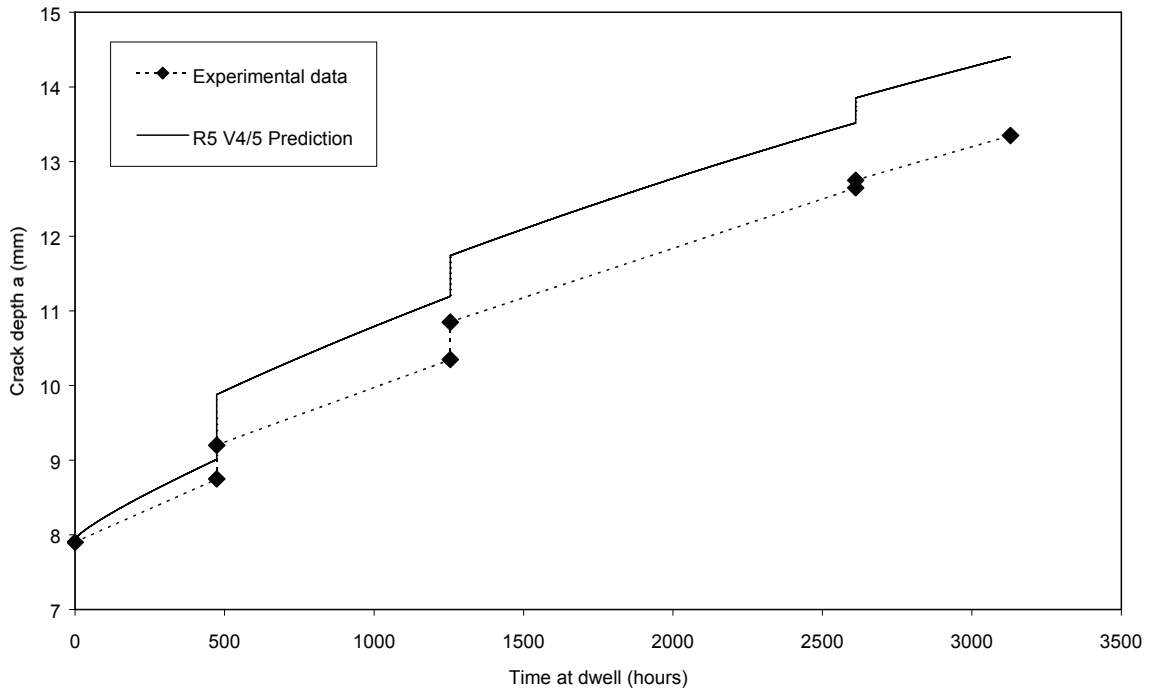


Figure A8.28 - Through-thickness crack growth (Example 7)

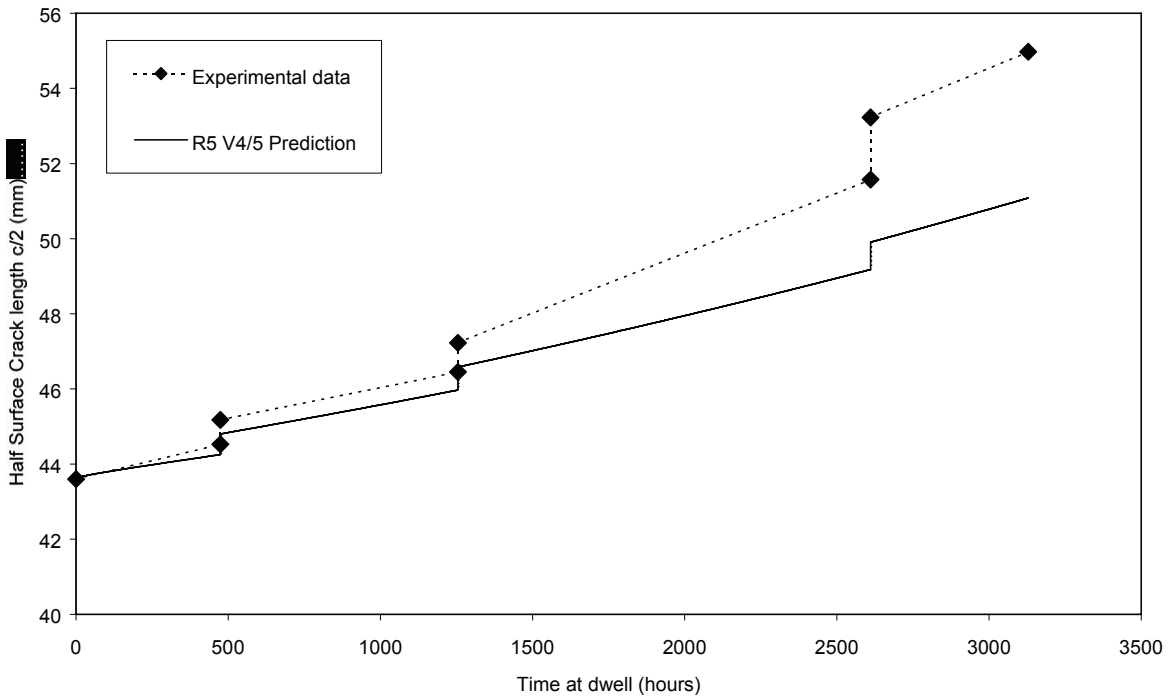


Figure A8.29 - Surface crack growth (Example 7)

13.5 Case Studies for CORROSION

13.5.1 Pipeline Local Thinned Area Assessment

Specimen :	Pipe
Loading :	Internal pressure
Material :	API 5L X65
Defect :	LTA
Temperature :	

Objective

Assessment of a pipeline containing a local thinned area due to corrosion

Background

This example shows the assessment of a pipeline containing an isolated local thinned area (LTA) due to corrosion. The local thinned areas were found during an internal inspection of the pipeline using a magnetic flux intelligent pig. The largest reported LTA has a length equal to 220 mm and a depth equal to 30% of the wall thickness. The inspection accuracy quoted by the inspection tool provider is that the defect depth will be reported within a $\pm 10\%$ tolerance of the wall thickness with confidence level equal to 80%. The standard deviation in the length measurement is less than 20 times the standard deviation in the depth measurement. The maximum allowable operating pressure of the line is 150 bar. The dimensions and the material properties are summarised as follows:

- outside diameter = 812.8 mm
- wall thickness = 19.1 mm
- specified minimum tensile strength = 530.9 MPa (API 5L grade X65)

FFS analysis

The local thinned areas have been assessed using the DNV recommended practice RP-F101 for corroded pipelines published in 1999. Within this recommended practice the accuracy of the inspection technique/tool used can be taken into account, see the DNV RP-F101 for details. The maximum allowable pressure of the pipeline containing the above corrosion defect is calculated using the following equation:

$$p_{corr} = \gamma_m \frac{2t SMTS \left(1 - \gamma_{\Delta} (d/t)^*\right)}{(D-t) \left(1 - \frac{\gamma_{\Delta} (d/t)^*}{Q}\right)}$$

where

$$Q = \sqrt{1 + 0.31 \left(\frac{l}{\sqrt{Dt}}\right)^2}$$

$$(d/t)^* = (d/t)_{measured} + \varepsilon_{\Delta} StD [d/t]$$

with

- d = depth of corroded region
- t = nominal wall thickness
- D = nominal outside diameter
- l = longitudinal length corroded region

The other parameters are a function of the accuracy of inspection and are listed below (see the DNV RP-F101 for details):

- γ_m = 0.74
- γ_d = 1.28
- ε_d = 1.00
- $StD(d/t)$ = 0.08

The calculated maximum allowable pressure with the corrosion is 14.87 MP (148.7 bar), which is lower than the required maximum allowable pressure of 150 bar.

Refinement

Since the calculated safe allowable pressure of the pipeline with corrosion (148.7 bar) is only slightly lower than the required maximum allowable operating pressure (150 bar) it is decided to perform a more accurate inspection of the corroded area, using manual UT.

Using the accuracy sizing accuracy of UT ± 0.2 mm, see the table on “performance of NDE methods used in accordance with existing codes and standards” in this guideline, the following parameters are obtained:

- γ_m = 0.77
- γ_d = 1.04
- ε_d = 0.00
- $StD(d/t)$ = 0.01

The calculated maximum allowable pressure with the corrosion is now 17.41 MPa (174.1 bar), which is higher than the current maximum allowable pressure of 150 bar.

Mitigation

When a more accurate sizing is impossible, because of limited access, the line would be determined to be unsafe. In this case the maximum allowable operating pressure could be reduced to a value below the 14.87 MPa (148.7 bar).

Conclusions

It was determined, on the basis of the intelligent pig results that the pipeline is unsafe to operate at the required maximum operating pressure of 150 bar.

Based on a more accurate verification using manual UT, it was shown that it is safe to operate at 150 bar.

When a more accurate sizing is impossible, the line could be de-rated to a maximum allowable operating pressure below the calculated failure pressure of 14.87 MPa (148.7 bar) if this does not result in unacceptable financial losses.

It should be noted that separate action is required to either monitor future extension of the corrosion damage and/or measures should be taken to stop the corrosion.

Bibliography

DNV Recommended Practice RP-F101, *Corroded Pipelines* (1999).

13.5.2 Checklist for FFS Assessment

item	input/results/comments
1 General (also see Information Check List)	
1.1 Structure/equipment identification (detail)	Pipeline
1.2 Design code (pressure vessel, bridge, offshore etc.)	B31
1.3 Environment	Gas
1.4 Material	API 5L grade X65
1.5 Dimensions (width, thickness, etc)	outside diameter = 812.8 mm wall thickness = 19.1 mm
1.6 Post weld heat treatment	no
1.7 Consequence of failure:	
1.7.1 Brittle fracture (yes or no)	no
1.7.2 Potential risk to a person (yes or no)	no
1.7.3 Potential risk to personnel (yea or no)	no
1.7.4 Potential risk to the environment (yes or no)	no
1.7.5 Potential financial consequences (yes or no)	Yes, (unplanned) repair loss of production and costs (volume per day during shutdown plus any delivery penalties)
1.7.6 Target reserve factor or probability of failure	During design the pipeline was qualified as Safety Class “Normal” accordingly to DNV OS-F101 which corresponds with a annual failure probability equal to $< 10^{-4}$
2 Loading conditions	
2.1 Design conditions e.g. temperature, pressure, static/dynamic loading, proof testing, design life etc.	Maximum allowable operating pressure = 150 bar
2.2 Operating conditions e.g. temperature, environment, pressure, static/ dynamic loading, re-hydrotesting, period to shutdown, etc.	Maximum allowable operating pressure = 150 bar
2.3 Design stress analysis available	yes
2.4 Define stresses	-
Primary stresses (tension, bending)	Internal pressure and no unsupported span to cause bending
Secondary thermal/residual stresses (post weld heat treatment)	Not applicable. No welds involved and plastic collapse is the failure mode
Proof testing (level of stress and temperature)	Yes, but not relevant for plastic collapse
2.5 Indication of over- or unconservatism in the loading conditions	Accurate. Due to pressure relief valves.
3 Material properties	
3.1 Material specification (base, weld) (Minimum requirements for tensile and impact properties)	API 5L grade X65 SMUTS = 530.9. MPa
3.2 Measured tensile and impact properties (base, weld)	Unavailable
Tensile Properties	-
Impact Properties	-
Full stress strain curve	-
Weld Configuration (max. weld bead heights, bevel angles, width of weld and HAZ, etc.	Inapplicable. No welds involved.
3.3 Fracture toughness	Inapplicable. Plastic collapse is failure mode. No welds involved.
Estimated from Charpy V Data	-
Estimated from a fracture toughness database	-
Material qualification data (CTOD, K, J, R-curve)	-
3.4 Transition temperature	Inapplicable. Plastic collapse is failure mode.
3.5 Crack growth law (e.g. fatigue), stress corrosion cracking, hydrogen embrittlement.	Corrosion

item	input/results/comments
3.6 Embrittlement, ageing (temper embrittlement, irradiation embrittlement, hydrogen embrittlement)	Inapplicable
3.7 Weld mismatch	Inapplicable. No weld involved.
3.8 Modulus of elasticity and Poisson's ratio	-
3.9 Indication of over- or unconservatism in materials properties	Minimum specified yield is used as input.
4 Flaw data and NDE aspects Inspection history (frequency and extent of inspections)	
4.1 Flaw type and cause (fatigue, lack of fusion, planar, volumetric, fabrication, in service etc.)	Corrosion damage
4.2 Flaw location (weld metal, fusion line etc.)	Base material
4.3 Flaw size and orientation	Largest 200mm length and 30% of wall thickness
4.4 Basis for flaw data (NDE method) NDE method(s) used and indicate procedure(s) used)	Inspection accuracy specified by provider of the magnetic flux inspection tool.
Probability of detection (influences-accessibility difficulties, less than 100% coverage)	
Defect accuracy (influences-accessibility difficulties, conditions)	Depth 10% of wall thickness
Extent of defects e.g. distribution of the defects, number of defects per metre, part(s) of the weld and part(s) of the equipment, etc.	Single corrosion patches
Defect growth rates (estimated defect growth rates (also corrosion rates) from periodic inspections)	Unknown. To be monitored
4.5 Defect interaction (evaluation (including the recategorisation of subsurface to surface defects))	No interaction
4.6 Indication of over- or unconservatism in defect data	Inspection accuracy specified by tool provider and is based on tool qualification tests performed on a test loop with known defects
5 Analysis option	
5.1 Decide if FFS is unnecessary e.g. a superficial repair is possible	FFP required. A repair is costly and would introduce unwanted high residual stresses
5.2 Applied assessment procedure and level of analysis	DNV RP-F101, Corroded Pipelines
5.3 Fracture initiation (brittle fracture, ductile fracture initiation)	Plastic collapse is the failure mode of a critical corrosion defect in the base material, see 6.1
5.4 Applied constraint factor (CTOD-K conversion)	Inapplicable, see 5.3 and 6.1.
5.5 Ductile tearing analysis (specify fracture resistance curve)	Inapplicable, see 5.3 and 6.1
5.6 Crack growth (e.g. fatigue), (See Part I Figure 12)	Corrosion to be monitored
5.7 Leak before break or redundancy (See Part I Figure 13) or redundancy	The 220 mm long corrosion patch is not leak before break.
5.8 Probabilistic analysis (See Part I Figure 19)	
Applied method	DNV RP-F101, Corroded Pipelines
Applied distributions	
6 Limit load and stress intensity factor solution	
6.1 Applied limit load solution (plastic collapse)	DNV RP-F101, Corroded Pipelines
Definition of flow stress	-
6.2 Applied stress intensity factor solution	Not applicable, see 5.3 and 6.1.
Stress concentration factor	-
6.3 Indication of conservatism or unconservatism in solutions chosen	The applied solutions are conservative and by taking into account the inaccuracy of inspection the defect sizes, upperbound defect sizes were implicitly used in the analysis.
7. Significance of results	
7.1 Results sensitivity analysis	No sensitivity analysis was carried out. Inaccuracy taken into account using partial safety factors.
7.2 Reserve factor as a function of e.g. defect size, fracture toughness etc. versus consequences of	See item 6.3 and item 7.1.

failure (Check against item 1.7)	
----------------------------------	--